

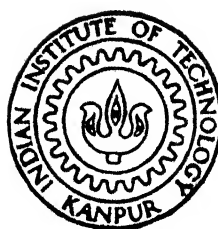
# PROCESSING AND PROPERTIES OF MODIFIED WC - 10Co CEMENTED CARBIDES

*by*

**SUBIR KUMAR BHAUMIK**

ME  
1992  
D  
BHA  
PRO

TH  
ME/1992/D  
B 469p



DEPARTMENT OF METALLURGICAL ENGINEERING  
INDIAN INSTITUTE OF TECHNOLOGY KANPUR

FEBRUARY, 1992

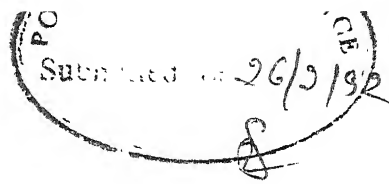
to the  
DEPARTMENT OF METALLURGICAL ENGINEERING  
INDIAN INSTITUTE OF TECHNOLOGY KANPUR  
FEBRUARY, 1992

PE-1992-D-GMA-PRO

20 OCT 1992 /MET

Doc. No. **116575**

715  
671.37  
F 11.16



## CERTIFICATE

This is to certify that the thesis entitled 'Processing and Properties of Modified WC-10Co Cemented Carbides' submitted by Mr. S.K. Bhaumik has been carried out under our supervision and has not been submitted elsewhere for a degree.

G.S. Upadhyaya

Professor

M.L. Vaidya

Professor

Department of Metallurgical Engineering  
Indian Institute of Technology Kanpur  
Kanpur 208 016

## ACKNOWLEDGEMENTS

The author gratefully places on record his indebtedness to Professors G.S. Upadhyaya and M.L. Vaidya who have kindly supervised the work described in this thesis. Their keen involvement and competent guidance during this study are acknowledged with feelings of the deepest reverence.

The author would like to thank Dr. R. Balasubramaniam and Dr. S. Bhargava for useful discussions.

The author is fortunate in his labmates, Hamid, Pradip, Rajendra, Bhaskar, Sujata, and Prasanta, who have helped and encouraged him at various times.

Experimental work of this magnitude requires the cooperation of many associated with the laboratories. The assistance rendered to the author by Shri S.C. Soni, Shri M.N. Mongole, Shri P.K. Pal, Shri K.P. Mukherjee and Shri B.K. Jain, in this connection has been crucial.

Shri K.N. Islam has done an excellent job of typing the thesis. Vijayan, Manindra, Rajesh, Brajesh, Anoop, Shreesh, Varun, Amitav, Aniruddha, Navdeep, Nagarajan, Yudvir, Rajiv, Jyoti, Alok, Santos, Vinay, Sujay, the author's close friends have made the stay at IIT Kanpur memorable in many pleasant ways.

The author's family has been generous with encouragement and moral support throughout.

Shri T. Bose and his family are specially acknowledged for their advice and love.

Finally, and most importantly, the author has been supported by Bithi with encouragement, patience and friendship.

Subir Kumar Bhaumik

## PUBLICATIONS

Based on the present thesis the following papers have been published :

1. Alloy design of WC-10Co hard metals with modifications in carbide and binder phases, International Journal of Refractory Metals and Hard Materials, Vol.10, No.3, 1991.
2. Properties and microstructures of WC-TiC-Co and WC-TiC-Co(Ni) cemented carbides, Material Science and Technology, Vol. 7, 1991, 723.
3. SEM study of the fracture behavior of some WC based cemented carbides, Practical Metallography, Vol.28, 1991, 238.
4. Mechanical properties and microstructures of carbide and binder modified WC-10Co cemented carbides, Proceedings of 'International P/M Conference and Exhibiton', 9-12 June, 1991, Chicago, Metal Powder Industries Federation, Princeton, Vol.6, 1992.
5. Effect of TiN addition on sintering behavior and mechanical properties of WC-10Co hard metals containing MoC and Ni, Journal of Material Science, (in press).
6. Fracture behavior of WC-TiN-Co and WC-TiN- $\text{Mo}_2\text{C}$ -Co(Ni) cemented carbides. A SEM study, Practical Metallography, (in press).
7. TEM study of WC-10Co cemented carbide with modified hard and binder phases, Material Characterisation, (in press).
8. Microstructure and mechanical properties of WC-TiN-Co and WC-TiN- $\text{Mo}_2\text{C}$ -Co(Ni) cemented carbides, Ceramics International, (in press).

# CONTENTS

	Page
List of Tables	ix
List of Figures	x
Abstract	xv
 CHAPTER I      LITERATURE REVIEW	 1
I.1    Introduction	1
I.2    WC-Co cemented carbide	4
I.2.1    Sintering	4
I.2.2    Microstructure	7
I.2.3    Mechanical properties	12
(a)    Hardness	12
(b)    Compressive strength	14
(c)    Tensile strength	14
(d)    Transverse rupture strength	15
(e)    Fracture toughness	17
(f)    Fracture behavior	19
I.2.4    Magnetic properties	21
(a)    Coercive force	21
(b)    Magnetic saturation	23
I.2.5    Oxidation resistance	23
I.2.6    Thermal shock resistance	24
I.2.7    Wear resistance	25
I.3    WC-Co cemented carbide with modified binder phase	28
I.3.1    WC bonded with nickel	28
I.3.2    WC bonded with nickel based alloys	29
I.3.3    WC bonded with iron	31
I.3.4    WC bonded with iron, nickel and cobalt	31
I.4    WC-Co cemented carbide with modified hard phase	32
I.4.1    Effect of refractory carbide additions	33

I.4.2	Effect of refractory nitride additions	36
I.5	WC-Co cemented carbide with modified hard and binder phases	37
I.6	Scope of the present investigation	37
CHAPTER II	EXPERIMENTAL PROCEDURE	41
II.1	Raw materials and their characteristics	41
II.2	Premix preparation	43
II.3	Milled premix powder characterisation	44
II.4	Room temperature compaction	45
II.5	Dewaxing and sintering	45
II.6	Hot isostatic pressing (HIP'ing)	46
II.7	Sintered density and porosity evaluation	47
II.8	Microstructural studies	47
II.8.1	Pore morphology and its distribution	47
II.8.2	Scanning Electron Microscopy (SEM) and quantitative metallography	47
II.8.3	Transmission Electron Microscopy (TEM)	49
II.9	Mechanical properties evaluation	49
II.9.1	Transverse Rupture Strength (TRS)	49
II.9.2	Hardness	50
II.9.3	Indentation Fracture Toughness	50
II.10	Magnetic properties measurements	50
II.11	Oxidation study	51
II.12	Thermal shock resistance evaluation	52
II.13	Cutting tool life estimation and failure analysis	52
CHAPTER III	EXPERIMENTAL RESULTS	56
III.1	Powder premix characterisation	56
III.2	WC-10Co cemented carbide (Alloy A)	56
III.2.1	Sintered density	56

	page
III.2.2 Microstructural study	56
III.2.3 Magnetic properties	57
III.2.4 Mechanical properties	57
III.2.5 Fractographic study	57
III.2.6 Oxidation behavior and thermal shock resistance	58
III.2.7 Cutting performance	59
III.3 WC-TiC ( $\text{Mo}_2\text{C}$ )-Co(Ni) cemented carbides	59
III.3.1 WC-8TiC-12Co cemented carbide (Alloy B)	59
III.3.2 WC-8TiC-6Co-6Ni cemented carbide (Alloy C)	62
III.3.3 WC-6TiC-2 $\text{Mo}_2\text{C}$ -6Co-6Ni cemented carbide (Alloy D)	66
III.4 WC-TiN( $\text{Mo}_2\text{C}$ )-Co(Ni) cemented carbides	69
III.4.1 WC-8.7TiN-12Co cemented carbide (Alloy E)	69
III.4.2 WC-8.7TiN-6Co-6Ni cemented carbide (Alloy F)	74
III.4.3 WC-7.5TiN-1.8 $\text{Mo}_2\text{C}$ -6Co-6Ni cemented carbide (Alloy G)	76
III.5 WC-Ti(C,N)/ $\text{Mo}_2\text{C}$ -Co/Ni cemented carbides	79
III.5.1 WC-8.3Ti(C,N)-12Co cemented carbide (Alloy H)	80
III.5.2 WC-8.3Ti(C,N)-6Co-6Ni cemented carbide (Alloy I)	82
III.5.3 WC-7Ti(C,N)-2 $\text{Mo}_2\text{C}$ -6Co-6Ni cemented carbide (Alloy J)	85
CHAPTER IV DISCUSSION	165
IV.1 WC-10Co cemented carbide (Alloy A)	165
IV.1.1 Densification behavior	165
IV.1.2 Microstructural characterisation	167
IV.1.3 Mechanical properties and fracture behavior	170

	page
IV.1.4 Oxidation and thermal shock resistance	171
IV.1.5 Cutting performance	172
IV.2 WC-8TiC-12Co cemented carbide (Alloy B)	173
IV.3 WC-8TiC-6Co-6Ni cemented carbide (Alloy C)	178
IV.4 WC-6TiC-2Mo <sub>2</sub> C-6Co-6Ni cemented carbide (Alloy D)	183
IV.5 WC-8.7TiN-12Co cemented carbide (Alloy E)	187
IV.5.1 Liquid phase sintered alloy	187
IV.5.2 Hot isostatically pressed alloy	188
IV.6 WC-8.7TiN-6Co-6Ni cemented carbide (Alloy F)	193
IV.7 WC-7.5TiN-1.8Mo <sub>2</sub> C-6Co-6Ni cemented carbide (Alloy G)	194
IV.7.1 Liquid phase sintered alloy	194
IV.7.2 Hot isostatically pressed alloy	195
IV.8 Cemented carbides containing Ti(C,N)	197
IV.8.1 Liquid phase sintered alloys	197
IV.8.2 Hot isostatically pressed alloys	198
IV.9 Comparative role of different refractory compound additives on microstructure and properties of WC-10Co cemented carbides.	201
CHAPTER V CONCLUSIONS	208
REFERENCES	210

## LIST OF TABLES

Table		Page
1.1	: Different ISO grades of cemented carbides and their properties	40
2.1	: Nominal compositions of different alloys in volume and mass percent	53
3.1	: Mean linear intercept of hard phase particles in various powder premixes	89
3.2	: Mean linear intercept of WC, contiguity of carbide phase and mean binder free path of alloy A	90
3.3	: Mechanical and magnetic properties of alloy A	90
3.4	: The oxides identified and the rate law constants of alloys A, B, C, D, E and G after oxidation in air at 800 <sup>o</sup> C (1073K)	91
3.5	: Thermal shock resistance ( $\Delta T$ ) of various grades of cemented carbides	92
3.6	: Sintered density of alloys A, B, C and D after H <sub>2</sub> sintering.	93
3.7	: Mean linear intercept length of hexagonal and cubic phases in various cemented carbides	94
3.8	: Percent sintered porosity in various grades of cemented carbides after liquid phase sintering and HIP'ing.	95

## LIST OF FIGURES

Figure		Page
2.1	A schematic drawing of the quenching apparatus used for thermal shock resistance measurements.	54
2.2	A schematic drawing of the tool geometry.	55
3.1	Cumulative frequency distribution of hard phases intercept lengths in alloys A and B after milling.	96
3.2	Cumulative frequency distribution of hard phases intercept lengths in alloys C and D after milling.	97
3.3	Cumulative frequency distribution of hard phases intercept lengths in alloys E and F after milling.	98
3.4	Cumulative frequency distribution of hard phases intercept lengths in alloys G and H after milling.	99
3.5	Cumulative frequency distribution of hard phases intercept lengths in alloys I and J after milling.	100
3.6	Pore morphology and SEM microstructure of alloy A.	101
3.7	TEM micrographs of alloy A.	102
3.8	SEM fractographs of alloy A.	103
3.9	Weight gain Vs time plot of alloy A during oxidation in air at 800 °C (1073K).	104
3.10	SEM micrographs of oxidised surface.	105
3.11	SEM pictures of tool made of alloy A after cutting test.	106
3.12	Effect of sintering temperature on hardness of alloys A, B, C and D.	107
3.13	Effect of sintering temperature on TRS and indentation fracture toughness of alloys A, B, C and D.	108
3.14	Effect of sintering temperature on magnetic properties of alloys A, B, C and D.	109

Figure		Page
3.15	SEM micrographs of alloys A, B, C, and D.	110
3.16	Cumulative frequency distribution of hard phases intercept lengths in alloys A, B, C and D after sintering.	111
3.17	Mean binder free path and contiguity in Alloys A, B, C and D.	112
3.18	TEM microstructure of alloy B.	113
3.19	Magnetic properties variations in alloys A, B, C and D.	114
3.20	Hardness variations of alloys A, B, C and D.	115
3.21	TRS and indentation fracture toughness variations of alloys A, B, C and D.	116
3.22	SEM fractographs of alloy B.	117
3.23	Weight gain Vs time plot of alloys A, B, C and D during oxidation in air at 800 <sup>o</sup> C (1073K).	118
3.24	Tool life variations of alloys A,B,C and D.	119
3.25	SEM pictures of tool made of alloy B after cutting test.	120
3.26	TEM microstructures of alloy C.	121
3.27	SEM fractographs of alloy C.	122
3.28	SEM pictures of tool made of alloy C after cutting test.	123
3.29	TEM microstructure of alloy D.	124
3.30	SEM fractographs of alloy D.	125
3.31	SEM pictures of the worn surfaces of the tool made of alloy D.	126
3.32	Effect of sintering temperature on percent sintered porosity, and hardness of alloys E, F and G.	127
3.33	Effect of sintering temperature on TRS and indentation fracture toughness of alloys E,F and G.	128
3.34	Effect of sintering temperature on magnetic properties of alloys E, F and G.	129

Figure	Page
3.35	Pore morphology and distribution in alloys E, F, and G after liquid phase sintering. 130
3.36	SEM microstructures of alloys E, F and G after liquid phase sintering. 131
3.37	Cumulative frequency distribution of hard phases intercept lengths in alloys E, F and G after liquid phase sintering. 132
3.38	Pore morphology and distribution in alloys E and G after HIP'ing. 133
3.39	SEM microstructures of alloys E and G after HIP'ing. 134
3.40	Cumulative frequency distribution of hard phases intercept lengths in alloys E and G after HIP'ing. 135
3.41	Mean binder free path and contiguity variations in alloys A, E and G. 136
3.42	TEM microstructures of alloy E. 137
3.43	Magnetic properties variations in alloys E and G. 138
3.44	Hardness variations in alloys A, E and G. 139
3.45	Transverse rupture strength and indentation fracture toughness variations in alloys A, E and G. 140
3.46	SEM fractographs of alloy E. 141
3.47	Weight gain Vs time plot of alloys A, E and G during oxidation in air 800°C (1073K). 142
3.48	Tool life variations of alloys E and G after HIP'ing. 143
3.49	SEM picture of tool made of alloy E after cutting test. 144
3.50	TEM micrographs of alloy G. 145
3.51	SEM fractographs of alloy G. 146
3.52	SEM pictures of tool made of alloy G after cutting test. 147

Figure		Page
3.53	Effect of sintering temperature on percentage sintered porosity and hardness of alloys H, I and J.	148
3.54	Effect of sintering temperature on TRS and indentation fracture toughness of alloys H, I and J.	149
3.55	Effect of sintering temperature on magnetic properties of alloys H, I and J.	150
3.56	Pore morphology and distribution in alloys H, I and J after liquid phase sintering.	151
3.57	SEM microstructures of alloys H, I and J after liquid phase sintering.	152
3.58	Cumulative frequency distribution of hard phases intercept lengths in alloys H, I and J after liquid phase sintering.	153
3.59	Pore morphology and distribution in alloys H, I and J after HIP'ing.	154
3.60	SEM microstructures of alloys H, I and J after HIP'ing.	155
3.61	Cumulative frequency distribution of hard phases intercept lengths in alloys H, I and J after HIP'ing.	156
3.62	Mean binder free path and contiguity variations in alloys H, I and J.	157
3.63	Magnetic properties variations in alloys H, I and J.	158
3.64	Hardness variations in alloys H, I and J.	159
3.65	TRS and indentation fracture toughness variations in alloys H, I and J.	160
3.66	SEM fractographs of alloy H.	161
3.67	SEM fractographs of alloy I.	162
3.68	SEM fractographs of alloy J.	163
3.69	Weight gain Vs time plot of alloys H, I and J during oxidation in air at 800°C (1073K).	164

Figure		Page
4.1	Hardness variations in various cemented carbides as a function of hard phase additives and binder phase compositions.	206
4.2	TRS and indentation fracture toughness variations in various cemented carbides as a function of hard phase additives and binder phase compositions.	207

## ABSTRACT

Cemented carbides are some of the most successful powder metallurgy products in industrial and engineering applications due to a unique combination of their high hardness and fracture toughness. At least 70% of the cutting tools employed today are cemented carbides, out of which a major part is WC-Co. This extensive usage makes tungsten and cobalt among the most strategically important materials in the world. Though WC free cemented carbides have been developed, they could not replace WC based cemented carbides in most of the applications because of their relatively lower toughness and WC based cemented carbides by far remain the major competent material in the field of cutting and wear resistant applications. The most developed approaches, therefore, seem to be dilution of WC by other refractory compounds and partial replacement of cobalt by nickel, iron or their alloys so that at least some of these strategically important materials could be saved.

The present study deals with the partial replacement of WC in WC-10Co cemented carbide by other refractory compounds without sacrificing strength and toughness. The refractory compounds chosen are TiC, TiN and Ti(C,N). In order to maintain equivalent properties such addition necessitated the binder modification. The starting composition of the cemented carbide i.e. WC-10Co corresponded to approximately 17 vol% binder phase. All the subsequent compositions developed later were tailored so that the volume fraction of hard phases and binder remained constant as that of the initial WC-10Co cemented carbide. The systems studied were WC-17 vol% Co, WC-20 vol% X - 17 vol% Co, WC-20 vol% X - 8.5 vol% Co - 8.5 vol% Ni and WC - 17 vol% X - 3 vol% Mo<sub>2</sub>C - 8.5 vol% Co - 8.5 vol% Ni, where X is the refractory compound additive i.e.

TiC / TiN/Ti (C,N). In all the cases, the milling of the constituent powders was carried out in acetone medium in centrifugal ball mill for 32 hrs. The vacuum dried powder premixes were subsequently cold compacted at pressure range 350-450 MPa to obtain Transverse Rupture Strength (TRS) test pieces. Straight WC-10Co and TiC, containing cemented carbides were sintered in hydrogen and vacuum, whereas TiN and Ti(C,N) containing cemented carbides were sintered in  $H_2$  and  $H_2+N_2$  (50:50) mixture. Hot isostatic pressing (HIP'ing) was carried out for those alloys which were not fully densified by liquid phase sintering alone. The study starting from alloy processing through microstructural and properties evaluation including some important technical properties viz. oxidation resistance, thermal shock resistance and cutting performance were carried out for a comparative study of the role of different refractory compounds/binders on WC-10Co cemented carbide.

Sintering experiments have shown that the addition of TiC to WC-10Co cemented carbide requires a higher sintering temperature to achieve full density irrespective of any binder composition, whereas it is virtually impossible to achieve full density with TiN/Ti(C,N) addition by liquid phase sintering alone. HIP'ing is, therefore, required for TiN/Ti(C,N) containing cemented carbides to eliminate the closed pores in liquid phase sintered alloys. As far as the sintering atmosphere is concerned, WC-10Co and TiC containing cemented carbides give better properties after vacuum sintering, but TiN/Ti(C,N) containing cemented carbides have to be sintered in  $H_2+N_2$  mixture to avoid denitrification of the nitrogen bearing refractory compounds.

TiC addition to WC-10Co cemented carbide results in a nonuniform microstructure with relatively large TiC grains, which gives rise to poor TRS and indentation fracture toughness. Such

grain coarsening effect in TiC is thought to be due to inadequate wetting of TiC by cobalt. TEM studies confirm that the modification of the binder cobalt by incorporating nickel and molybdenum results in the formation of well-wettable Mo-rich shell around TiC grain and thus helps in producing a rather uniform microstructure, which subsequently results in an improved TRS and indentation fracture toughness.

TiN/Ti(C,N) addition to WC-10Co cemented carbide does not lead to any observable nonuniformity in microstructure. Though TiN/Ti(C,N) has poor wettability with cobalt, the grain growth suppression in TiN/Ti(C,N) appears to be due to spinodal decomposition. In case of TiN/Ti(C,N) addition, with cobalt binder the TRS and indentation fracture toughness are better than those containing TiC. Any change in binder chemistry imparts some deterioration in properties in such system.

Both TiN and Ti(C,N) containing cemented carbides have better TRS and indentation fracture toughness than those of TiC containing ones for any particular binder composition. However, among TiN and Ti(C,N) containing cemented carbides, the former has better properties than those of latter.

Oxidation and thermal shock resistance of all the investigated alloys were determined. The results show that addition of TiC/TiN/Ti(C,N) to WC-10Co cemented carbide improves the oxidation resistance, but deteriorates the thermal shock resistance. Presence of molybdenum in any of the systems has deleterious effect on both oxidation and thermal shock resistance.

Cutting test was performed on EN 9 steel (VHN 200), which showed a superior performance in case of TiN addition with cobalt binder among all the alloys.

In general, the properties of Ti(C,N) containing cemented carbides are intermediate to those containing TiC and TiN,

irrespective of the change in the binder chemistry. The properties of the former are, however, much closer in magnitude with those containing TiN. This has been interpreted on the basis of the change in the contribution of chemical bonds in such refractory compounds, which contributes to the overall composite strength.

In conclusion, it is possible to substitute reasonable amount of WC by TiC/TiN/Ti(C,N) in WC-10Co cemented carbide without much sacrifice in strength and toughness with due modifications in the binder phase. However, a greater control over sintering atmosphere and post sintering treatment such as HIP'ing are required for cemented carbides with TiN/Ti(C,N) substitution. *greater control*

# CHAPTER - I

## LITERATURE REVIEW

### I.1 INTRODUCTION

Cemented carbides typically consist of hard refractory compounds bonded with a relatively soft metal from group VIII of the Periodic Table. These materials are processed using conventional powder metallurgy technique including liquid phase sintering. The product is a composite structure of interwoven phases with synergistic combination of properties. The unique combination of elastic modulus, compressive strength, hardness and fracture toughness of cemented carbides has made them indispensable in a variety of scientific and industrial applications. The single largest application, in economic terms, is that of indexable inserts used for the machining of metals. Major applications also exist in the fields of underground coal and ore mining, surface mining, deep hole drilling, dies, rolls and other components used in metal forming as well as in a broad variety of wear and special applications. Most commercial grades have WC as the prime ingredient with a metal binder, usually Co, and are referred as 'straight grades' in this text. However, many grades, especially those used in the machining of steel contain a substantial quantity of TiC, TaC and/or NbC. They are primarily added to reduce chemical reactivity with the hot substrate in metal cutting. They also act as grain growth inhibitors, and improve deformation resistance at high temperature.

Cemented carbides are typical examples of systems undergoing liquid phase sintering during consolidation. From technical point of view, liquid phase sintering is very

attractive as it provides faster sintering and complete densification without the need for any external pressure. The sintering kinetics are dictated by the interaction between the constituents as represented by basic thermodynamic features which include a wetting liquid, low solubility of the liquid in the solid, segregation of the liquid to solid-solid interfaces and rapid diffusivity during sintering [1-2]. In this respect WC-Co cemented carbides are very often cited as ideal liquid phase sintering system, since the liquid phase produced during sintering in such compositions satisfies all the basic requirements mentioned above.

The decisive breakthrough leading to the modern cemented carbide products was achieved by Schroter [3] in the early 1920s. Most of the two phase tungsten carbide-cobalt (WC-Co) cemented carbides were developed in the period 1926 to 1939 and with minor changes, these developments have persisted in wide use to the present day. Schwarzkopf's [4] discovery that solid solutions of more than one carbide are superior to one carbide led to the development of multcarbide cutting tools for high speed machining of steel. By the early 1950s most of the basic steps essential to an understanding of the production processes and properties measured for quality control i.e. hardness and transverse rupture strength were known, and technical development on an empirical basis was close to the saturation level. From this point the research in cemented carbides took a new dimension and more emphasis was laid upon physical metallurgy aspects including physical and mechanical properties, the wear and other failure mechanisms, and the development of new applications. During this period many of the classical mysteries of cemented carbide were resolved or more clearly understood. Since then the increasing

demand of such unique materials with stringent requirements led the scientists to develop a number of grades suited for specific applications within narrow range. It also became necessary to understand the structure-property relationship more meaningfully. A large amount of literature is available in this regard and by now a quantitative relationship between the microstructure and properties is fairly well understood. Modern applications demand materials with high strength, corrosion resistance, and improved fatigue and creep properties. This led to the development of cemented carbides with modified hard and binder phases. However, future developments are also related with the raw materials supply, economic factors, the general object to save energy and raw materials apart from the increasing demand to have special materials with defined and optimised properties. The resources of tungsten and cobalt have come to appear critical, and this has motivated a great deal of research to develop alternate cemented carbides. Cemented carbides based on TiC-Ni compositions have been developed, but they could not replace WC based cemented carbides in most of the applications because of their relatively lower toughness and WC based cemented carbides by far remain the major competent material in the field of cutting and wear resistant applications.

In this chapter WC based cemented carbides have been reviewed in terms of their processing, mechanical and technical properties, microstructure - property relationship and the scope of the present investigation has been highlighted.

## I.2 WC-Co CEMENTED CARBIDE

### I.2.1 Sintering

The classic theory [1, 5-6] of liquid phase sintering suggests that in systems like WC-Co densification takes place in three overlapping stages; an initial fluid flow stage in which rearrangement of the particle occurs, a subsequent solution reprecipitation stage that gives closer packing, and a final coalescence stage in which densification shows to the rate pertinent to the solid phase sintering. However, according to the updated theory [2,7], there is considerable solid-state sintering during heating to sintering temperature. The degree of densification and microstructural coarsening during heating depend on the solubility of the mixed components and heating rate. Therefore, the liquid phase sintering process in cemented carbides is actually composed of four stages which takes into account the chemically driven diffusion and dissolution process that occur prior to liquid formation.

Most important feature in WC-Co system is that the high density is obtained at the very first stage of sintering. Considerable shrinkage takes place even before the eutectic liquid is formed [1-2,8]. Cobalt flow in the carbide matrix occurs well below the eutectic temperature [9,10] and thus results in greatest possible reduction in surface free energy. The rapid densification of the carbide particles, which takes place at the early stage of sintering is due to enhanced and interfacial diffusion forming close packed boundaries, which first occurs in cobalt rich regions around the cobalt particles, leading to localised densification, or aggregation of carbide particles [11]. The initial size of such aggregates

depends on the size and distribution of cobalt. The distribution of the particles in the formation of aggregates gives rise to an overall shrinkage of the compact. Further, a good solubility of WC in cobalt is observed well below the eutectic temperature [12], which helps in surface smoothening of the particles leading to an enhanced rearrangement in the solid state.

Once the liquid is formed, its further formation and spreading over the particles are fast due to surface energy reasons. The liquid penetrates the particle boundaries soon after its formation and a tremendous capillary force is developed by the wetting liquid on the solid particles, which leads to the particle rearrangement for closer packing. Solubility of the solid in the liquid further aids rearrangement because of particle smoothening concurrent with capillary attraction. Simultaneously pore elimination takes place because the system tries to minimise its total surface energy which is the main driving force for densification in all the stages of liquid phase sintering. The amount of densification attained by rearrangement is dependent on the amount of liquid phase, particle size, solubility of the solid in the liquid, contact angle, dihedral angle etc [1]. Though various other events do take place concurrently with rearrangement, the kinetics of rearrangement are dominant at the initial stage of sintering in the presence of liquid phase and contributes maximum to the densification.

As densification by rearrangement slows down, the solubility and diffusivity effects become dominant and the second stage of classic liquid phase sintering starts. For WC-Co system where high density is achieved at the initial stage, it would be expected that the solution-reprecipitation

mechanisms could be more significant at lower cobalt content since here the volume of liquid is not sufficient enough to fill all the voids after rearrangement. However, the densification at this stage is associated with grain shape accommodation, which takes place by contact flattening at grain contacts, dissolution of small grains with reprecipitation on large grains, and coalescence involving grain boundary migration and cooperative solution reprecipitation [1,6]. Densification by contact flattening takes into account that the surface tension forces create an excess pressure in the liquid films between particles. This results in a high chemical potential for solubility at these points, which then dissolve away while material is deposited elsewhere, so that particles come into closer contact [6]. The other mechanism involves the dissolution of small particles and reprecipitation on the large particles. In this case, large grains grow and undergo shape accommodation at the expense of neighboring small grains which ultimately leads to the availability of liquid phase for filling the pores. The actual grain shape is determined by the relative solid-liquid and solid-solid interfacial energies, the amount of liquid and any anisotropy in surface energy of the solid [1]. Although any deviation from a spherical shape results in enlarged solid-liquid interface area, grain shape accommodation gives rise to elimination of porosity and the higher energy interfaces associated with pores [2].

In most of the technical WC-Co cemented carbides full density is achieved before the final stage of liquid phase sintering starts and further holding at this sintering temperature does not lead to any densification. However, microstructural changes of practical importance take place at this stage. Of those the notable ones are grain size and size

distribution, grain shape and binder phase distribution. The maximum density attained in the final stage is highly dependent on the characteristics of the pores and any internal gas trapped in the pores. Normally porosity gets sealed off from the surrounding atmosphere when 90 percent density is reached [1,8]. If the entrapped gas is insoluble then the pores shrink until the balance is attained between surface energy and the excess pressure in the pores. Furthermore, the skeletal microstructure formed provides rigidity to the compact and inhibits pore elimination. At this situation prolonged holding does not cause any further densification, but the grain coarsening continues by diffusion. Moreover, the residual pores containing entrapped gas may grow giving rise to compact swelling. In general, the properties are deteriorated after prolonged final stage sintering and hence is not recommended [2].

### I.2.2 Microstructure

WC-Co cemented carbide has a microstructure consisting of hard carbide phase (WC) cemented together by a ductile cobalt binder phase. WC particles exhibit typical crystal shape with straight edges. This has a highly anisotropic structure and therefore, develops such crystal shapes during liquid phase sintering which can be described as flat triangular prisms with truncated edges [11,13]. Although in most of the technical compositions this shape is not fully developed due to impingement with other crystals or coalescence, the crystal sections observed on the polished surface can easily be interpreted by this equilibrium configuration [13,14]. Two crystallographic planes play an important role in the formation of tungsten carbide interfaces, the  $\{10\bar{1}0\}$  prismatic plane and the  $\{0001\}$  basal plane [15],

which are the main facets of WC crystals. Crystal defects are also observed in WC but the density is fairly low. They appear due to the deformation of the WC crystals during milling and partly due to the residual stresses during sintering process which are accommodated by plastic deformation [13-17].

WC grain size and size distribution in the sintered microstructure are largely dependent on the milled powder. Once the milled powder is produced, the only remaining operation that can affect the grain size is sintering [18]. Two distinct modes of normal grain growth are observed in cemented carbides, namely, coalescence and solution reprecipitation [19-20]. Discontinuous grain growth is superimposed upon normal grain growth under certain conditions which include application of excessive sintering period or activated powders, and other reasons, such as recarburation of eta phase [21-22]. The composition of cemented carbides has also influence on grain growth. Grain growth during sintering is dependent on carbon content because this alters the characteristics of liquid phase markedly. A slight increase in carbon content is reported [18, 23] to result <sup>in</sup> more rapid grain growth. Cobalt content also plays an important role since grain growth in WC-Co cemented carbide is strongly dependent on the amount of solvent phase available for material transport, and secondly, it determines the mode of grain growth. These effects have been discussed in detail by Exner and Fischmeister [24].

Grain growth inhibition is exercised in practice by adding other transition metal carbides, especially those of Vth group elements [18]. Grain refinement has been reported to occur with Li, Na, K, Ni, Sn, V, Mo, Cr,  $\text{SiO}_2$ ,  $\text{Al}_2\text{O}_3$ , while Ni, P, and C have reported to increase the tendency for normal grain growth [21,25-27]. The linear intercepts in the carbide

grains normally show a distribution very close to a logarithmic Gaussian distribution [21,28,29]. The size range in the distribution depends on the size distribution in the milled powder and sintering conditions. However, the size distribution widens and loses its log-normal shape when discontinuous grain growth occurs[27].

The binder phase cobalt is present in the microstructure as a continuous thin film separating the carbide particles and it is normally associated with high dislocation density and stacking faults [16,17]. Cobalt has an fcc structure above  $417^{\circ}\text{C}$  and transforms to hcp structure, a martensitic kind of transformation while cooling [30]. In cemented carbides, the binder phase is actually a dilute cobalt alloy containing tungsten and carbon as solute atoms and can exist in either of two allotropic forms hcp or fcc. Both tungsten and carbon stabilise the fcc phase [31,32] which is the high temperature form, by reducing the transformation temperature [33,34]. Carbon is more effective than tungsten [31] and generally it is found that in most cemented carbides the Co-W-C binder is present as a mixture of fcc and hcp structure [33]. The ratio of the two is determined in bulk alloys by prior processing treatment and composition [17]. The relative ease of interchangeability of the two forms, fcc and hcp, is related to the low stacking fault energy of dilute cobalt alloys. For example, a small parallel array of stacking faults in the fcc structure represents a finite amount of hcp phase in the form of thin lamella [35].

The average size of the binder phase is represented by the quantitative parameter, mean binder free path. This is defined by the arithmetic mean of the distances from one carbide/binder interface to the other measured in the binder

phase. Very little is known about the distribution of this length, mainly because of the resolution problem during microscopic evaluation. However, there is indirect evidence based on magnetic properties measurements, which suggests that the cobalt distribution in the WC-Co cemented carbide is strongly dependent on carbon content, which seems to control its redistribution during heating to the sintering temperature [36].

Mixing during milling also has influence on the distribution of cobalt. Insufficient mixing results in large cobalt pool in the microstructure and may cause porosity [37,38]. For a given cobalt content, the mean binder free path varies inversely with the specific carbide/binder interface area [13] or varies directly with the carbide particle size.

One of the important aspects of the microstructure of cemented carbides is the degree to which a continuous skeleton of the carbide exists. Whether the carbide grains form a continuous skeleton or not is still debatable [39]. According to the generally adopted proposal by Gurland [40], the degree of continuity of the carbide phase can be quantitatively defined by the ratio of WC/WC grain boundary area to total interface of the carbide grains. Contiguity decreases with the increase in amount of binder and carbide grain size [19]. The mean binder free path ( $L_{Co}$ ), the mean linear size of the carbide grains ( $L_{WC}$ ) and contiguity ( $C$ ) are interrelated through the following theoretical equation [41,42] :

$$L_{WC} = L_{Co}(1 - C)(1 - V_{Co})/V_{Co}$$

where  $V_{Co}$  is the volume fraction of the binder phase.

Like contiguity, a great deal of controversy also exists on the nature of grain boundaries between the carbide crystals [20]. Many authors [43,44] have discussed the

different possible configurations of WC grain boundaries with or without a continuous cobalt film or with segregated cobalt phase. Several physical analysis methods have been put to work and the most recent studies by lattice fringe imaging [45] and HREM [46] confirm the contiguity of some grain boundaries which do not contain any cobalt phase. According to Vicens et al. [15] most grain boundaries between two WC crystals rotated around  $\langle 10\bar{1}0 \rangle$  axis are parallel to prismatic plane and are classified as twist grain boundaries. On the other hand, the grain boundaries rotated around  $\langle 11\bar{2}0 \rangle$  axis are described as asymmetric tilt boundaries. The second type of interfaces present in WC-Co cemented carbide is WC/Co interface. The orientation relationships between WC and cobalt at these interfaces are important. However, no clear relationship between these two phases has been reported so far in literature.

The carbon deficiency in WC-Co cemented carbide leads to the formation of a third phase ('eta' phase) other than carbide and binder phase. 'Eta' phase is a ternary compound of tungsten, cobalt and carbon. It can exist in two forms, either  $M_6C$  carbide ranging from  $Co_{3.2}W_{2.8}C$  to  $Co_2W_4C$  or  $M_{12}C$  carbide of fixed composition  $Co_6W_6C$  [47]. Both  $M_6C$  and  $M_{12}C$  are indistinguishable physically and  $M_6C$  may represent a metastable form which may undergo insitu decomposition to  $M_{12}C$  by a fairly sluggish reaction [48]. However, in commercial WC-Co cemented carbides with relatively fast cooling rate the presence of  $M_6C$  is more probable than that of  $M_{12}C$  [49].

Positive deviation from stoichiometric carbon content results in precipitation of free carbon which appears like pores on the polished surface. It may form during liquid phase sintering or precipitate during slow cooling. In the

first case, large crack like features are visible in the microstructure, while small black spots occur in second case [50].

Pores, on the other hand, can hardly be completely avoided by normal sintering. Pores due to different causes have different appearances, and a full range of shapes and sizes may exist in poorly produced grades [20]. The causes of residual porosity have been reviewed by many authors [37,38] and are fairly well understood. The common method of examining the porosity is by the means of optical microscopy, using the ISO norm 4505 [51]. Hot isostatic pressing is a common post-sintering treatment used to eliminate the residual porosity in those cases where large pores are especially harmful[37,38,52].

### I.2.3 Mechanical properties

#### (a) Hardness :

Table 1.1 summarises the general trend of hardness variation in cemented carbides with respect to their grades.

The hardness of WC-Co cemented carbide primarily depends on average carbide grain size and cobalt content and varies little with the processing route chosen to achieve the microstructure [18]. A considerable amount of research work [40,41,53,195] has been devoted to find out the microstructural relationship with hardness. Most of the reports do agree with each other except the controversy over continuous carbide skeleton formation. In this case the plastic deformation of the alloy would require considerable plasticity in the carbide, since the carbide skeleton would have to deform in compatibility with the binder phase. Lee and Gurland [41] suggest that the carbide grains form a partially connected structure with the long range continuity through direct

carbide-carbide contacts. The concept of plastic limit analysis was used to evaluate the effect of the continuous carbide phase on the hardness of WC-Co cemented carbides and the following equation was proposed [41] which includes other quantitative microstructural parameters such as mean carbide grain size ( $L_{WC}$ ) and mean binder free path ( $L_{Co}$ ) :

$$H_C = H_{WC} \cdot V_{WC} \cdot C + H_m (1 - V_{WC} \cdot C)$$

where  $V_{WC}$  and  $C$  are volume fraction of WC and contiguity respectively.

The hardness of the carbide and matrix phases are the functions of  $L_{WC}$  and  $L_{Co}$  respectively and are related by the empirical relations :

$$\begin{aligned} H_{WC} &= 1382 + 23.1(L_{WC})^{-1/2} \text{ Kg/mm}^2 \\ H_m &= 304 + 12.7(L_{Co})^{-1/2} \text{ Kg/mm}^2 . \end{aligned}$$

It is reported [54] that a good agreement exists between the measured hardness and the hardness values calculated from these equations.

Hot hardness of WC-Co cemented carbides is basically derived from the hot hardness of the individual components. The studies on WC brought forth contradictory results [55-57], where a different range of temperature has been mentioned over which the polycrystalline WC or single crystal losses their hardness rapidly. However, the study on WC-Co suggests that hardness does not vary linearly with temperature over the entire range [58]. An inflection in the temperature range 620-720<sup>o</sup>K is observed which is thought to be related with the recovery or recrystallisation of the cobalt phase and with the allotropic transformation of hcp cobalt to fcc.

## (b) Compressive strength :

In the complex form of loading to which cemented carbides are subjected during the machining of metals and rock drilling, compression invariably plays a major part. Also, increasingly more recognition is being given to the relevance of compression tests which impart information on both flow stress and plastic strain [17]. It is reported [59] that the flow stress in compression at 0.2% plastic strain of WC-Co cemented carbide has reciprocal dependence of WC grain size and can be expressed as

$$\sigma_{0.2} = K' + K'' L_{WC}^{-1/2}$$

where  $K'$  and  $K''$  are constants and  $K'$  is a function of volume fraction of cobalt. The ability of WC grains to accommodate substantial plastic deformation without occurrence of brittle fracture is well understood [60-62] and therefore, the deformation of WC-Co cemented carbide should incorporate the deformation behavior of both WC and cobalt. Roebuck and Almond [17] suggest that although cobalt volume fraction and mean free path correlate well with flow stress in compression, other parameters such as deformation of WC and contiguity are relevant and must be accounted for in order to produce usefully predictive models. Compressive strength of WC-Co increases with decreasing cobalt content and WC grain size [59,63,64] and depending on temperature and grain size, it passes through a maximum at a particular cobalt content [53].

## (c) Tensile strength :

Very little has been published on the tensile strength of cemented carbides because of experimental difficulties. A predominant feature in room-temperature

tensile-deformation of cemented carbides is the initiation of fracture from pores [65]. It is reported [66] that the ratio of transgranular/intergranular fracture of WC increases with increase in grain size, but there has been controversy over the relative contribution of the WC and cobalt phases [44,67,68]. Viswanadham et al. [67,68] suggest that the predominant fracture path is through the binder phase, whereas according to Lea and Roebuck [44] about 50% of the fracture passes through WC/WC interface.

(d) Transverse Rupture Strength :

Transverse rupture strength (TRS) is the calculated maximum tensile stress at failure of a carbide beam loaded midway between the supports. It is a combination of shear strength, compressive strength and tensile strength and is used as a general measure of toughness of the sintered cemented carbides. The TRS test, because of its simplicity, and because of the lack of better methods, is widely used to evaluate the fracture strength of cemented carbides. Table 1.1 summarises the general trend of TRS variation in various grades of cemented carbides.

Cemented carbides are intrinsically very strong but this strength is not realised in practice because of the inevitable presence of defects in the structure or at the surfaces at which stress concentration arises when a stress is applied. The fracture load is a function of both the intrinsic strength of the cemented carbide grade concerned and the nature and distribution of the defects in the structure [39]. In broken TRS test pieces, the vast majority of the fractures can be shown to have initiated at internal defects in the material, and not at the tensile surface of the test piece [65,69,70].

These defects are normally voids, inclusions, abnormally large WC grains, segregated areas or lakes of binder phase. Therefore, the scatters in the TRS values are closely related to the distribution of such defects [39]. However, modern cemented carbides manufacturing methods assure avoidance of such defects with much less sintered porosity. Recent study [52,71-73] indicates that even small amount of porosity has significant effect on TRS. It has been shown that cemented carbides follow classic Griffith-type brittle fracture with failure initiating from pre-existing flaws in the material. The strength improvement after hot isostatic pressing is thus thought to be essentially entirely due to the reduction in size of the critical flaw population [66,72,73].

The most important parameter which has maximum influence on TRS is the cobalt content. The TRS improves with increasing cobalt content and passes through a maximum depending on the carbide grain size [40,42,74,195]. Carbon content of the alloy has strong influence on TRS as well. The strength decreases in both carbon deficient and carbon excess alloys. It is reported [22] that the strength decrease along carbon deficiency is much more pronounced than the carbon excess. However, a contradictory opinion exists about the decrease of strength with carbon excess. One school of thought [75] suggests that TRS decreases slightly in presence of free carbon, whereas according to others [76,77] the decrease is comparable to that of the 'eta' phase. According to Lardner [78] TRS values remain constant when the cemented carbides contain between 0.5 vol% graphite and 0.5 vol% 'eta' phase and outside this range the value substantially decreases. In the two phase region, TRS increases with increasing carbon content [75].

(e) Fracture toughness :

Fracture toughness measurement of cemented carbide cannot be done in accordance with the recommended British [79] or American [80] standard test method as it is not possible to precrack these materials by fatigue. Precracking is further complicated by the fact that the stress intensity required to initiate a precrack in these materials is often very close to their critical stress intensity factor,  $K_{IC}$  [81]. Such a problem ultimately led the scientists to develop a number of methods [81-88] to determine fracture toughness of WC-Co cemented carbides. Unfortunately none of them could attract the industry to incorporate it into routine testing for quality control or material development because all of them suffer from some drawbacks [89]. The main problems with the methods requiring precracked single end notched beam specimen [81,83,85] are as follows :

- (i) Thermal damage at the notch root
- (ii) Notch root radius produced is too large to satisfy the plain strain condition
- (iii) A plastically deformed zone is produced on indentation which is very difficult to remove.

Other available methods [84,86-88] can give valid fracture toughness values but the disadvantages are that they are complicated and expensive, requiring closely controlled laboratory conditions and are unsuitable for routine fracture toughness testing. Apart from this, some of the methods [84,88] are not attractive due to relatively large and complex design of the test samples. However, the 'short rod' fracture toughness test may eventually simplify the measurement of basic fracture toughness parameters and can be used as important tool for the

development of new cemented carbide grades [90-92]. It is also claimed [90] that the results obtained in 'short rod' test are most consistent among all the methods.

Indentation with Vickers pyramid to assess the fracture toughness of semibrittle cemented carbides was first introduced by Palmqvist [93] in as early as 1957. The test provides a measure of the indentation crack resistance of brittle material, namely,

$$W = \frac{P}{L}$$

where  $W$  is the surface crack resistance,  $P$  is the load on Vickers diamond indenter, and  $L$  is the total length of the surface cracks emanating from the corners of the indentation. There was a great deal of controversy about the validity of Palmqvist method of toughness measurement over years. Initial doubts about the reproducibility and relevance of the measurements were resolved when the influence of residual stresses due to grinding was clarified [94-96]. It is now accepted [95, 97-100] that with proper precautions in surface preparation, the Palmqvist method gives results with good accuracy and thus the quantity,  $W$  measured constitutes a material property, called indentation fracture toughness [39]. In recent years this method has aroused attention because of its simplicity in specimen preparation and easiness in measurement, but it suffers the weakness of its complexity in analysing the state of stresses [100]. A considerable amount of efforts [101-102] has been made to establish the relation of Palmqvist crack resistance to bulk fracture toughness,  $K_{IC}$  or critical strain energy release rate,  $G_{IC}$ , which indicates that a relation should exist. However, the theoretical expressions vary according to the treatment of the stress field and the

assumption made for the crack contour and the predictions are only in qualitative agreement with experiment.

The fracture toughness,  $K_{IC}$  of WC-Co alloys is known to increase as binder phase volume fraction ( $V_{Co}$ ), mean carbide grain size ( $L_{WC}$ ), and mean binder free path ( $L_{Co}$ ) are increased, while increased carbide contiguity ( $C$ ) causes a decrease in the fracture toughness [103]. Bolton and Keely [89] suggest that there is significant correlation between  $K_{IC}$  and each of these four microstructural parameters which can be expressed through following equation :

$$K_{IC} = a_0 + a_1 V_{Co} + a_2 L_{WC} + a_3 L_{Co} + a_4 C,$$

where  $a_0$ ,  $a_1$ ,  $a_2$ ,  $a_3$  and  $a_4$  are linear coefficients of regression analysis. In a recent study [100] it is reported that the quantitative effects of  $L_{WC}$  and  $L_{Co}$  on bulk fracture toughness ( $K_{IC}$ ) and Palmqvist indentation fracture toughness ( $W$ ) are different.  $K_{IC}$  obeys a parabolic relation with  $L_{Co}$  and  $L_{WC}$ , while  $W$  obeys an exponential relation with them, which means that  $W$  and  $K_{IC}$  do not measure exactly the same properties of alloys.

Nonstoichiometric carbon content in WC-Co results in precipitation of a third phase, either free graphite or 'eta' phase and both of them are responsible for a decreased fracture toughness. It is reported [48] that for a given composition, the maximum fracture toughness appears to arise in slightly substoichiometric alloys where the quantity of binder phase is not reduced by 'eta' phase formation.

#### (f) Fracture behavior :

Fracture study of cemented carbides is important since a more complete understanding of the exact nature of

fracture path in these composite materials should significantly contribute towards efforts aimed at new materials development. The subject of fracture paths in cemented carbides is one of continuing controversy, and many differing views having been expressed [40,104]. The early work of Gurland and Bradzil [40] suggested that transgranular fracture was the predominant feature in WC-Co. This led to the assumption that fracture was controlled by the properties of carbide particles. Another school of thought [104] correlated the fracture path in WC-Co with the amount and distribution of the cobalt phase. The dominant contribution of the cobalt to the fracture resistance of WC-Co was made obvious since the values reported for the fracture energy of WC-Co cemented carbides were evidence of considerable plastic work during fracture when compared to typical cleavage energies of WC and other brittle materials [81,87,105]. However, it was soon realised that the fracture mode in WC-Co is dependent on both carbide and binder phases. Since then a lot of effort has been aimed at correlating the microstructural parameters with the fracture behavior [89, 105-109]. Auger electron spectroscopy has also been used [44,67,68] to study the fracture surface in detail in order to quantify the fracture modes. Viswanadham et al.[67,68] suggest that the predominant fracture path is through the binder phase. Recently Dusza et al.[103] have studied the fracture processes in WC-Co from the viewpoint of initiation and propagation of the fracture with relevance to the internal defects and the microstructural parameters. From Weibull statistical analysis of fractured samples they showed that the volume fraction of the binder represents the most important factor in controlling scatter in the bend strength. They have also explained the

individual micromechanism which causes the cleavage fracture in WC grains and ductile fracture in cobalt.

The mode of fracturing in WC is governed by its grain size. It is reported [106] that WC grains of size greater than 5  $\mu\text{m}$  are generally favored in fracturing transgranularly and smaller grains ( $< 2 \mu\text{m}$ ) in fracturing intergranularly. However, the critical grain size for transgranular fracture is also a function of cobalt content of the alloy [107].

Recent study of Spiegler et al. [110] suggests that binder phase normally fails by void nucleation, growth and coalescence or by necking. Void formation is favored if the bond strength between the matrix and the hard phase is strong enough to withstand interface separation, where as necking is the typical failure mechanism where debonding at the matrix hard phase interface can easily occur. Former produces dimples on the fracture surface and in the latter case, the binder phase is present as fractured ligaments between the carbide grains.

#### I.2.4 Magnetic properties

##### (a) Coercive force :

The cobalt binder phase is ferromagnetic and therefore, cemented carbides can be characterised by the parameter, coercive force ( $H_c$ ). The coercive force measures the ease with which the ferromagnetic domain walls are aligned by an induced magnetic field. Obstacle of the domain walls movement is caused by structures, particularly non-magnetic inclusions and material imperfections [111]. According to the 'Foreign body' theory domain walls are attracted to these

imperfections because the wall energy and the magnetostatic energy are thereby reduced [112]. WC being non-magnetic, in cemented carbide, the total surface area of the WC grains is considered to be main imperfection [111]. Hence, interesting conclusions can be drawn as to the degree of sintering, cobalt distribution, carbon balance and grain size of the carbide phase which have influence on coercive force.

Literatures [24,60,111,113] are available, describing the variation of coercive force with composition, grain size etc. All of them report that for a fixed WC grain size, the coercive force decreases as the cobalt volume fraction increases, where as for a fixed volume fraction of cobalt, it increases as the grain size decreases. Exner and Fischmeister [24] reported that a linear relationship exists between coercive force and specific cobalt surface in cemented carbides consisting of WC and cobalt.

Dissolved tungsten and carbon in the binder cobalt also have effects on coercive force [75,114,115] as they produce internal stress due to solution and precipitation hardening. Coercive force increases with the increase in tungsten content in the binder cobalt. As far as the carbon balance is concerned, it is reported [49] that coercive force increases when the composition is out of the two phase region i.e. in both carbon deficient and carbon excess alloys. The increase being more pronounced in carbon deficient alloy than the carbon excess alloy, which is related to the hardening effect caused in the binder cobalt by the finely dispersed 'eta' phase.

(b) Magnetic saturation :

The measurement of magnetic saturation is used as an indirect method of measuring the carbon content of sintered cemented carbides. Magnetic saturation measurements enable to estimate carbon content to an accuracy of 0.01% if the test pieces are prepared with closely comparable conditions. It's great advantages are speed, simplicity and sensitivity.

The magnetic saturation drops sharply in three phase region,  $\eta + WC + Co$  due to reduction in the amount of the magnetic phase when cobalt is incorporated in the non-magnetic ' $\eta$ ' phase [49]. Various authors [22,116] reported that the magnetic saturation of the sintered cemented carbide increases as the amount of tungsten as solid solution in cobalt phase decreases and vice versa. Magnetic saturation in the two phase region is, therefore, an indication of the amount of dissolved tungsten in binder phase. However, according to Freytag and Exner [49], magnetic saturation is not only sensitive to the carbon deficient alloy but also to the carbon excess alloy cooled quickly from sintering temperature. Thus, magnetic saturation is not a safe indication for the amount of tungsten dissolved in the binder phase.

### I.2.5 Oxidation resistance

While cutting metals and alloys, the tool tip is invariably subjected to a temperature of 600-1000°C depending on the cutting speed. As a consequence, the oxidation of tool materials becomes an important factor in determining the tool life. The oxidation study of these alloys is, therefore, important for meaningful alloy design and development.

Though oxidation behavior of pure refractory compounds like WC, TiC, Mo<sub>2</sub>C [117], TiC, TiN [118] etc. has

been studied extensively, not much work is reported on cemented carbides. Kang and Fromm [117] reported that the oxidation process in WC-Co can be described quantitatively by the data of carbon diffusion and of vaporisation rates of volatile oxides. According to them, the results of theory and experiments are in good agreement. The weight gain curves of WC-Co alloys show additional effects in comparison to pure WC which are due to evaporation and/or oxidation of the binder cobalt, especially at higher temperatures and  $O_2$  pressures [117].

WC-Co cemented carbides follow linear to parabolic type of oxidation behavior depending on temperature and cobalt content [118]. The oxides form in such systems have Pilling-Bedworth ratios greater than one [119], and thus give rise to porous oxide layer on the substrate.

#### I.2.6 Thermal shock resistance

The retention of high strength and hardness to a large degree at elevated temperature is a factor which favors WC-Co as a material over others for cutting and mining applications. High temperatures are often combined with temperature differences and thermal stresses arise which may lead to serious damage in the tools. In intermittent cutting, thermal cracking has long been recognised as a mode of failure [120]. Studies of the mechanics of rock drilling also point to thermal fatigue as a failure mechanism, especially in the rotary drilling of soft, non-abrasive rock [121]. The complexity of rock drilling and intermittent cutting does not allow sufficient separation of thermal and mechanical tool response so that one grade of carbide might be recognised as more resistant to thermal effects than another [121]. However, applying the theory of thermo-elasticity and fracture

mechanics, it is, in principle, possible to predict the thermal behavior of such cemented carbides [122,123].

Though various methods of thermal shock resistance measurement techniques have been reported [121-125], water quenching experiments are probably most frequently used to characterise the thermal shock behavior of ceramics [123]. At the outset of quenching, only a small surface layer of the specimen cools down, whereas the inner part remains at the initial higher temperature. Therefore, the contraction of the surface layer due to the thermal expansion is hindered by the inner still hotter part and tangential tensile surface stresses occur which are balanced by compressive stresses inside the body [122]. This results in micro-crack formation and growth. The number of micro-cracks that will grow under certain applied quenching temperature difference,  $\Delta T$  depends on the thickness of the sample and fracture toughness of the material [122-124], which in turn is a function of intrinsic properties and microstructure.

#### I.2.7 Wear resistance

Cemented carbides are generally considered to be highly resistant to abrasive wear and this property is vital for the selection of these materials for a large number of applications. In practice the destruction of a cutting edge results from the interaction of many effects. It is difficult to find out which are purely wear mechanisms and which are to be considered as micro-scale mechanical failures [121]. However, different mechanisms account for the wear of cemented carbides, which vary with the service conditions, and with compositions and microstructure of the alloy. In machining operation, three

types of wear mechanisms are generally noticed that are major factors in tool wear, viz. abrasive wear, attrition wear and diffusion wear.

For cemented carbides abrasive wear mechanism is most readily understood and has been studied in detail [120, 126-131]. This is the type of wear that occurs when a hard particle is rubbed across a surface. Generally, the abrasive particle should be harder, but this is not essential. Abrasive wear is very closely related to hardness of the tool material and in consequence, to the composition and structural features that control hardness [127]. The rate of wear by abrasion depends on several factors but the only microstructural parameter which has a clear cut effect on abrasive wear resistance is the mean binder free path [120,126]. With increasing mean free path, the number of hard abrasive particles of a size capable of directly contacting the binder region increases and also the effective hardness of the binder decreases. Both these effects increase abrasive wear. The precise mechanism of abrasive wear depends on the hardness of the abrasive particles relative to the bulk cemented carbide hardness [126, 128, 129]. While describing a model of abrasive wear, Hack and Peter [130] have proposed that the use of hardness as a direct measure of wear resistance, is invalid. According to them, wear resistance is functionally related to the plain strain bulk fracture toughness. Abrasive wear increases as the fracture toughness of the cemented carbide increases. This hypothesis has been supported by Peters and Brabyn [131], who found wear characteristics of WC-7Co-3Ni and WC-10Co cemented carbides to be similar though they were having significant differences in hardness.

The term 'attrition wear' is used to describe a wear process in which particles of microscopic size are detached from the tool surface and carried away in the stream of work material [132]. Attrition wear is closely related to the more basic adhesive wear mechanisms [127]. It is due to the cold welding effect which can occur readily in metal cutting, especially at low cutting speeds. The motion of work piece and chip continually breaks the junctions so formed and discrete particles of tool material are carried away. This type of wear seems to occur mainly by the plucking away of complete grains of WC and the wear rate is associated with grain size rather than hardness [127].

The term 'diffusion wear' is used to describe a wear mechanism in which the tool shape is changed by diffusion of atoms into the work material, equivalent to a dissolution of the tool surface by the chip material flowing over it [132]. Technically this is known as cratering. Clearly, this depends upon the solubility of tool material in the work material and the interface temperature obtained during cutting. The cratering phenomenon results from diffusion of carbon from cemented tungsten carbide to the steel chip sliding over the rake face of the tool [132-135]. This type of wear is exceptionally severe with straight WC-Co cemented carbides when cutting steel, so much so that such alloys have no practical application for cutting steel in continuous chip producing operation at economic cutting speed [127] and are mainly used for cutting cast irons, non-ferrous metals and in all rock drilling operations.

### I.3 WC-Co CEMENTED CARBIDE WITH MODIFIED BINDER PHASE

From the early history of cemented carbides, cobalt has been the traditional and predominant binder metal for WC, although nickel and iron are cited as alternatives. The use of cobalt in preference to iron and nickel is believed to be due to higher solubility of WC in cobalt [13]. Secondly, cobalt has superior comminution characteristics and hence a better distribution of cobalt is achieved on the WC particles during milling, which subsequently during sintering leads to a better microstructural development [136]. However, economic and strategic considerations have motivated several attempts to find a suitable alternative to cobalt binder. If cobalt is excluded, then the choice is limited to iron, nickel and their alloys. Several reports [137-140] are available, where it has been mentioned that an equivalent or even superior properties to that of WC-Co cemented carbide can be achieved through either Ni or a combination of Ni+Fe and Ni+Fe+Co. Moreover, new applications in wear resistant cemented carbide parts have led to the use of tools in corrosive environments, and cemented carbides stable under such exposure are demanded.

#### I.3.1 Tungsten carbide bonded with nickel

The data available for Fe-W-C, Co-W-C and Ni-W-C [137] indicate that a higher sintering temperature is required in WC-Ni cemented carbide than that of WC-Co cemented carbide. According to Tracy and Hall [138] the sintering temperature of nickel bonded cemented carbide is  $50-75^{\circ}\text{C}$  greater than that of cobalt bonded one. They also claim that when nickel is combined with stoichiometric WC, it gives rise to detrimental free carbon in the system which is the main reason of inferior

TRS. Suzuki et al. [139,140] have also reported that the TRS in nickel bonded cemented carbide is dependent on carbon content. In their study on WC-16Ni cemented carbide, the maximum TRS was obtained when the carbon content of WC was 6.05 weight percent. Nickel is said to be more prone than cobalt to the formation of 'eta' phase when the Ni-W-C system is deficient in carbon [140]. As far as the solubility of WC in nickel is concerned, there is a great deal of controversy. One group [12] says that at higher temperature WC has higher solubility in cobalt than in nickel, while others [136,138] disagree, such that the solubility at high temperature is about the same in presence of excess carbon within the stipulated range for cemented carbide composition. Though nickel bonded WC does not have any significant difference in microstructure from cobalt bonded one, the presence of excess carbon in the former increases the fluidity of the melt during sintering and hence a greater degree of grain coarsening results [141]. However, WC-Co and WC-Ni cemented carbides are not widely different and the latter can be manufactured successfully with no major technical problems [142].

### I.3.2 Tungsten carbide bonded with nickel based alloys

Since complete replacement of cobalt by nickel reduces the mechanical properties rather extensively [143], a partial substitution of cobalt by nickel has been tried. It has been reported by Precht et al. [144], that WC bonded with cobalt-nickel has superior abrasion resistance to that of only cobalt bonded one. According to them, the effect is due to stabilisation of the relatively ductile fcc cobalt phase by Ni, preventing it from transforming to the less ductile hcp phase during deformation.

The corrosion resistance as well as the strength and toughness of WC-Co-Ni grades are possible to get raised by adding suitable alloying constituents. Recently a number of such grades have been reported [145,146] having binder phases Ni-Co-Cr and Ni-Co-Cr-Mo. An improved strength and toughness is achieved by the solution strengthening of the binder phase by the alloying elements such as Cr and Mo, and the corrosion resistance is imparted by both Cr and Ni. Tungsten carbides bonded with either Co-Ni-Cr or Co-Ni-Cr-Mo are claimed to have shown better performance than WC-Co cemented carbides of equivalent compositions, where corrosion plays an important role in components' failure [145,146]. A similar nickel free corrosion resistant grade has been reported [146] with Co-Cr-Mo binder. It is reported that compared to WC-Co, WC-Co-Cr-Mo cemented carbides have improved corrosion and erosion resistance, whereas the mechanical properties are maintained at a level which is obtained by standard WC-Co alloys depending on the amount of binder phase.

The possibility of replacing the binder phase in WC-Co cemented carbides by nickel alloys based on super alloy composition has also been explored [144,147,148]. This group of cemented carbides find application where creep resistance is the additional requirement apart from the good strength and toughness. Binder phase strengthening through  $\gamma'$ -precipitation combined with solid solution hardening by Cr and Mo in WC-Co-Ni-Cr-Mo-Al alloy have been reported [147]. It is also claimed that such compositions offer the possibilities of enhanced resistance to creep and corrosion, and properties that could be varied by heat treatment to meet specific properties.

### I.3.3 Tungsten carbide bonded with iron

Efforts have been made to substitute cobalt in WC-Co cemented carbide by iron as well. If similar procedure as that of cobalt bonded WC are employed in the preparation of iron bonded WC so that WC of theoretical carbon content is bonded with iron, the formation of 'eta' phase is noticed [149]. Through addition of the required amounts of carbon to the starting powders, the tendency of iron to form the deleterious 'eta' carbide can be avoided. It is reported by Moskowitz et al. [149] that excess carbon addition between 0-1.4% cannot suppress the 'eta' carbide formation, while carbon addition between 1.4 to 3.0% results in a microstructure free of both graphite and 'eta' phase. Therefore, for an optimum combination of hardness and strength, a judicious choice of excess carbon addition has to be done. However, WC-Fe cemented carbide did not become popular, probably because of inferior strength and processing difficulties.

### I.3.4 Tungsten carbide bonded with Fe, Ni and/Co alloys

A number of literature [149-151] are available for this group of cemented carbides. With Fe-Ni binder, the tendency of Ni to form free carbon to some extent is compensated for the tendency of iron to form the mixed 'eta' carbide [150]. As a result the carbon requirement to avoid 'eta' phase formation is lowered. For certain binder phase compositions Moskowitz et al. [149] reported TRS values higher with Fe+Ni than those for Co. However, the exact carbon content and the phase constitution were not reported.

Prakash et al. [150] developed a family of WC-Fe-Co-Ni cemented carbides comparable to those of WC-Co. In some cases, through appropriate heat treatment, specific

properties superior to those of WC-Co were achieved. Recently Viswanadham and Lindquist [151] applied the concept of transformation toughening in such cemented carbides by binder composition control and thermomechanical treatment. According to them, the metastable phase, austenite can be stabilised to various degree by controlling binder phase composition and proper thermo-mechanical treatment, which undergoes insitu martensitic transformation in the stress field of propagating crack and thus results in transformation toughening.

#### I.4 WC-Co CEMENTED CARBIDE WITH MODIFIED HARD PHASE

Straight WC-Co cemented carbides are not universally applicable and find applications to machining of cast iron, nonferrous metals and in all rock drilling operations. Poor crater resistance of such cemented carbides is the major limitation while machining steel. Similarly, straight WC-Co cemented carbide cannot be used in high temperature wear resistant parts, where oxidation resistance and hot hardness are very important. To extend the use of WC-Co cemented carbides in the above mentioned applications, the modification of the hard phase is a must. In normal practice these are achieved through the addition of IVth and Vth group transition metal carbides such as TiC, TaC, NbC etc. to WC-Co cemented carbide. Such additions also promote the production of cemented carbide with fine tungsten carbide grain size since they act as grain growth inhibitor during sintering.

A major part of the cutting tools and wear resistant materials employed today is cemented carbides, out of which atleast 70% constitutes WC-Co based cemented carbide. This extensive usage makes tungsten among the strategically important metals. Efforts have been made for partial

substitution of WC in WC-Co based cemented carbide by other readily available refractory compounds, without sacrificing strength and toughness. So far not much work has been reported in this regard.

#### I.4.1 Effect of refractory carbide additions on WC-Co cemented carbides

##### (a) Microstructure :

Small addition of other transition metal carbides as grain growth inhibitors has been a long practice in cemented carbide industries. Such additions become especially important when producing extremely fine grained cemented carbide for high abrasive wear resistant applications [18,71]. It is reported [18,71,152-156] that carbide additives such as TaC, NbC, VC, TiC,  $\text{Cr}_3\text{C}_2$  and  $\text{Mo}_2\text{C}$  restrict the grain growth in WC-Co alloys. The effectiveness of grain growth inhibition for a given amount of addition is related to the thermodynamic stability of the carbide, whereas the amount of inhibitor required is proportional to the amount of binder phase [152]. The fact that the addition of other transition metal carbides restricts the grain growth in WC-Co alloys is known since long but the mechanism of grain growth inhibition is not fully understood. According to Kim and Accary [155], such grain growth inhibitors partly get dissolved in the binder phase and decrease the anisotropy of the WC/binder interfacial energy restricting the grain growth during sintering.

Apart from the grain growth inhibition, the objectives of such additives is to impart some special properties e.g., crater resistance, hot hardness etc. to WC-Co cemented carbide, where a greater amount of additions are

required [196]. Since these carbide additives do not have adequate wettability with cobalt, they have the tendency to form large grain and chain like structure in the sintered microstructure which have deleterious effects on mechanical properties especially strength and toughness [164]. In practice they are, therefore, added in the form of solid solutions such as (W,Ti)C, (W,Ta)C, (W,Ti,Ta)C etc., since these solid solutions have somewhat better wettability with cobalt as compared to the individual monocarbides.

(b) Hardness :

Table 1.1 summarises the general trend of mechanical properties variations in cemented carbides containing other cubic refractory carbides.

The addition of TiC, TaC increases the resistance of WC-Co cemented carbides to plastic deformation and the strength loss which increases the ability of these multcarbide composites to resist the cutting edge deformation [134,157, 158]. The effect of NbC addition on hardness is similar to that of TaC [159]. Since these cubic carbides do not exist as individual monocarbides, their contribution to the increased hot hardness may be due to the appreciably higher hardness of their complex solid solutions, i.e., (W, Ti)C, (W, Ta)C, (W, Ti, Ta)C as compared to their individual monocarbides [55]. Cobalt does not wet these solid solutions properly as it does in case of WC, and therefore, such refractory carbide additions tend to form a chain like structure. This morphology is believed to retard the WC grain boundary sliding during the high temperature deformation [160].  $\text{Cr}_3\text{C}_2$  which is added normally as grain growth inhibitor and for oxidation resistance

also increases the hot hardness of WC-Co cemented carbides[156].

(c) Strength and toughness :

Addition of TiC is known to increase the crater resistance of WC-Co cemented carbide, but it has an adverse effect on room temperature TRS. On the other hand, TaC addition to WC-TiC-Co increases the room temperature strength [157]. The effect of NbC addition to the WC-Co cemented carbide is more or less similar as that of TaC as far as the strength is concerned [159].  $\text{Cr}_3\text{C}_2$ , used as grain growth inhibitor, increases TRS [156], because it prevents the transformation of cobalt from fcc to hcp, thus improving the ductility of the binder phase.

The toughness variation of WC-Co cemented carbides containing other carbides as additives is similar to that of TRS variation [156,157,159,161].

(d) Wear and oxidation resistance :

The high hardness and chemical stability of TiC impart excellent resistance to crater wear [134]. As a matter of fact, when TiC is added to WC-Co base composition, it forms (W,Ti)C solid solution which has better chemical stability at higher temperature. The increase in crater resistance after such addition is, therefore, basically due to the reduction of carbon diffusion from carbide tool to the steel chip. It is significant to note that though TiC is much harder than WC, the addition of TiC to WC-Co reduces the abrasion resistance. This suggests that the over all picture of composite must be taken into account rather than a singular hard phase. In contrast, addition of the softest of the carbides under discussion, TaC,

increases abrasion-resistance. The effect of TaC is to inhibit grain growth, and it is the finer grain of such composition that provides within limit the improved abrasion resistance [133]. Secondly, TaC addition decreases co-efficient of friction between tool and work piece. Sometime NbC is also used in conjunction with TaC to have similar type of effect as to that of TaC addition [134]. Although TiC does in fact reduce abrasion resistance, it is added in steel cutting grades for improved resistance to cratering.

Additions of TiC, TaC and NbC cause important changes in the oxidation characteristics of WC-Co cemented carbide. Addition of TiC causes the formation of TiO surface layer that effectively isolates the tool from the part to be cut and, in a sense, protects the tool from rapid wear [162]. The compound WC forms  $WO_3$ , which is volatile and therefore, offers no protection. On the other hand, additions of TaC and NbC raise the melting temperature of the carbide solid solution and increase the oxidation resistance over that of WC-TiC-Co [162].  $Cr_3C_2$  addition also does improve the oxidation resistance of WC-Co cemented carbide [156], where as  $Mo_2C$  addition has deleterious effect [117].

#### I.4.2 Effect of refractory nitride additions

As far as the role of refractory nitride addition on WC-Co cemented carbide is concerned, only limited study has been made. It is reported [164] that TiN addition to WC-Co cemented carbide results in slightly decreased hardness, but better TRS and oxidation resistance as compared to equivalent TiC addition.

## I.5 WC-Co CEMENTED CARBIDE WITH MODIFIED HARD AND BINDER PHASES

Not much work have been reported on WC based cemented carbides with the modification in both hard and binder phases. Schwarzkopf and Kieffer [163] developed a series of WC-Mo<sub>2</sub>C-TiC-Ni-Co cemented carbides. They reported that addition of Mo<sub>2</sub>C to WC-TiC-Co alloys increased the hardness at the expense of the strength. Moreover, higher Mo<sub>2</sub>C additions led to tougher alloys if nickel, rather than cobalt, was used as the binder metal. In general, these cemented carbides have been reported to have inferior strength and toughness. Schwarzkopf and Kieffer, however, did not highlight on the processing and microstructural details of such cemented carbides.

## I.6 SCOPE OF THE PRESENT INVESTIGATION

The continued increase in the consumption of WC based cemented carbides and the threat from the depleting resources of tungsten and cobalt led to a great deal of research to develop alternate cemented carbides compatible with WC-Co based ones. Although WC free cemented carbides have been developed based on TiC-Ni compositions, these materials have not been used extensively in metal cutting applications as they do not meet the toughness requirement for most of the metal cutting and rock drilling operations. Therefore, at this juncture the most developed approaches seem to be dilution of WC by other refractory compounds and partial replacement of cobalt by nickel, iron or their alloys, so that at least some of these strategically important materials can be saved. As already reviewed earlier, the partial or full substitution of traditional cobalt binder by nickel, iron or their alloys has

been fairly well successful, but not much attempt has been made for the partial replacement of WC by other refractory compounds. The exception being the steel cutting grades of WC based cemented carbides, where TiC addition is a must, and which has been an established practice in cemented carbide industries.

The objective of the present investigation is to study the possibilities of partial replacement of WC in WC-Co cemented carbide by other refractory compounds without much sacrifice in strength and toughness. The refractory compounds chosen are TiC, TiN and Ti(C,N), which are cheap, abundant, and relatively light.

A change in the chemistry of alloy brings forth a change in the interfacial energy between solid and melt which would affect the wettability and thus the first stage of liquid phase sintering i.e. rearrangement. This in its own turn would affect the solubility behavior of different constituents of hard phase into the binder and hence the microstructural evolution. A systematic study was, therefore, proposed to be carried out to estimate the influence of the refractory compound additives on the microstructure and properties of the base WC-Co cemented carbide and also to see how far a concurrent change in the binder chemistry becomes essential in order to maintain the end properties. Cobalt, cobalt-nickel and cobalt-nickel-molybdenum binder compositions were tried in this regard and a rationale was sought after.

As the reports of various workers do not pertain necessarily with the same grade of starting tungsten carbide powder, it was still more imperative to centre the whole study on a particular starting powder. This would facilitate to appreciate the results better.

The present study starting from alloy processing through microstructural and properties evaluation including some important technical properties viz. oxidation resistance, thermal shock resistance and cutting performance were carried out for a comparative study of the role of different refractory compounds/binders on WC-10Co cemented carbide.

Table 1.1 : Different ISO grades of cemented carbides and their properties [170]

Designations	Compositions						Properties		
ISO application code	WC	TiC	Ta(Nb)C	Co	Ni	Mo	Density g/cm <sup>3</sup>	Hardness HV	TRS MPa
P 01	-	80	-	-	10	10	5.8	1900	850
P 01	50	35	7	6	-	-	8.5	1900	1100
P 05	78	16	-	6	-	-	11.4	1820	1300
P 10	69	15	8	8	-	-	11.5	1740	1400
P 15	78	12	3	7	-	-	11.7	1660	1500
P 20	79	8	5	8	-	-	12.1	1580	1600
P 25	82	6	4	8	-	-	12.9	1530	1700
P 30	84	5	2	9	-	-	13.3	1490	1850
P 40	85	5	-	10	-	-	13.4	1420	1950
P 50	78	3	3	16	-	-	13.1	1250	2300
M 10	85	5	4	6	-	-	13.4	1590	1800
M 20	82	5	5	8	-	-	13.3	1540	1900
M 30	86	4	-	10	-	-	13.6	1440	2000
M 40	84	4	2	10	-	-	14.0	1380	2100
K 01	97	-	-	3	-	-	15.2	1850	1450
K 05	95	-	1	4	-	-	15.0	1780	1550
K 10	92	-	2	6	-	-	14.9	1730	1700
K 20	94	-	-	6	-	-	14.8	1650	1950
K 30	91	-	-	9	-	-	14.4	1400	2250
K 40	89	-	-	11	-	-	14.1	1320	2500

Very considerable variation between the products of different manufacturers is possible.

## CHAPTER - II

### EXPERIMENTAL PROCEDURE

The detailed experimental procedures carried out in the present investigation are described in this chapter.

#### II.1 RAW MATERIALS AND THEIR CHARACTERISTIC

The characteristics of the raw materials used in the present study are indicated below :

##### Tungsten carbide (WC) powder

Source : WIDIA (INDIA) LTD.

Average particle

size : 3.2  $\mu\text{m}$  (FSSS)

Total carbon : 6.12%

Free carbon : 0.10%

##### Titanium carbide (TiC) powder

Source : Treibacher Chemische Werke,  
Austria

Average particle

size : 3.45  $\mu\text{m}$  (FSSS)

Chemical analysis :

Fe	0.05%
O	0.06%
C	19.40% (Total)
	0.08% (Free)
Ti	Balance

Molybdenum carbide ( $\text{Mo}_2\text{C}$ ) powder

Source : USSR make

Average particle

size : 3-4  $\mu\text{m}$  (FSSS)

Titanium nitride ( $\text{TiN}$ ) powder

Source : H.C. Starck, Germany

Average particle

size : 3-4  $\mu\text{m}$  (FSSS)

Titanium carbonitrides,  $\text{Ti}(\text{C}, \text{N})$  powder

Source : Treibacher, Austria

Average particle

size : 2.10  $\mu\text{m}$  (FSSS)

Chemical analysis :

C (total)	9.87%
C (free)	0.04%
Fe	0.12%
O	0.07 %
N	11.0%

Cobalt powder

Source : H.C. Starck, Germany

Average particle

size : 2.3  $\mu\text{m}$  (FSSS)

Chemical analysis :

Ni	0.20%
Fe	0.04%
O	3500 ppm
Co	Balance

Nickel powder

Source : INCO (U.K.)

Type 123

Average particle

size : 3.7  $\mu\text{m}$  (FSSS)

Chemical analysis :

C 0.06%

Fe 0.005%

O 0.05%

Co 0.0003%

N<sub>2</sub> 0.003%

S 0.003%

Other elements 0.001%

Ni Balance

Molybdenum powder

Source : Metallwerk Plansee, Austria

Average particle

size : 4-6  $\mu\text{m}$  (FSSS)Paraffin wax powder

Source : La Ceresene, France

Melting point : 60-62°C

Density at 25°C : 0.88 g/cm<sup>3</sup>

Maximum oil percentage : 0.07

Acidity index : Nil

## II.2 PREMIX PREPARATION

The premix of carbides and binder metals were prepared by conventional ball milling technique. Wet milling of the powders in acetone was performed in a Fritsch

'Pullverisette-5' centrifugal type ball mill using  $1.8 \times 10^{-2}$  m diameter WC balls. The ratio of feed to ball by mass was kept at 1:3. The additive hard phases i.e. TiC,  $\text{MO}_2\text{C}$ , TiN and Ti(C,N) were initially milled with binder powders for 8 hrs followed by WC addition with an additional 28 hrs wet milling. 4 hrs before the completion of milling 2 mass% micronised wax powder was added in the charge. After the milling operation, the wet powder slurry was dried in vacuum oven.

The starting composition of cemented carbide, i.e. WC-10Co corresponded to approximately 16.5 vol% binder phase. All the subsequent compositions developed later were tailored so that the volume fractions of hard phases and binders remained constant as that of the initial WC-10Co cemented carbide. The respective mass percent additives in various cemented carbide compositions are given in Table 2.1

### II.3 MILLED POWDER CHARACTERISATION

The as received milled powders were characterised in terms of average particle size and size distribution using quantitative metallographic method.

Cylindrical green compacts of  $1.27 \times 10^{-2}$  m diameter and approximately  $0.8 \times 10^{-2}$  m height were prepared from the ball milled powder premix. They were subsequently infiltrated with silver at  $900^\circ\text{C}$  in  $\text{H}_2$  atmosphere to provide sufficient strength and reduce the porosity in the compacts for successful metallographic sample preparation. The silver impregnated compacts were then polished metallographically and observed on a JSM 840A scanning electron microscope to determine the average particle size and size distribution. The metallographic sample preparation technique and the

quantitative metallographic method will be described in later Section II.8 in detail.

#### II.4 ROOM TEMPERATURE COMPACTION

Rectangular green compacts of  $24.7 \times 7.7 \times 6.2 \text{ mm}^3$  (approximately) were prepared from the ball milled powder premix. A manually operated single acting hydraulic press (Apex construction Ltd., U.K.) of 200 tonnes capacity was used for this purpose. The compaction was done at a pressure range of 350–450 MPa so as to obtain a constant green density (approximately 55% of theoretical density) for all the compositions. The die made of high chromium high carbon steel and lined with WC, was cleaned with acetone and lubricated with Zn-stearate prior to powder filling for each compaction.

#### II.5 DEWAXING AND SINTERING

Dewaxing of the green compacts was carried out in a silicon carbide resistance heated tubular furnace at  $400^\circ\text{C}$  for 2 hrs under a dry hydrogen (dew point  $-35^\circ\text{C}$ ) atmosphere. The heating rate was maintained at a relatively low rate of about  $2^\circ\text{C}/\text{min}$  to make sure that no damage was done to the green compacts during dewaxing. The hydrogen used as atmosphere was dried and cleaned by passing through a purification train before introducing it into the furnace. The hydrogen purification train consisted of a hydrogen purifier, DEOXO, Model 0.15/3.5 of Engelhard Industries, Gloucestershire (U.K.) and tubes containing calcium chloride for drying and glass wool/cotton for removing any suspended particles. The dew point of the hydrogen after such drying was  $-35^\circ\text{C}$  which was measured using a SHAW MOISTURE meter (U.K. make).

The dewaxed compacts were subsequently sintered in the same tubular furnace in a temperature range of  $1450^{\circ} - 1500^{\circ} \pm 5^{\circ}\text{C}$  (at an interval of  $25^{\circ}\text{C}$ ) for 1 hr with the exception of alloy A (WC-10 Co) which was sintered at  $1425^{\circ}\text{C}$ . Heating rate was around  $8^{\circ}\text{C}/\text{min}$ . The sintering atmosphere was either  $\text{H}_2$  or  $\text{H}_2\text{-N}_2$  mixture (50:50) depending on the cemented carbide composition. Alloys A to D i.e. TiC containing cemented carbides were sintered in  $\text{H}_2$ , where as alloys E to J i.e. TiN and Ti(C,N) containing cemented carbides were sintered in  $\text{H}_2$  and  $\text{H}_2\text{-N}_2$  atmosphere respectively. The nitrogen used was dried by passing it through a Matheson 6406 gas purifier. The purified and dried hydrogen and nitrogen were passed through a Matheson made gas flowmeter cum mixer into the sintering furnace. The optimum sintering temperature was found out by evaluating sintered properties and microstructural studies. Vacuum sintering of alloy A (WC - 10Co) and all TiC containing cemented carbides i.e. Alloys B to D were also carried out at  $10^{-3}$  torr pressure in an industrial production furnace.

## II.6 HOT ISOSTATIC PRESSING (HIP'ing)

As it would be evident from the next chapter it was not possible to achieve a fully dense product out of TiN/Ti(C,N) containing cemented carbides, irrespective of any variation in the sintering atmosphere. It was, therefore, decided to HIP these cemented carbides after liquid phase sintering. HIP'ing was carried out in Ar of 1000 bars pressure for 45 minutes at 1400 and  $1450^{\circ}\text{C}$  respectively in a production unit of a cemented carbides manufacturing plant.

## II.7 SINTERED DENSITY AND POROSITY EVALUATION

The sintered density was measured according to the following formula as suggested by Arthur [165] by using displacement method :

$$\text{Sintered density (gm/cc)} = \frac{a}{b-c}$$

where, a = weight of the compact in air (gm)

b = weight of the xylene impregnated compact in air(gm)

c = weight of the xylene impregnated compact in water (gm).

Theoretical density of each composition was calculated from the simple rule of mixture, taking the theoretical density of the various elements/compounds from the literature [166].

## II.8 MICROSTRUCTURAL STUDIES

### II.8.1 Pore morphology and its distribution

The selected sintered compacts were wet polished primarily on a cast iron wheel using 7  $\mu\text{m}$  diamond paste, followed by fine polishing by the diamond paste of decreasing grit size viz. 6  $\mu\text{m}$ , 2.5  $\mu\text{m}$  and 1  $\mu\text{m}$  respectively. The unetched polished samples were observed under optical microscope at a magnification of 200X in order to compare their pore sizes and distribution.

### II.8.2 Scanning Electron Microscopy (SEM) and Quantitative Metallography

The polished samples were electroetched by using 5% HCl solution at a potential difference of 3V for 10-20 sec. and were observed under a JSM 840A scanning electron microscope (SEM) in secondary electron mode at an operating voltage of 20KV. For each sample about 10 photomicrographs were taken arbitrarily from different places at 10,000

magnification which were subsequently used for quantitative metallographic study.

The different microstructural parameters viz. mean linear intercept grain size, contiguity and the binder mean linear intercept distance were measured in accordance with the method suggested by Gurland [167] using the following formulae:

(i) The carbide mean linear intercept grain size

$$L_{\alpha} = \frac{2(V_v)_{\alpha}}{2(N_L)_{\alpha\alpha} + (N_L)_{\alpha\beta}}$$

where,  $(V_v)_{\alpha}$  is the volume fraction of the carbide phase and  $(N_L)_{\alpha\beta}$  and  $(N_L)_{\alpha\alpha}$  are the average number of intercepts per unit length of test lines with the traces of the carbide/binder interface and carbide/carbide grain boundaries respectively.

(ii) The contiguity of the carbide phase

$$C_{\alpha} = \frac{2(N_L)_{\alpha\alpha}}{2(N_L)_{\alpha\alpha} + (N_L)_{\alpha\beta}}$$

(iii) The binder mean linear intercept distance, i.e., the mean free path

$$L_{\beta} = \frac{2(V_v)_{\beta}}{(N_L)_{\alpha\beta}}$$

where,  $(V_v)_{\beta}$  is the volume fraction of the binder phase. Fracture surfaces obtained after 3-point bend test were also examined in SEM in secondary electron mode at an operating voltage of 20 KV.

### II.8.3 Transmission Electron Microscopy (TEM)

Slices of thickness 0.5 - 0.6 mm were prepared from the bulk sintered specimens by using a thin diamond wafering blade. 3 mm discs were removed from these slices by spark erosion and were mechanically polished to a thickness of 60 - 70  $\mu\text{m}$  using 1  $\mu\text{m}$  diamond paste. These discs were finally thinned to perforation by ion etching using a German make Gattan 600 DIF duo ion milling unit. Thin foils thus obtained were examined in a JEM 200 CX transmission electron microscope (TEM) at an operating voltage of 160 KV.

## II.9 MECHANICAL PROPERTIES EVALUATION

### II.9.1 Transverse Rupture Strength (TRS)

TRS of as sintered and HIP'ped specimens was determined under three point loading as per ASTM specifications (B406-76). The specimens were placed in a fixture having two WC rolls of 3 mm diameter and 15 mm length which were kept 14.9 mm apart. The testing was performed in a MTS machine with a cross head speed of 0.2 mm/min. The maximum rupture load at the failure point of the test piece was used in the following formula for calculating the TRS :

$$\text{TRS (MN/m}^2\text{)} = \frac{3PL}{2WT^2}$$

where, P = breaking load (MN)

L = length (m)

W = width (m)

T = thickness (m).

For each set of specimens eight tests were performed, and the average value was reported.

### II.9.2 Hardness

Hardness of the sintered compacts was measured on a Vickers hardness testing machine model HPO 250 of 'Fritz Heckert Leipzig' make, using a load of 30 Kg. About five indentations were taken on each polished specimen, and the average value was reported.

### II.9.3 Indentation fracture toughness

Indentation fracture toughness was measured according to the method suggested by Shetty, Wright, Mincer and Clauer [98,168] based on Palmqvist crack geometry.

$$K_C \text{ (MN/m}^{3/2}\text{)} = 0.0937 P/a\ell^{1/2}$$

where,  $P$  = indentation load (MN)

$a$  = half indentation diagonal (m)

$\ell$  = Palmqvist crack length (m).

Testing was carried out at a load of 60 Kg using the Vickers hardness testing machine and crack length measurement was carried out on a precision graduated microscope. Reproducibility in results required the removal of the subsurface damage which could persist after normal diamond lapping and polishing. This was achieved through doubling the duration of each lapping/polishing stage as suggested by Laugier [97]. About five indentations were taken on each sample, and the average values were reported.

## II.10 MAGNETIC PROPERTIES MEASUREMENTS

Magnetic properties like coercivity and magnetic saturation were measured to get an idea of metal phase distribution, amount of porosity, and the presence of 'eta' phase in the structure. The properties were also measured for a quick identification of the reproducibility of the test

samples for each set of experiments. A Dr. Foester make coercivity meter was used for this purpose.

## II.11 OXIDATION STUDY

Specimens of  $6 \times 4 \times 3 \text{ mm}^3$  size were machined from the bulk sintered fully dense transverse rupture strength (TRS) pieces using a diamond cutter. All the surfaces of the specimens were polished to a  $1 \mu\text{m}$  finish using diamond paste. Isothermal weight gain measurements were made on a thermogravimetric unit (Make Anisworth, USA). The test temperature was  $800^\circ\text{C} \pm 5^\circ\text{C}$  (a realistic service temperature at the tool tip). The test was carried out in air for periods upto 8 hours. The rate constant of the oxidation reaction for all the systems was determined using the general empirical relationship

$$(\Delta m)^n = Kt$$

where,  $\Delta m$  = weight gain/unit area ( $\text{gm}/\text{m}^2$ )

$t$  = time (sec)

$K$  = rate constant

$n$  = power index.

The values of 'n' and 'K' for each systems were calculated using the least square method.

X-ray diffraction studies were conducted on the oxide surface by means of a Rich-Seifert X-ray diffractometer using  $\text{CuK}_\alpha$  radiation and the oxides present in the systems were identified. JSM 840A Scanning Electron Microscope was used to study the morphology of the resulting oxides.

## II.12 THERMAL SHOCK RESISTANCE EVALUATION

Specimens of  $6 \times 4 \times 3 \text{ mm}^3$  size were machined from the bulk sintered TRS pieces using a diamond cutter. All specimen surfaces were finished by grinding and were subsequently polished to a  $1 \text{ }\mu\text{m}$  finish by using diamond paste. All the corners of the specimens were chamfered to  $0.5 \text{ mm}$  (approximately). The specimens were put into a container filled with  $\text{N}_2$  gas as shown in Fig. 2.1. They were heated up to temperature  $T_1$  ( $400$  to  $800^\circ\text{C}$  at an interval of  $50^\circ\text{C}$ ) and a holding period of 10 minutes was allowed for homogenisation of the temperature. The shutter was opened and the specimens were dropped into the water bath at room temperature ( $T_2$ ) to impart a thermal shock. The surfaces of the specimens were then examined for cracking with an optical microscope at  $100\times$ . Two test pieces from each set of specimen were tested at each temperature. The minimum value for  $\Delta T = T_1 - T_2$  ( $^\circ\text{C}$ ) leading to cracking for each specimen was reported.

## II.13 CUTTING TOOL LIFE ESTIMATION AND FAILURE ANALYSIS

The tool geometry used for cutting tool life estimation is shown in Fig. 2.2. The tools were made from the broken TRS pieces using diamond wheel grinder. Special care were taken while grinding to minimise the surface damage which might otherwise add some extraneous factors to cause failure of the tools. The continuous cutting tests were performed on EN 9 steel ( $0.3\text{--}0.6\%$  Mn,  $0.5\text{--}0.6\%$  C) having a hardness of BHN 200 with a feed of  $0.2\text{mm/rev}$ . and  $2\text{mm}$  depth of cut at a cutting speed of  $180 \text{ m/min}$  and  $220 \text{ m/min}$  respectively. The tests were conducted on 50 HP CNC WIDMA lathe according to ISO 3685-1977 specification for tool life testing with single point turning tools [197].

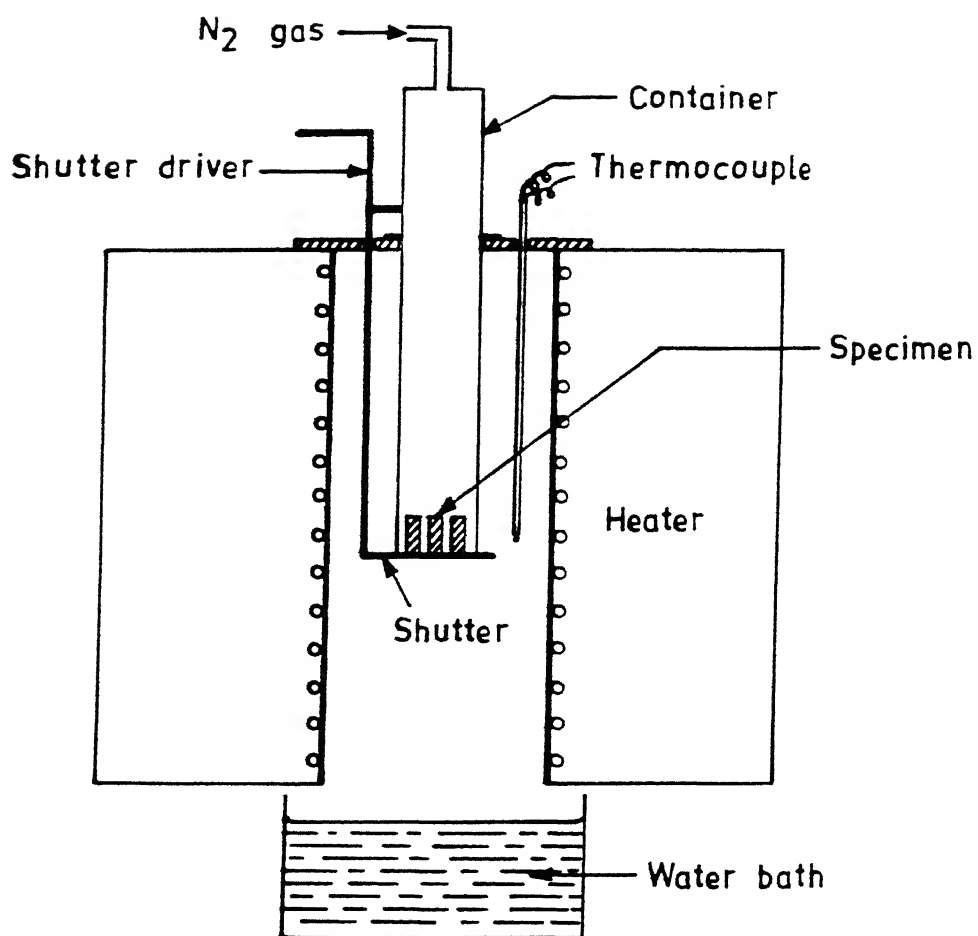


Figure 2.1 A schematic drawing of the quenching apparatus used for thermal shock resistance measurements.

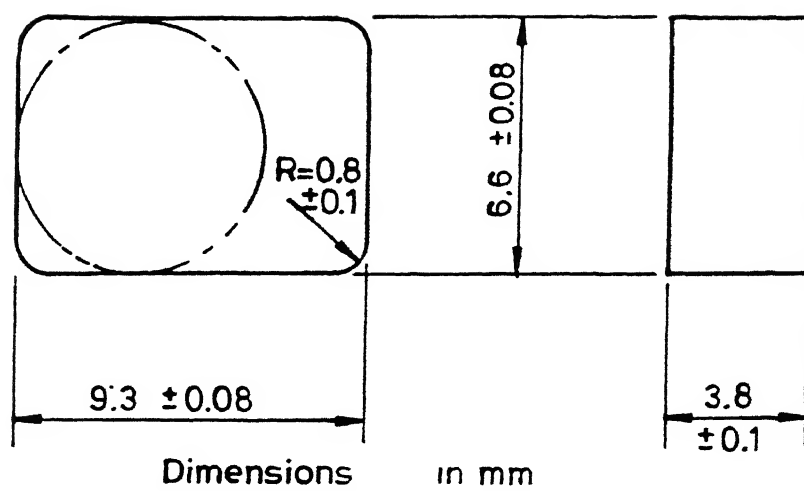


Figure 2.2 A schematic drawing of the tool geometry.

# CHAPTER - III

## EXPERIMENTAL RESULTS

### III.1 POWDER PREMIX CHARACTERISATION

The particle size and their distribution in the powder premixes after wetball milling are presented in Figs. 3.1-3.5 and Table 3.1. It was observed that the average particle size and the size distribution in the powder premixes of all the alloys after milling were almost similar.

### III.2 WC-10Co CEMENTED CARBIDE (ALLOY A)

#### III.2.1 Sintered density

The full density of alloy A was achieved after sintering at 1425°C. The unetched polished sample showed only type 'A' porosity having a concentration of ' $A_{O_2}$ ' (Fig. 3.6a). However, the change in sintering atmosphere from hydrogen to vacuum resulted in higher sintered density.

#### III.2.2 Microstructural study

Fig. 3.6b shows the typical SEM microstructure of polished and etched samples of alloy A. The microstructure consisted of sharp angular WC grains embedded in the cobalt matrix. Table 3.2 lists the mean WC grain size, mean binder free path and the contiguity values. The TEM structures are illustrated in Fig. 3.7. WC grains exhibited the simple geometric forms with straight edges (Fig. 3.7a). It also appears that each WC grain was in contact with one or more neighbouring grains. The structure in WC grains revealed that in general they had low dislocation density (Fig. 3.7b) and in fact many of them were free from any such defect structure. On

the other hand, the binder phase cobalt was associated with a high density of stacking faults which is clearly evident from Fig. 3.7c. There were basically two kind of interfaces in this two phase microstructure viz. carbide/ carbide and carbide/binder interfaces. The nature of these interfaces are shown in Figs. 3.7a and d.

The change in sintering atmosphere from hydrogen to vacuum did not apparently lead to any drastic change in sintered microstructure. However, the quantitative metallographic study showed that the vacuum sintering resulted in a decreased mean binder free path and contiguity values (Table 3.2).

### III.2.3 Magnetic properties

The magnetic properties viz. coercivity and magnetic situation of alloy A are presented in Table 3.3. The variation in sintering atmosphere did not show any noticeable change in magnetic properties.

### III.2.4 Mechanical properties

Hardness, TRS and indentation fracture toughness of alloy A are listed in Table 3.3. The results show that vacuum sintering resulted in higher TRS and indentation fracture toughness, but lower hardness as compared to that sintered in hydrogen.

### III.2.5 Fractographic study

The different microstructural features observed on the fracture surfaces of alloy A are illustrated with SEM fractographs in Fig. 3.8. The typical fracture surfaces of this kind of cermet are composed of features of both brittle and

ductile modes. Figs. 3.8a, c and d illustrate such fracture surfaces which show both transgranular fracture of WC grain and ductile fracture of cobalt. WC of grain size greater than 5  $\mu\text{m}$  were fractured transgranularly (Fig. 3.8b) whereas smaller grains ( $<2 \mu\text{m}$ ) fractured intergranularly. Many cleaved WC grains of smaller average grain size were also observed on the fracture surfaces. However, the ductile fracture of cobalt left a pattern of dimples or tear ridges on the fracture surface. The other common features observed were secondary cracks (Figs. 3.8a and c) and de-bonding of interfaces i.e. WC/Co or WC/WC (Fig. 3.8d).

### III.2.6 Oxidation behavior and thermal shock resistance

The plot of weight gain versus time at  $800^\circ\text{C}$  for alloy A is presented in Fig. 3.9. The values of 'n' and 'K' for the equation  $(\Delta m)^n = Kt$  were calculated from the oxidation results using least square method which are tabulated in Table 3.4. Results indicate that alloy A followed a parabolic type of oxidation behavior ('n' = 1.36). The morphological study of the oxides by SEM indicates that the oxide layers forming on this alloy were brittle (Fig. 3.10a). Cracks were also visible in the oxides, and were not just a surface phenomena but extended through the oxide layer. For example, Fig. 3.10b shows the cracks in the oxide extending from the metal/oxide interface to the oxide/gas interface. The oxides identified in this alloy were  $\text{WO}_3$ ,  $\text{CoWO}_4$ ,  $\text{Co}_2\text{O}_3$  and  $\text{Co}_3\text{O}_4$ .

Thermal shock resistance which was described as  $\Delta T$ , the minimum value for the temperature difference in quenching test leading to cracking of the specimen, is listed in Table 3.5.

### III.2.7 Cutting performance

Continuous cutting test was performed on EN 9 steel (Hardness BHN 200). The other cutting conditions viz. feed, depth of cut have been mentioned in section II.13. The tool lives obtained in alloy A are 377 sec. and 270 sec. at a cutting speed of 180 m/min and 220 m/min respectively. The SEM pictures of tools after cutting test are illustrated in Fig. 3.11 which show that the diffusion wear was the major wear mechanism in limiting the tool life.

### III.3 WC-TiC ( $\text{MO}_2\text{C}$ )-Co(Ni) CEMENTED CARBIDES

#### III.3.1 WC-8TiC-12Co cemented carbide (Alloy B)

##### (a) Selection of optimum sintering temperature :

Optimum sintering temperature of alloy B was found out by evaluating sintered properties viz. percent sintered porosity, hardness, TRS, indentation fracture toughness, coercivity and magnetic saturation. Table 3.6 shows that the full density of the present cemented carbide composition was achieved only when the sintering temperature was above  $1475^{\circ}\text{C}$ . The unetched polished fully dense sample showed type 'A' pores with the distribution same as mentioned in alloy A (Fig. 3.6a). With the increase in sintering temperature, hardness (Fig. 3.12) and TRS (Fig. 3.13a) were somewhat improved but remained almost constant after  $1475^{\circ}\text{C}$  sintering. Indentation fracture toughness (Fig. 3.13b) variation showed a maximum value after  $1475^{\circ}\text{C}$  sintering followed by a drop at higher sintering temperature. Magnetic properties viz. coercivity and magnetic saturation (Fig. 3.14) did not show apparently any variation with sintering temperature.

On the basis of the present experimental results, the optimum sintering temperature for alloy B was selected as  $1475^{\circ}\text{C}$ . Further studies on this composition were, therefore, carried out on the samples sintered only at  $1475^{\circ}\text{C}$ .

(b) Microstructural study :

The introduction of TiC into alloy A led to a very nonuniform microstructure, specifically large TiC grains (Fig. 3.15b). The changes in different microstructural parameters viz. mean grain size, size distribution, mean binder free path and contiguity which were brought about by the change in carbide phase chemistry are demonstrated through Figs. 3.16, 3.17 and Table 3.7. It is evident from Fig. 3.16 that the major microstructural changes were the mean grain size and the grain size distribution of the cubic carbide (TiC) phase. However, a similar behavior was also observed in WC, but the changes were marginal as compared to TiC. The mean binder free path (Fig. 3.17a) followed the same trend as that of mean grain size, but the contiguity value dropped from 0.61 to 0.56.

Table 3.7 clearly indicates that the mean grain size of both WC and TiC remained almost constant irrespective of sintering atmosphere, i.e., either hydrogen or vacuum. However, the other microstructural parameters viz. mean binder free path (Fig. 3.17a) and contiguity (Fig. 3.17b) showed lower values when the sintering was done under vacuum.

WC grains in alloy B had typical angular shape with straight edges (Fig. 3.18a). The defect structure in WC grains and the WC/Co interfaces were similar to those described in alloy A. However, TiC grains in the microstructures were characterised by their rounded nature.

Some of the TiC grains seem to be completely spherical in shape (Fig. 3.18b). Most of the TiC grains were free from any defect structures. Some of them were observed to have small cobalt inclusions, which were located near the centre of the grains (Fig. 3.18b). The binder phase cobalt appeared to be highly dislocated.

(c) Magnetic properties :

The introduction of TiC into WC-10Co cemented carbide resulted in a decrease in coercivity (Fig. 3.19a), but the magnetic saturation remained almost same (Fig. 3.19b). After vacuum sintering coercivity increased and showed a value even greater than that of alloy A, whereas a slight drop was observed in magnetic saturation value.

(d) Mechanical properties :

The mechanical properties of alloy B are presented in Figs. 3.20 and 3.21. The incorporation of TiC into alloy A resulted in a drastic fall in both TRS and indentation fracture toughness (Fig. 3.21). In contrast, the hardness value showed an increase (Fig. 3.20). Vacuum sintering resulted in improved TRS and toughness, but slightly lower hardness compared to that sintered in hydrogen.

(e) Fractographic study :

SEM images of the fracture surfaces of alloy B are presented in Fig. 3.22. The fractograph in Fig. 3.22a hardly shows any dimpled ductile fracturing of cobalt as compared to alloy A (Figs. 3.8a, c and d). A careful examination reveals that on the fracture surface most of the transgranularly fractured carbides were large TiC grains. The predominant

local fractures in the present alloy were of transgranular type in the carbide grains (mainly TiC), and WC/WC, WC/TiC or TiC/TiC interface separations (Fig. 3.22c).

(f) Oxidation behavior and thermal shock resistance :

The oxidation results of alloy B are presented in Fig. 3.23 and Table 3.4. Like alloy A, this alloy also followed parabolic type of oxidation behavior ( $n = 1.20$ ). The morphology of the oxides and their characteristics were same to those of alloy A mentioned earlier (Fig. 3.10). However, with the addition of TiC to alloy A the oxidation resistance enhanced (Fig. 3.23). In the present alloy,  $TiO_2$  was also detected in addition to the oxides present in alloy A (Table 3.4). Thermal shock resistance of alloy B was much inferior to alloy A (Table 3.5).

(g) Cutting performance :

The tool life test result of alloy B is presented in Fig. 3.24. Compared to alloy A, alloy B showed very poor cutting performance. The failure of the tools took place at a very early stage. The SEM pictures of the tools after cutting test are shown in Fig. 3.25. The picture of failed tool (Fig. 3.25a) is indicative of the fact that the failure took place by crack initiation at the cutting edge followed by its quick propagation.

### III.3.2 WC-8TiC-6Co-6Ni cemented carbide (Alloy C)

(a) Selection of optimum sintering temperature :

As mentioned earlier in case of alloy B (Section II.3.1), the optimum sintering temperature of alloy C was also

found out in a similar way. The sintered properties of the present composition with the variation in sintering temperature are shown in Figs. 3.12, 3.13 and 3.14 and Table 3.6. Densification behavior of alloy C was better than that of alloy B and it achieved almost full density at  $1450^{\circ}\text{C}$  (Table 3.6). TRS remained almost constant when the sintering temperature was above  $1475^{\circ}\text{C}$ , but indentation fracture toughness showed a maximum at  $1475^{\circ}\text{C}$  followed by a sharp drop at  $1500^{\circ}\text{C}$  (Fig. 3.13). Coercivity decreased steadily with the increase in sintering temperature, where as magnetic saturation remained constant at all sintering temperatures (Fig. 3.14).

Based on the experimental results the optimum sintering temperature for alloy C was selected as  $1475^{\circ}\text{C}$ .

(b) Microstructural study :

Presence of nickel in the binder phase helped in producing a better microstructure (Fig. 3.15c) as compared to that of alloy B (Fig. 3.15b). This is further confirmed by the mean carbide grain size (Table 3.7) and size distribution (Fig. 3.16) of WC and TiC. The modification of alloy B, by incorporating nickel in binder cobalt resulted in a higher contiguity and lower mean binder free path (Fig. 3.17). The change in sintering atmosphere from hydrogen to vacuum did not bring out any noticeable change in the microstructure. However, quantitative metallographic results showed a drop in both contiguity and mean binder free path.

The TEM structures obtained after modification in the binder phase chemistry are presented in Fig. 3.26, which showed that the microstructure consisted of straight edged WC and rounded TiC grains. The shape and defect structures in WC grains were similar to those described for alloy A or alloy B.

However, in alloy C some of the TiC grains showed dislocation substructure but of a very low density (Fig. 3.26b). The nature of WC/binder interface in this alloy was similar to that in alloy A. On the other hand, the TiC/binder interface observed in this alloy (Fig. 3.26b) was very different from those observed in alloy B (Figs. 3.18a-b). A still higher magnified view of the TiC/binder interface is shown in Fig. 3.26c, where an interfacial interaction between the two phases can be noticed.

(c) Magnetic properties :

The magnetic properties of alloy C are illustrated through Fig. 3.19. Alloy C had a higher coercivity and a lower magnetic saturation values than those of alloy B. The variation in sintering atmosphere did not lead to any change in magnetic properties.

(d) Mechanical properties :

Substitution of 50 vol% binder metal cobalt by nickel resulted in a marginal decrease in hardness (Fig. 3.20) but the TRS increased by about 325 MPa (Fig. 3.21a). Indentation fracture toughness showed an opposite trend in relation to alloy B. Vacuum sintering resulted in a better TRS and indentation fracture toughness and an inferior hardness as compared to that sintered in hydrogen atmosphere.

(e) Fractographic study :

The differences in the fracture surfaces due to change in binder phase composition can be evidenced in Fig. 3.27. As compared to alloy B, the fracture surface showed a reasonable amount of ductile fracturing of binder phase apart

from the transgranular fracture of WC and TiC grains (Fig. 3.27a). A comparison of Figs. 3.8 a, c, d and 3.27a reveals an important change in the fractured binder phase. In alloy A, the rupturing of cobalt left a pattern of dimples or tear ridges on the fracture surface. But in alloy C the binder phase was present as a ruptured ligaments between carbide particles (Fig. 3.27a). Many small smooth carbide particles were also observed on the fracture surface as a result of de-bonding of carbide/binder interfaces. The characteristic feature on the fracture surface of the present alloy was that the transgranularly fractured TiC very often left a river pattern on the fracture surface (Figs. 3.27b-c). From the river pattern it can be easily determined that the local fracture initiation in the TiC grains was either from carbide/binder (Fig. 3.27b) or carbide/carbide interface (Fig. 3.27c). The basic modes of local fracture as highlighted in the earlier sections can also be evidenced along a secondary crack in Fig. 3.27d.

(f) Oxidation behavior and thermal shock resistance :

The oxidation results of alloy C are presented in Fig. 3.23 and Table 3.4. The addition of nickel in the binder cobalt (alloy C) did not drastically affect the oxidation behavior but led to only a marginal improvement with respect to alloy B (Fig. 3.23). Moreover,  $\text{NiWO}_4$  and  $\text{Ni}_2\text{O}_3$  were also present in the oxides in addition to other oxides mentioned in alloy B (Table 3.4), when nickel was present in the binder metal cobalt. The SEM study of the oxides layer indicated that it had more or less the same morphology and characteristics to those of either alloy A or alloy B (Fig. 3.10). The result from Table 3.5 indicates that the modification in binder phase

chemistry by incorporating nickel improved the thermal shock resistance of alloy C.

(g) Cutting performance :

Alloy C showed a better tool life than that of alloy B, but it was still shorter than that of alloy A (Fig. 3.24). The SEM images of the failed tools are shown in Fig. 3.28. It is clearly evident from Figs. 3.25a and 3.28a that the failed tools of alloys B and C had almost similar structural features.

### III.3.3 WC-6TiC-2Mo<sub>2</sub>C-6Co-6Ni cemented carbide (Alloy D)

(a) Selection of optimum sintering temperature :

The results show that the densification behavior of the previously mentioned cemented carbide (Alloy C) was further improved with the presence of molybdenum in the binder phase (Table 3.6). It attained almost full density when sintered at 1450°C. Both TRS and indentation fracture toughness showed a maximum at 1475°C followed by a sharp drop at 1500°C (Fig. 3.13). Hardness variation showed just the opposite trend to that of strength (Fig. 3.12). It had the minimum value at 1475°C. The magnetic properties i.e., coercivity and magnetic saturation increased steadily with the increase in sintering temperature (Fig. 3.14). Based on the experimental results, the optimum sintering temperature for the present alloy was selected as 1475°C.

(b) Microstructural study :

It is clearly evident from Figs. 3.15b-d, that alloy D had the most uniform microstructure amongst all TiC

containing cemented carbides viz. alloys B, C and D. A partial substitution of TiC by  $\text{Mo}_2\text{C}$  in alloy C brought down the mean carbide grain size and the range of grain size distribution of both WC and TiC (Fig. 3.16 and Table 3.7). The observed changes in microstructure were much more in cubic phase (TiC) than in WC. Both mean binder free path and the contiguity values decreased with reference to that of alloy C (Fig.3.17). Vacuum sintering did not bring out any noticeable change in the mean carbide grain size or their distribution (Table 3.7), but the mean binder free path and contiguity (Fig.3.17) were decreased further as compared to that in hydrogen sintering.

No major changes were observed in TEM microstructure of this alloy in comparison to alloy C at low magnification (Fig. 3.29a). However, in some places of the specimen the binder phase (Fig. 3.29b) showed a high density of intersecting stacking faults. Fig. 3.29b also reveals the distinctive nature of WC/binder and TiC/binder interfaces which have almost similar kind of appearance as in alloy C (Figs. 3.26b and c). The magnified view of TiC/binder interface (Fig. 3.29c) reveals that the TiC grain had a diffused interface showing a rim around the TiC grains.

#### (c) Magnetic properties :

Fig. 3.19a indicates that the coercivity of the present cemented carbide maintained the same level to that of alloy C, but the magnetic saturation value (Fig.3.19b) dropped from 140 Gauss to 115 Gauss when sintered in  $\text{H}_2$ . However, vacuum sintering enhanced both coercivity and magnetic saturation to a level almost same to alloy C.

(d) Mechanical properties :

The TRS and indentation fracture toughness improved significantly (Fig. 3.21) when the TiC in alloy C was partially substituted by  $\text{Mo}_2\text{C}$ . In fact the present alloy showed TRS almost equivalent to that of alloy A. Hardness value did not change much with respect to alloy C due to the modification in alloy chemistry. Sintering atmosphere too had influence on the mechanical properties. Vacuum sintering enhanced the strength and toughness further, while a drop was observed in hardness value.

(e) Fractographic study :

SEM fractographs of the present alloy are illustrated through Figs. 3.30a-c. A comparison of Figs. 3.30a and 3.27a reveals that the appearance of the fracture surfaces, especially the binder phase got changed appreciably. Fig. 3.30a (Alloy D) shows a much more dimpled structure than that of alloy C (Fig. 3.27a). As far as the carbides are concerned they behaved in a similar manner to those for alloy C (Figs. 3.30 b and c). Cleaved TiC grains were easily distinguishable from WC as they showed prominent river patterns on the fracture surface. The other modes of local fracture viz. carbide/binder and carbide/carbide interface separation were also observed.

(f) Oxidation behavior and thermal shock resistance :

In contrast to mechanical properties, addition of  $\text{Mo}_2\text{C}$  in alloy C had deleterious effects on oxidation resistance. From Fig. 3.23 and Table 3.4 it is clearly evident that alloy D was most prone to oxidation amongst the alloys mentioned so far. The oxide morphology and characteristics resembled very much to that of alloy A mentioned earlier (Fig.

3.10). With the presence of  $\text{Mo}_2\text{C}$  in the system, the oxide  $\text{MoO}_3$  was formed in addition to other oxides previously mentioned (Table 3.4).

Thermal shock resistance of alloy D (Table 3.5) was of the same order as that of alloy C but much less than that of alloy A.

(g) Cutting performance :

Cutting performance of alloy C was greatly improved by incorporating  $\text{Mo}_2\text{C}$  in it. In fact, alloy D showed the best cutting life among the alloys A, B, C and D (Fig. 3.24). The SEM pictures of alloy D after cutting test (Fig. 3.31a) depict that the wear on the rake face was responsible for limiting the tool life. SEM studies of the worn surface showed that it was covered with a thick layer of oxides (Fig. 3.31b). The morphology of the oxides were similar to that observed in oxidation study (Fig. 3.10a).

#### III.4 WC - $\text{TiN}(\text{Mo}_2\text{C})$ - Co(Ni) CEMENTED CARBIDES

##### III.4.1 WC - 8.7 TiN - 12Co cemented carbide (Alloy E)

###### Part I : Liquid phase sintered alloy

(a) Selection of optimum sintering temperature and atmosphere :

Introduction of TiN into WC-10Co cemented carbide (alloy A) resulted in high sintered porosity. The maximum attainable sintered density was achieved at  $1475^\circ\text{C}$  (Fig.3.32a). A great improvement in sintered density was observed when the sintering atmosphere was changed to  $\text{H}_2\text{-N}_2$  mixture (50:50) from

straight  $H_2$ . Even then, the maximum density obtained was about 96% of the theoretical density. Hardness variation (Fig. 3.32b) showed that it attained the maximum value at  $1475^{\circ}\text{C}$  and remained constant at higher sintering temperature when sintered in  $H_2$ . TRS and indentation fracture toughness values (Fig. 3.33) decreased steadily with the increase in sintering temperature in  $H_2$  atmosphere. But a different kind of behavior was observed when sintering was done in  $H_2-N_2$  atmosphere. Hardness remained constant at all sintering temperatures, whereas both TRS and indentation fracture toughness increased with the increase in sintering temperature. They attained maximum at  $1475^{\circ}\text{C}$  followed by a drop at  $1500^{\circ}\text{C}$ . The magnetic properties variation (Fig. 3.34) shows that both coercivity and magnetic saturation were higher when sintered in  $H_2-N_2$  atmosphere as compared to those sintered in  $H_2$ .

On the basis of the experimental results the optimum sintering temperature and sintering atmosphere were selected as  $1475^{\circ}\text{C}$  and  $H_2-N_2$  mixture (50:50) respectively.

(b) Metallographic study :

The pore morphology and their distribution in the present alloy after sintering at  $1475^{\circ}\text{C}$  in  $H_2-N_2$  are shown in Fig. 3.35a. Fig. 3.36a shows the SEM microstructure of polished and etched sample. The microstructure consisted of angular WC (white phase) and equiaxed TiN (grey phase). The addition of TiN in WC-10Co (Alloy A) resulted in increased WC grain size and wider range of size distribution (Fig. 3.37 and Table 3.7).

## Part II : Hot isostatically pressed alloy

### (a) Pore morphology and distribution :

Nearly full density with residual porosity of about 0.15% was achieved when HIP'ing of the liquid phase sintered alloy was done at  $1450^{\circ}\text{C}$  (Table 3.8). The pore size and the distribution in the HIP'ped cemented carbide of the present composition are shown in Figs. 3.38a and b. Large pores in the as sintered compacts were mostly eliminated by HIP treatment. The pore size was further reduced when the HIP'ing temperature was increased to  $1450^{\circ}\text{C}$  from  $1400^{\circ}\text{C}$ . HIP'ing at  $1450^{\circ}\text{C}$  resulted in finer pores and a better distribution than those at  $1400^{\circ}\text{C}$ .

### (b) Metallographic study :

SEM microstructures of HIP'ped alloy in Figs. 3.39 a and b do not show much difference from those of as sintered one (Fig. 3.36a). Quantitative metallographic study showed that HIP treatment resulted in grain coarsening of both WC and TiN (Fig. 3.40 and Table 3.7). Mean binder free path decreased slightly after such treatment, but the contiguity reached a value of 0.70 as compared to 0.61 in alloy A (Fig. 3.41).

The TEM microstructure of HIP'ped alloy E are demonstrated through Figs. 3.42a-c. The general microstructure consisted of straight faceted WC grains and equiaxed TiN grains (Fig. 3.42a). Compared to alloy A (Fig. 3.7), alloy B (Fig. 3.18), alloy C (Fig. 3.26) and alloy D (Fig. 3.29), the hard phases in the present alloy showed a very high dislocation density. Another characteristics feature of the microstructure was the formation of shear bands (Fig. 3.42b). However, the

shear bands were mostly observed in TiN phase only. The micrographs in Figs. 3.42a and c clearly indicate that each WC/TiN grain was in contact with many neighbouring WC/TiN grains. The binder phase cobalt was associated with high dislocation density (Fig. 3.42a) and did not contain any stacking fault. The hard phases/binder interface observed in this alloy (Fig. 3.42c) was very similar to that of WC/Co interface in alloy A. But the hard phase/hard phase interfaces were very different from those observed in alloy A, which can be clearly noticed from Fig. 3.42c, where WC grain (grey) seems to be intruded into TiN grain (centre white grain).

(c) Magnetic properties :

HIP'ing at  $1400^{\circ}\text{C}$  resulted in an increase in coercivity, but the magnetic saturation maintained the same level as that of liquid phase sintered alloy in  $\text{H}_2\text{-N}_2$  (Fig. 3.43). Just the opposite happened when HIP'ing was done at  $1450^{\circ}\text{C}$ , such that both coercivity and magnetic saturation values decreased.

(d) Mechanical properties :

From Figs. 3.44 and 3.45 it is clearly evident that HIP'ing resulted in a great enhancement in all the investigated mechanical properties. The only exception was the indentation fracture toughness value after HIP'ing at  $1400^{\circ}\text{C}$  which showed a decrease. The addition of TiN in WC-10Co (Alloy A) resulted in a lower hardness (Fig. 3.44), but the TRS and indentation fracture toughness obtained after HIP'ing at  $1450^{\circ}\text{C}$  (Fig. 3.45) were equivalent to those of alloy A.

(e) Fractographic study :

Though the introduction of TiN into WC-10Co did not result in any appreciable change in TRS, noticeable changes were observed on the fracture surface. The major changes were in the binder phase. Here the binder phase was mostly present as ruptured ligaments on the hard phase grains and rough tear ridges around the grains (Figs. 3.46a-b). As far as the transgranularly fractured TiN grains were concerned, they showed a well defined smooth cleaved surface with steps (Fig. 3.46c). In general, the predominant local fracture took place by the interfacial decohesion of grain boundary followed by intergranular or transgranular fracture (Fig. 3.46d).

(f) Oxidation behavior and thermal shock resistance :

With the addition of TiN to WC-10Co cemented carbide (Alloy A), the oxidation resistance was enhanced (Fig. 3.47 and Table 3.4). It is important to note that TiC addition also enhanced the oxidation resistance of WC-10 Co cemented carbide (Fig. 3.23 and Table 3.4), but the enhancement was more pronounced for TiN addition compared to TiC addition. The morphology and characteristics of the oxide layer were same as those mentioned earlier in alloy A (Fig. 3.10). The oxides identified in the oxide layer were same as those observed in alloy B (Table 3.4).

Though the TiN addition to WC-10Co cemented carbide deteriorated the thermal shock resistance marginally, it is worth mentioning that the present alloy had a better thermal shock resistance than any of the TiC containing cemented carbides (Table 3.5) mentioned earlier.

(g) Cutting performance :

Fig. 3.48 shows the cutting performance of alloy E after HIP'ing. A significant increase in tool life was observed when the HIP'ing temperature was increased to  $1450^{\circ}\text{C}$  from  $1400^{\circ}\text{C}$ . Unlike mechanical properties, the addition of TiN to WC-10Co cemented carbide increased the tool life to a great extent while cutting steel at a speed of 180 m/min. SEM pictures taken from the worn tool after cutting test are illustrated through Fig. 3.49, which shows that the wear around the nose radius was of significance in this particular case.

#### III.4.2 WC-8.7TiN-6Co-6Ni cemented carbide (Alloy F)

(a) Selection of optimum sintering temperature and atmosphere :

Partial substitution of cobalt by nickel did not improve the densification behavior for alloy F. Sintered density increased with the increase in sintering temperature but remained almost constant after  $1475^{\circ}\text{C}$  sintering (Fig. 3.32a). However, a great improvement in sintered density was observed when the sintering atmosphere was changed to  $\text{H}_2\text{-N}_2$  from straight  $\text{H}_2$ . The mechanical properties viz. Hardness, TRS and indentation fracture toughness attained the maximum value at a sintering temperature of  $1475^{\circ}\text{C}$  (Figs. 3.32b and 3.33a-b). The change in sintering atmosphere from  $\text{H}_2$  to  $\text{H}_2\text{-N}_2$  enhanced the mechanical properties except hardness which showed a decrease. Magnetic properties variation (Fig.3.34) shows that the coercivity increased with the increase in sintering temperature. A further improvement in coercivity values were observed when sintering was done in  $\text{H}_2\text{-N}_2$ . On the other hand, magnetic saturation decreased steadily with the

increase in sintering temperature during  $H_2$  sintering (Fig. 3.34b). However, it showed an opposite trend in  $H_2-N_2$ , such that it increased upto sintering temperature of  $1475^{\circ}C$  and then remained constant at higher sintering temperature.

On the basis of the present experimental results, the optimum sintering temperature and the atmosphere were selected as  $1475^{\circ}C$  and  $H_2-N_2$  respectively.

#### (b) Metallographic study

The pore morphology and their distribution in the present alloy after sintering in  $H_2-N_2$  are presented in Fig. 3.35b. The binder phase modification by incorporating nickel in the cobalt binder resulted in an increase in the density of larger pores. Fig. 3.36b indicates that the present alloy had almost similar microstructure to that of previous alloy (Alloy E). However, the quantitative metallographic study (Fig. 3.37 and Table 3.7) showed that the partial substitution of cobalt binder metal by nickel resulted in an increased hard phase (WC and TiN) grain size and a wider grain size distribution. The size distribution became more wider in case of WC (Fig. 3.37a) than in TiN (Fig. 3.37b).

#### (c) Mechanical properties

In general the mechanical properties deteriorated when nickel was introduced in Alloy E.

Since the modification of the binder phase chemistry did not show any promising results either by improving the densification behavior or by enhancing the mechanical properties, it was decided not to carry out any further detailed study on the present alloy composition.

### III.4.3 WC-7.5TiN-1.8Mo<sub>2</sub>C-6Co-6Ni cemented carbide (Alloy G)

#### Part I : Liquid phase sintered alloy

##### (a) Selection of optimum sintering temperature :

By now on the basis of the experimental results, it was already established that H<sub>2</sub>-N<sub>2</sub> mixture was the proper sintering atmosphere for the cemented carbides containing TiN. It was, therefore, decided to sinter the present alloy in H<sub>2</sub>-N<sub>2</sub> atmosphere only.

Fig. 3.32a shows that the addition of Mo<sub>2</sub>C in Alloy F improved the densification behavior significantly. The maximum attainable density was achieved at 1475°C and no further improvement was observed at higher sintering temperature. The hardness variation (Fig. 3.32b) showed a minimum value at 1475°C. TRS attained the maximum value at 1475°C followed by a drop at higher sintering temperature (Fig. 3.33a). Indentation fracture toughness reached maximum for the specimen sintered at 1475°C, while remained constant till 1500°C (Fig. 3.33b). With the increase in sintering temperature, the coercivity decreased for samples sintered upto 1475°C, followed by a marginal increase at 1500°C (Fig. 3.34a). Magnetic saturation remained almost constant at all sintering temperatures (Fig. 3.34b).

The results showed that the best combination of properties for the present alloy composition was obtained at a sintering temperature of 1475°C.

##### (b) Metallographic study :

It is clearly evident from Figs. 3.35b and c that the addition of Mo<sub>2</sub>C resulted in a decrease in pore size and

Mo<sub>2</sub>C ,

its better distribution as compared to that of the previous composition i.e. Alloy E. Though it is not possible to differentiate the SEM microstructure of the present alloy (Fig. 3.36c) from alloy F. Fig. 3.37 and Table 3.7 clearly indicate that the addition of  $\text{Mo}_2\text{C}$  helped in producing a better micro-structure as compared to that of alloy F in terms of average hard phase grain size and its distribution.

## Part II : Hot isostatically pressed alloy

### (a) Pore morphology and distribution :

Large pores in the as sintered compacts of the alloy were mostly eliminated (Fig. 3.38c and d) and nearly full density was achieved with a residual porosity of about 0.10%, when the liquid phased sintered alloy was HIP'ped at  $1450^\circ\text{C}$ . HIP'ing at  $1400^\circ\text{C}$  did increase the density to about 99.7% of the theoretical density (Table 3.8), but many large pores were left out (Fig. 3.38c). Increase in HIP'ing temperature from  $1400^\circ\text{C}$  to  $1450^\circ\text{C}$  helped in eliminating most of the large pores and also resulted in their uniform distribution (Fig. 3.38d).

### (b) Metallographic study :

SEM microstructures in Figs. 3.39c and d do not show any significant difference from that of non-HIP'ped alloy (Fig. 3.36c). Quantitative metallographic study also showed that it had almost similar average grain size and size distribution (Fig. 3.40 and Table 3.7) to that of non-HIP'ped one (Fig. 3.37 and Table 3.7). However, HIP treatment resulted in an increase in both mean binder free path (Fig. 3.41a) and contiguity (3.41b). As far as the microstructural

changes due to the change in alloy chemistry are concerned, they were same as those mentioned for as sintered alloy.

The TEM structures of the present alloy system (Fig. 3.50) do not show much difference from that of alloy E shown in Fig. 3.42.

(c) Magnetic properties :

HIP'ing resulted in increase in both coercivity (Fig. 3.43a) and magnetic saturation (Fig. 3.43b).

(d) Mechanical properties :

It is evident from Figs. 3.44 and 3.45 that HIP'ing resulted in considerable enhancement in all the investigated mechanical properties and the trend was exactly same as that observed in alloy E. However, the present alloy had slightly inferior TRS and indentation fracture toughness, but a better hardness to that of HIP'ped ( $1450^{\circ}\text{C}$ ) alloy E.

(e) Fractigraphic study :

The basic modes of local fracture observed in the present alloy were same as those of alloy E as can be seen from Figs. 3.51 and 3.46 respectively. However, Fig. 3.51d reveals an important change in predominant local fracture modes in alloy G. From the fractograph it is evident that many small WC grains were pulled out leaving a clear impression on the fracture surface. Secondly, TiN grains were fractured transgranularly leaving river patterns on these grains.

(f) Oxidation behavior and thermal shock resistance :

As observed in alloy D, the incorporation of  $\text{Mo}_2\text{C}$  in the present alloy also deteriorated the oxidation resistance (Fig. 3.47 and Table 3.4). The morphology and characteristics of oxide layer were same as that of alloy A (Fig. 3.10). The oxides identified in the oxide layer were same as those observed in alloy D (Table 3.4).

$\text{Mo}_2\text{C}$  addition had the similar effect on thermal shock resistance as that on oxidation resistance (Table 3.5), but the deterioration was not much. As compared to TiC containing cemented carbides viz. alloys B, C and D the present alloy had a better thermal shock resistance.

(g) Cutting performance :

The modification of alloy E by adding nickel in the binder metal cobalt and  $\text{Mo}_2\text{C}$  in the hard phase reduced the tool life to a great extent (Fig. 3.48). However, the tool life was improved and it showed an equivalent performance to that of alloy D (Fig. 3.24) when the HIP'ing temperature was increased to  $1450^\circ\text{C}$ . SEM pictures in Fig. 3.52 show that the tool failed by nose breaking. The wear on the rake face was similar to that described in alloy D, but oxidation was much less in the present case.

### III.5 WC-Ti(C,N)/ $\text{Mo}_2\text{C}$ -Co/Ni CEMENTED CARBIDES

Based on the results in the previous section (III.4), all Ti(C,N) containing cemented carbides viz. alloys H, I and J were sintered in  $\text{H}_2\text{-N}_2$  mixture (50:50) only.

### III.5.1 WC-8.3Ti(C,N)-12Co Cemented Carbide (Alloy H)

#### Part I : Liquid phase sintered alloy

##### (a) Selection of optimum sintering temperature :

Addition of Ti(C,N) to WC-10Co cemented carbide (alloy A) resulted in relatively high sintered porosity (Fig. 3.53a). The maximum attainable sintered density was about 97% of the theoretical density after sintering at 1475°C, and remained constant at higher sintering temperature. Hardness variation (Fig. 3.53b) showed that it remained constant upto 1475°C sintering, but increased at higher sintering temperature. TRS and indentation fracture toughness values (Fig. 3.54) increased with the increase in sintering temperature, but the increase in TRS after 1475°C was marginal. The magnetic properties variation (Fig. 3.55) shows that both coercivity and magnetic saturation increased with the increase in sintering temperature and remained almost constant after 1475°C.

Based on the experimental results the optimum sintering temperature for alloy H was selected as 1475°C.

##### (b) Metallographic study :

The pore morphology and their distribution in the present alloy after sintering at 1475°C are illustrated through Fig. 3.56a. The SEM microstructure of the same sample after etching is shown in Fig. 3.57a. The microstructure consisted of angular WC (white phase) and equiaxed Ti(C,N) grains (grey phase). The microstructure of alloy H resembled very much with the cemented carbides containing TiN (Fig. 3.36). Though the average grain size of WC was almost same to

that of alloy A, the grain size distribution became slightly wider (Fig. 3.58 and Table 3.7).

## Part II : Hot isostatically pressed alloy

### (a) Pore morphology and distribution :

Almost full density with residual porosity of about 0.06% was obtained after HIP'ing the liquid phase sintered alloy at 1400°C. Large pores in the liquid phase sintered compacts were completely eliminated by HIP treatment. However, some micropores were still present in the HIP'ped alloy (Fig. 3.59a).

### (b) Metallographic study :

SEM microstructure of HIP'ped alloy (Fig. 3.60a) did not show any difference from that of the liquid phase sintered one (Fig. 3.57a) except the pores. The average grain size and their distribution of both WC and Ti(C,N) (Fig. 3.61 and Table 3.7) remained almost same after HIP treatment. HIP'ing did not lead to any grain coarsening effect as was seen in TiN containing cemented carbides viz. alloys E, F and G. HIP'ing resulted in a decrease in mean binder free path (Fig. 3.62a), but a substantial increase in contiguity value (Fig. 3.62b) was observed.

### (c) Magnetic properties :

Introduction of Ti(C,N) into alloy A resulted in an increase in coercivity (Fig. 3.63a) and a decrease in magnetic saturation (Fig. 3.63b). However, HIP'ing resulted in a decrease in both coercivity and magnetic saturation of the liquid phase sintered alloy.

(d) Mechanical properties :

It is evident from Figs. 3.64 and 3.65 that HIP'ing resulted in an enhancement of all the investigated mechanical properties. In general, the addition of Ti(C,N) to WC-10Co (alloy A) deteriorated hardness, TRS and indentation fracture toughness. However, the deterioration was not that much as was observed in case of TiC addition.

(e) Fractographic study :

The typical fracture surfaces of alloy H are shown in Fig. 3.66. The basic modes of local fracture were same as those mentioned earlier in case of alloy A. Fig. 3.66a reveals that the binder phase was present as a mixture of ruptured ligaments and dimpled structure, of which a large proportion consisted of the former. The predominant local fracture mode was the crack initiation at the contiguous boundaries followed by transgranular fracture of hard phases (Fig. 3.66b). Fig. 3.66c shows a typical transgranularly fractured Ti(C,N) grain.

(f) Oxidation and thermal shock resistance

With the addition of Ti(C,N) to WC-10Co cemented carbide, the oxidation resistance was enhanced (Fig. 3.69), but the thermal shock resistance decreased (Table 3.5). The enhancement is better than TiC and inferior to TiN for similar additions.

### III.5.2 WC-8.3 Ti(C,N)-6Co-6Ni cemented carbide (Alloy I)

#### Part I : Liquid phase sintered alloy

(a) Selection of optimum sintering temperature :

Modification of binder metal cobalt with nickel in alloy I slightly deteriorated the densification behavior (Fig. 3.53a). The maximum attainable density at a sintering temperature of  $1475^{\circ}\text{C}$  was about 97% of the theoretical density and it remained almost constant at  $1500^{\circ}\text{C}$ . Hardness value increased continuously with the increase in sintering temperature (Fig. 3.53b), where as both TRS and indentation fracture toughness remained almost constant upto  $1475^{\circ}\text{C}$  followed by a decrease at higher sintering temperature (Fig. 3.54). Coercivity and magnetic saturation followed the same trend, such as they increased for alloys sintered upto  $1475^{\circ}\text{C}$  and then dropped, the decrease being sharp in case of magnetic saturation (Fig. 3.55).

Analysing the results, the optimum sintering temperature for alloy I was selected as  $1475^{\circ}\text{C}$ .

(b) Metallographic study :

The pore morphology and their distribution in the present alloy i.e. 'I' after sintering at  $1475^{\circ}\text{C}$  are shown in Fig. 3.56b. The binder phase modification resulted in an increase in the density of larger pores. The SEM microstructure (Fig. 3.57b) did not show apparently any difference from that of alloy H (Fig. 3.57a). However, quantitative metallographic study showed that the average grain size of WC and  $\text{Ti}(\text{C},\text{N})$  increased though the distribution remained more or less similar (Fig. 3.58 and Table 3.7).

## Part II : Hot isostatically pressed alloy

### (a) Pore morphology and distribution :

Large pores in the sintered compacts were eliminated (Fig. 3.59b) and nearly full density with residual porosity of about 0.15% was obtained after HIP'ing alloy I at 1400°C. Though porosity level was little high, but they were distributed uniformly as fine pores.

### (b) Metallographic study :

As mentioned earlier in case of liquid phase sintered alloy, the microstructure of the present alloy (Fig. 3.60b) did not have any noticeable difference from alloy H. The average grain size and their distribution (Fig. 3.61) followed exactly the similar pattern as mentioned for liquid phase sintered alloy (Fig. 3.58). Apparently no grain coarsening with respect to liquid phase sintered alloy was observed after HIP'ing (Table 3.7). Quantitative metallographic study showed that HIP'ing resulted in a decrease in mean binder free path (Fig. 3.62a), but the contiguity value increased to a great extent (Fig. 3.62b).

### (c) Magnetic properties :

Incorporation of nickel in cobalt binder decreased both coercivity and magnetic saturation (Fig. 3.63). However, after HIP'ing, coercivity value got raised but the magnetic saturation further decreased.

### (d) Mechanical properties :

An enhancement in all the investigated mechanical properties viz. hardness, TRS and indentation fracture

toughness was observed after HIP treatment of the liquid phase sintered alloy (Figs. 3.64 and 3.65). A comparison between HIP'ped alloys H and I indicated that the change in binder phase chemistry led to inferior properties, the deterioration being more in TRS value.

(e) Fractographic study :

The typical fracture surfaces of alloy I are presented in Fig. 3.67. A distinctive difference in the binder phase fracturing of the present alloy (Fig. 3.67a) could be observed from that of previous alloy viz. Alloy H (Fig. 3.66a). In alloy I, the binder phase was present as fractured ligaments (Fig. 3.67a). The ligaments were interconnected forming a net like appearance on the fracture surface. Fig. 3.67b shows the typical transgranular fracture of Ti(C,N) phase. It can be easily found out from the river pattern that the fracture initiation took place at the hard phase contiguous boundary.

(f) Oxidation and thermal shock resistance

The binder phase modification by incorporating nickel in cobalt had the similar effect on oxidation and thermal shock resistance (Fig. 3.69 and Table 3.5) as was observed in alloy C, such that the former got enhanced, whereas the later deteriorated marginally.

### III.5.3 WC-7Ti(C,N)-2Mo<sub>2</sub>C-6Co-6Ni cemented carbide (Alloy J)

#### Part I : Liquid phase sintered alloy

(a) Selection of optimum sintering temperature :

Fig. 3.53a shows that the addition of  $\text{Mo}_2\text{C}$  in alloy I deteriorated the densification behavior. At  $1450^\circ\text{C}$  sintering the sintered porosity was as high as 8%, which decreased sharply with the increase in sintering temperature. Even at a sintering temperature of  $1500^\circ\text{C}$  the attainable density was about 96% of the theoretical density. There was enhancement in all the investigated mechanical properties (Figs. 3.53b and 3.54) with the increase in sintering temperature. However, the increment in TRS and indentation fracture toughness was not that pronounced. As far as the coercivity and magnetic saturation were concerned, they behaved in different manner, such that the former increased after  $1475^\circ\text{C}$  sintering followed by a drop at  $1500^\circ\text{C}$  (Fig. 3.55a) while the latter increased steadily with the increase in sintering temperature (Fig. 3.55b).

Based on the experimental results, the sintering temperature of the presently investigated alloy i.e. alloy J was selected as  $1500^\circ\text{C}$ .

(b) Metallographic study :

Though the amount of sintered porosity of the present alloy (Fig. 3.56c) was almost same to that of alloy I (Fig. 3.56b), the pore size was larger in the former. The SEM microstructure (Fig. 3.57c) did not show any noticeable difference. It had the same typical microstructure as mentioned in alloy H (Fig. 3.57a) or alloy I (Fig. 3.57b). However, there was minute change in grain size and distribution of both the hard phases viz. WC,  $\text{Ti}(\text{C},\text{N})$  (Fig. 3.58 and Table 3.7). Addition of  $\text{Mo}_2\text{C}$  resulted in marginal

decrease in average grain size of hard phases, though the distribution remained more or less similar.

## Part II : Hot isostatically pressed alloy

### (a) Pore morphology and distribution :

Incorporation of  $\text{Mo}_2\text{C}$  into the system resulted in high sintered porosity and larger pores, but HIP'ing at  $1400^\circ\text{C}$  helped in eliminating all large pores (Fig. 3.59c). Moreover, the residual porosity in the present alloy system after such treatment was less than that of the previous alloy i.e. alloy I (Table 3.8).

### (b) Metallographic study :

The SEM microstructure after HIP treatment (Fig. 3.60c) did not show any noticeable change from either alloy H (Fig. 3.60a) or alloy I (Fig. 3.60b). In fact, all the Ti(C,N) containing cemented carbides investigated in the present study are having similar microstructures. As far as the average grain size and their distributions are concerned (Fig. 3.61), they maintained almost similar values to those of non-HIP'ped ones. HIP'ing resulted in a decrease in mean binder free path (Fig. 3.62a) and an increase in contiguity (Fig. 3.62b). However, among the alloys H, I and J, the present alloy i.e. alloy J had the lowest mean binder free path and contiguity values.

### (c) Magnetic properties :

Magnetic properties viz. coercivity and magnetic saturation (Fig. 3.63) followed the same trend as was observed

in alloy I. After HIP'ing the present alloy had lower coercivity and magnetic saturation than those of alloy I.

(d) Mechanical properties :

It is evident from Figs. 3.64 and 3.65 that HIP'ing of the liquid phase sintered alloy resulted in a substantial improvement in all the investigated mechanical properties. Addition of  $\text{Mo}_2\text{C}$  in alloy J helped in improving the mechanical properties. Moreover, among all the Ti(C,N) containing cemented carbides viz. alloys H, I and J, the present alloy system had the best combination of mechanical properties (Figs. 3.64 and 3.65).

(e) Fractographic study :

The modification of alloy I by adding  $\text{Mo}_2\text{C}$  led to an appreciable change in the fracture behavior. The most important change could be observed in the binder phase. In alloy J the binder phase was present as dimpled structure (Fig. 3.68a). The binder phase in the previous alloy i.e. alloy I fractured mainly by rupturing the ligaments (Fig. 3.67a), which was more or less absent in the present alloy (Fig. 3.68a). The typical fracturing in hard phases is shown in Fig. 3.68b, which did not have much difference from that noticed for alloy H (Fig. 3.66c).

(f) Oxidation and thermal shock resistance

The effect of  $\text{Mo}_2\text{C}$  addition on oxidation resistance in alloy J (Fig. 3.69) was similar to that observed in alloys D and G. However, the present alloy had a better thermal shock resistance than that of the previous alloy i.e. alloy I by  $50^\circ\text{C}$  (Table 3.5).

Table 3.1 : Mean linear intercept,  $\bar{l}$ , of hard phase particles viz. WC, TiC/TiN/Ti(C,N) in various powder premixes ( n is the number of intercepts from which each value of  $\bar{l}$  was calculated and  $\sigma$  is the standard deviation)

Alloy	WC			Cubic phase (TiC/TiN/Ti(C,N))		
	n	$\bar{l}, \mu\text{m}$	$\sigma$	n	$\bar{l}, \mu\text{m}$	$\sigma$
A	283	1.55	1.35	-	-	-
B	302	1.52	1.40	251	1.49	1.47
C	311	1.55	1.35	233	1.52	1.42
D	297	1.55	1.35	287	1.58	1.44
E	232	1.55	1.35	312	1.51	1.40
F	267	1.51	1.37	198	1.50	1.35
G	284	1.54	1.48	215	1.53	1.37
H	327	1.50	1.37	263	1.52	1.48
I	295	1.52	1.37	282	1.50	1.35
J	308	1.54	1.35	297	1.55	1.37

Table 3.2 : Mean linear intercept ' $\bar{l}$ ' of WC, contiguity 'C' of carbide phase and mean binder free path ' $\bar{\lambda}$ ' of alloy A sintered at 1425°C in hydrogen and vacuum respectively.

Sintering atmosphere	$\bar{l}, \mu\text{m}$	$\bar{\lambda}, \mu\text{m}$	C
Hydrogen	1.33	0.337	0.61
Vacuum	1.31	0.323	0.58

Table 3.3 : Mechanical and magnetic properties of alloy A sintered in hydrogen and vacuum respectively at 1425°C

Sintering atmosphere	Mechanical properties			Magnetic properties	
	Hardness, HV 30	TRS, MPa	Indentation fracture toughness, MPam <sup>1/2</sup>	Coercivity, oersted	Magnetic saturation, Gauss
Hydrogen	1370	2320	11.20	144	228
Vacuum	1280	2380	11.87	142	236

**Table 3.5 : Thermal shock resistance ( $\Delta T$ ) of various grades of cemented carbides**

Alloy	Consolidation parameters	$\Delta T$
A	Liquid phase sintered at $1425^{\circ}\text{C}$ in $\text{H}_2$	800
B	Liquid phase sintered at $1475^{\circ}\text{C}$ in $\text{H}_2$	550
C	Liquid phase sintered at $1475^{\circ}\text{C}$ in $\text{H}_2$	650
D	Liquid phase sintered at $1475^{\circ}\text{C}$ in $\text{H}_2$	650
E	Liquid phase sintered at $1475^{\circ}\text{C}$ in $\text{H}_2\text{-N}_2$ followed by HIP'ing at $1450^{\circ}\text{C}$ .	750
G	Liquid phase sintered at $1475^{\circ}\text{C}$ in $\text{H}_2\text{-N}_2$ followed by HIP'ing at $1450^{\circ}\text{C}$ .	700
H	Liquid phase sintered at $1475^{\circ}\text{C}$ in $\text{H}_2\text{-N}_2$ followed by HIP'ing at $1400^{\circ}\text{C}$ .	700
I	Liquid phase sintered at $1475^{\circ}\text{C}$ in $\text{H}_2\text{-N}_2$ followed by HIP'ing at $1400^{\circ}\text{C}$ .	650
J	Liquid phase sintered at $1500^{\circ}\text{C}$ in $\text{H}_2\text{-N}_2$ followed by HIP'ing at $1400^{\circ}\text{C}$ .	700

Table 3.6 : Sintered density (% Th. density) of alloys A, B, C and D after H<sub>2</sub> sintering.

Alloy	Sintered density (% Th. density)			
	Sintering temperature, °C			
	1425	1450	1475	1500
A	100	—	—	—
B	—	98.7	100	100
C	—	99.6	100	100
D	—	99.8	100	100

Table 3.7 : Mean linear intercept length,  $\bar{l}$ , of hexagonal and cubic phases in various cemented carbides (n is the number of intercepts from which each value of  $\bar{l}$  was calculated and  $\sigma$  is the standard deviation).

Alloy	Sintering atmosphere	HIP'ped at, °C	Hexagonal phase, WC			Cubic phase TiC/TiN/Ti(C,N)		
			n	$\bar{l}$ , $\mu\text{m}$	$\sigma$	n	$\bar{l}$ , $\mu\text{m}$	$\sigma$
A	H <sub>2</sub>	-	383	1.33	0.514	-	-	-
	Vacuum	-	332	1.30	0.507	-	-	-
B	H <sub>2</sub>	-	337	1.40	0.595	191	2.84	1.15
	Vacuum	-	298	1.43	0.478	207	2.78	1.03
C	H <sub>2</sub>	-	321	1.43	0.637	178	2.53	0.946
	Vacuum	-	312	1.47	0.598	213	2.48	0.915
D	H <sub>2</sub>	-	332	1.22	0.537	216	2.00	0.344
	Vacuum	-	283	1.24	0.513	239	2.01	0.357
E	H <sub>2</sub>	-	277	1.28	1.27	187	1.32	1.22
	H <sub>2</sub> -N <sub>2</sub>	-	305	1.30	1.28	212	1.38	1.23
	H <sub>2</sub> -N <sub>2</sub>	1450	334	1.46	1.30	178	1.39	1.23
F	H <sub>2</sub>	-	293	1.24	1.25	243	1.34	1.20
	H <sub>2</sub> -N <sub>2</sub>	-	286	1.37	1.40	237	1.38	1.23
G	H <sub>2</sub> -N <sub>2</sub>	-	321	1.30	1.24	262	1.27	1.23
	H <sub>2</sub> -N <sub>2</sub>	1450	291	1.39	1.32	183	1.36	1.26
H	H <sub>2</sub> -N <sub>2</sub>	-	176	1.27	1.26	278	1.32	1.22
	H <sub>2</sub> -N <sub>2</sub>	1400	261	1.28	1.26	193	1.31	1.22
I	H <sub>2</sub> -N <sub>2</sub>	-	284	1.27	1.26	197	1.32	1.22
	H <sub>2</sub> -N <sub>2</sub>	1400	267	1.26	1.26	163	1.32	1.22
J	H <sub>2</sub> -N <sub>2</sub>	-	249	1.26	1.26	171	1.28	1.21
	H <sub>2</sub> -N <sub>2</sub>	1400	221	1.26	1.26	187	1.32	1.21

Table 3.8 : Percent sintered porosity in various grades of cemented carbides after liquid phase sintering and HIP'ing.

Alloy	Percent sintered porosity		
	After liquid phase sintering in $H_2-N_2$ mixture	Liquid phase sintered in $H_2-N_2$ mixture followed by HIP'ing at	
		1400°C	1450°C
E	3.64	0.41	0.15
G	3.25	0.30	0.10
H	2.39	0.06	-
I	3.36	0.15	-
*J	3.17	0.08	-

\*sintered at 1500°C and the rest of the alloys sintered at 1475°C

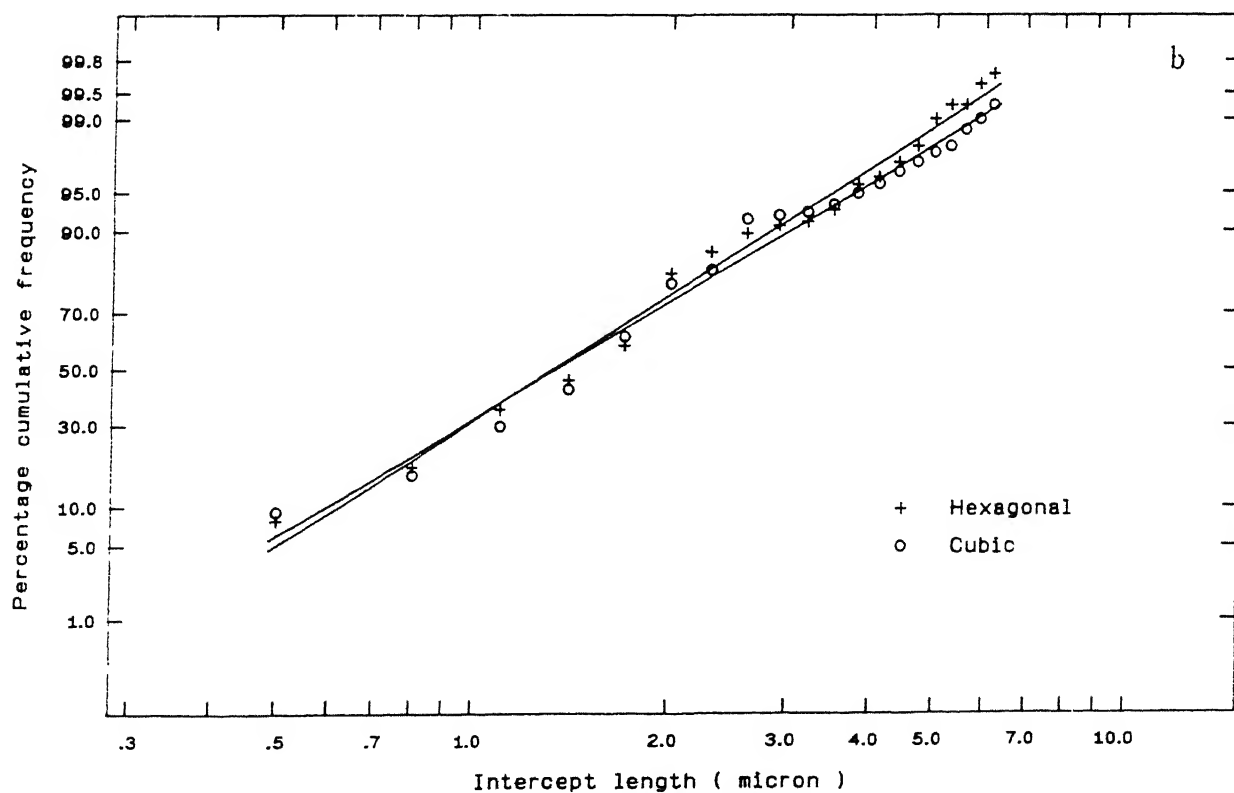
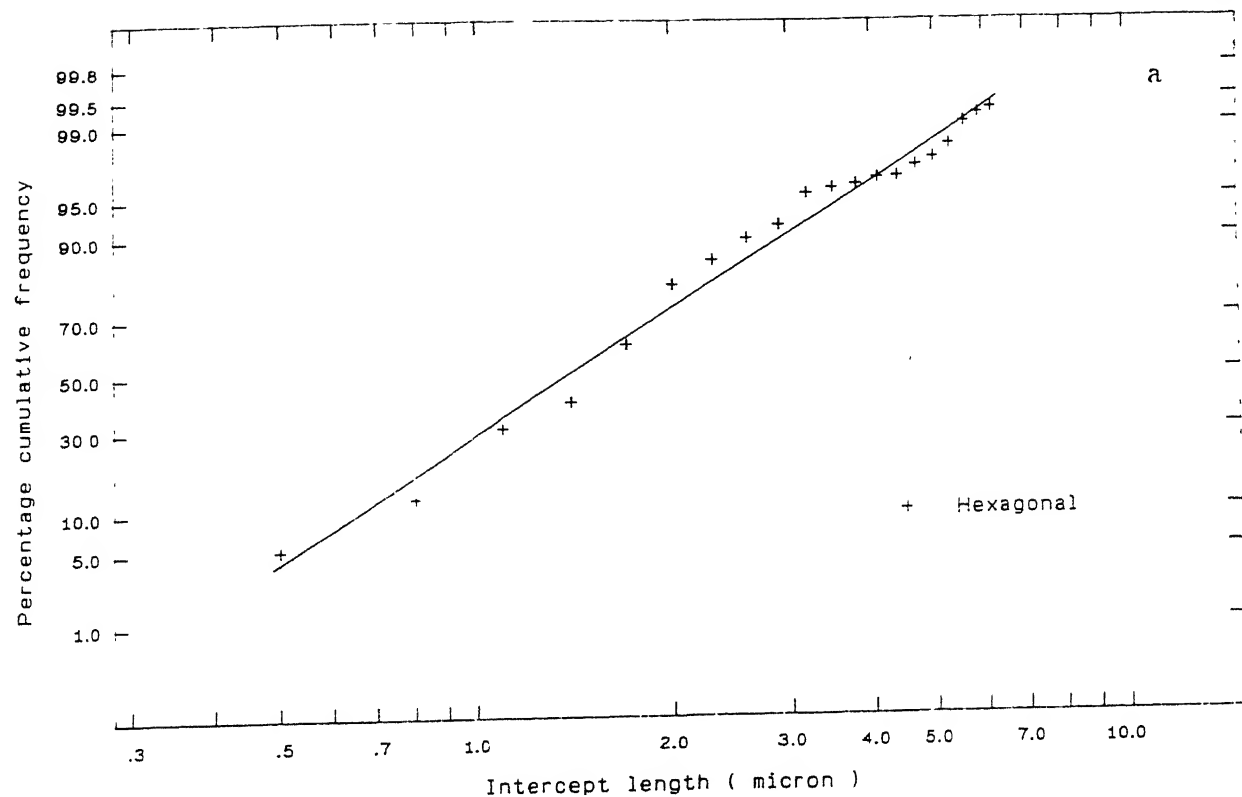


Figure 3.1 Cumulative frequency distribution of WC and cubic carbide (TiC) intercept lengths in the powder premix of alloy A (a) and alloy B (b) after milling.

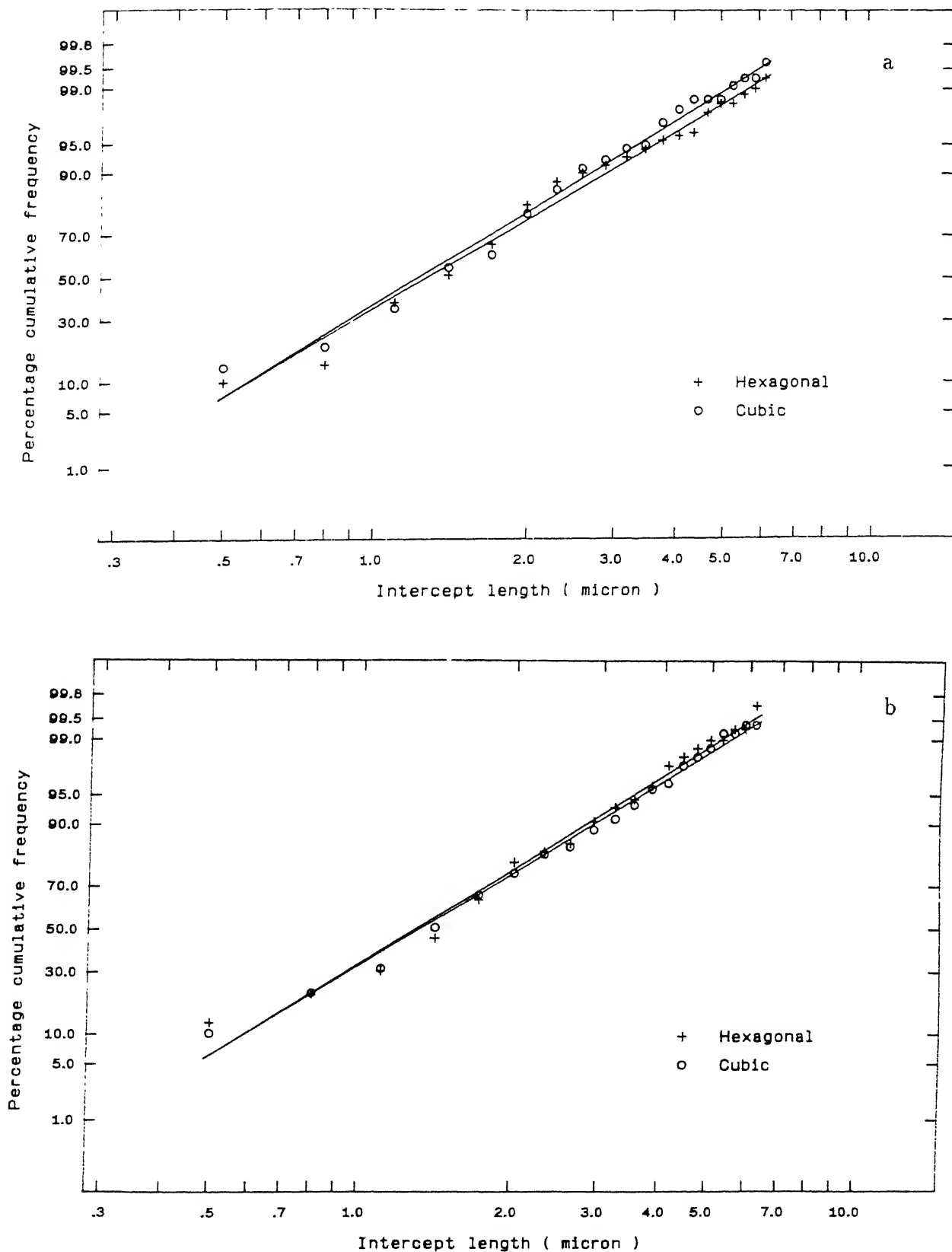


Figure 3.2 Cumulative frequency distribution of WC and cubic carbides ( $\text{TiC}/\text{Mo}_2\text{C}$ ) intercept lengths in the powder premix of alloy C (a) and alloy D (b) after milling.

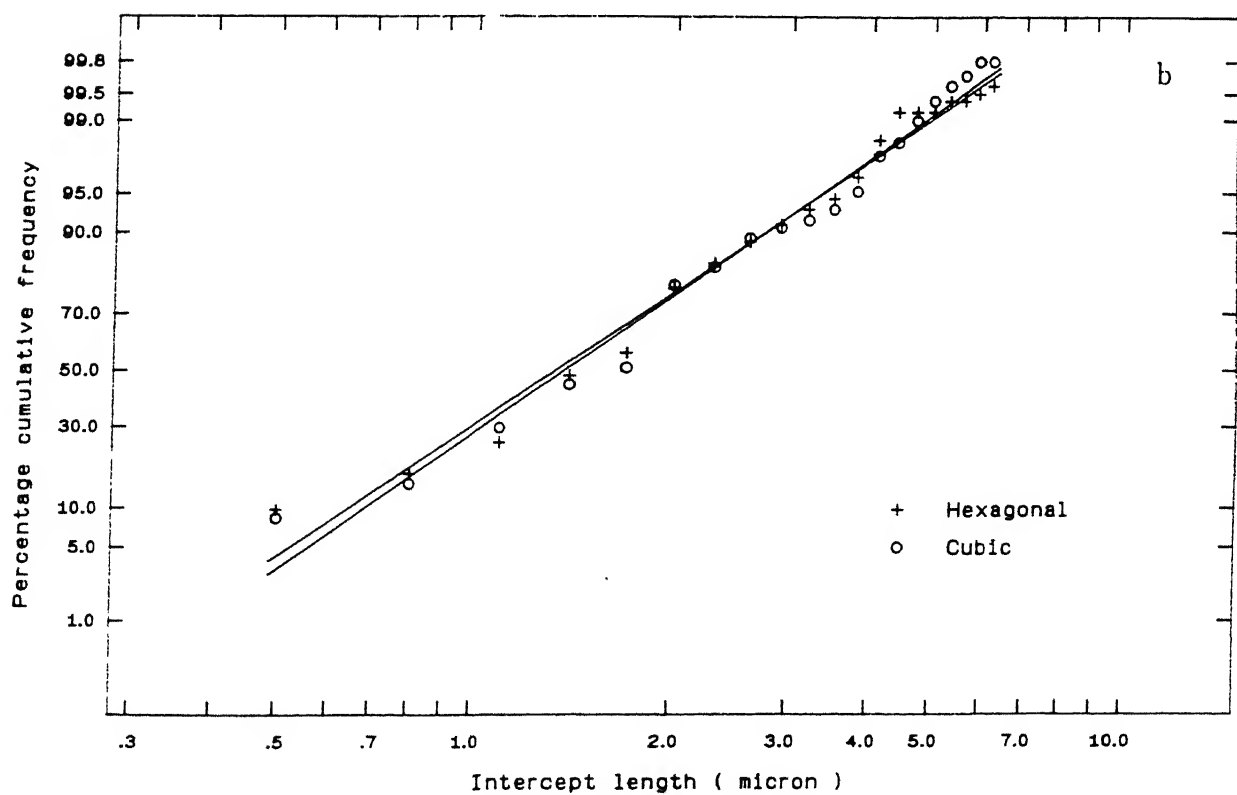
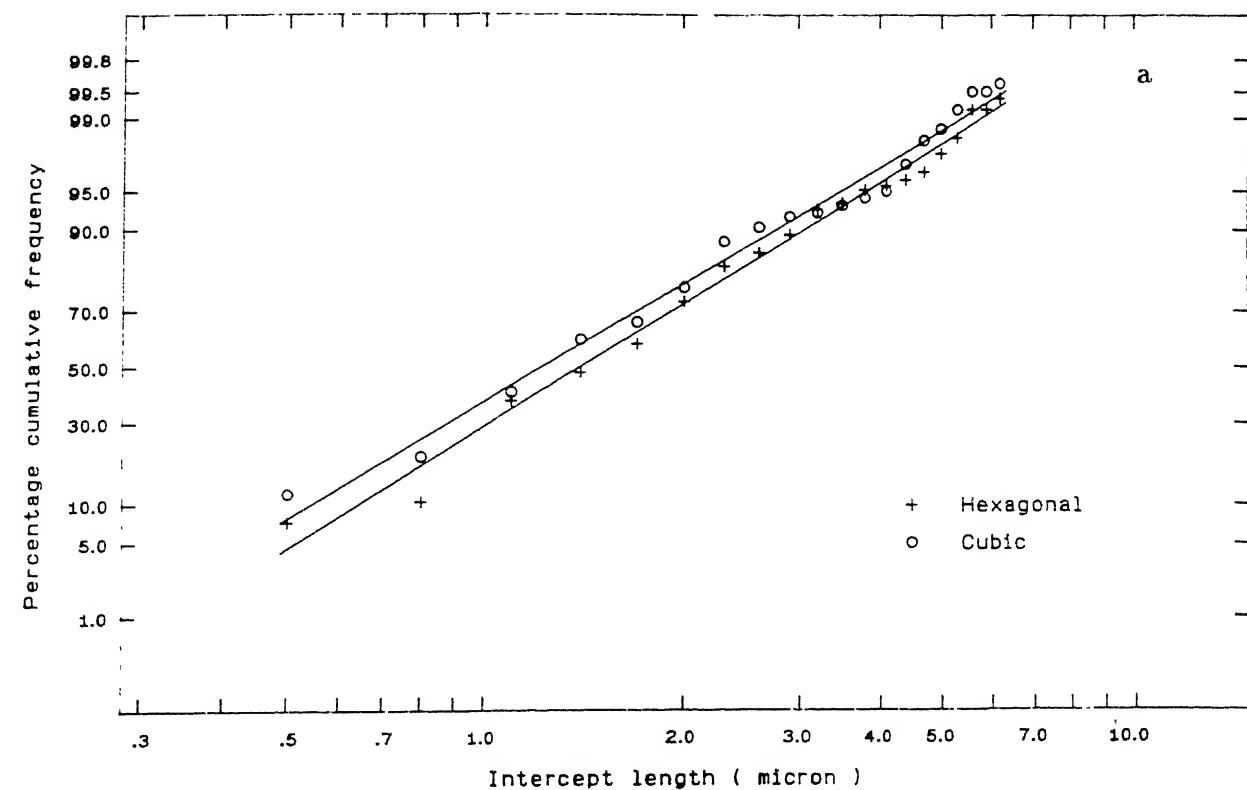


Figure 3.3 Cumulative frequency distribution of WC and cubic phase (TiN) intercept lengths in the powder premix of alloy E (a) and alloy F (b) after milling.

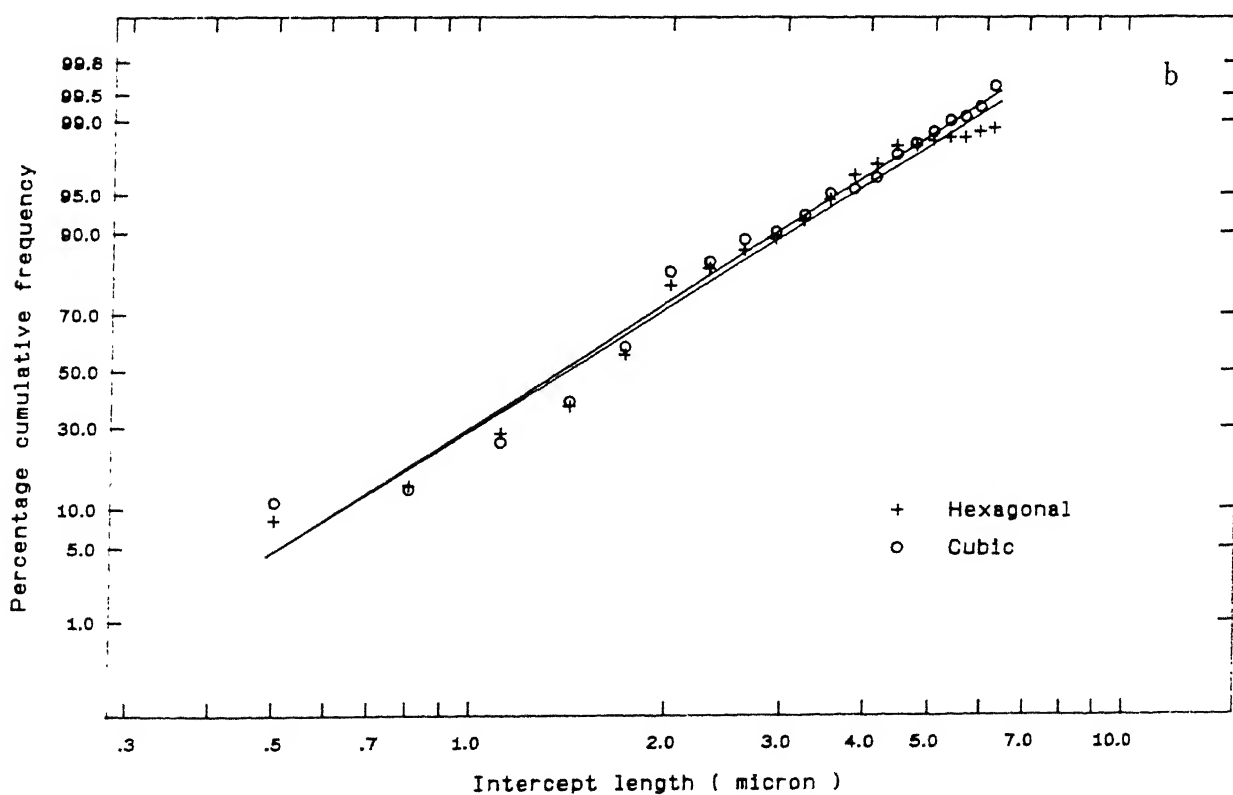
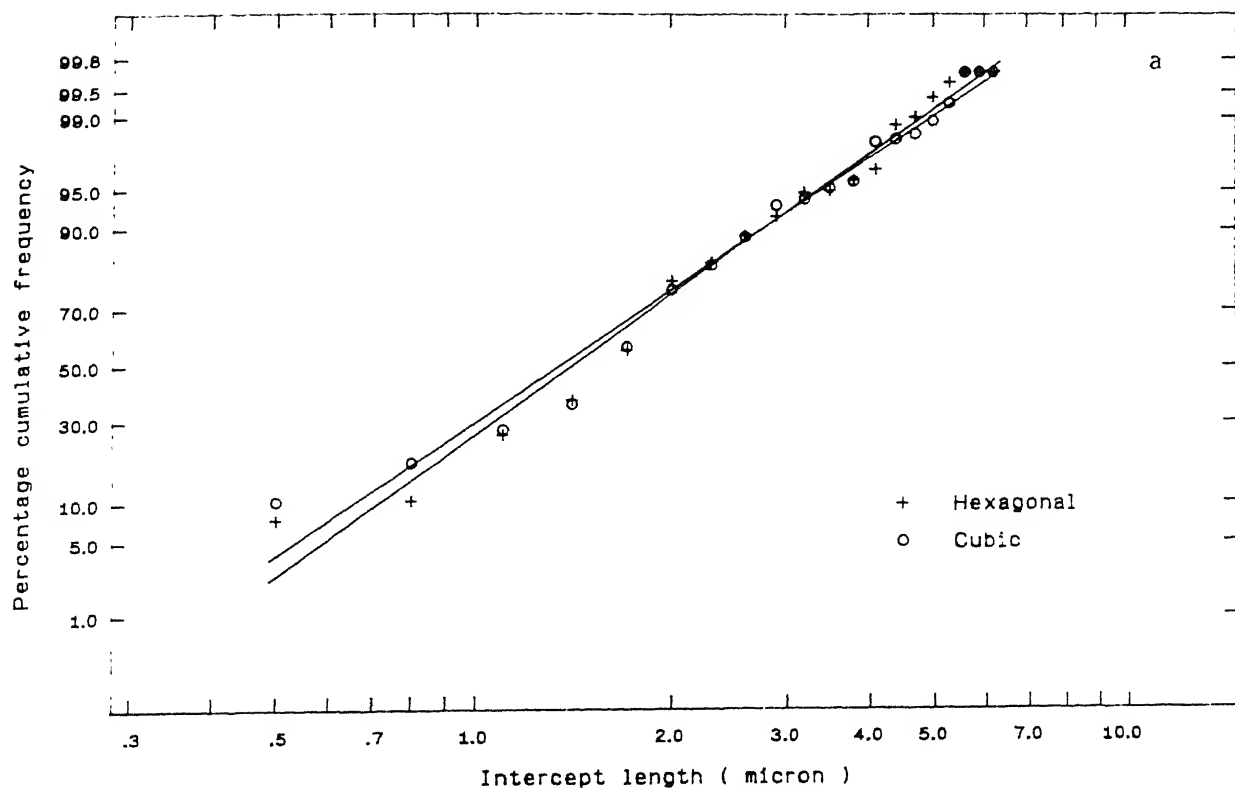


Figure 3.4 Cumulative frequency distribution of WC and cubic phase (TiN/Ti(C,N)/Mo<sub>2</sub>C) intercept lengths in the powder premix of alloy G (a) and alloy H (b) after

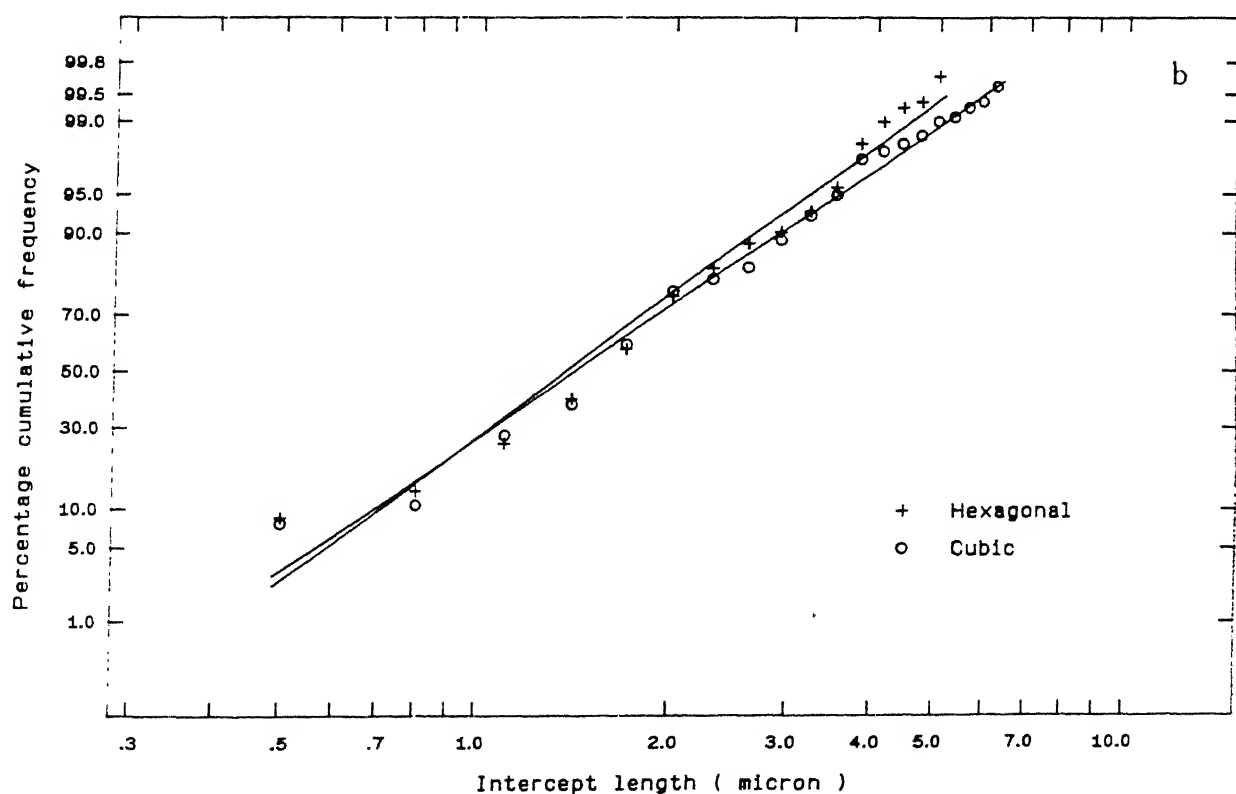
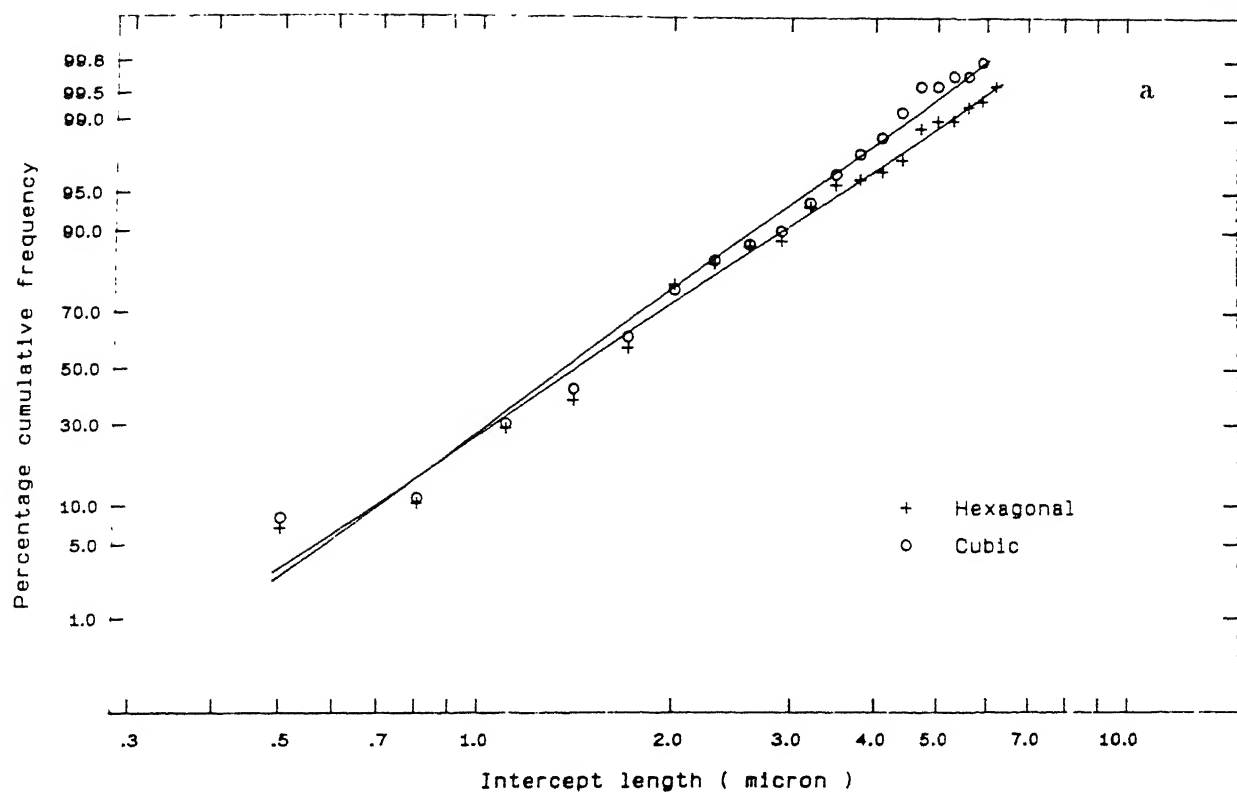


Figure 3.5 Cumulative frequency distribution of WC and cubic phase ( $\text{Ti}(\text{C},\text{N})/\text{Mo}_2\text{C}$ ) intercept lengths in the powder premix of alloy I (a) and alloy J (b) after milling.

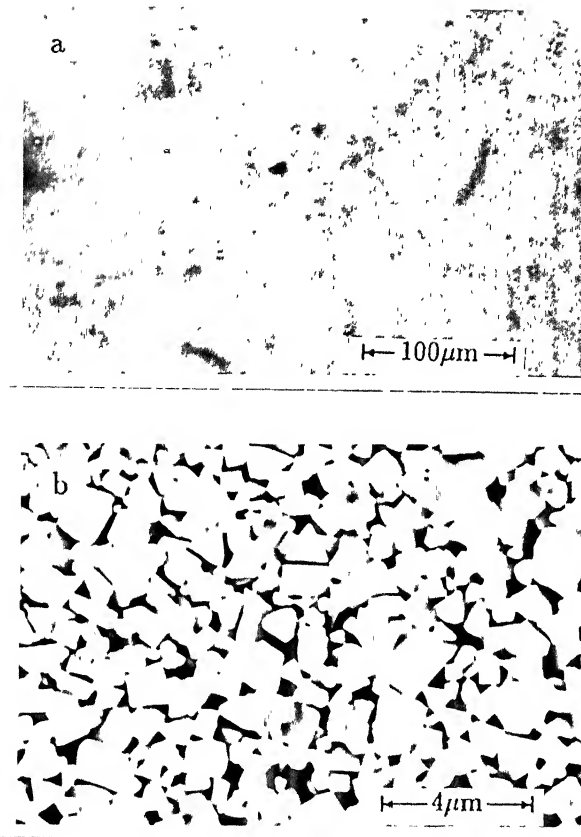


Figure 3.6 Pore morphology and distribution (a) and SEM microstructure (b) of alloy A sintered at 1425°C in H<sub>2</sub>.

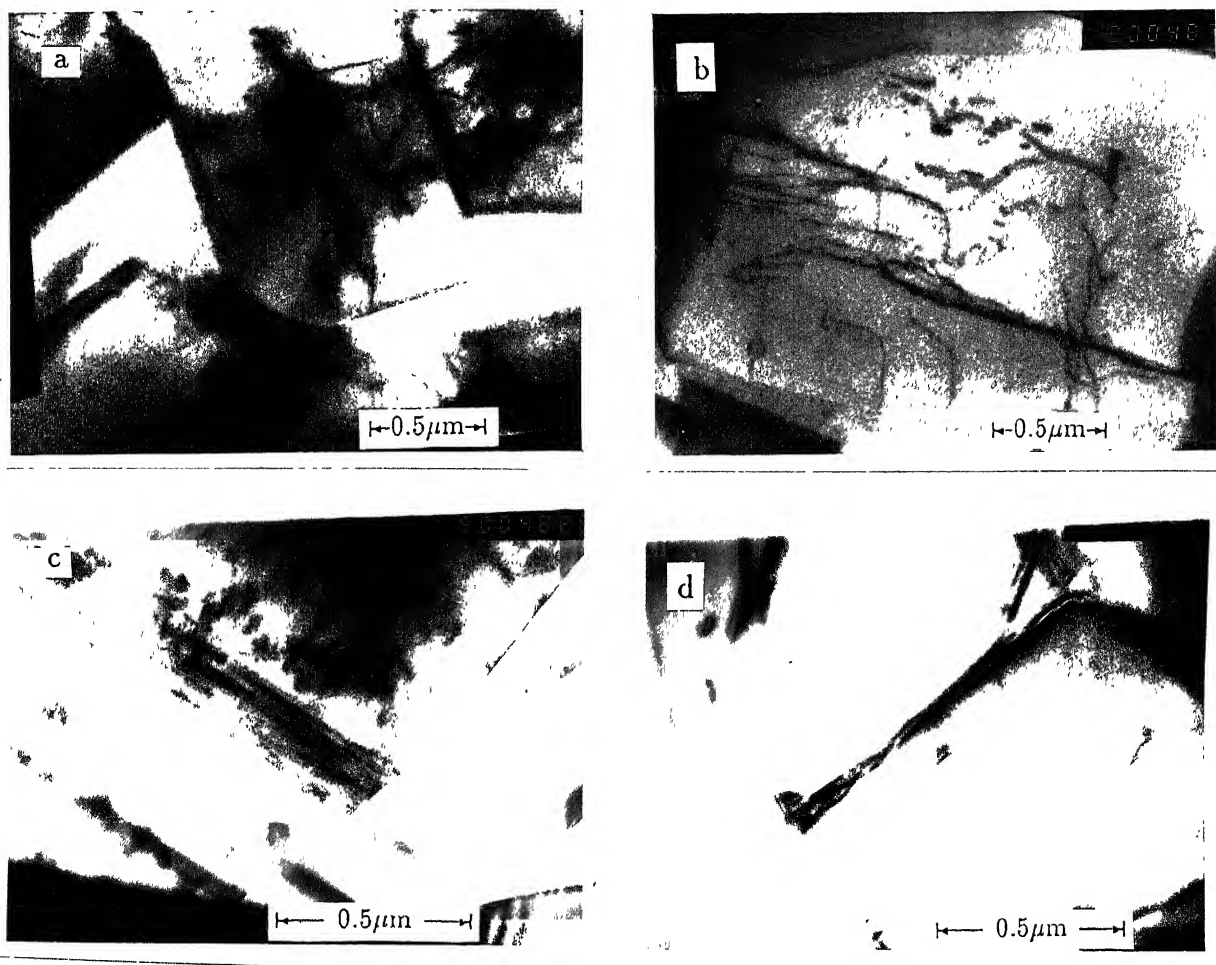


Figure 3.7 TEM micrographs of alloy A (sintered at 1425°C in  $H_2$ ), showing : (a) straight faceted WC grains, (b) dislocations in WC, (c) stacking fault in binder phase and WC/Co interface, and (d) WC/WC interface.

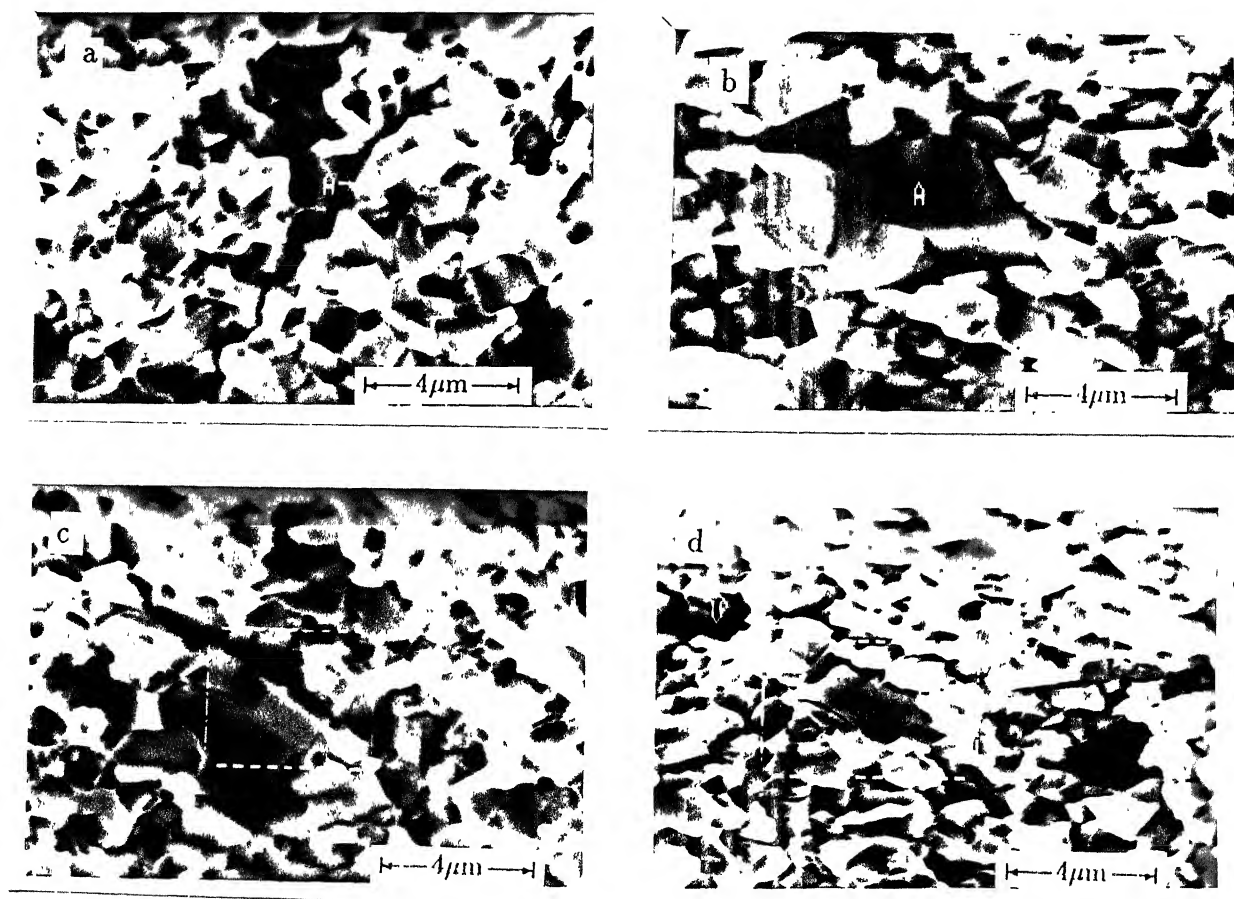


Figure 3.8 SEM fractographs of alloy A (sintered at 1425°C in  $H_2$ ), showing : (a) transgranular fracture of WC particles and ductile fracture of binder, (b) large WC particles with transgranular fracture (A), (c) secondary crack, and (d) de-bonding of interfaces.

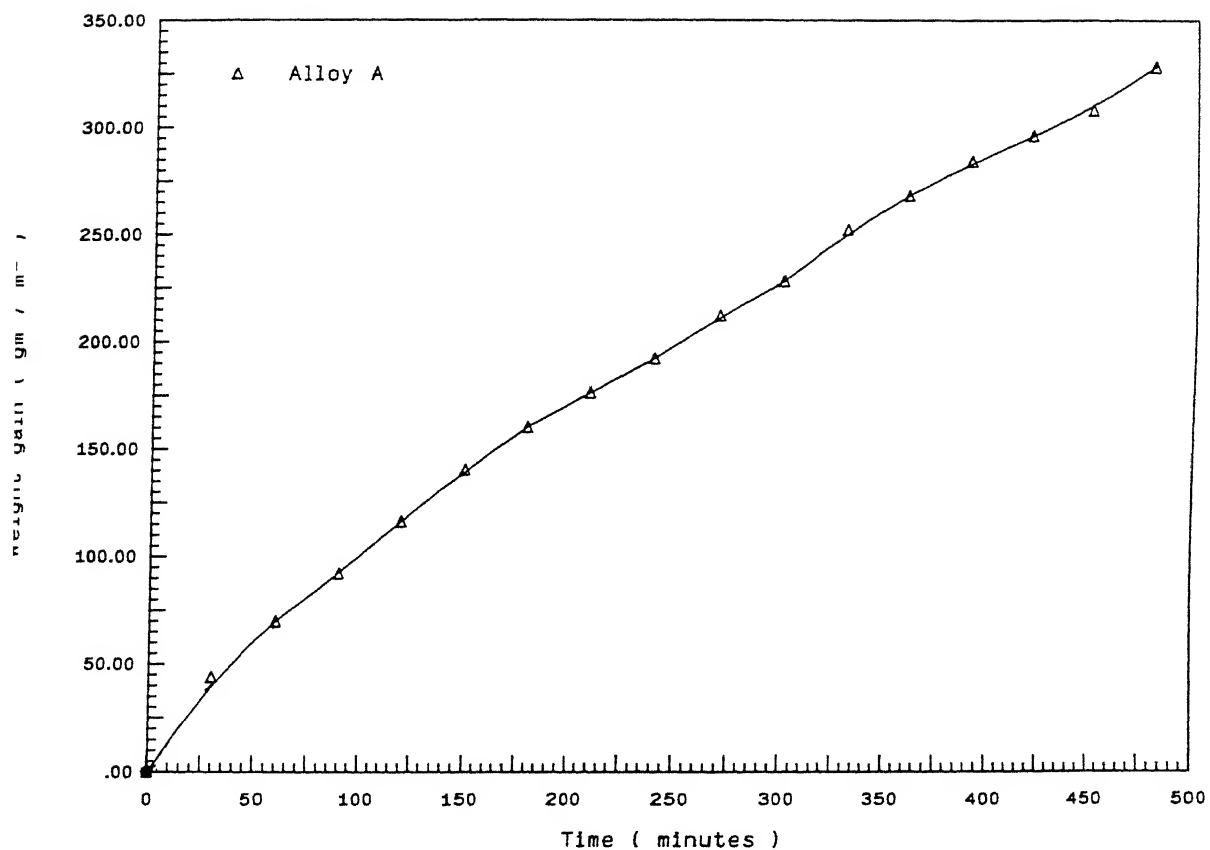


Figure 3.9 Weight gain Vs time plot of alloy A during oxidation in air at 800°C (1073K).

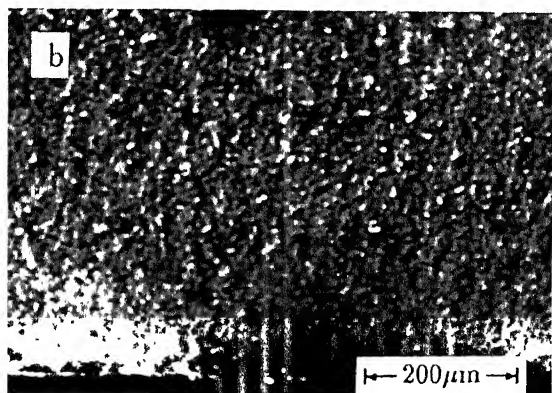
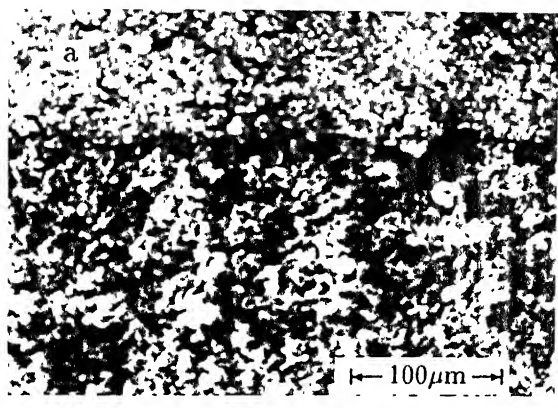


Figure 3.10 SEM micrographs of oxidised surface, showing :  
(a) morphology of oxide layer, and (b) a crack  
extending from metal/oxide interface to oxide/gas  
interface.

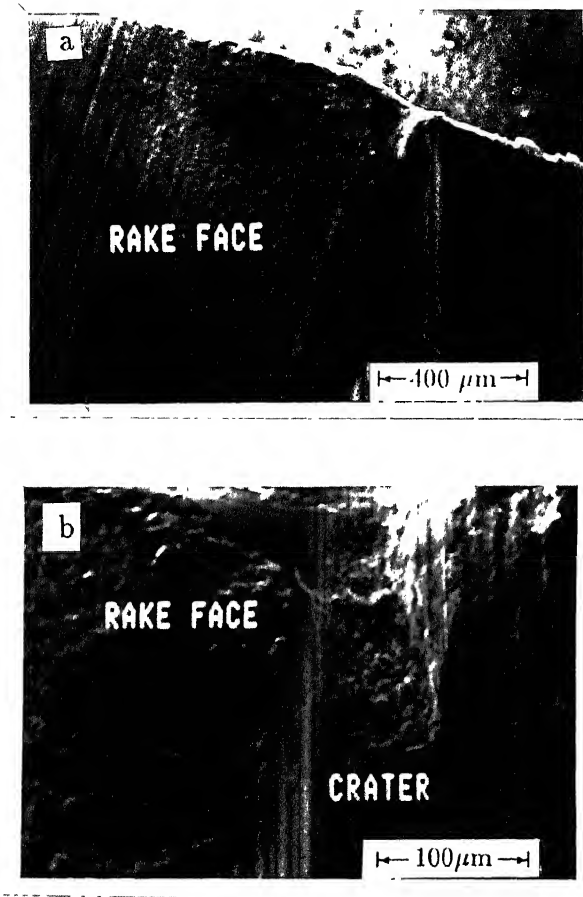


Figure 3.11 SEM pictures of tool made of alloy A, showing :  
(a) worn tool after cutting EN 9 steel at 180 m/min, and (b) cratering on the rake face.

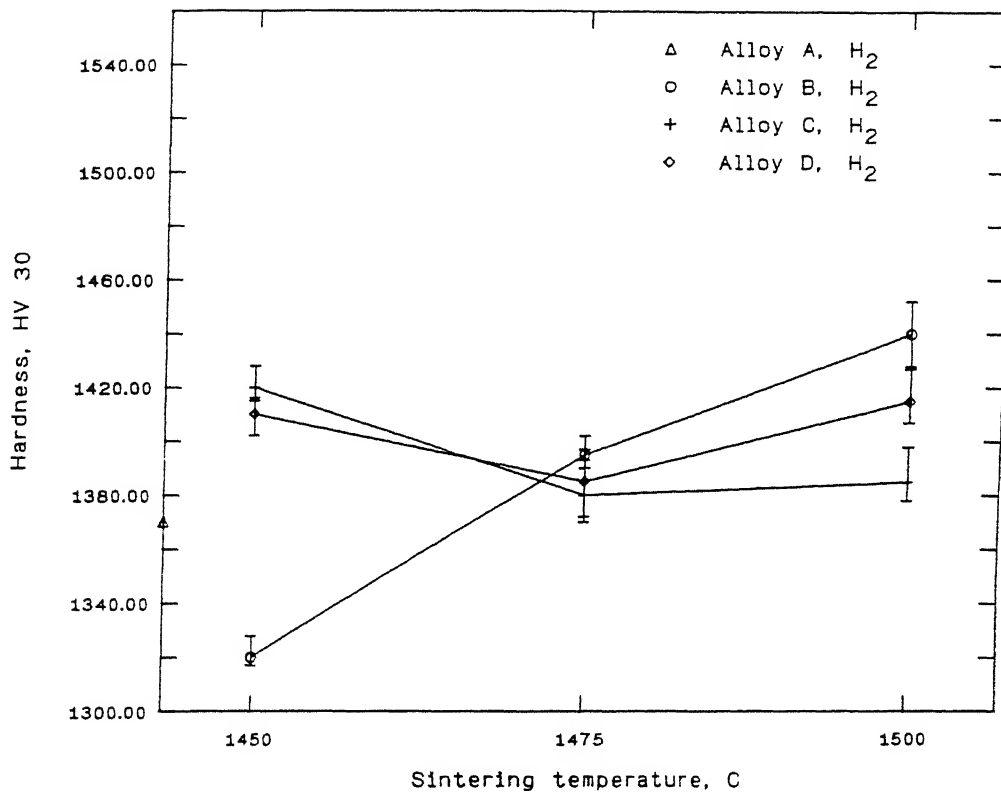


Figure 3.12 Effect of sintering temperature on hardness of alloys A, B, C and D (sintered in H<sub>2</sub>).

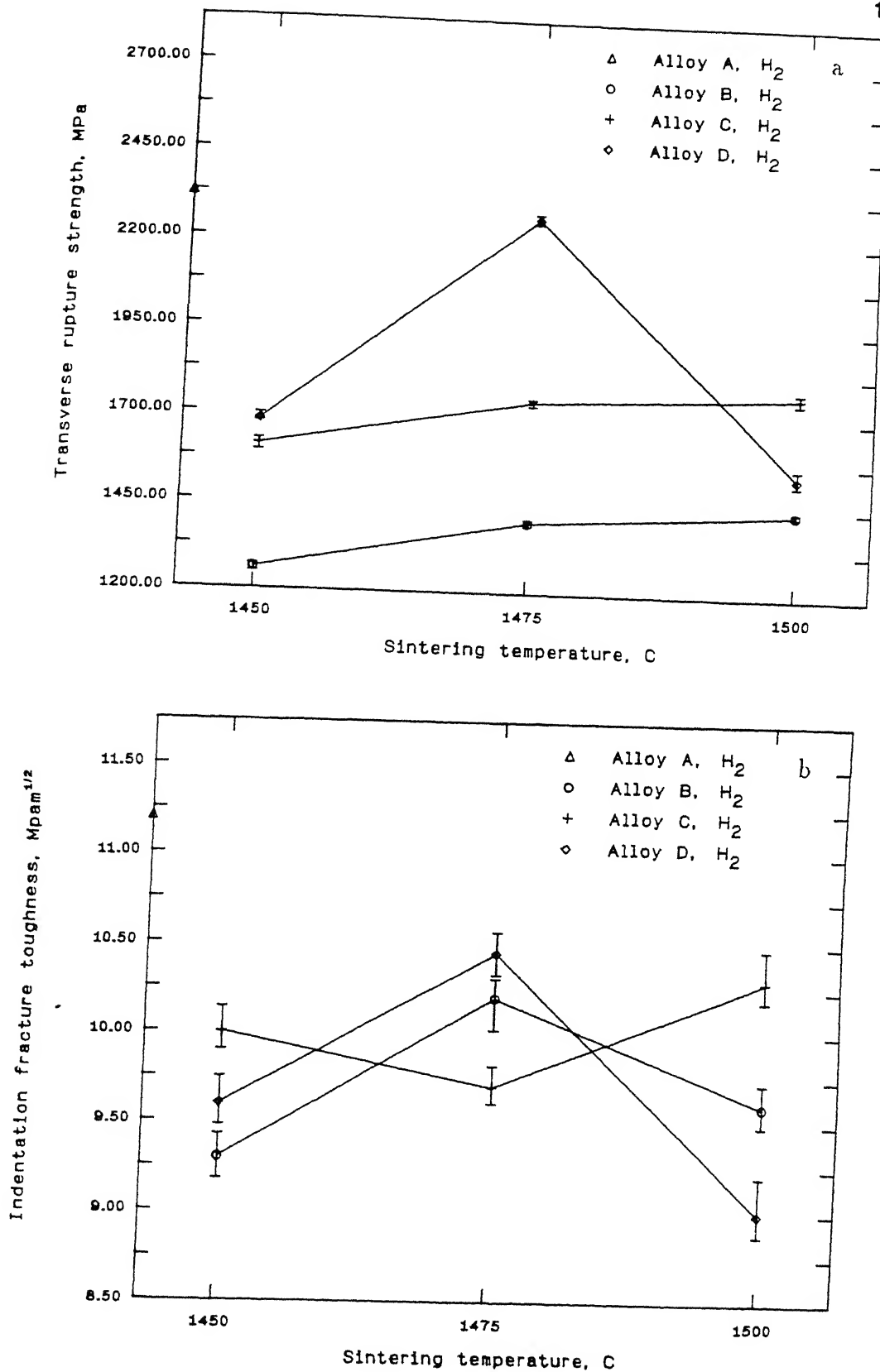


Figure 3.13 Effect of sintering temperature on TRS (a) and indentation fracture toughness (b) of alloys A, B, C and D (sintered in H<sub>2</sub>).

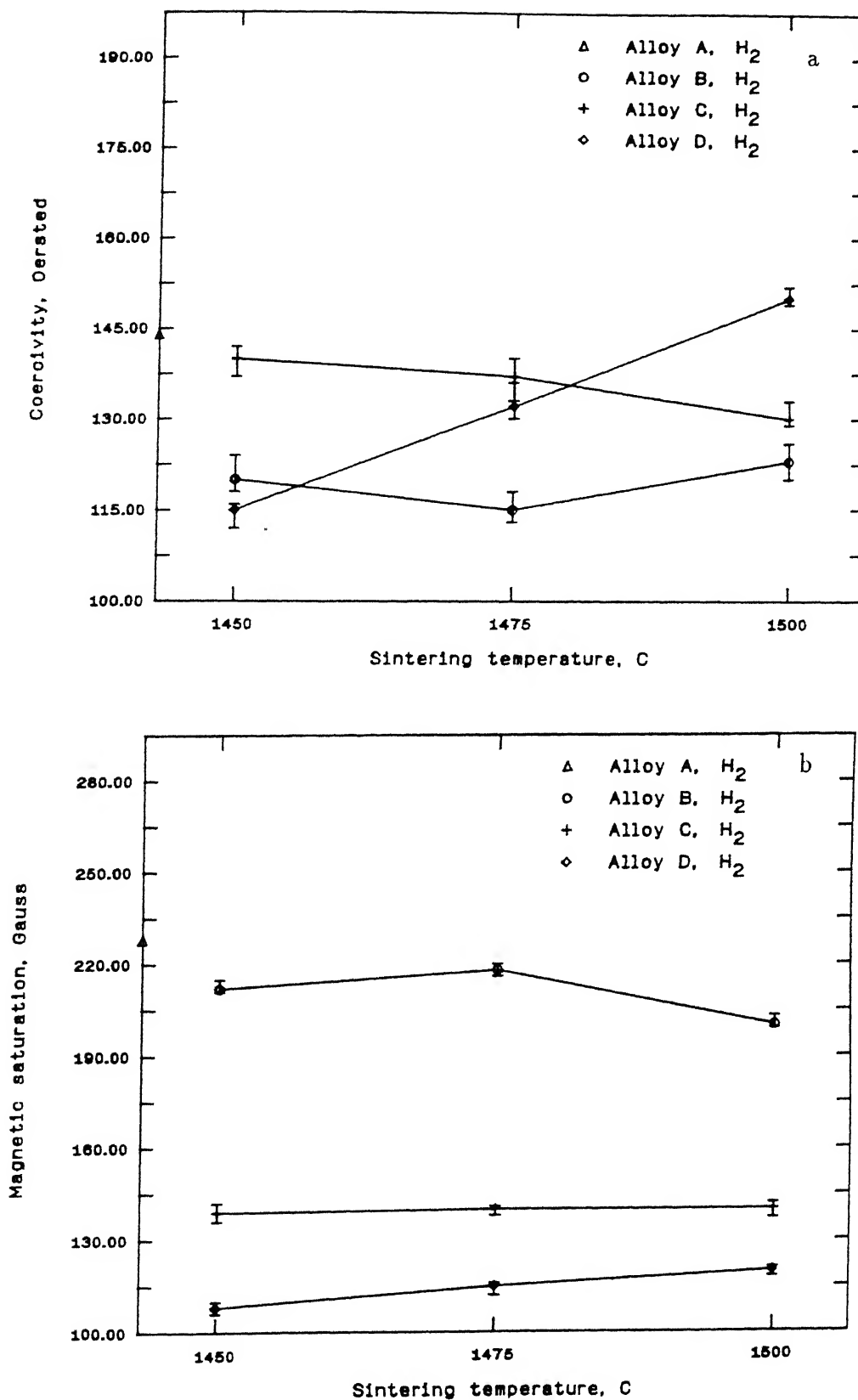


Figure 3.14 Effect of sintering temperature on magnetic properties : (a) coercivity, and (b) magnetic saturation of alloys A, B, C and D (sintered in  $H_2$ ).

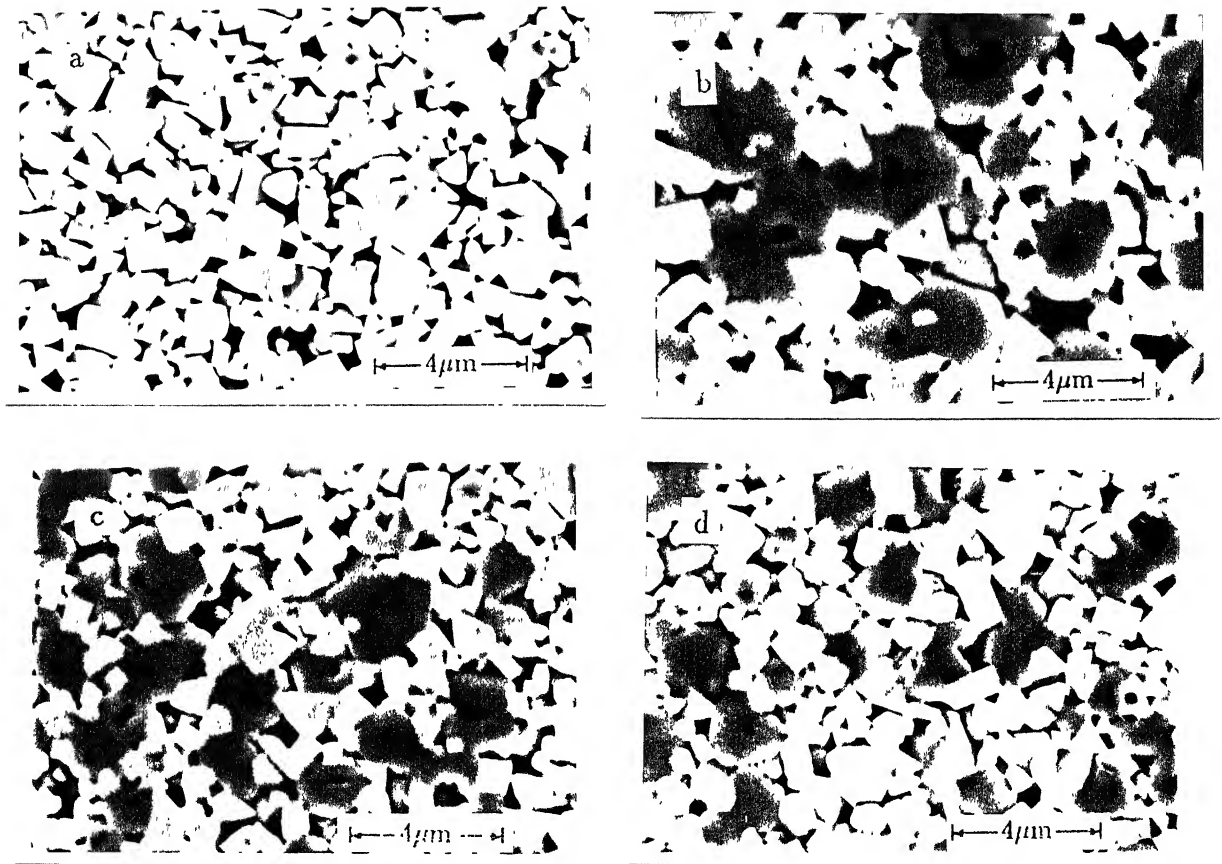


Figure 3.15 SEM micrographs of cemented carbides : (a) alloy A, (b) alloy B, (c) alloy C, and (d) alloy D.

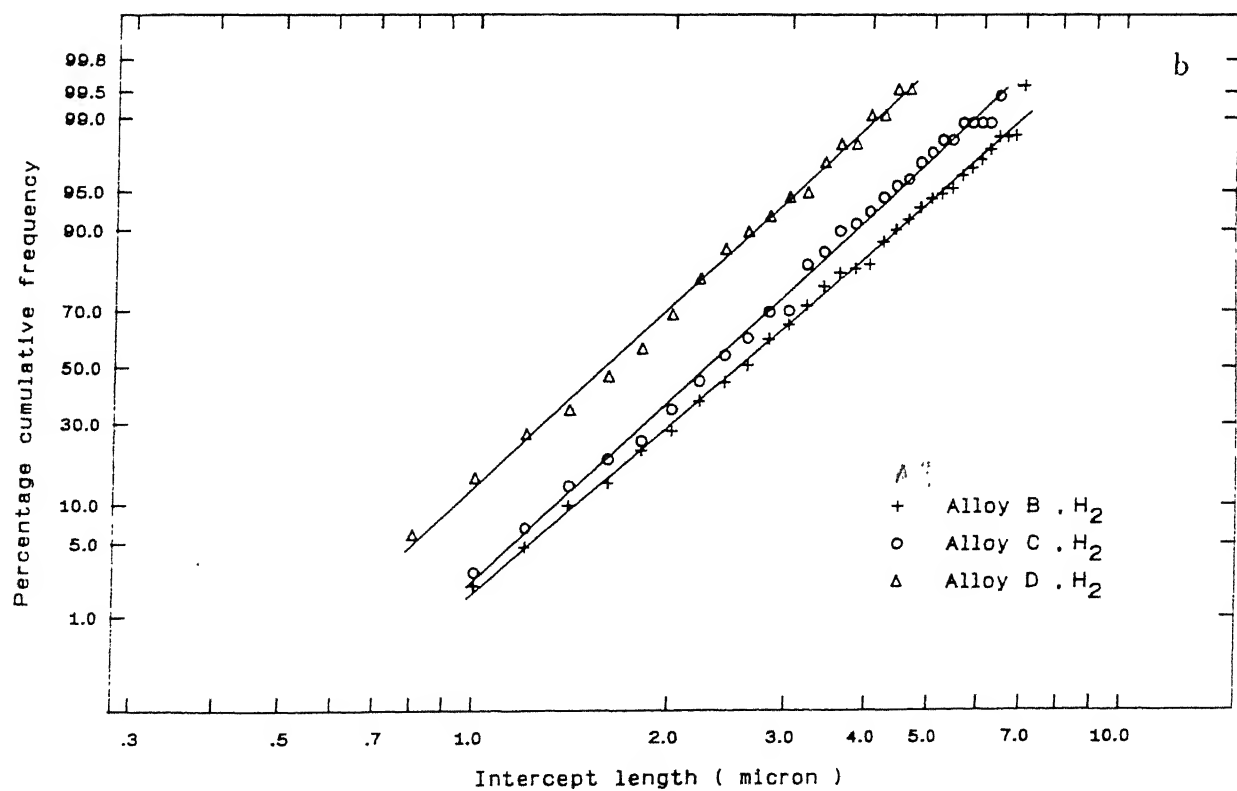
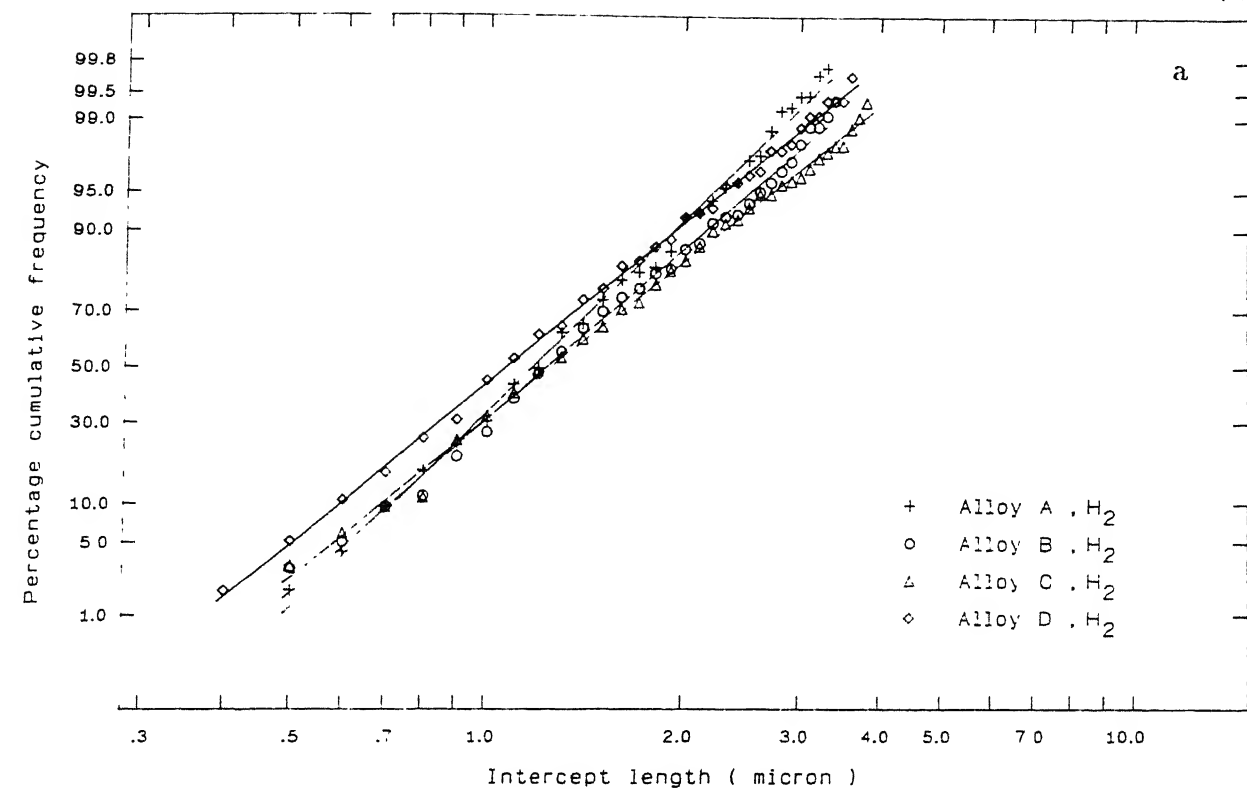


Figure 3.16 Cumulative frequency distribution of (a) WC and (b) cubic carbide (TiC) intercept lengths in alloys A, B, C and D (sintered in H<sub>2</sub>).

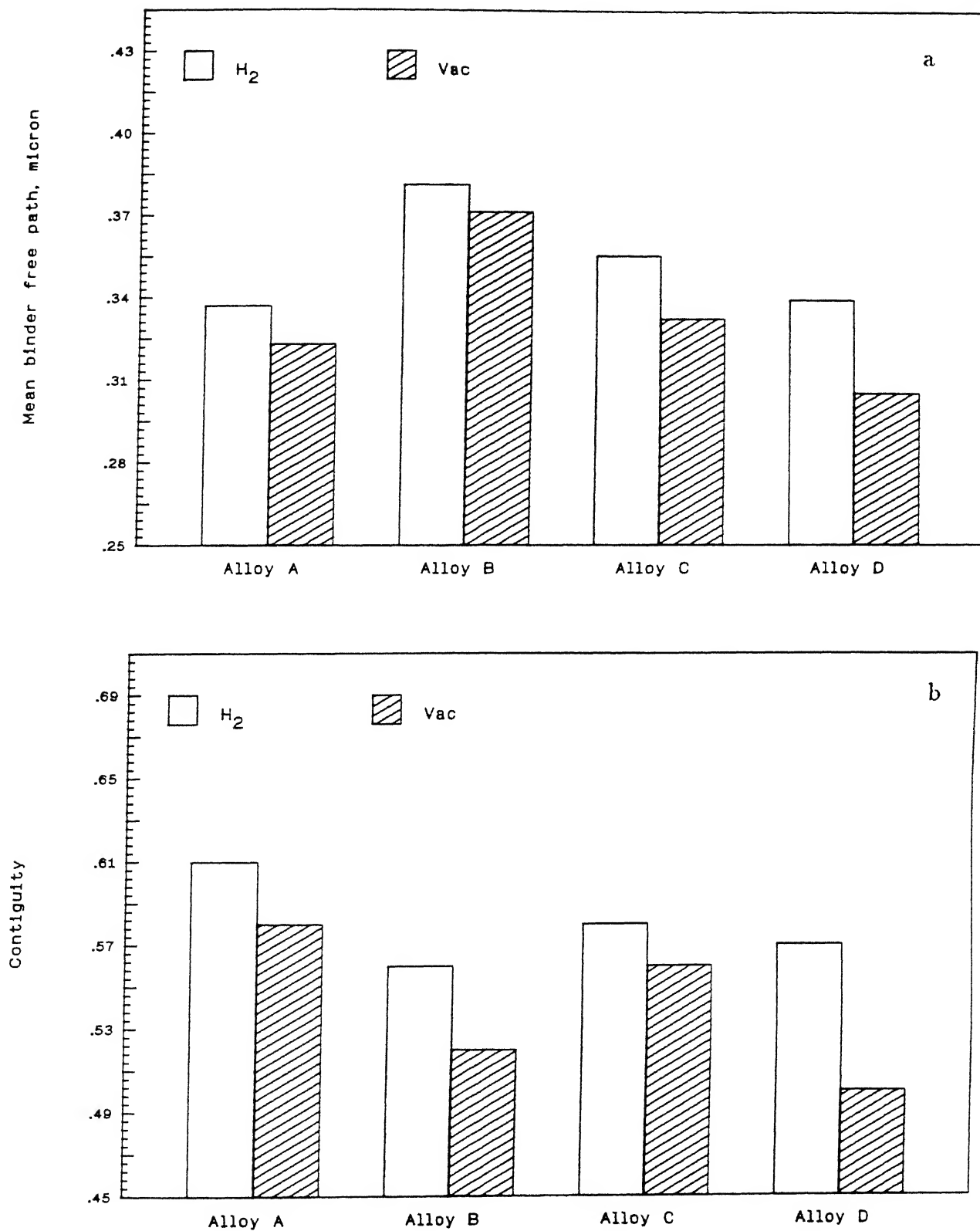


Figure 3.17 Mean binder free path (a) and contiguity (b) of alloys A, B, C and D sintered in  $H_2$  and vacuum respectively.



Figure 3.18 TEM microstructure of alloy B, showing: (a) straight faceted WC and rounded TiC grains and (b) binder with high dislocation density, WC/Co and TiC/Co interfaces, and cobalt inclusions in TiC grain.

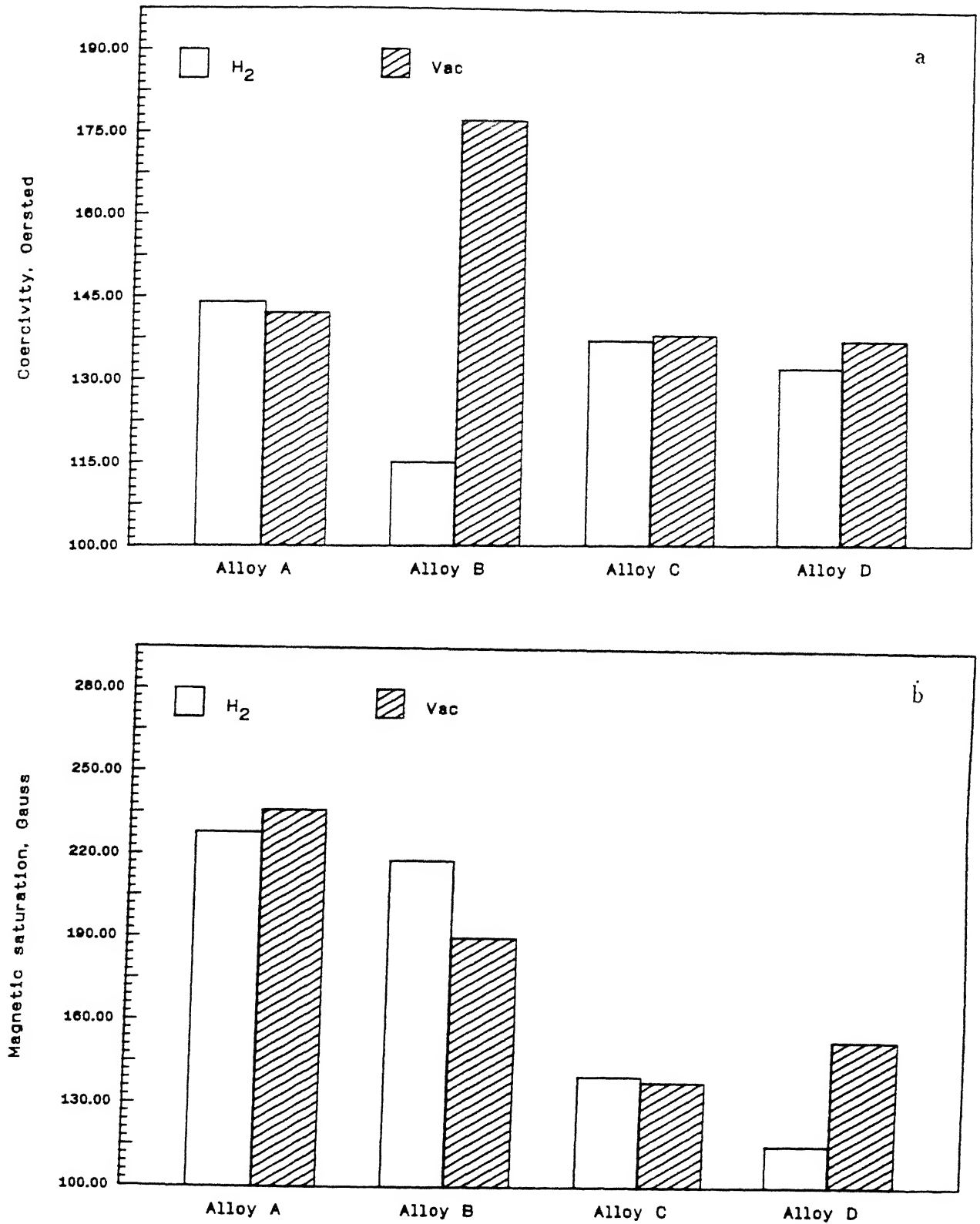


Figure 3.19 Magnetic properties variations of alloys A, B, C and D sintered in  $H_2$  and vacuum respectively :  
(a) coercivity and (b) magnetic saturation.

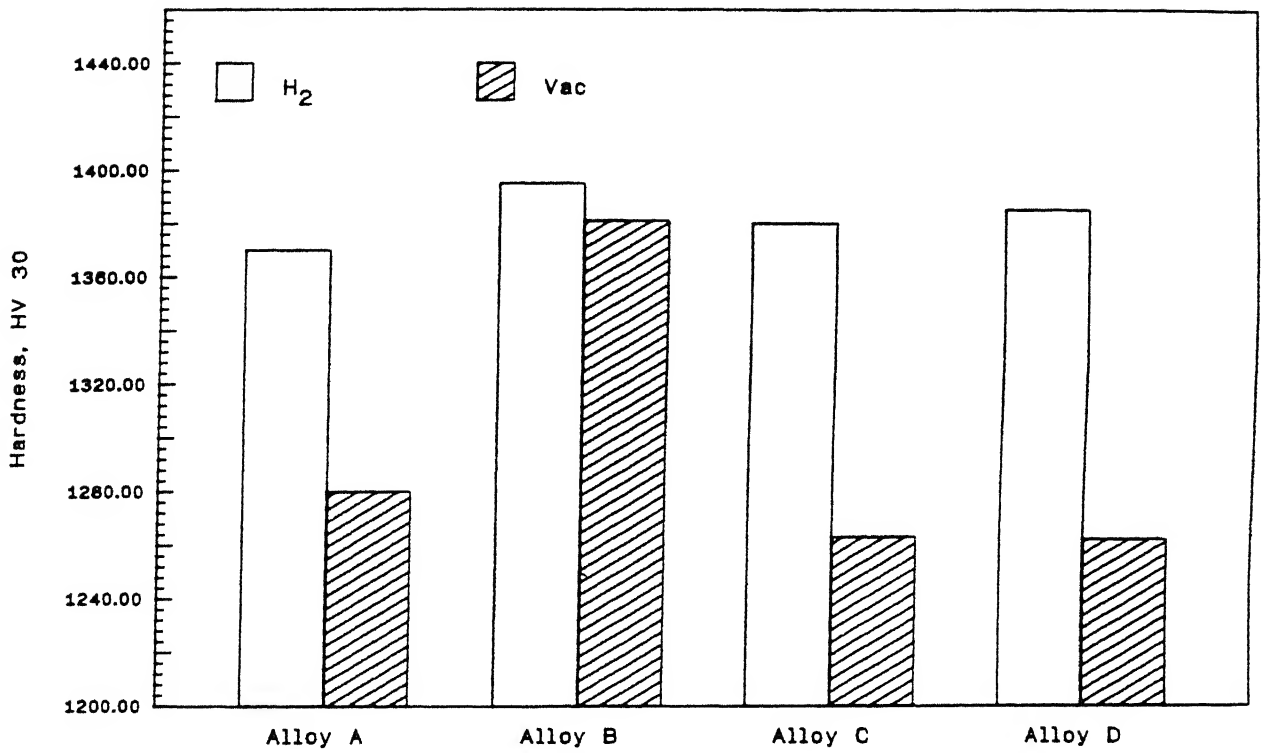


Figure 3.20 Hardness variations of alloys A, B, C and D sintered in  $H_2$  and vacuum respectively.

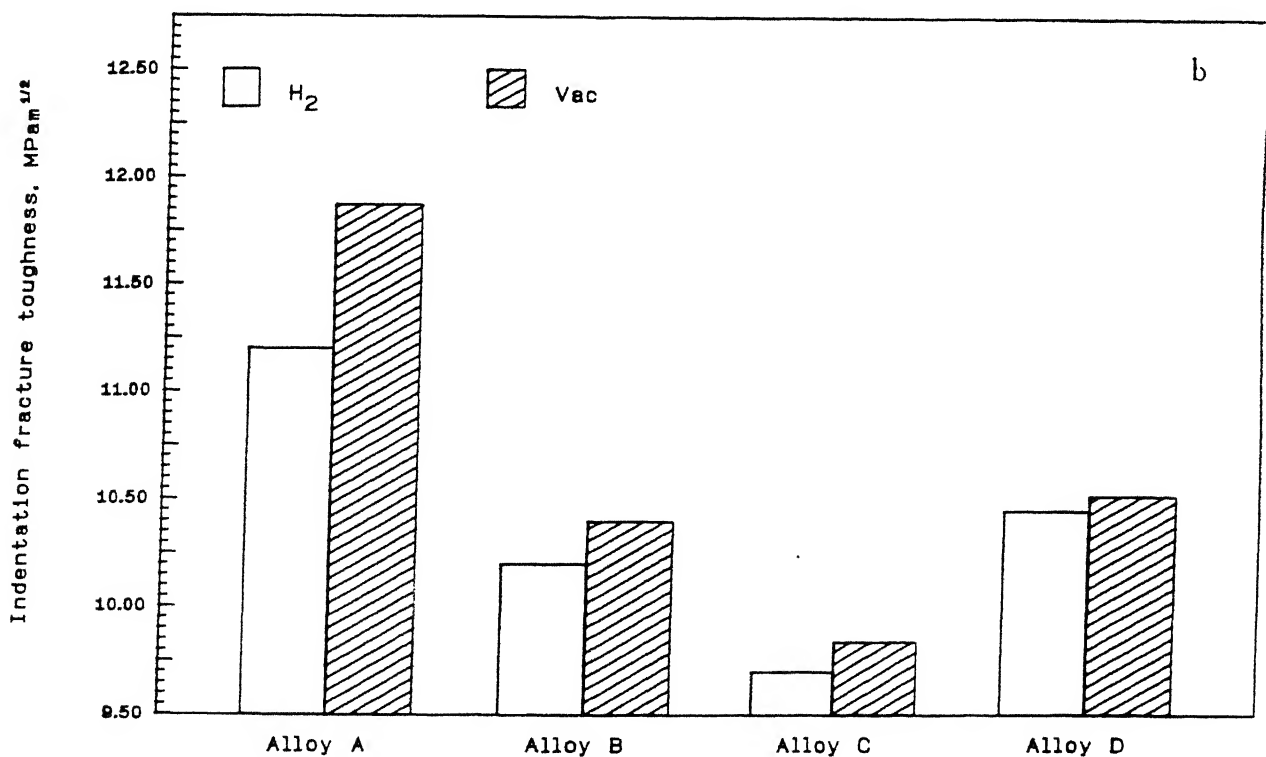
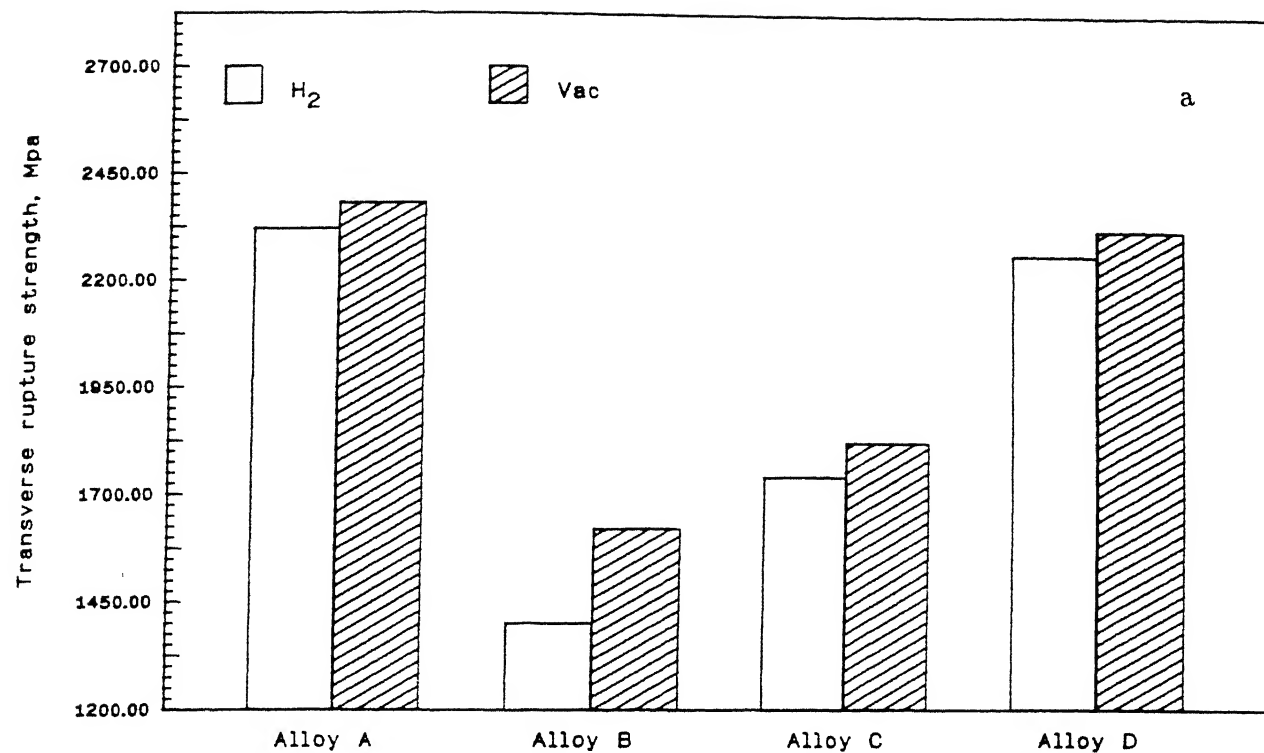


Figure 3.21 TRS (a) and indentation fracture toughness (b) variations of alloys A, B, C and D sintered in  $H_2$  and vacuum respectively.

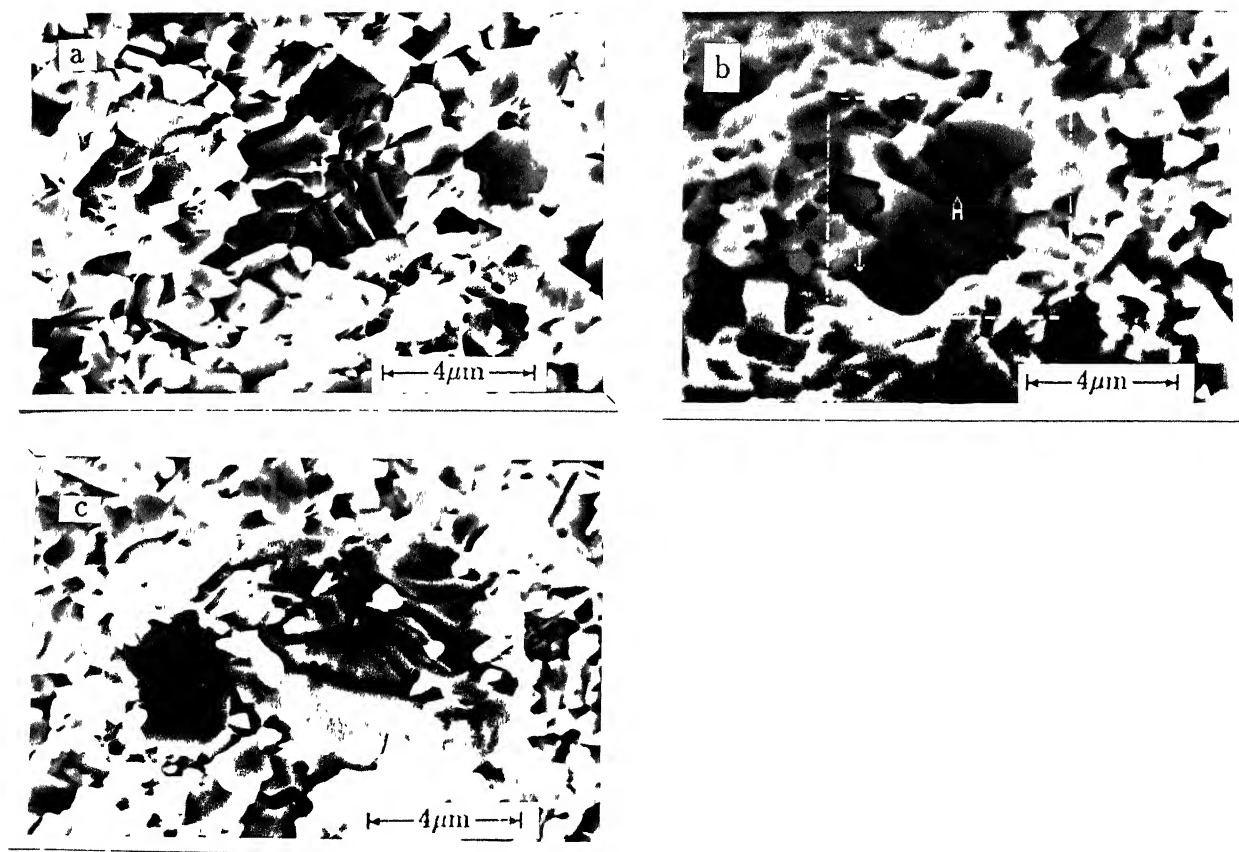


Figure 3.22 SEM fractographs of alloy B (sintered at 1475°C in H<sub>2</sub>), showing : (a) transgranular fracture of carbide grains, (b) transgranular fracture of large TiC grains (A), and (c) interface separation.

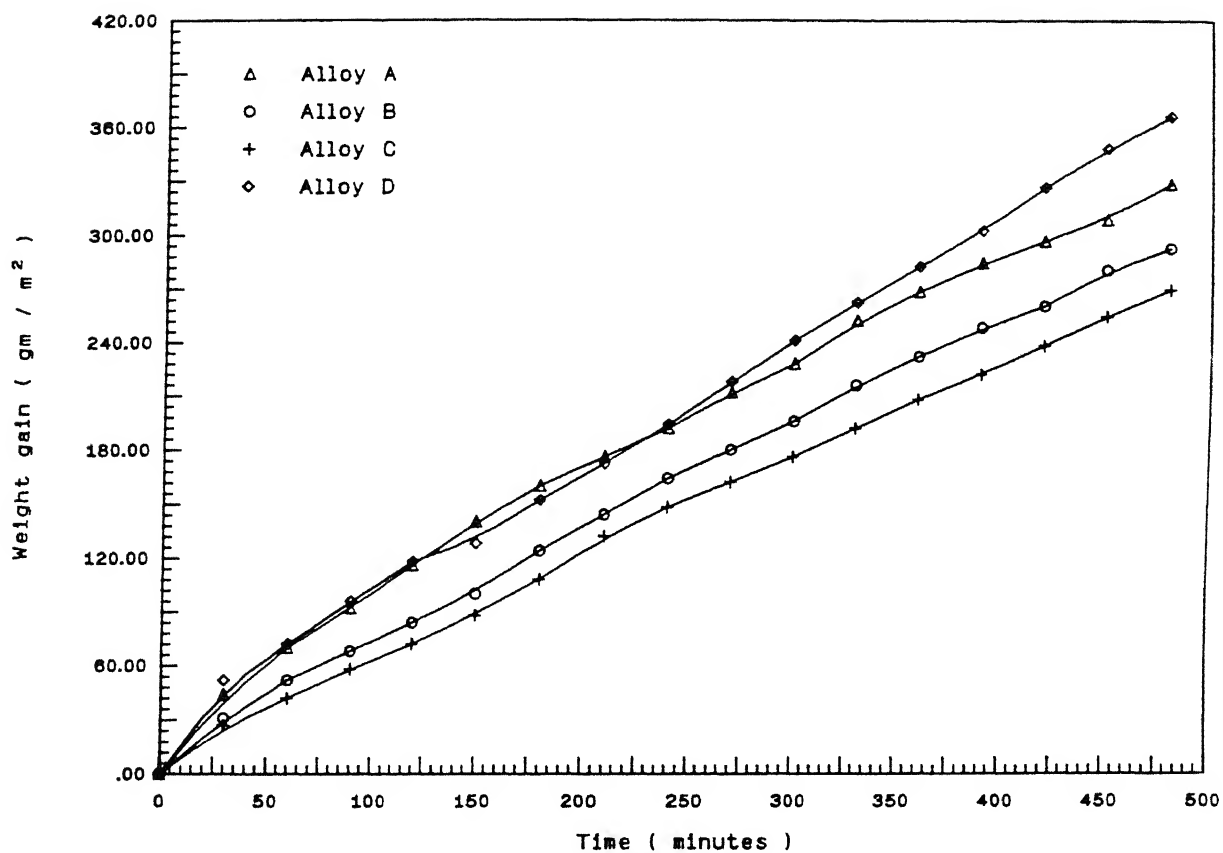


Figure 3.23 Weight gain Vs time plot of alloys A, B, C and D during oxidation in air at 800°C (1073K).

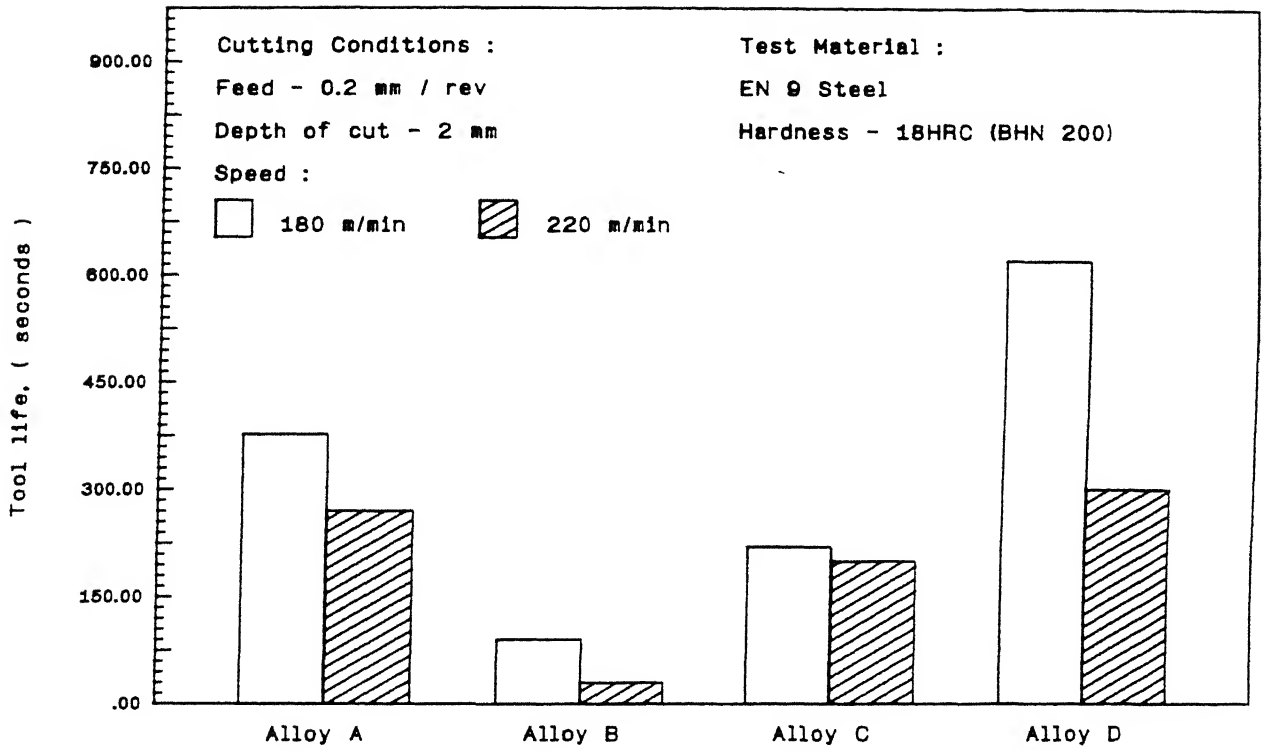


Figure 3.24 Tool life variations of alloys A,B,C and D (sintered in  $H_2$ ).

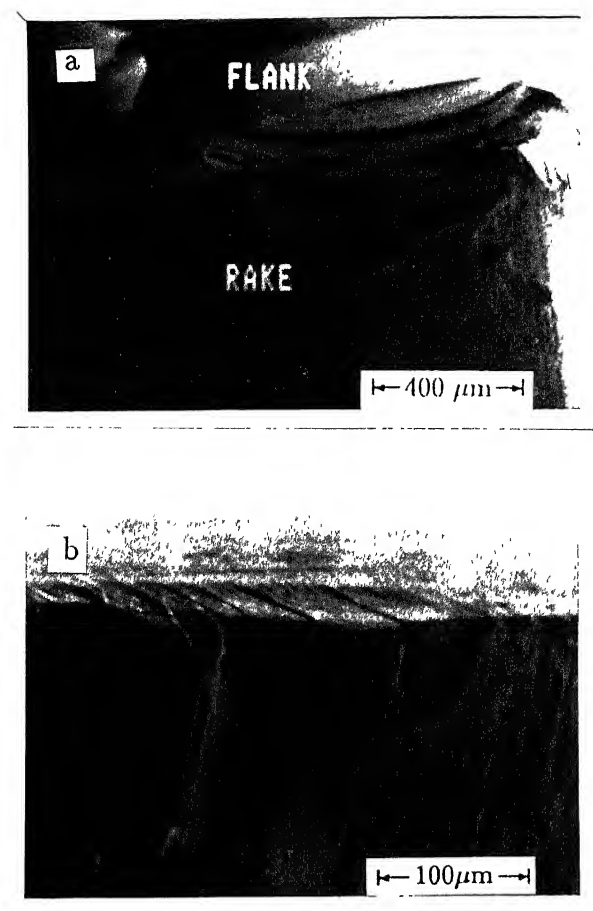


Figure 3.25 SEM pictures of tool made of alloy B, showing (a) cutting edge breaking, and (b) development of cracks on both rake and flank faces perpendicular to cutting edge when cutting EN 9 steel at 180m/min.

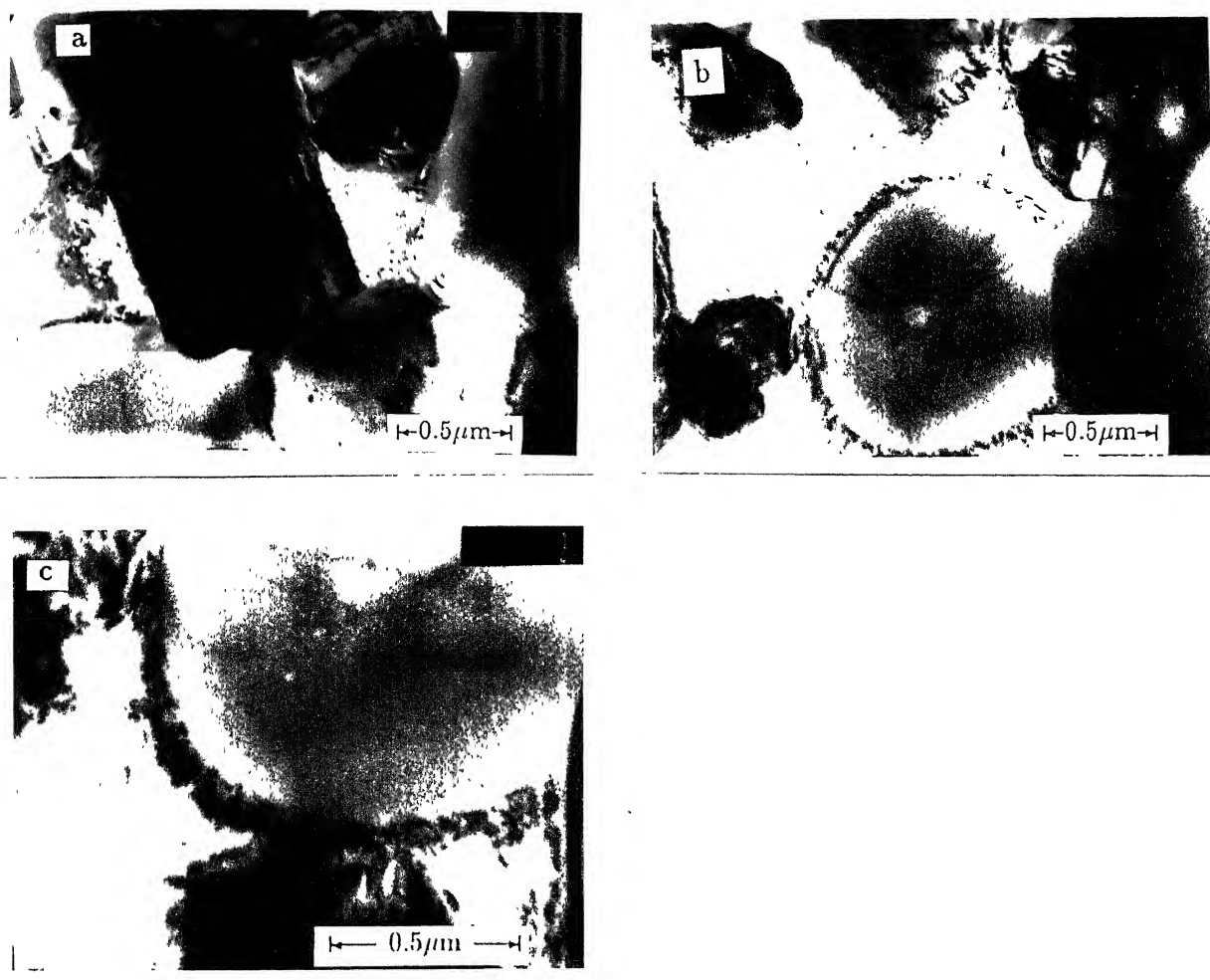


Figure 3.26 TEM microstructures of alloy C (sintered at  $1475^{\circ}\text{C}$  in  $\text{H}_2$ ), showing : (a) straight faceted WC and rounded TiC grains, (b) dislocations in TiC and TiC/Co interfaces, and (c) magnified view of TiC/Co interface in (b).

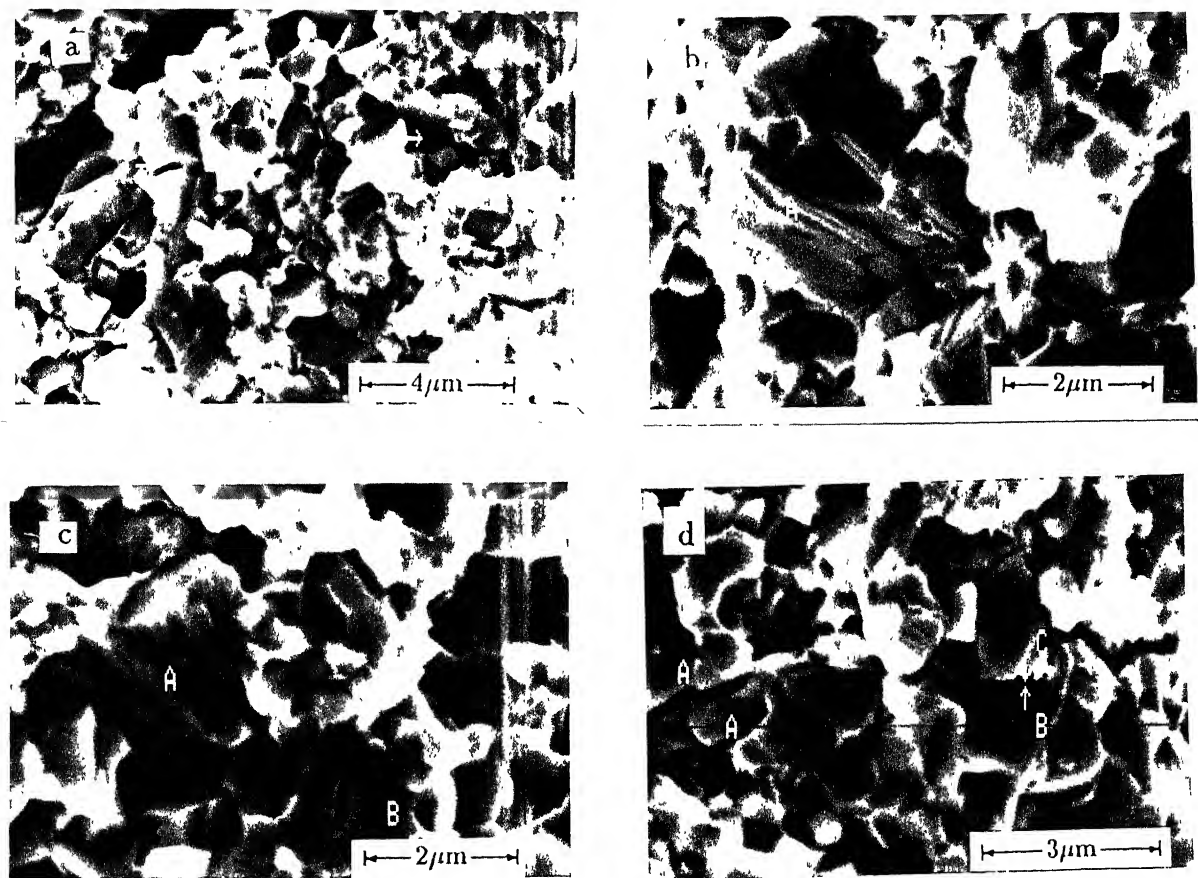


Figure 3.27 SEM fractographs of alloy C (sintered at 1475°C in H<sub>2</sub>), showing : (a) ruptured binder phase ligaments, (b) fracture initiation at carbide/binder interface, (c) fracture initiation at carbide/carbide interface, and (d) secondary crack.

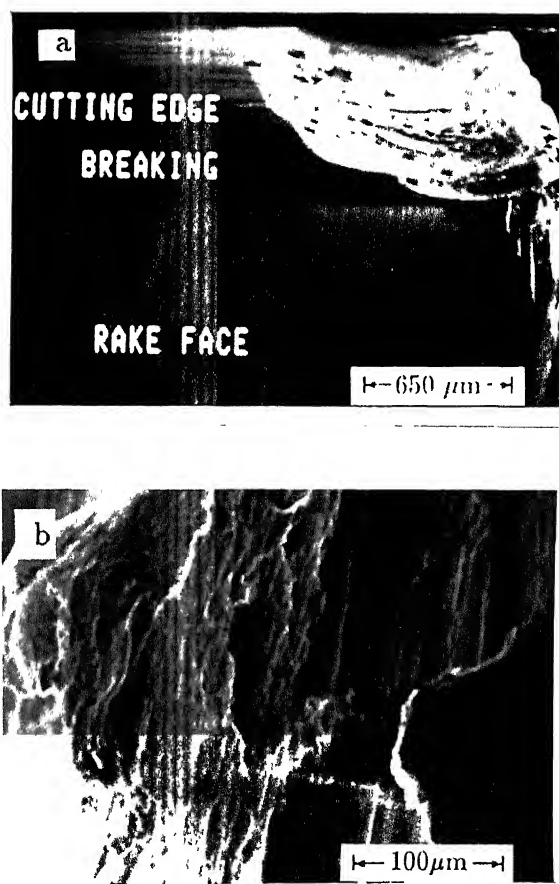


Figure 3.28 SEM pictures of tool made of alloy C after cutting test, showing : (a) cutting edge breaking, and (b) magnified view of the broken surface.

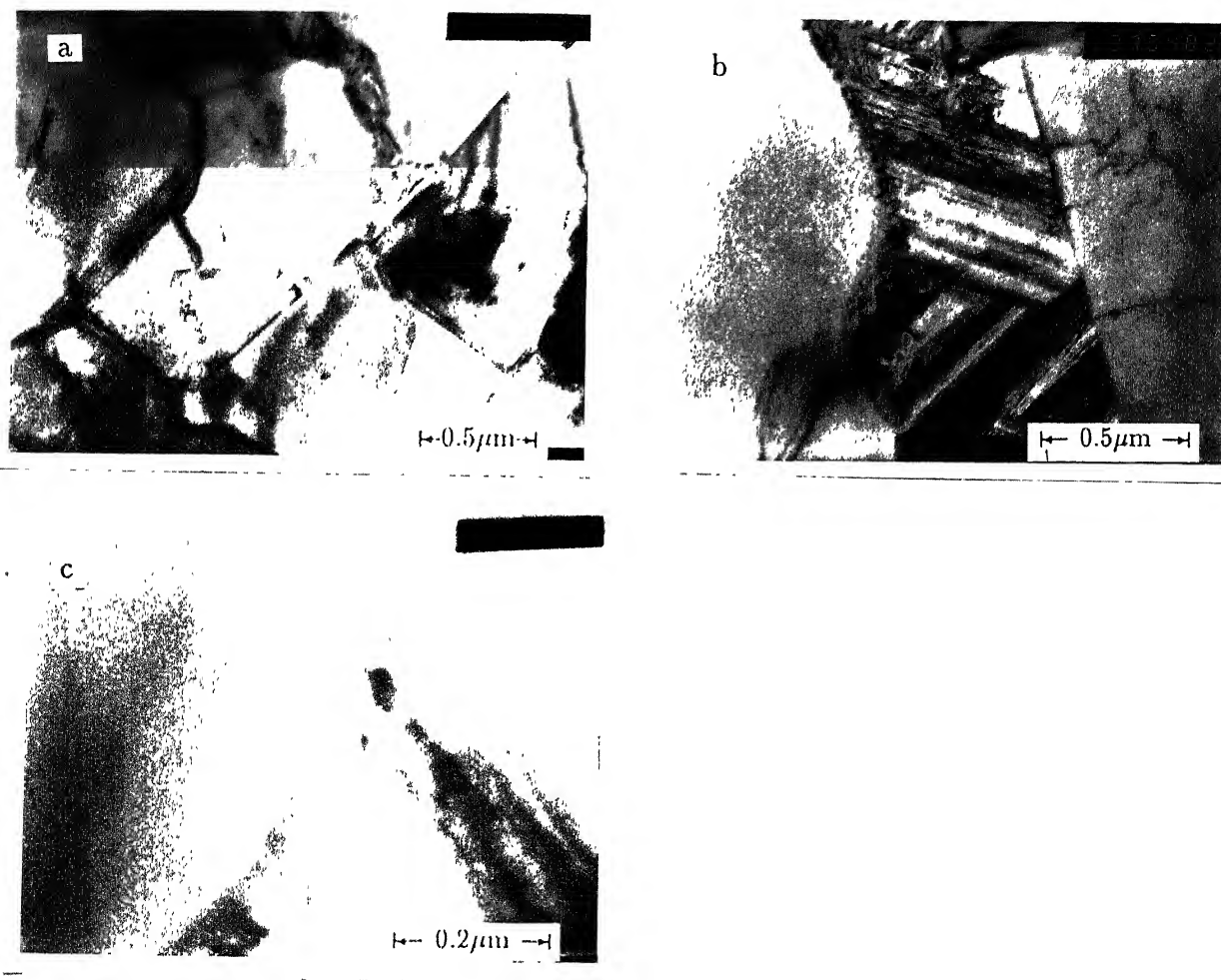


Figure 3.29 TEM microstructure of alloy D (sintered at  $1475^{\circ}\text{C}$  in  $\text{H}_2$ ), showing : (a) general microstructure, (b) stacking fault in binder phase, WC/Co and TiC/Co interfaces, and (c) a magnified view of TiC/Co interface in (b).

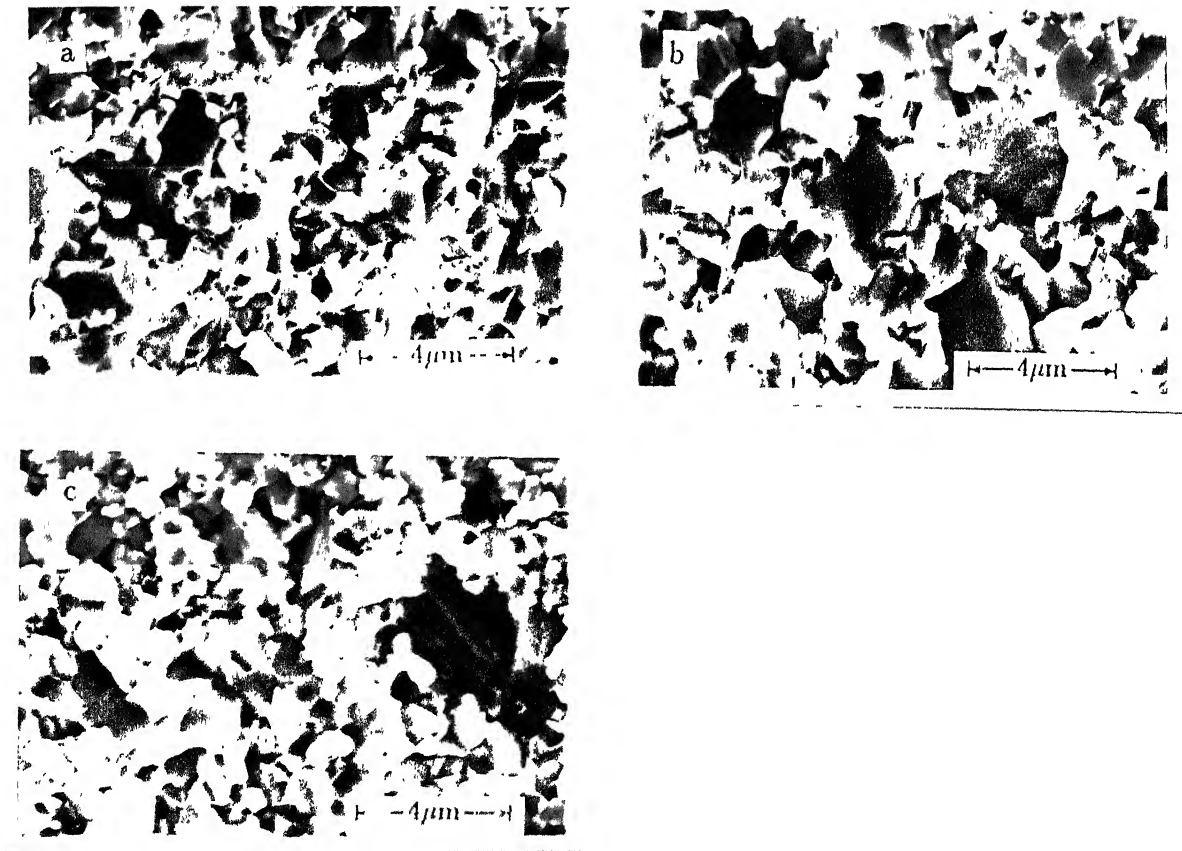


Figure 3.30 SEM fractographs of alloy D (sintered at  $1475^{\circ}\text{C}$  in  $\text{H}_2$ ), showing : (a) large fraction of dimpled fracture, (b) and (c) TiC particles discernible by river pattern.

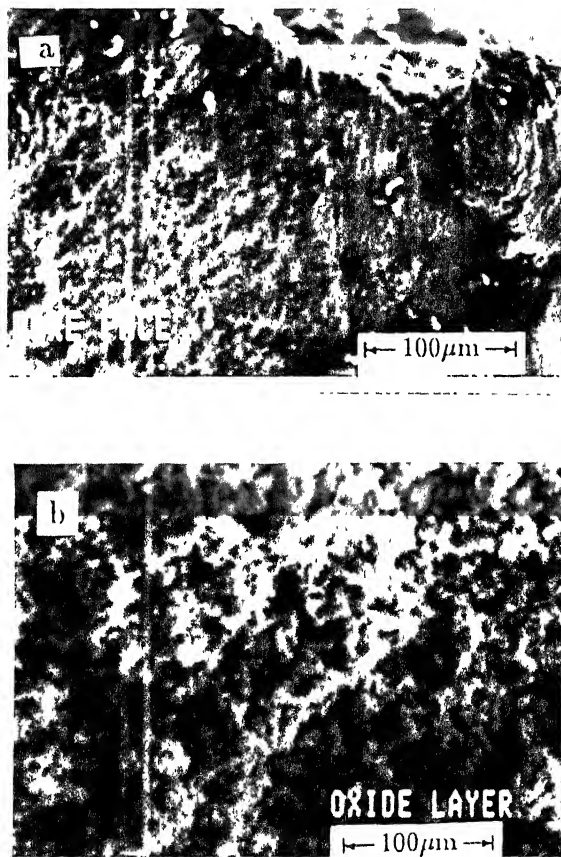


Figure 3.31 SEM pictures of the worn surfaces of the tool made of alloy D, showing : (a) worn rake face, and (b) oxide layer on the rake face.

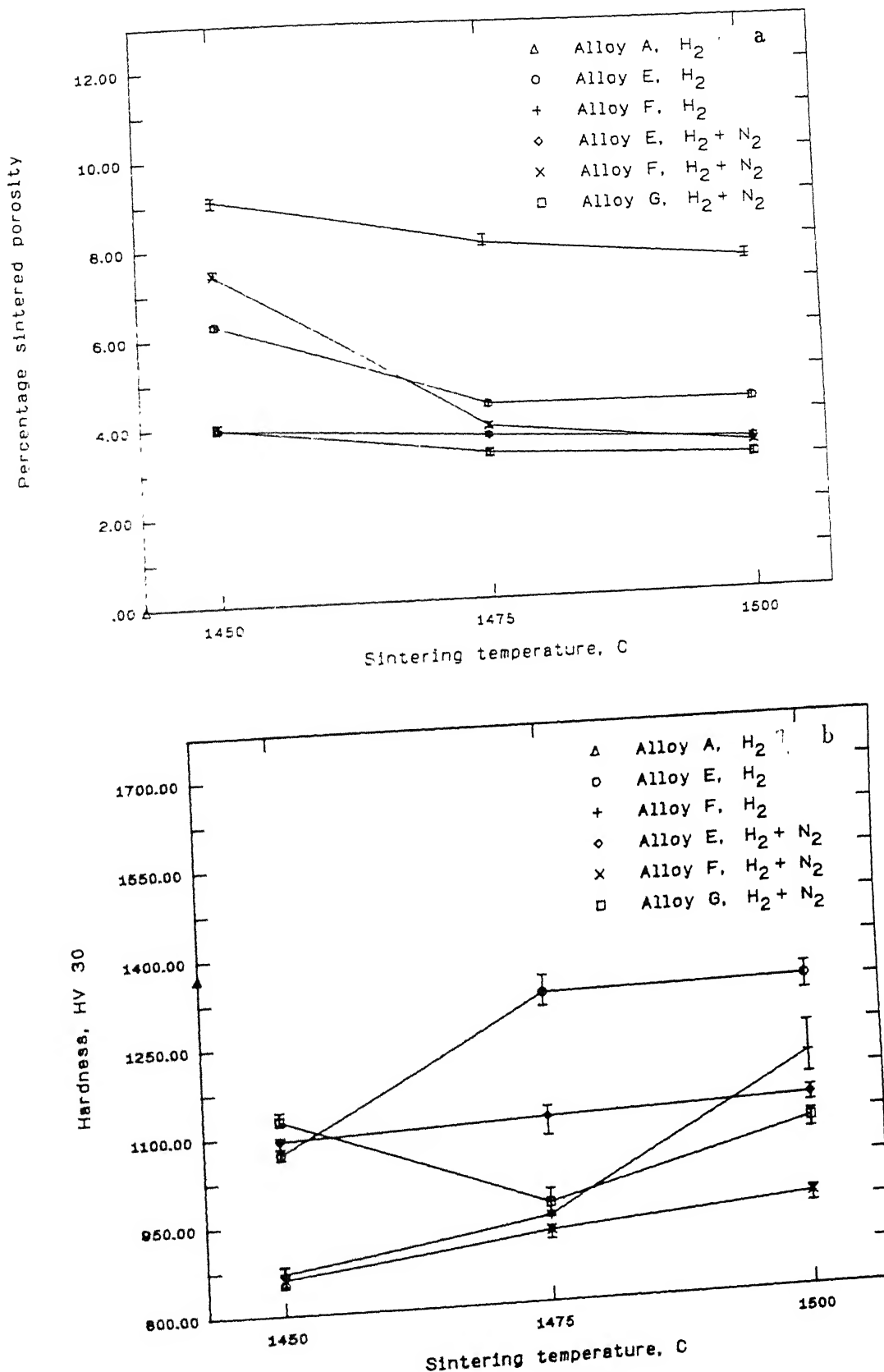


Figure 3.32 Effect of sintering temperature on (a) percent sintered porosity, and (b) hardness of alloys E, F and G sintered in  $H_2$  and  $H_2-N_2$  (50:50) mixture respectively.

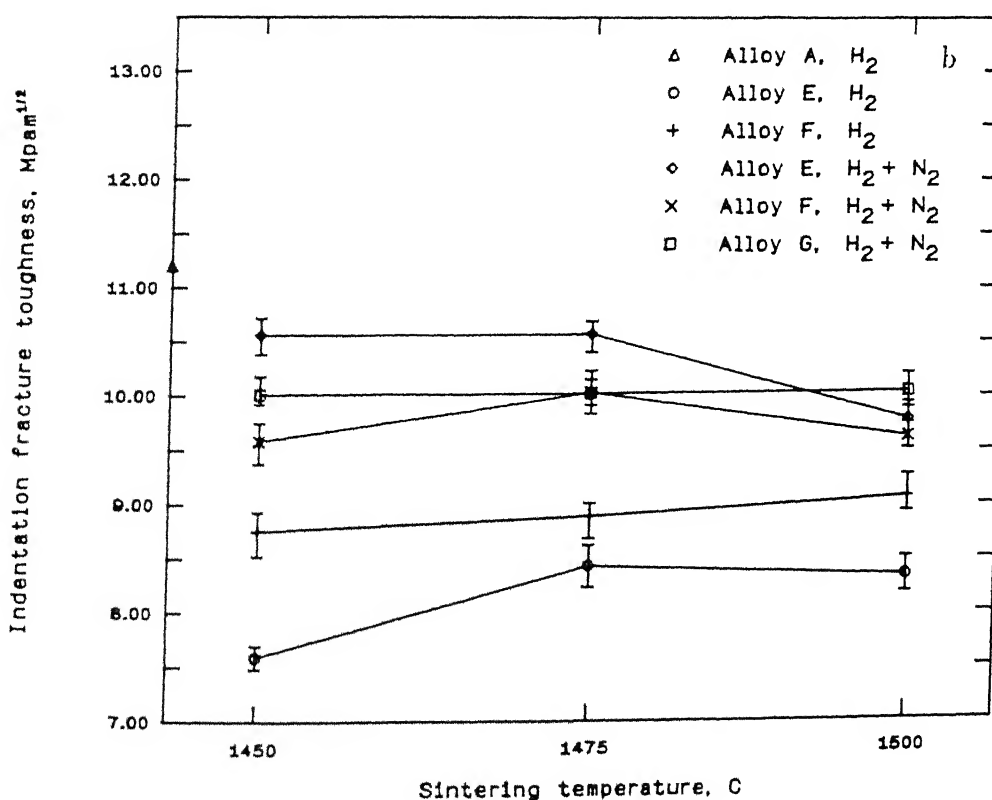
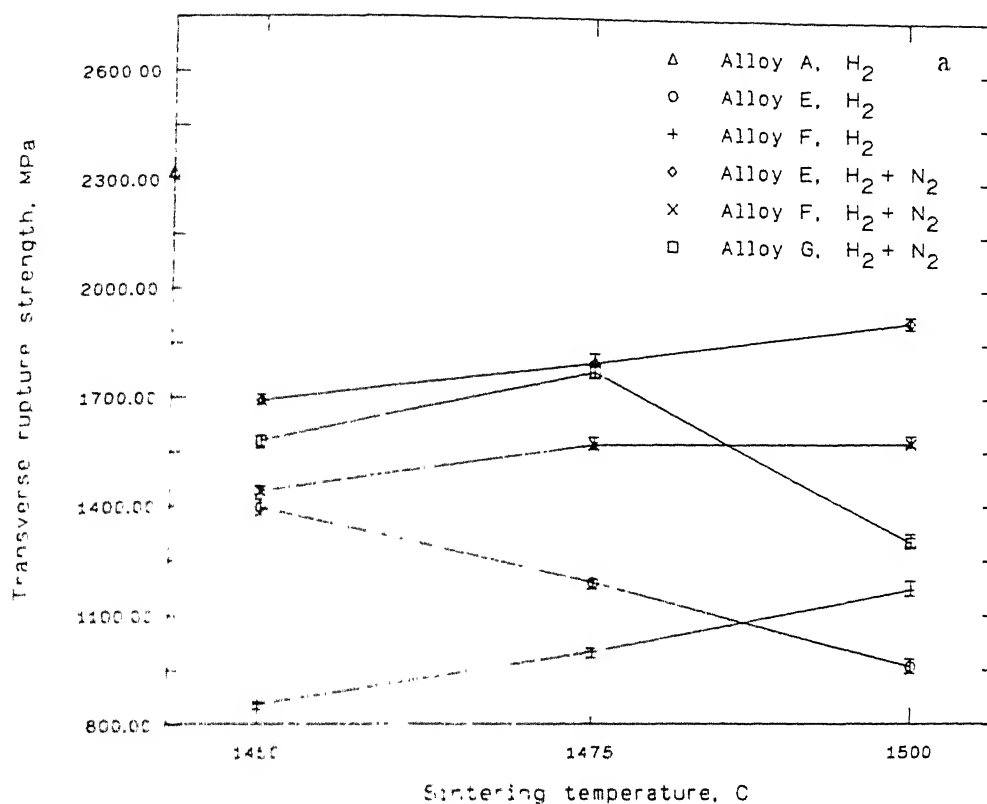


Figure 3.33 Effect of sintering temperature on (a) TRS and (b) indentation fracture toughness of alloys E, F and G sintered in H<sub>2</sub> and H<sub>2</sub>-N<sub>2</sub> (50:50) mixture

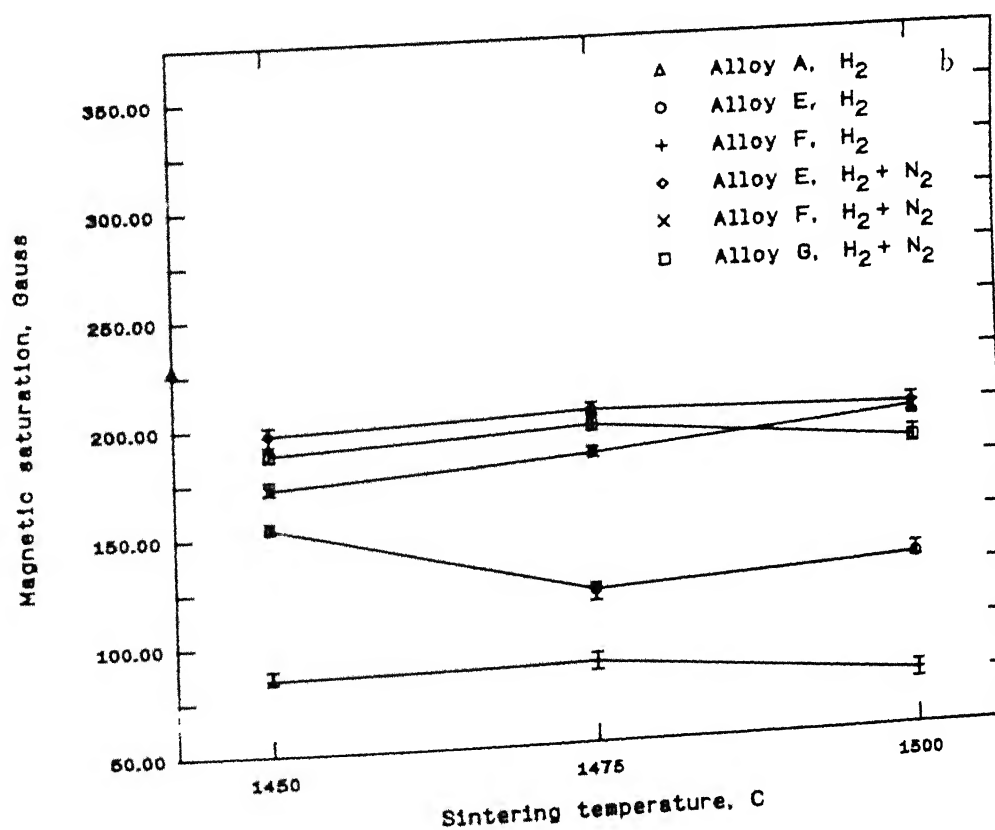
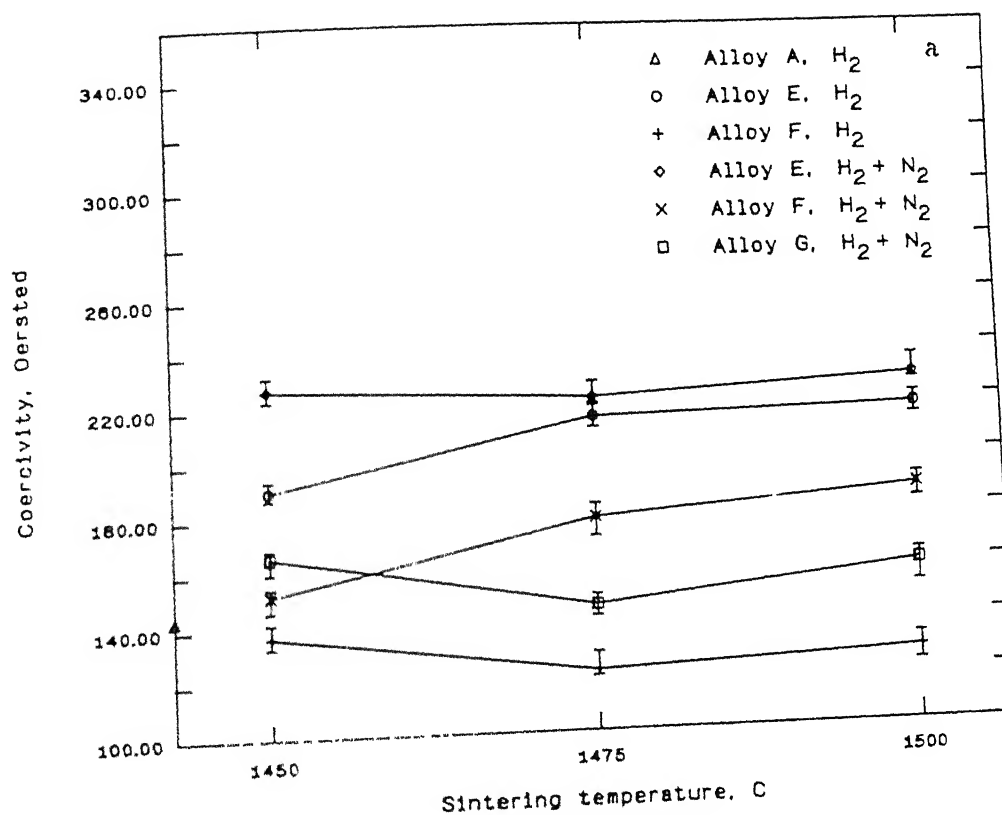


Figure 3.34 Effect of sintering temperature on (a) coercivity and (b) magnetic saturation of alloys E, F and G sintered in H<sub>2</sub> and H<sub>2</sub>-N<sub>2</sub> (50:50) mixture respectively

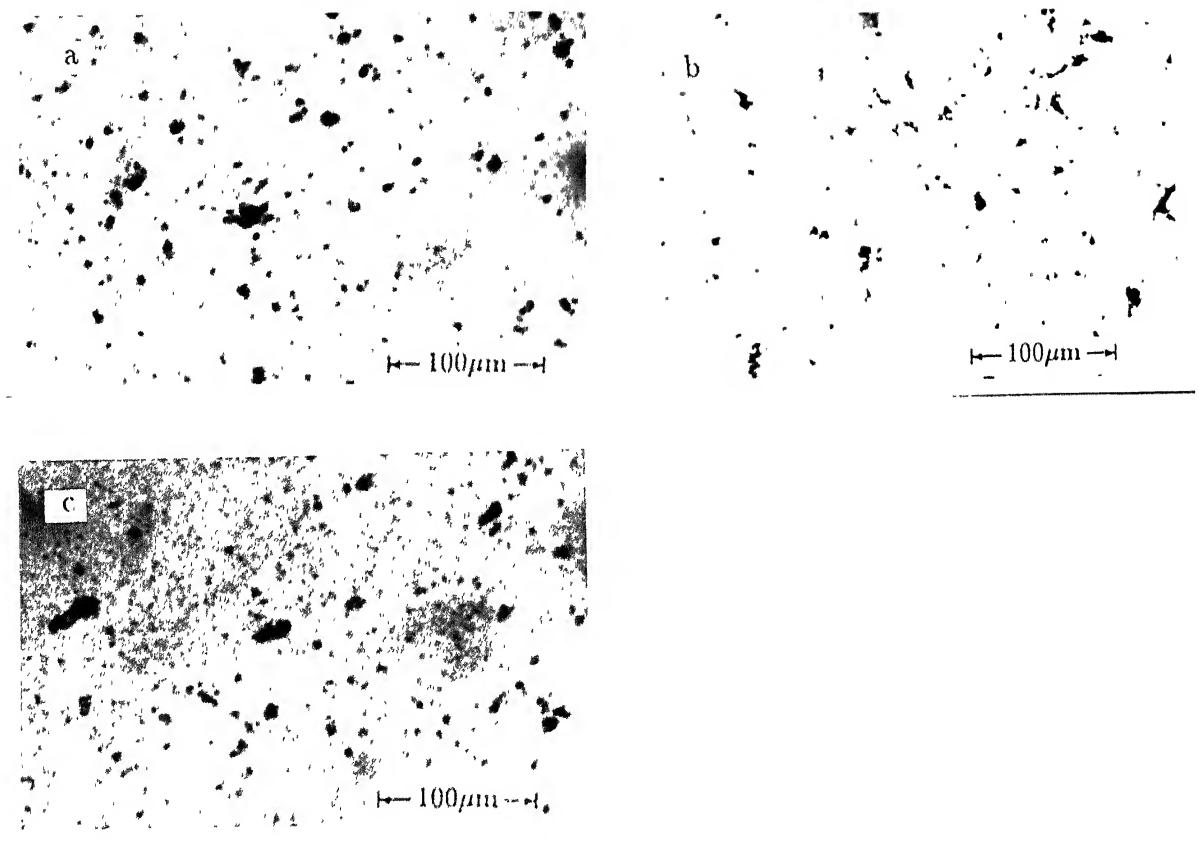


Figure 3.35 Pore morphology and distribution in (a) alloy E, (b) alloy F, and (c) alloy G sintered at 1475°C in  $\text{H}_2\text{-N}_2$  (50:50) mixture.

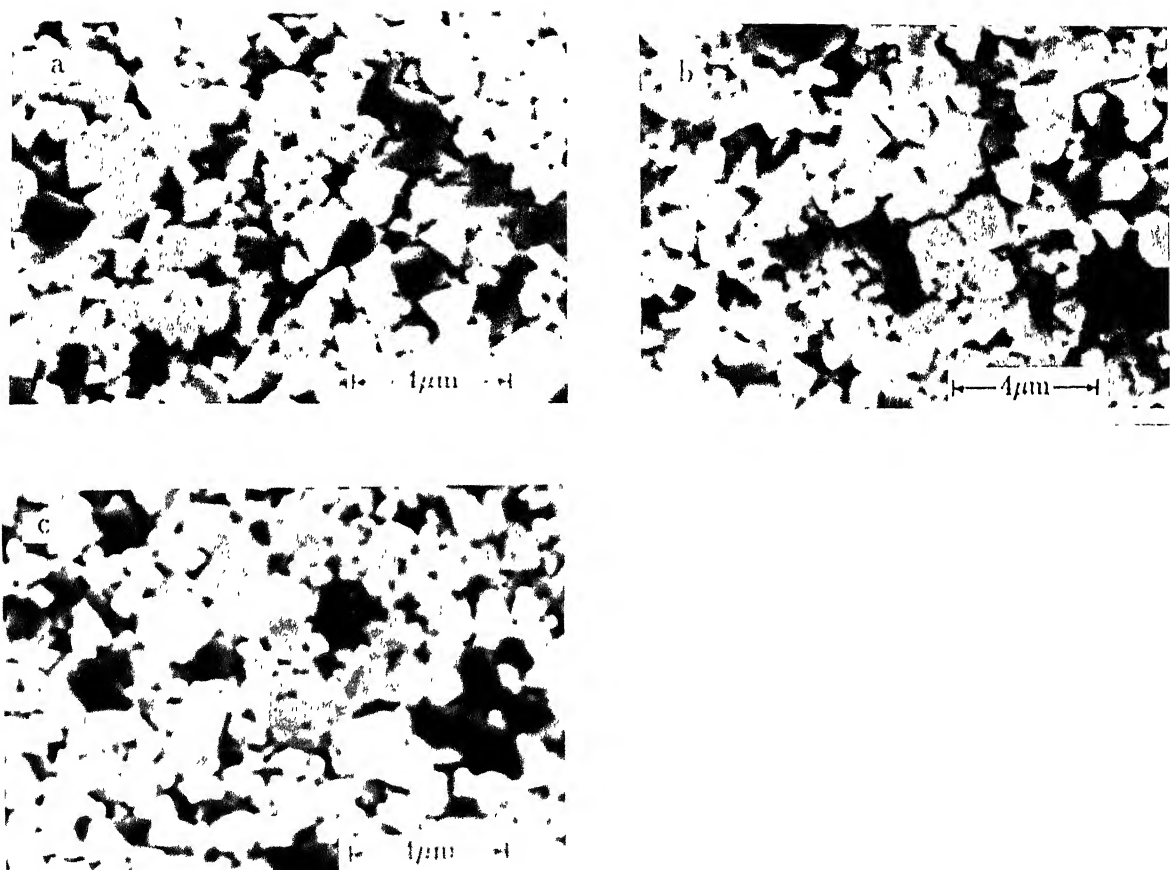


Figure 3.36 SEM microstructures of (a) alloy E, (b) alloy F, and (c) alloy G sintered at 1475°C in  $\text{H}_2\text{-N}_2$  (50:50) mixture.

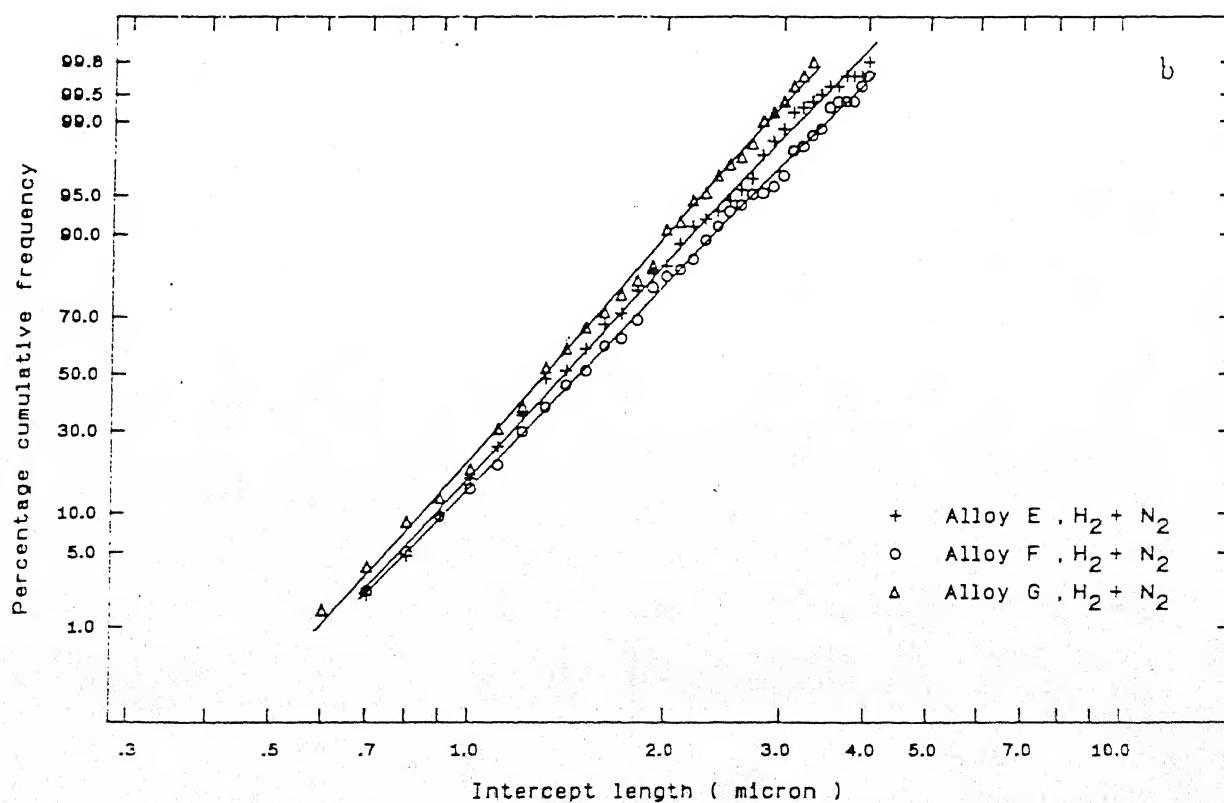
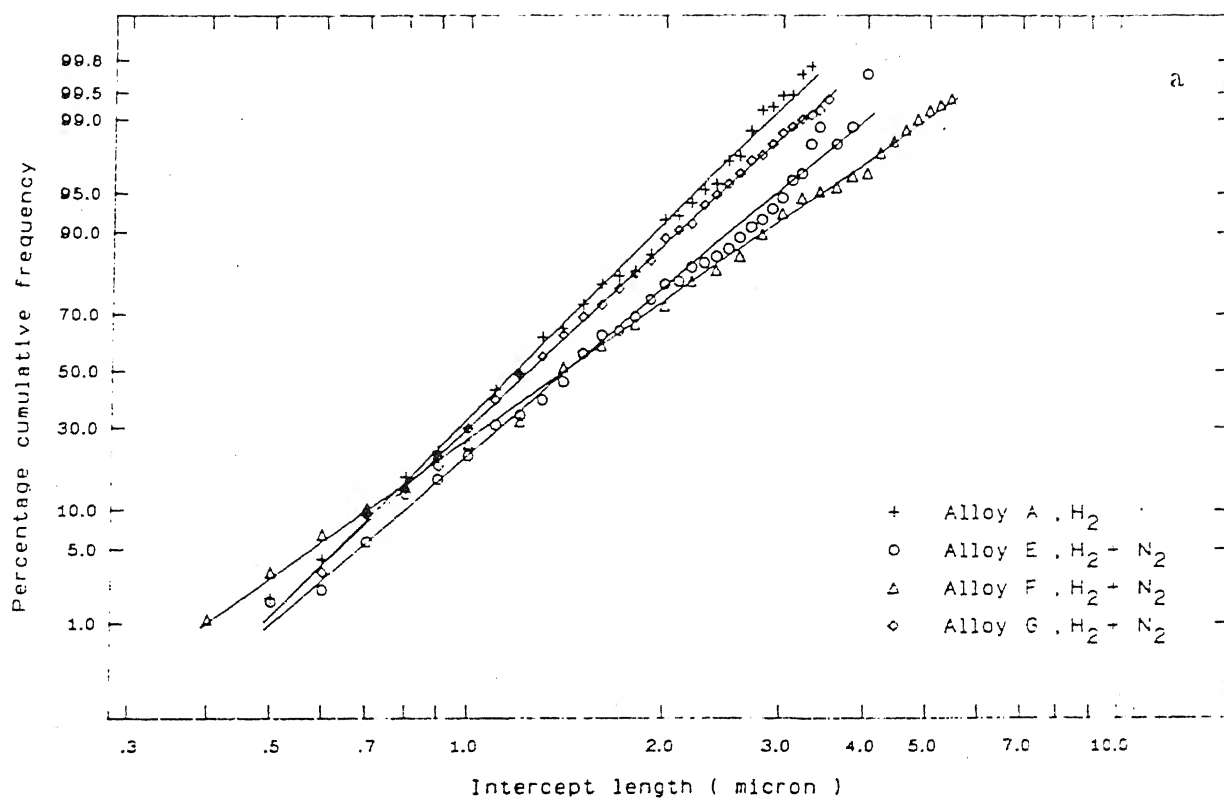


Figure 3.37 Cumulative frequency distribution of (a) WC and (b) cubic phase (TiN) intercept lengths in alloys E, F and G sintered at 1475°C in H<sub>2</sub>-N<sub>2</sub> (50:50) mixture.

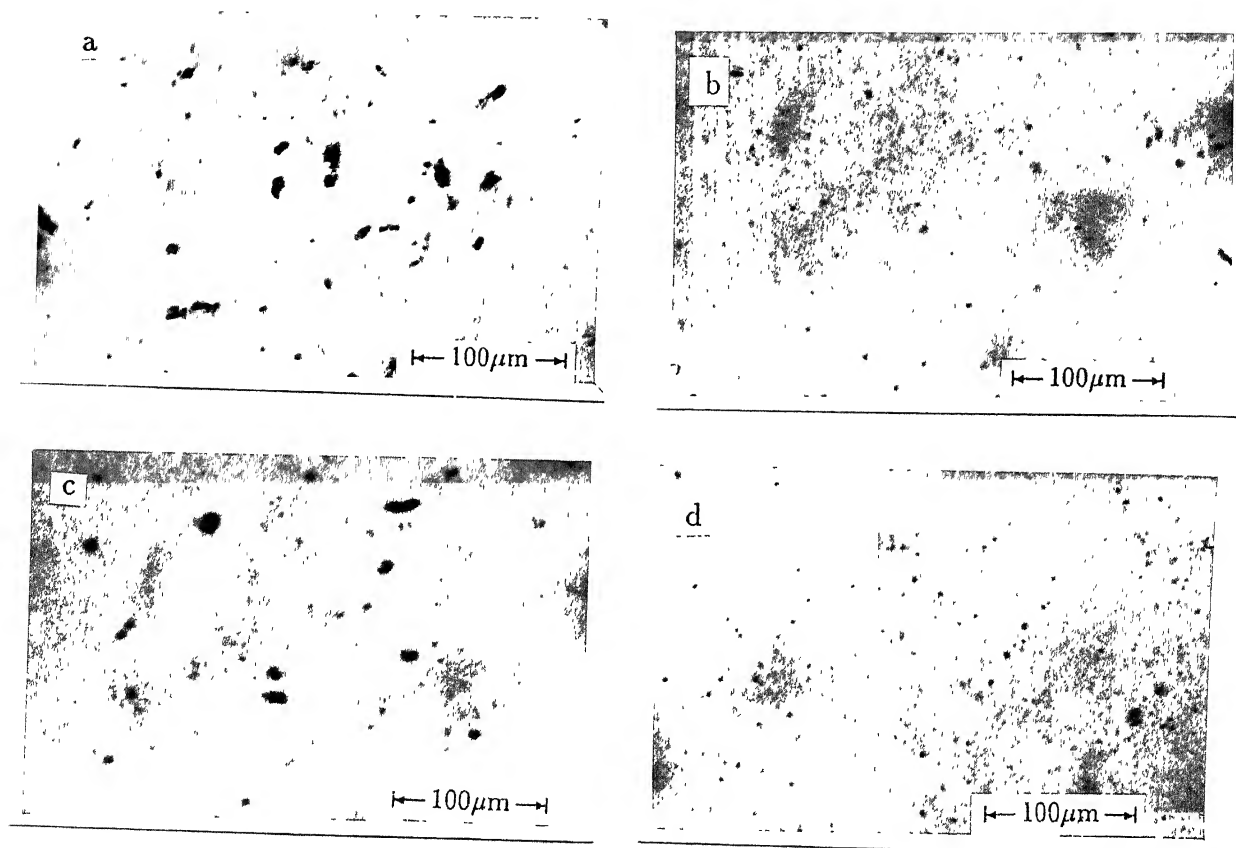


Figure 3.38 Pore morphology and distribution in (a) alloy E, HIP'ped at 1400 °C, (b) alloy E, HIP'ped at 1450 °C, (c) alloy G, HIP'ped at 1400 °C, and (d) alloy G, HIP'ped at 1450 °C.

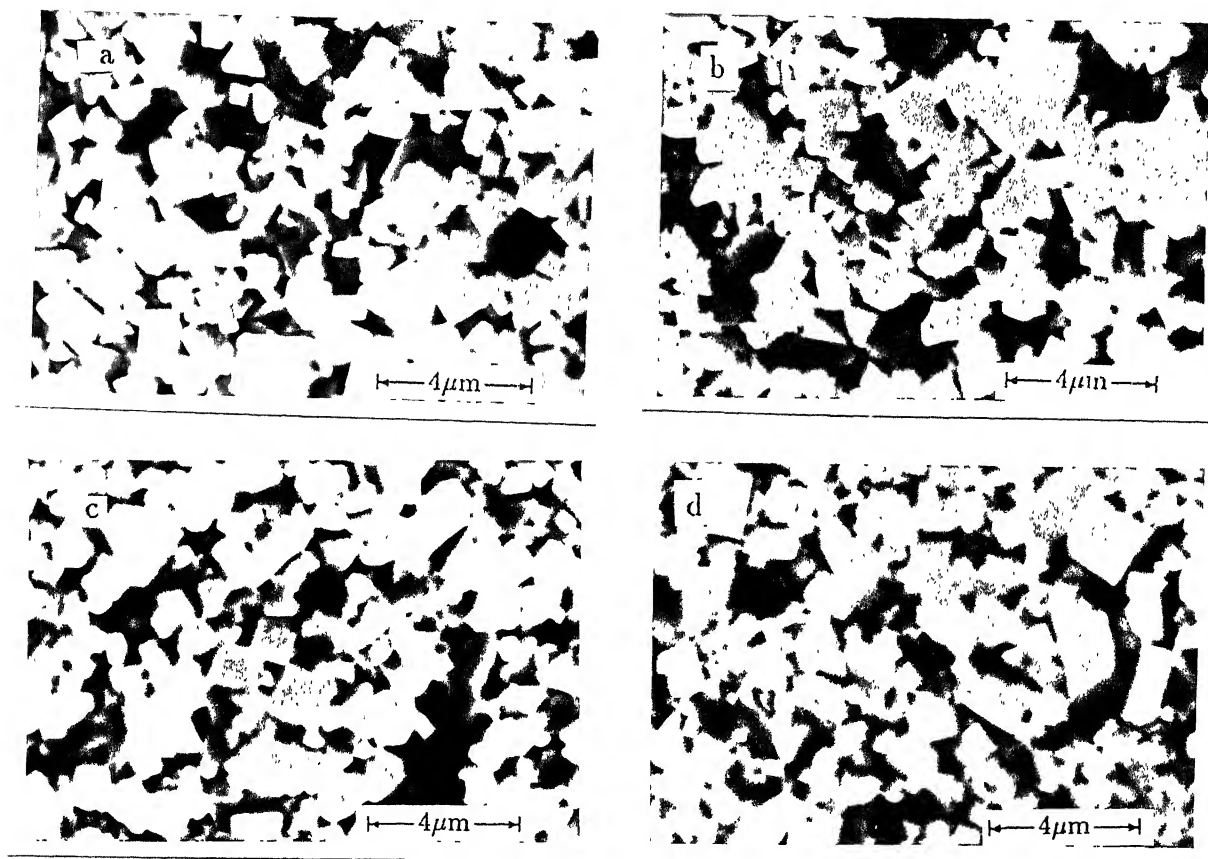


Figure 3.39 SEM microstructures of (a) alloy E, HIP'ped at 1400°C, (b) alloy E, HIP'ped at 1450°C, (c) alloy G, HIP'ped at 1400°C, and (d) alloy G, HIP'ped at 1450°C.

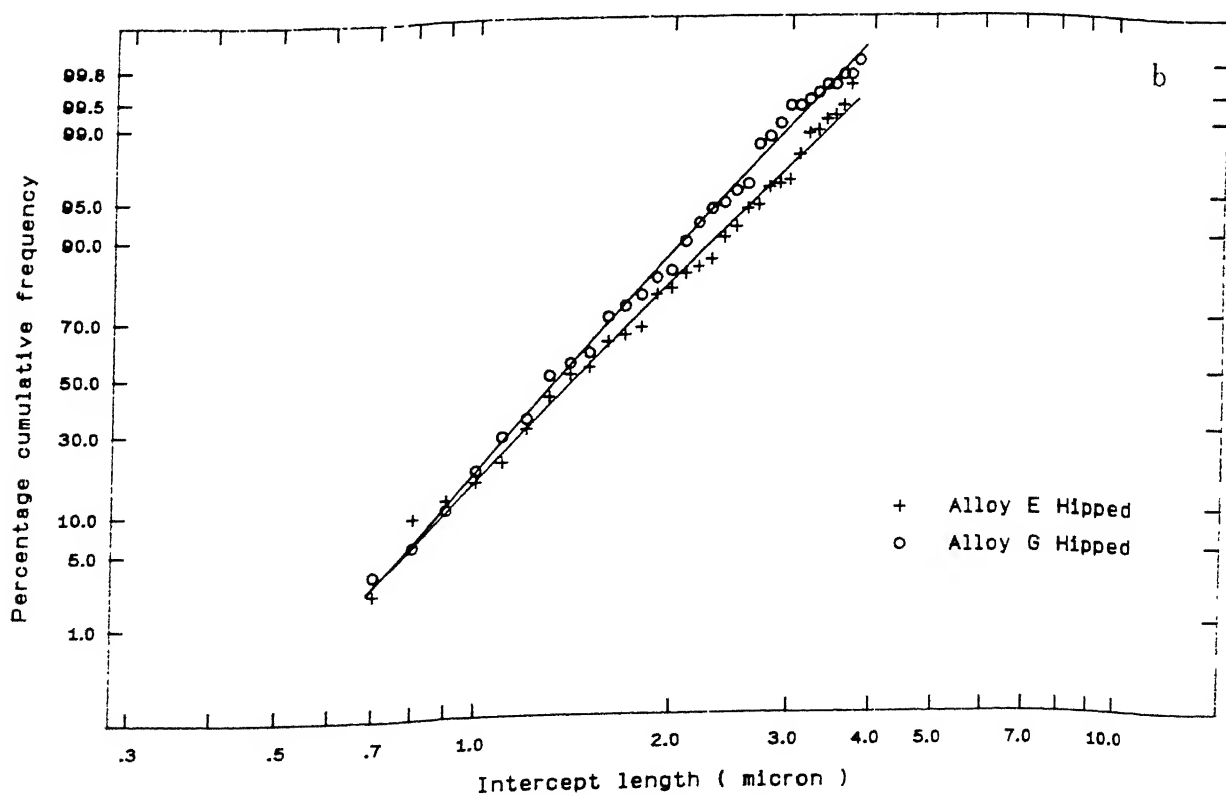
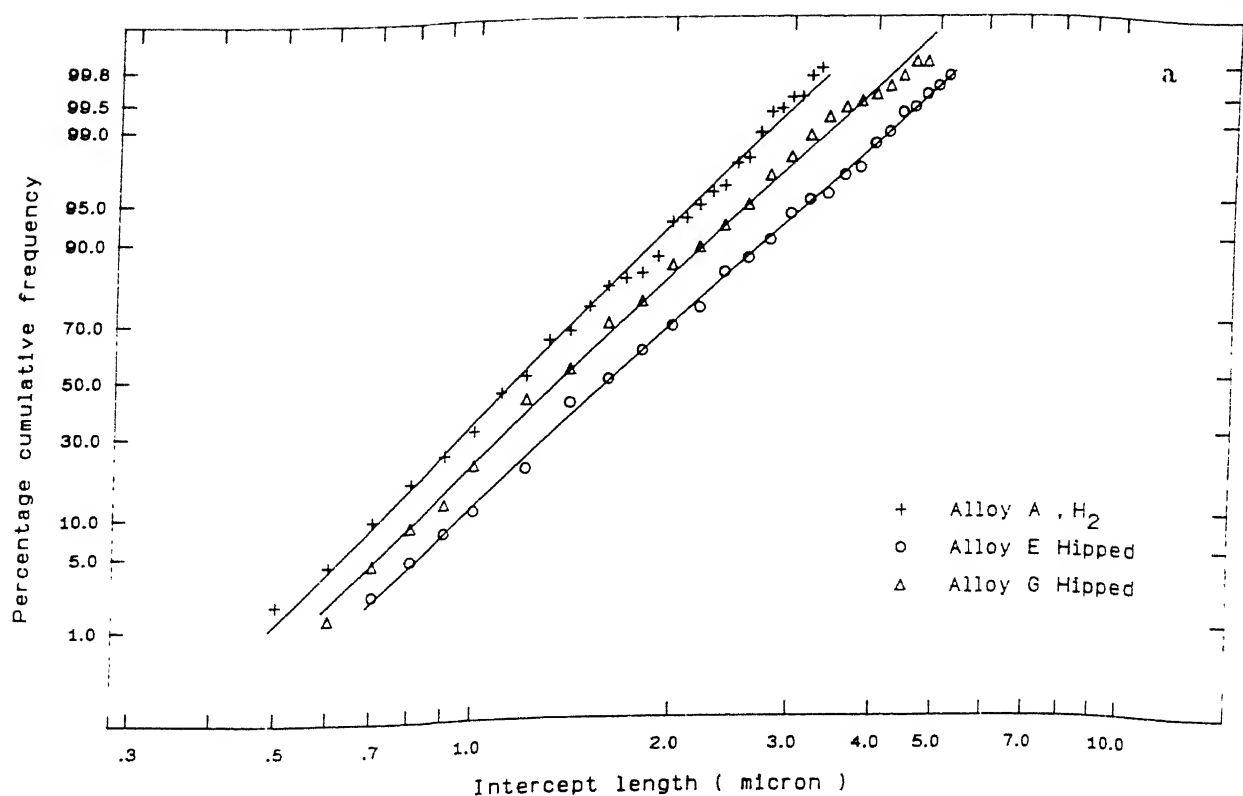


Figure 3.40 Cumulative frequency distribution of WC and cubic phase (TiN) intercept lengths in alloys E and G after HIP'ing at 1450°C.

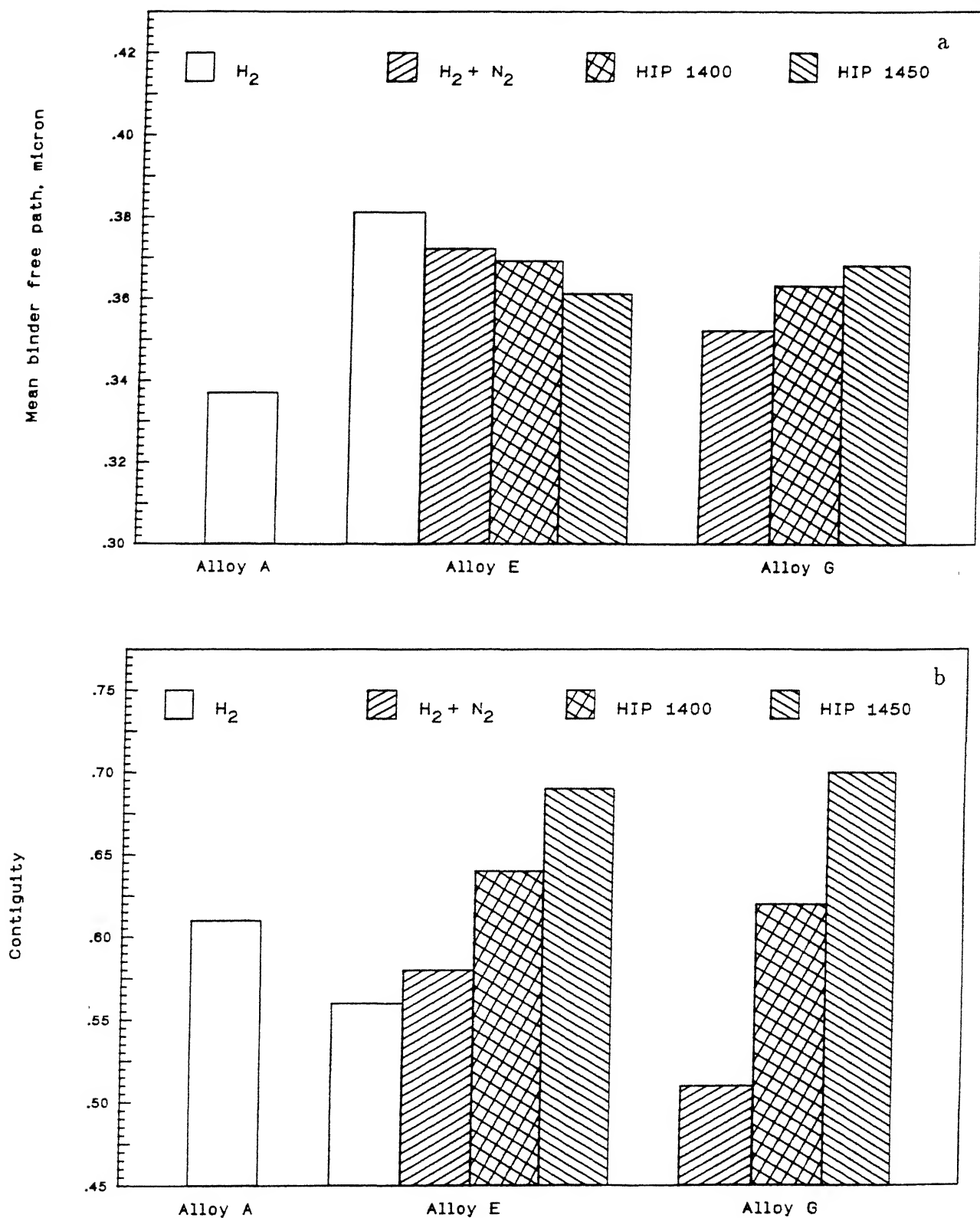


Figure 3.41 Mean binder free path (a) and contiguity (b) variations in alloys A, E and G.

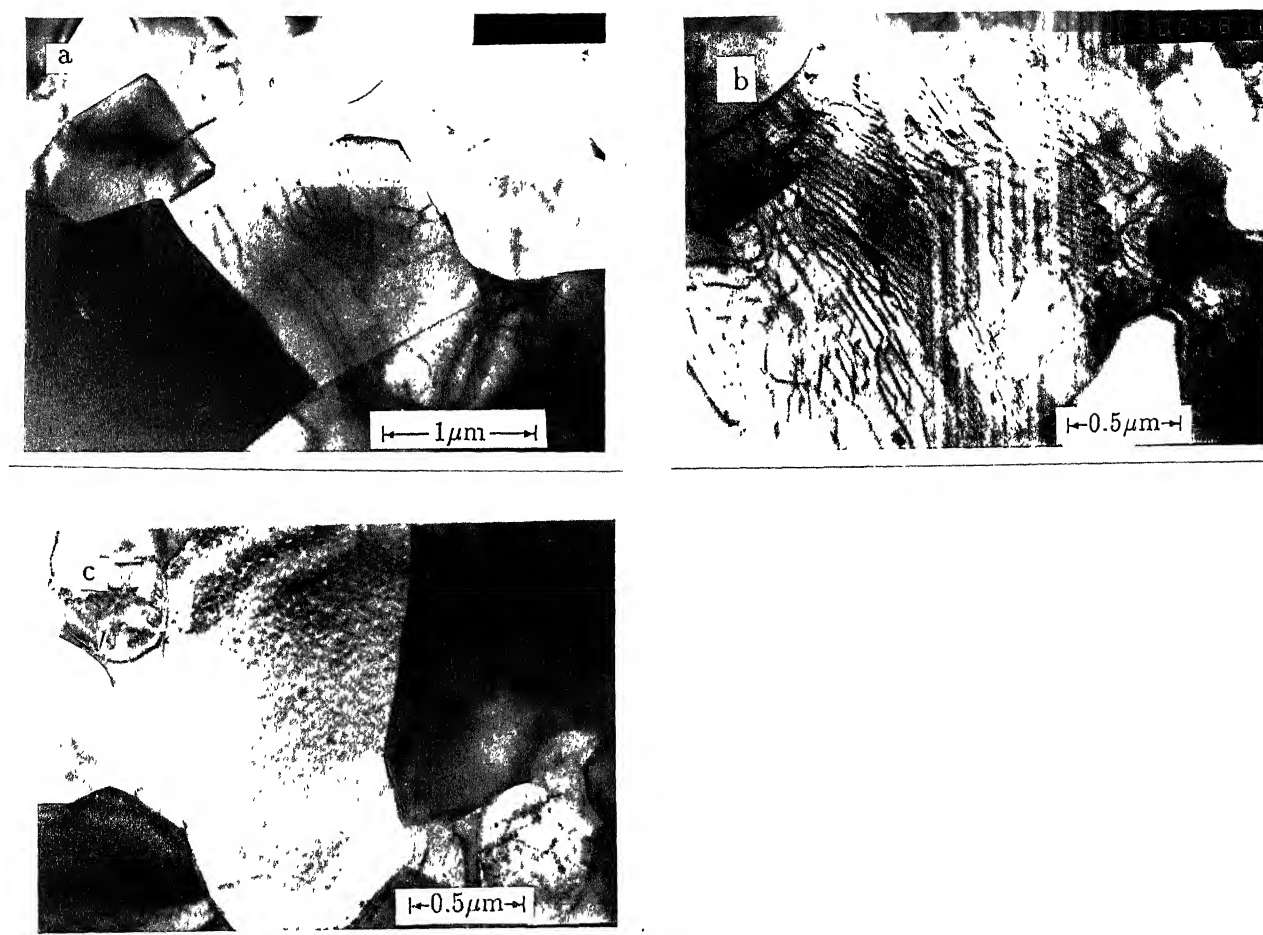


Figure 3.42 TEM microstructures of alloy E, (liquid phase sintered at 1475°C in  $H_2-N_2$  followed by HIP'ing at 1450°C), showing : (a) straight faceted WC (grey) and equiaxed TiN (white) grains, (b) shear bands in TiN grain, and (c) TiN grain with high dislocation density, WC/Co and TiN/Co interfaces and intruded WC grain (grey) in TiN grains (white).

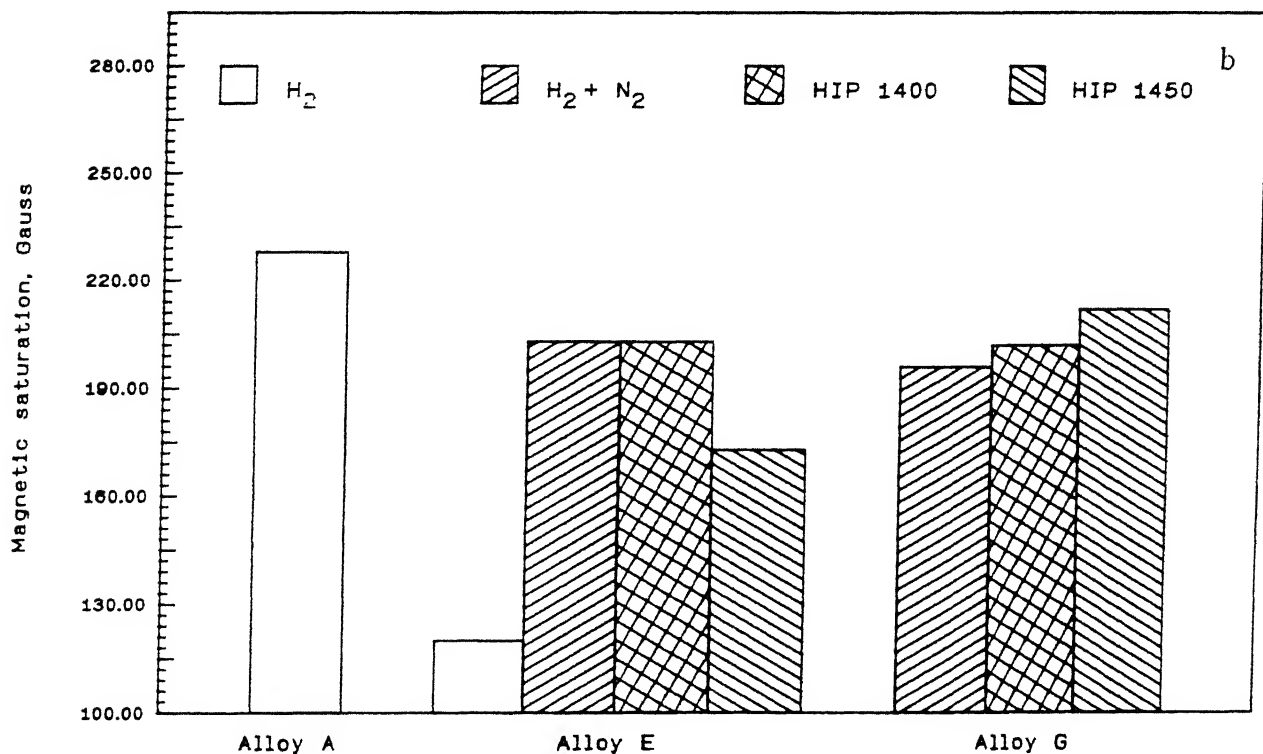
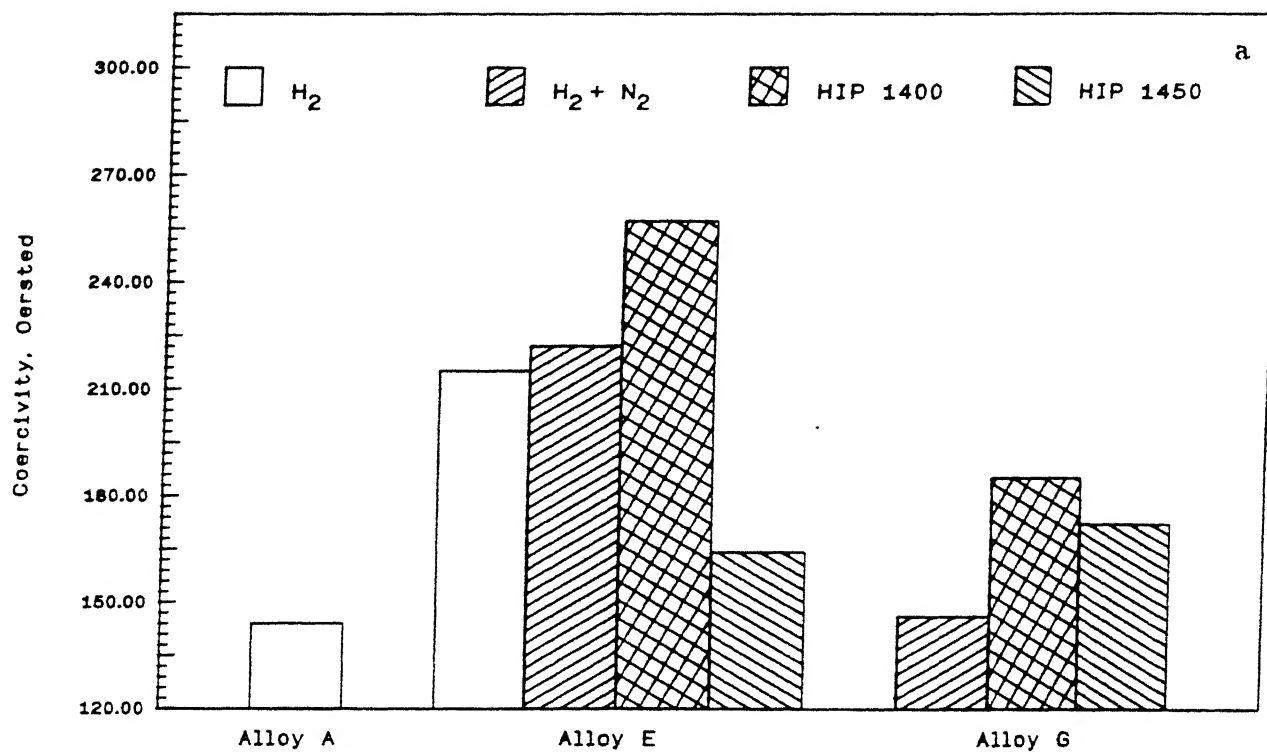


Figure 3.43 Coercivity (a) and magnetic saturation (b) variations in alloys A, E and G.

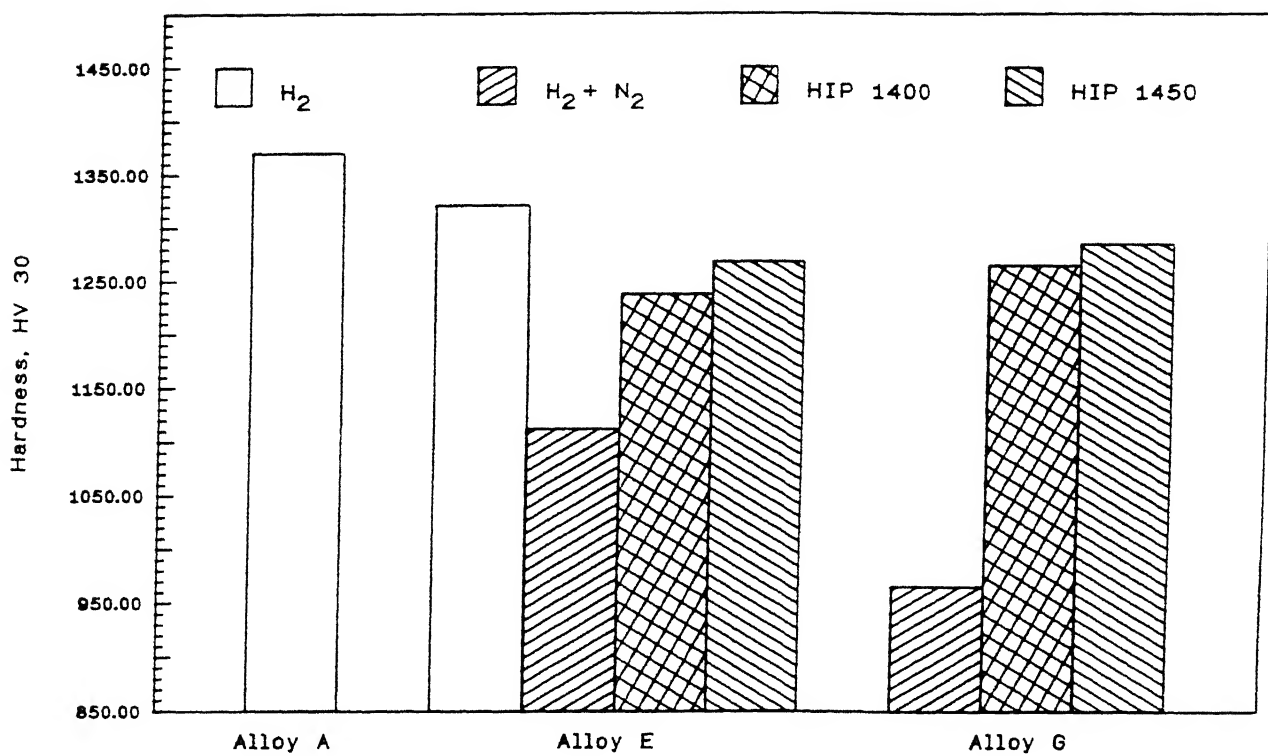


Figure 3.44 Hardness variations in alloys A, E and G.

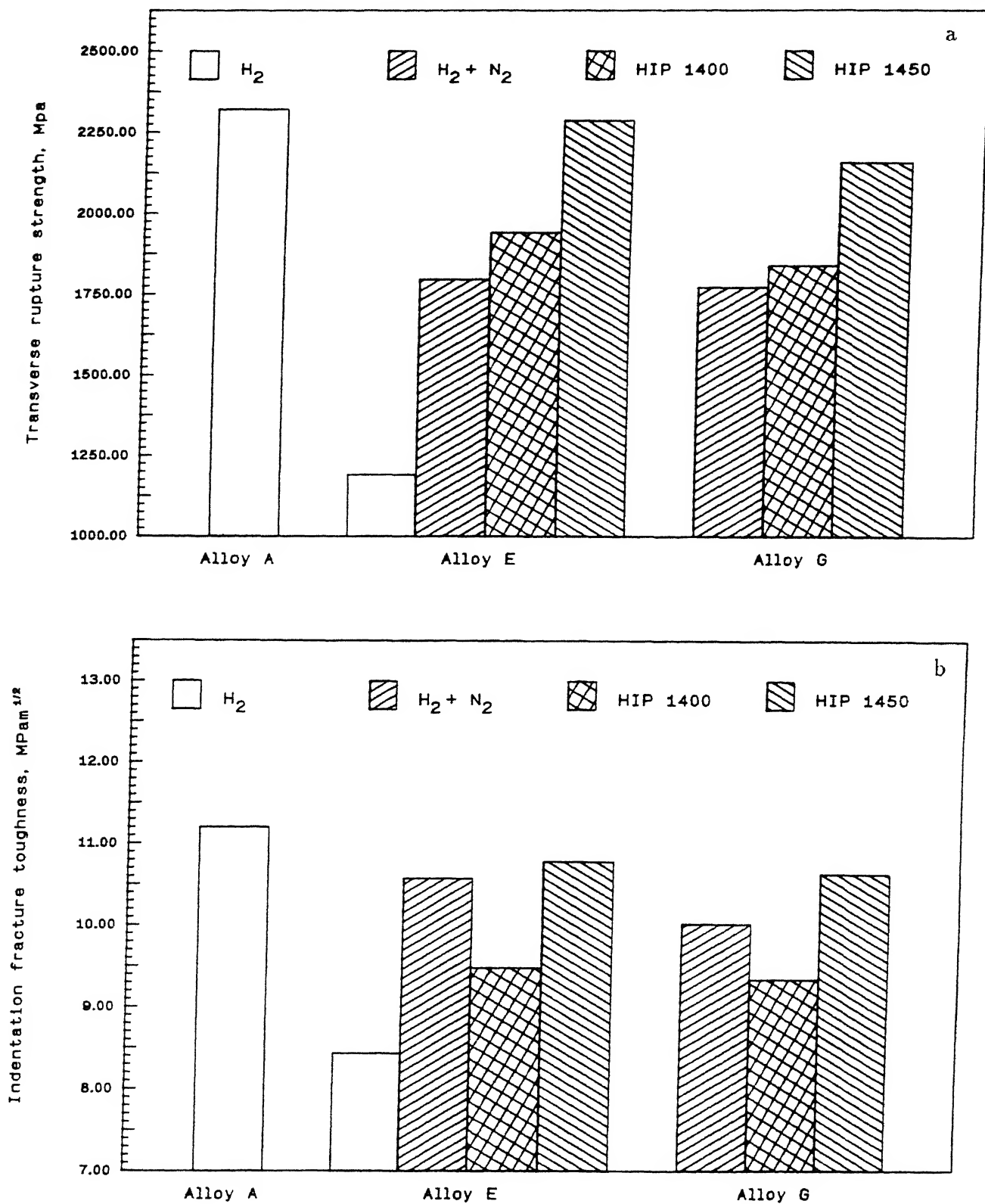


Figure 3.45 Transverse rupture strength (a), and indentation fracture toughness (b) variations in alloys A, E and G.

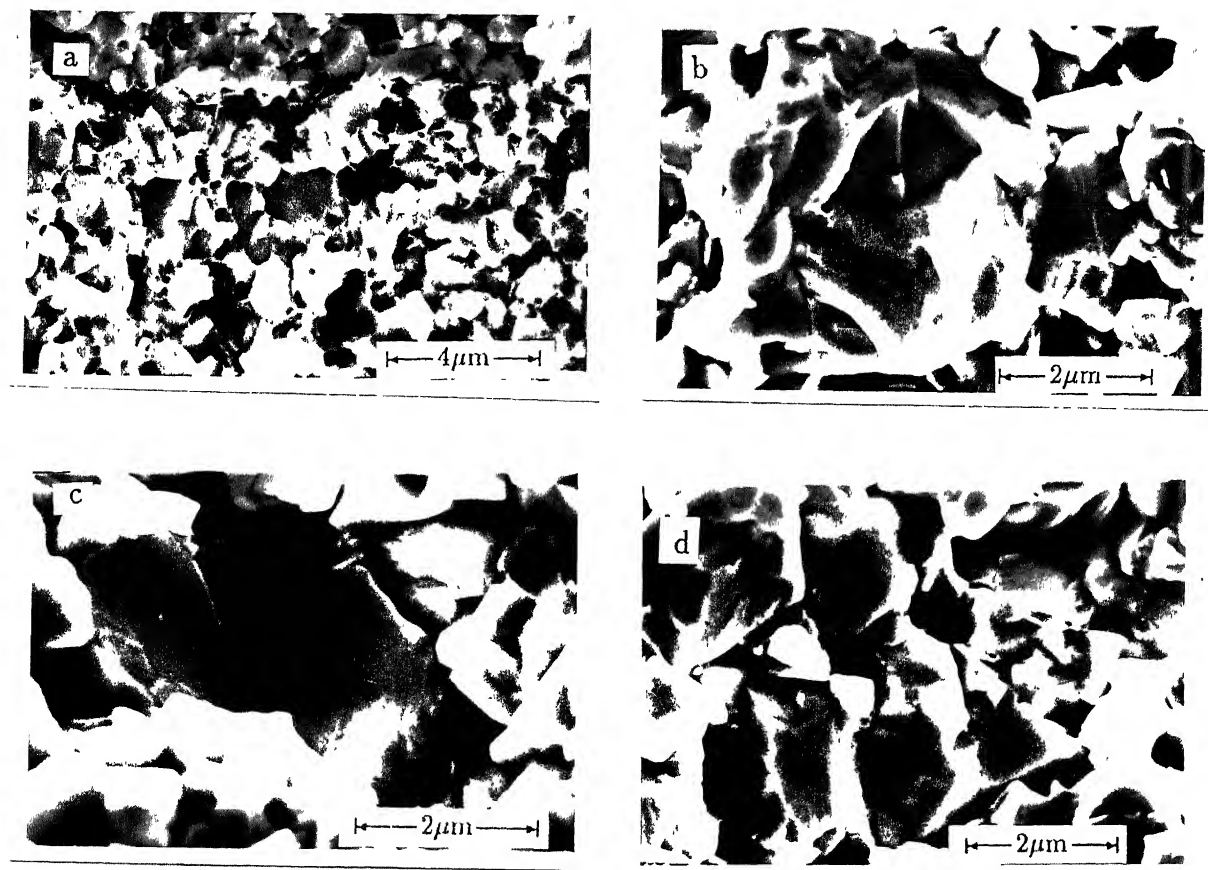


Figure 3.46 SEM fractographs of alloy E, showing : (a) ruptured binder phase, (b) ductile fracture of binder phase around the hard phase grains (c) transgranular fracture in large TiN grains, and (d) fracture initiation at the WC/WC, WC/TiN and TiN/TiN interfaces due to high contiguity.

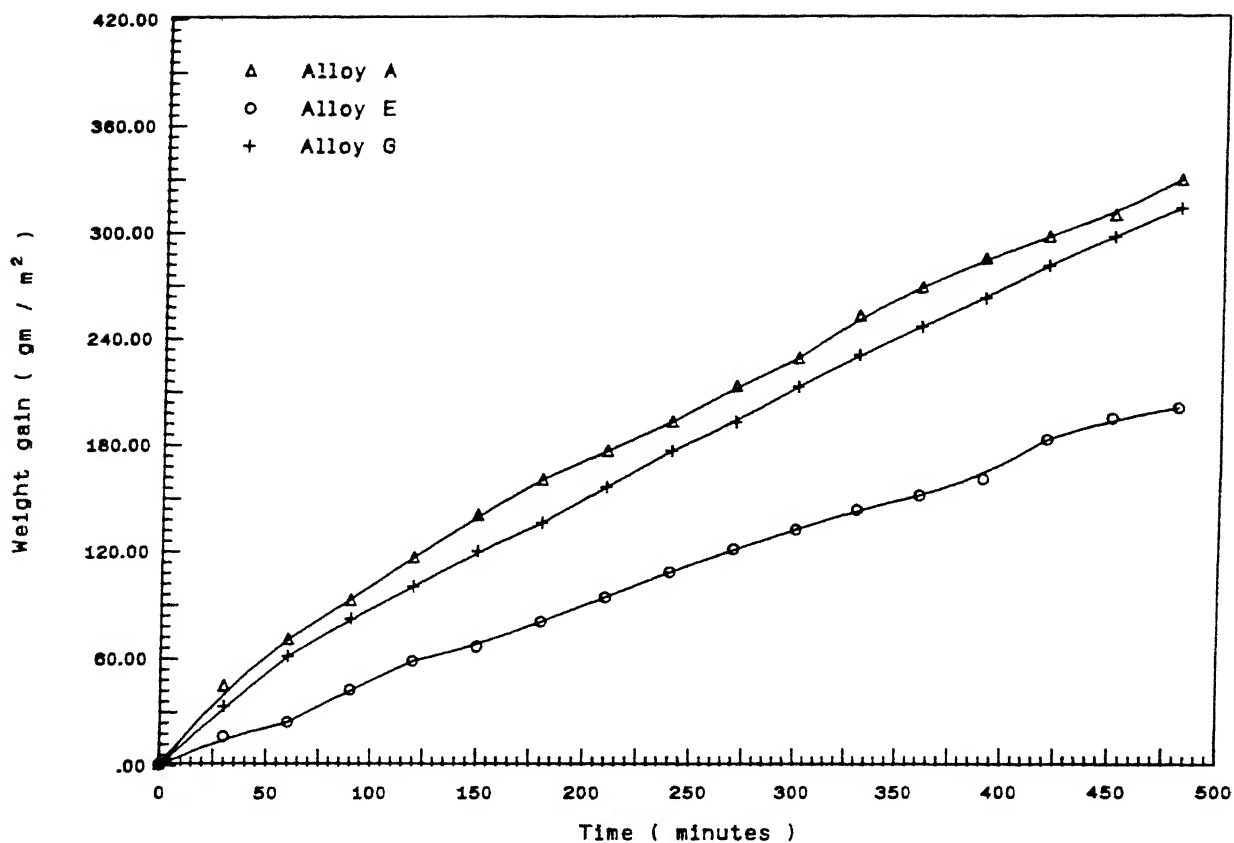


Figure 3.47 Weight gain Vs time plot of alloys A,E and G during oxidation in air 800°C (1073K).

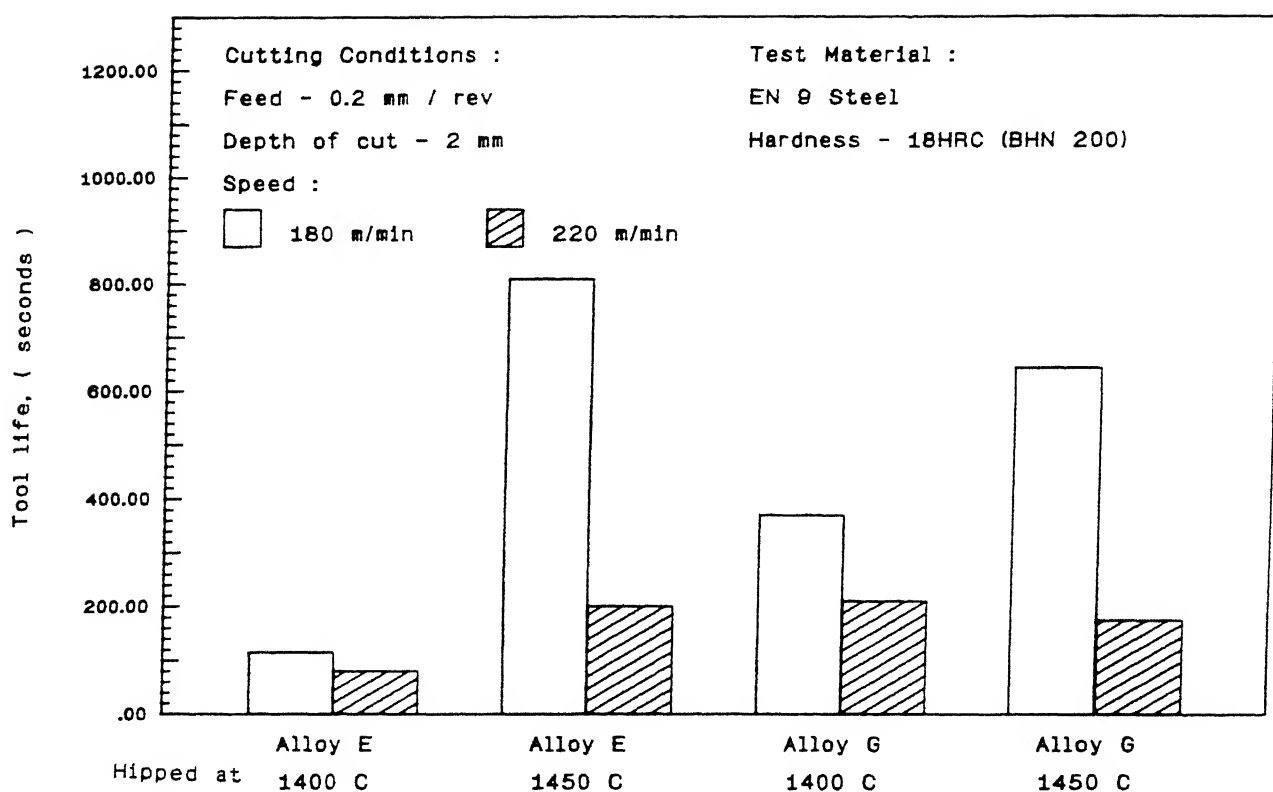


Figure 3.48 Tool life variations of alloys E and G HIP'ped at 1400°C and 1450°C respectively.

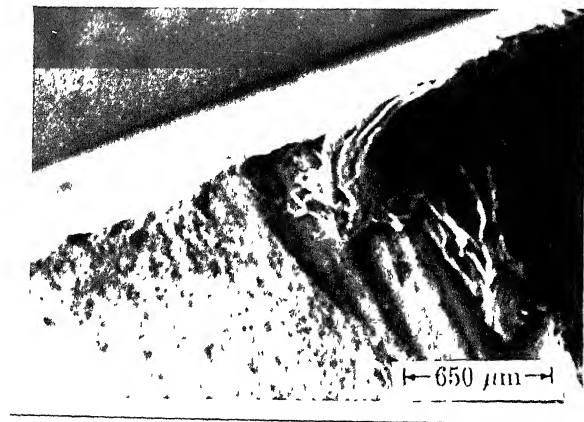


Figure 3.49 SEM picture of tool made of alloy E after cutting EN 9 steel at 180 m/min, showing nose radius wear.

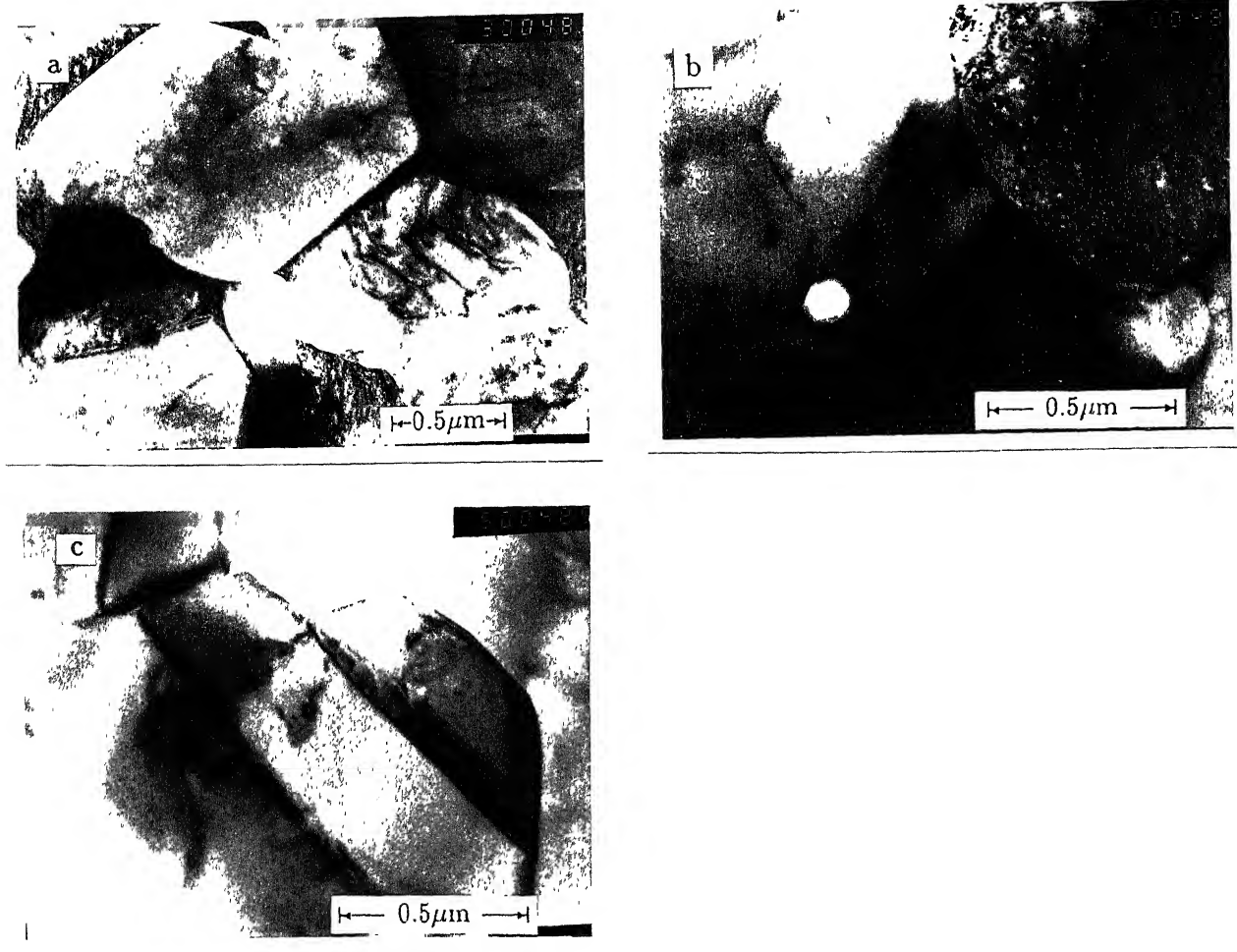


Figure 3.50 TEM micrographs of alloy G, showing (a) general microstructure containing equiaxed TiN grain, straight faceted WC and binder with high dislocation density, (b) deformed WC/TiN interface, and (c) deformed WC grain.

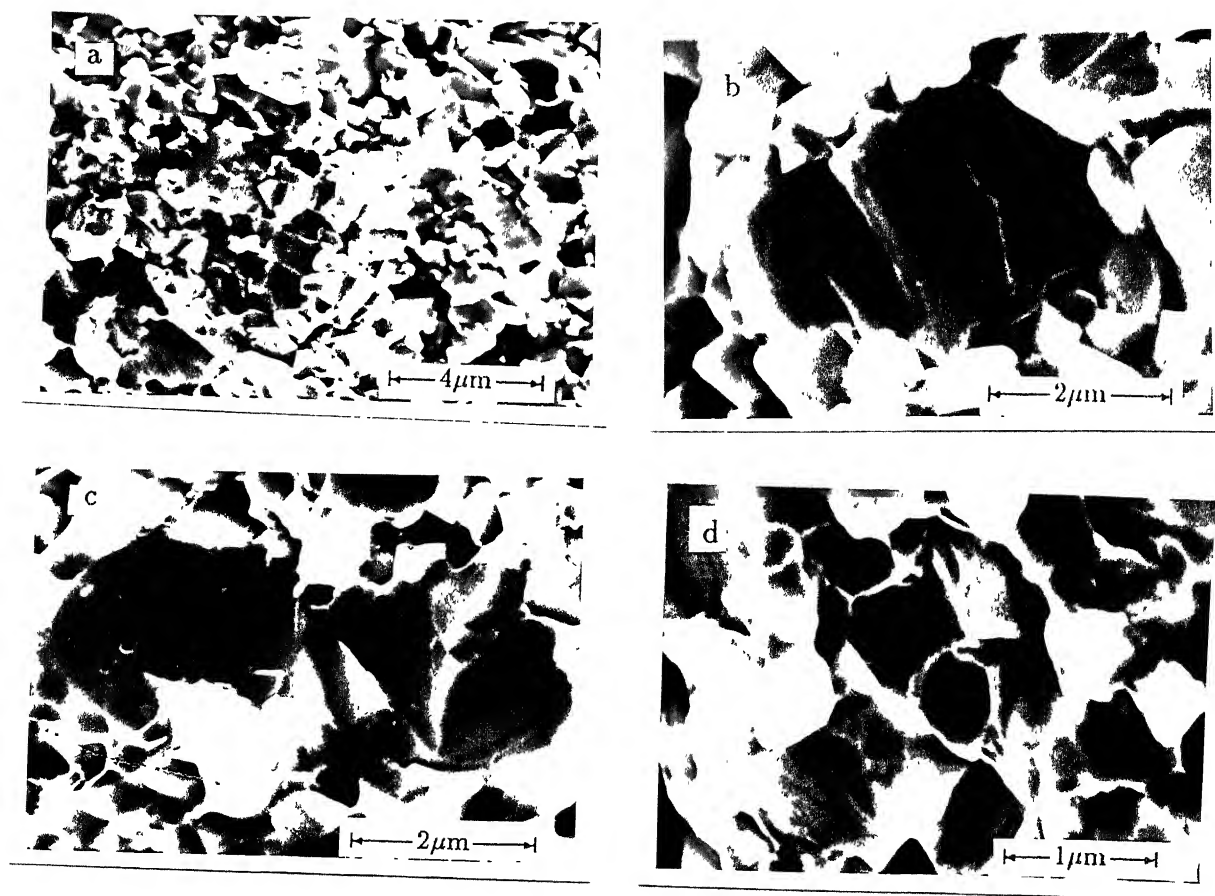


Figure 3.51 SEM fractographs of alloy G, showing : (a) transgranular fracture of hard phase grains and ductile fracture of binder phase, (b) and (c) typical transgranular fracture in TiN grains and (d) impression of small WC grains pull out from the matrix.

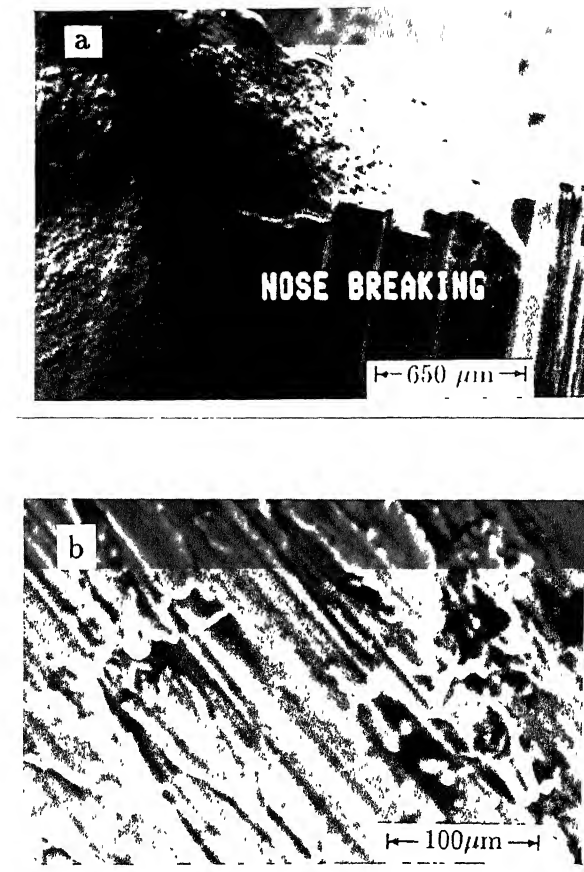


Figure 3.52 SEM pictures of tool made of alloy G after cutting E9 steel at 180 m/min., showing : (a) nose breaking, and (b) magnified view of the broken surface.

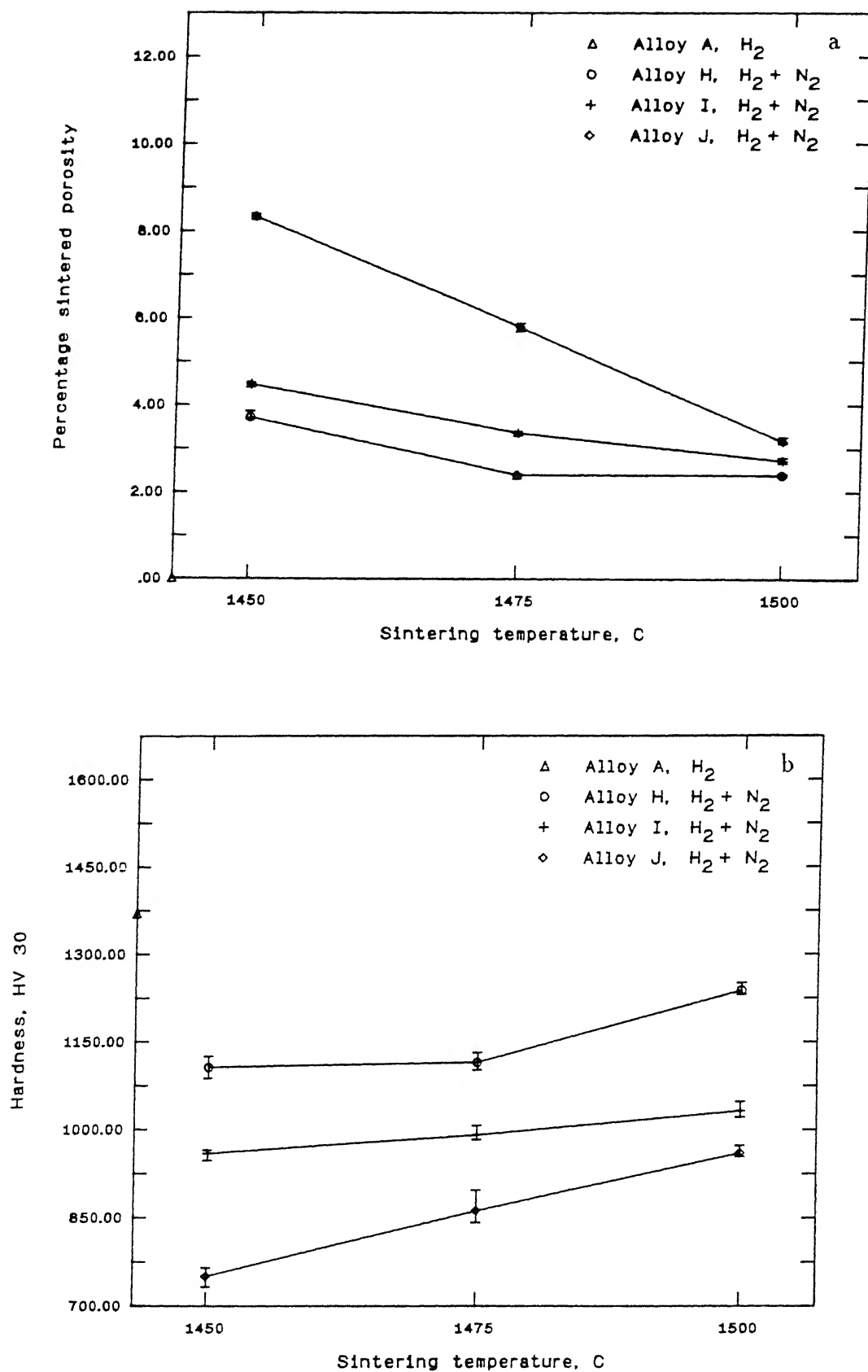


Figure 3.53 Effect of sintering temperature on percentage sintered porosity (a), and hardness (b) of alloys H, I and J (sintered in  $H_2 + N_2$ ).

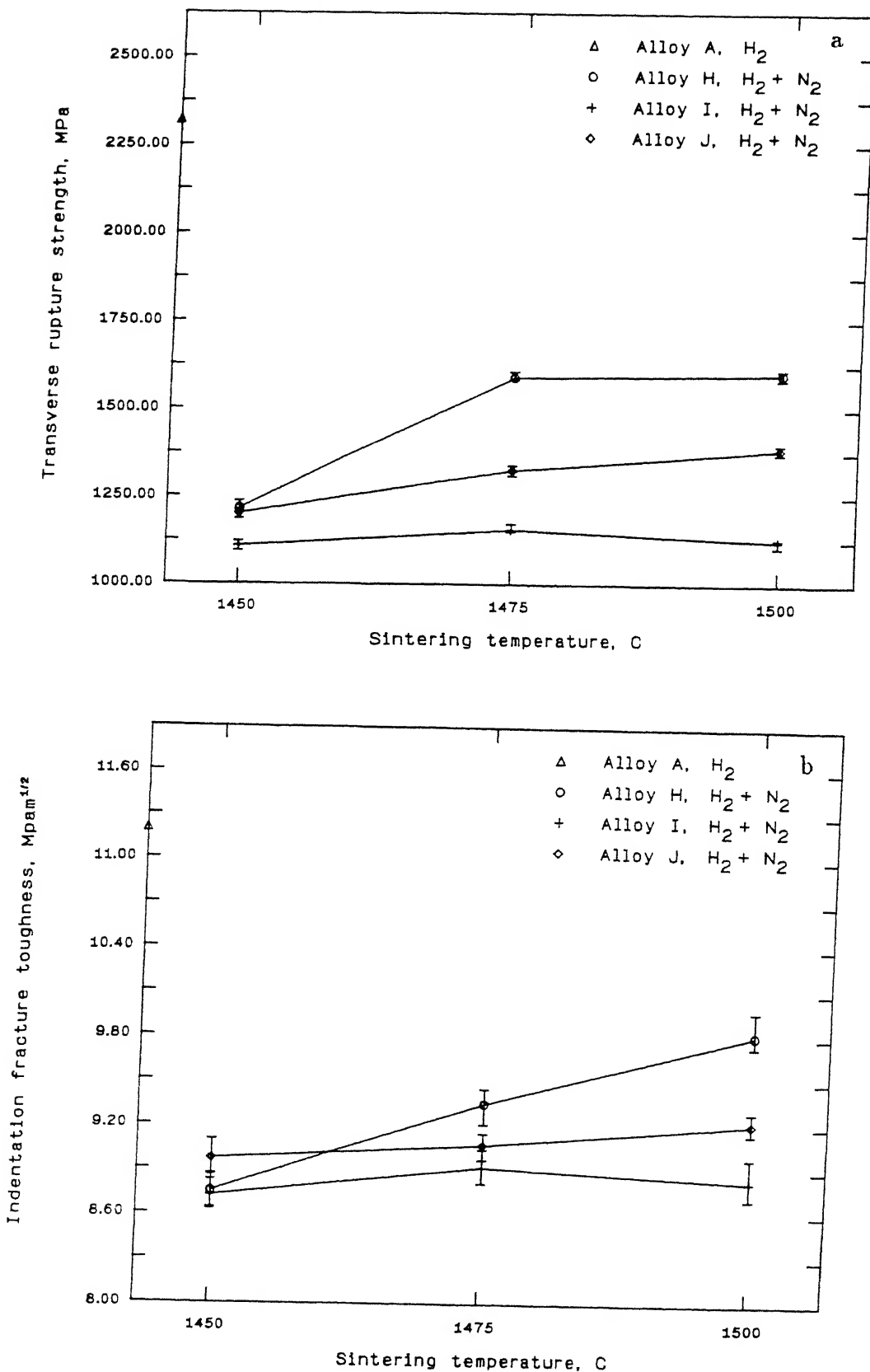


Figure 3.54 Effect of sintering temperature on TRS (a), and indentation fracture toughness of alloys H, I and J (sintered  $H_2 + N_2$ ).

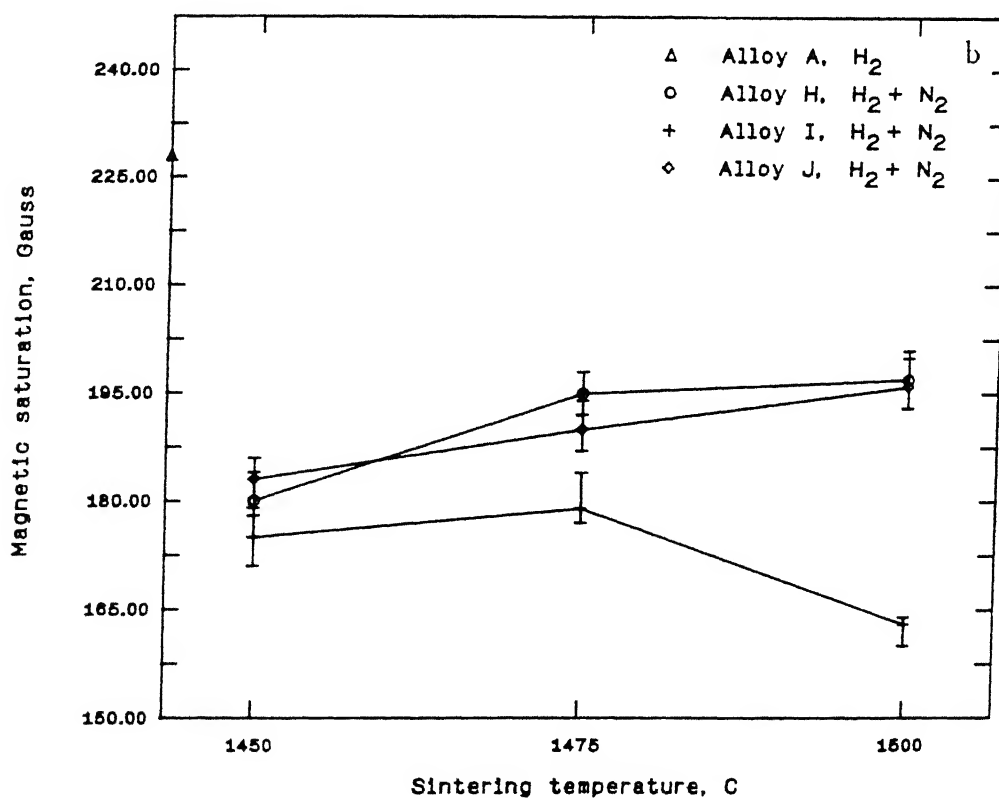
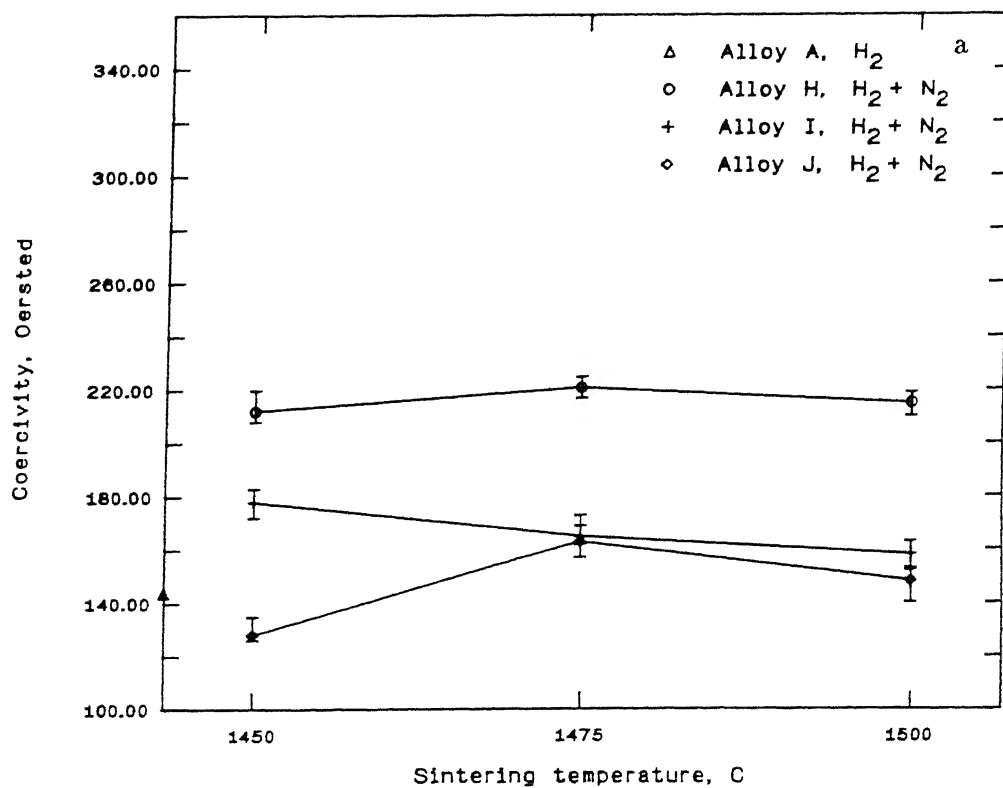


Figure 3.55 Effect of sintering temperature on magnetic properties : (a) coercivity, and (b) magnetic saturation of alloys H, I and J (sintered in  $H_2 + N_2$ ).

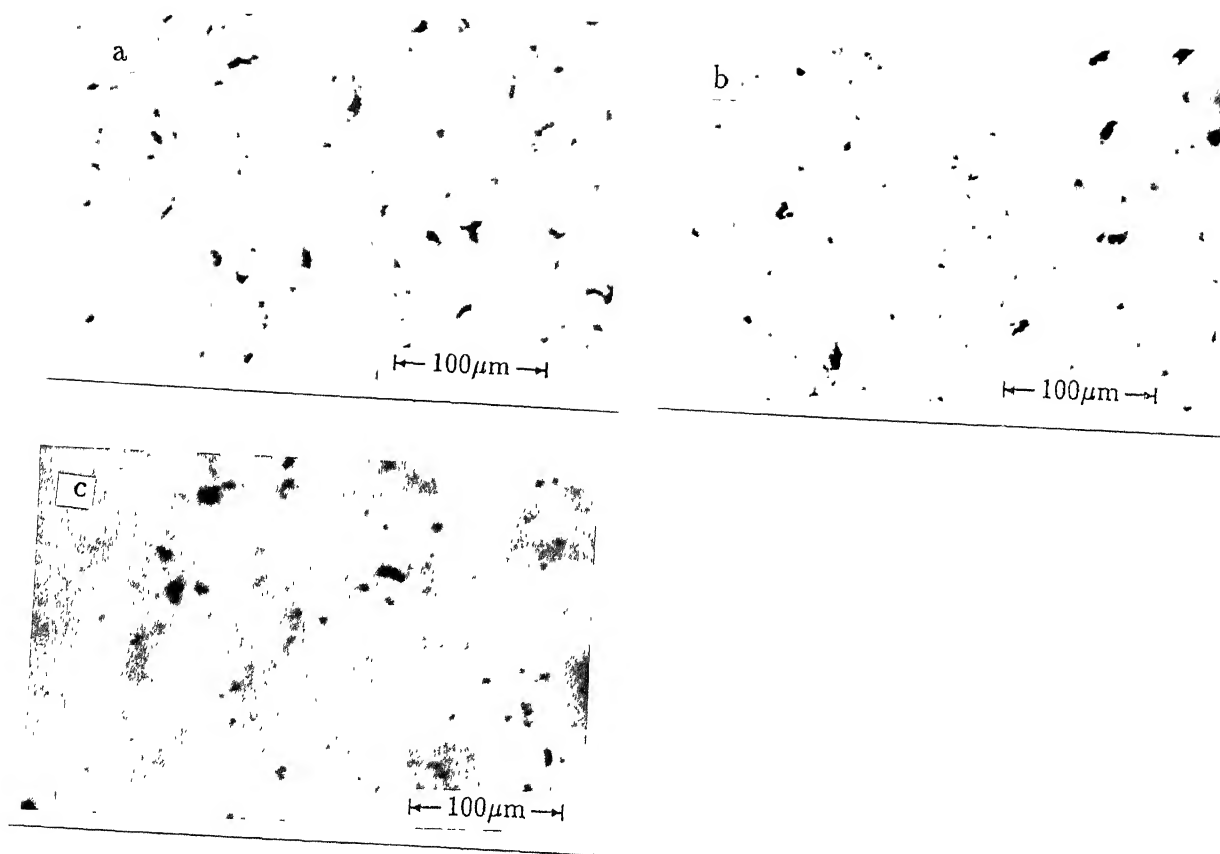


Figure 3.56 Pore morphology and distribution in (a) alloy H, sintered at 1475°C, (b) alloy I, sintered at 1475°C, and (c) alloy J, sintered at 1500°C in H<sub>2</sub>+N<sub>2</sub> mixture.

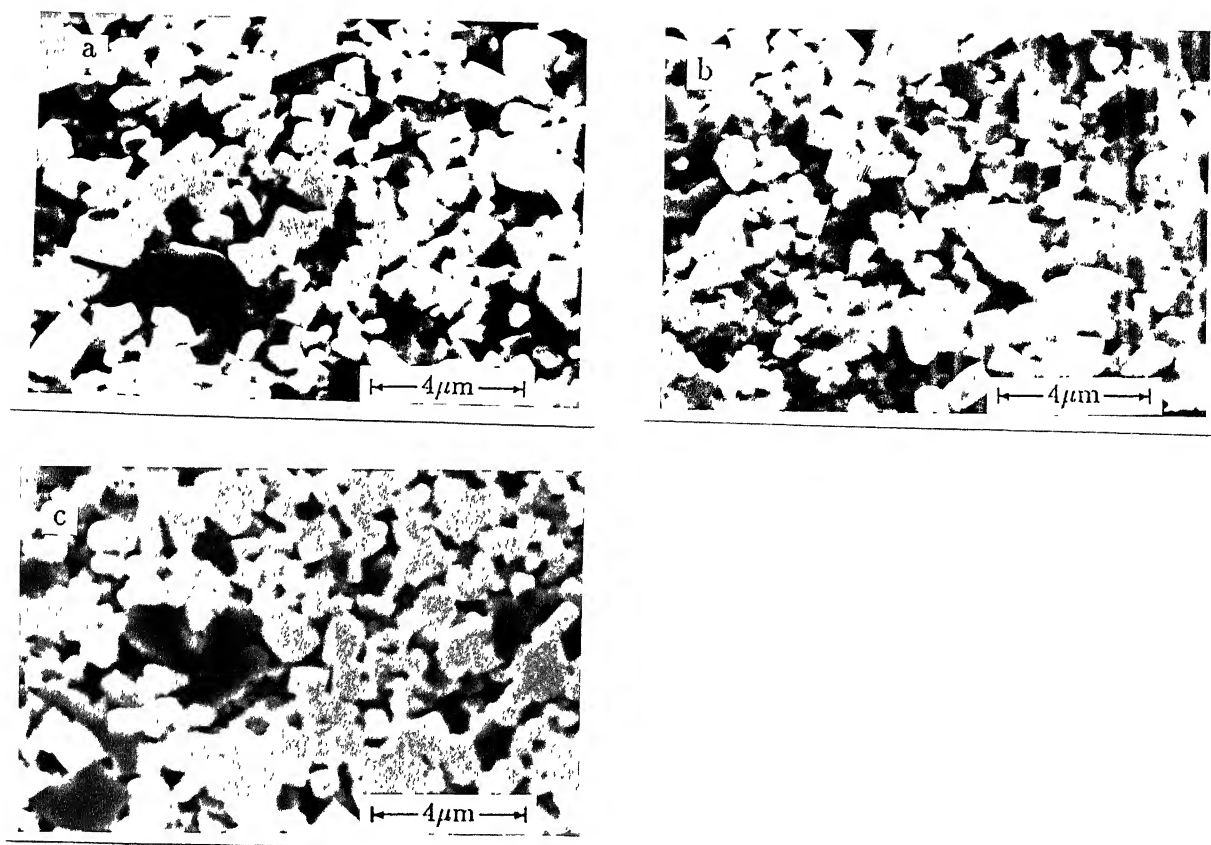


Figure 3.57 SEM microstructures of (a) alloy H, sintered at 1475°C, (b) alloy I, sintered at 1475°C, and (c) alloy J, sintered at 1500°C in  $\text{H}_2 + \text{N}_2$  mixture.

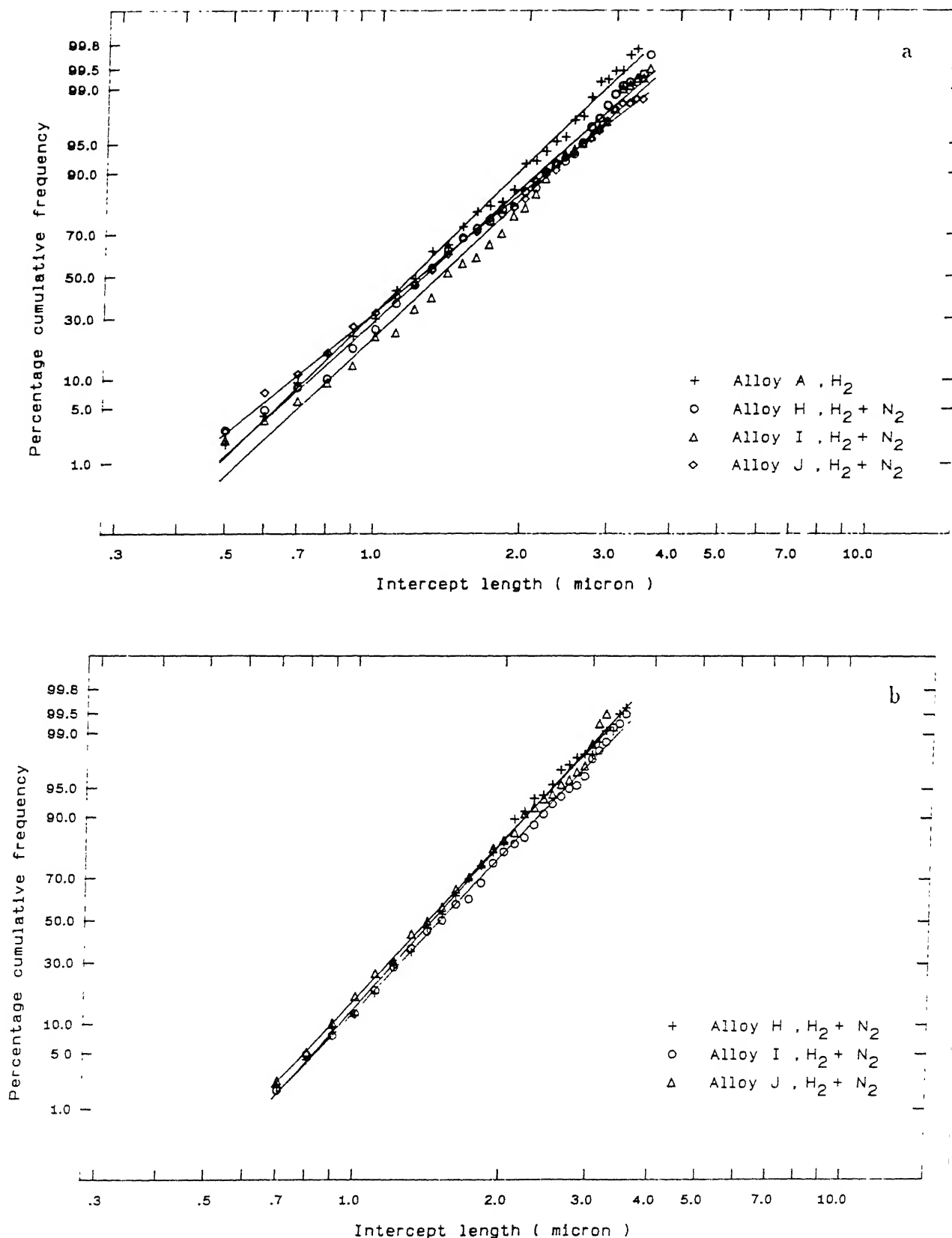


Figure 3.58 Cumulative frequency distribution of (a) WC, and (b) Ti(C,N) intercept lengths in alloys H, I and J sintered at 1475°C and 1500°C respectively in  $H_2 + N_2$  mixture.

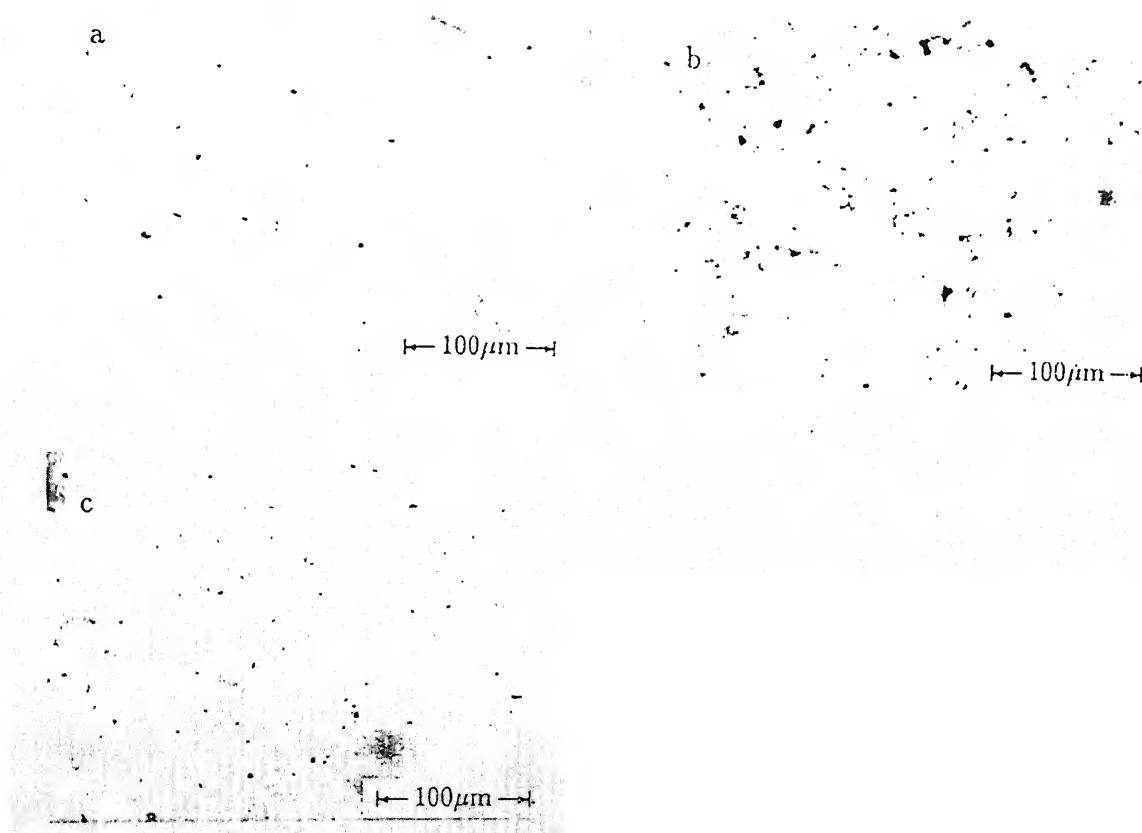


Figure 3.59 Pore morphology and distribution in alloy H (a), alloy I (b), and alloy J (c), after HIP'ing at 1400 °C.

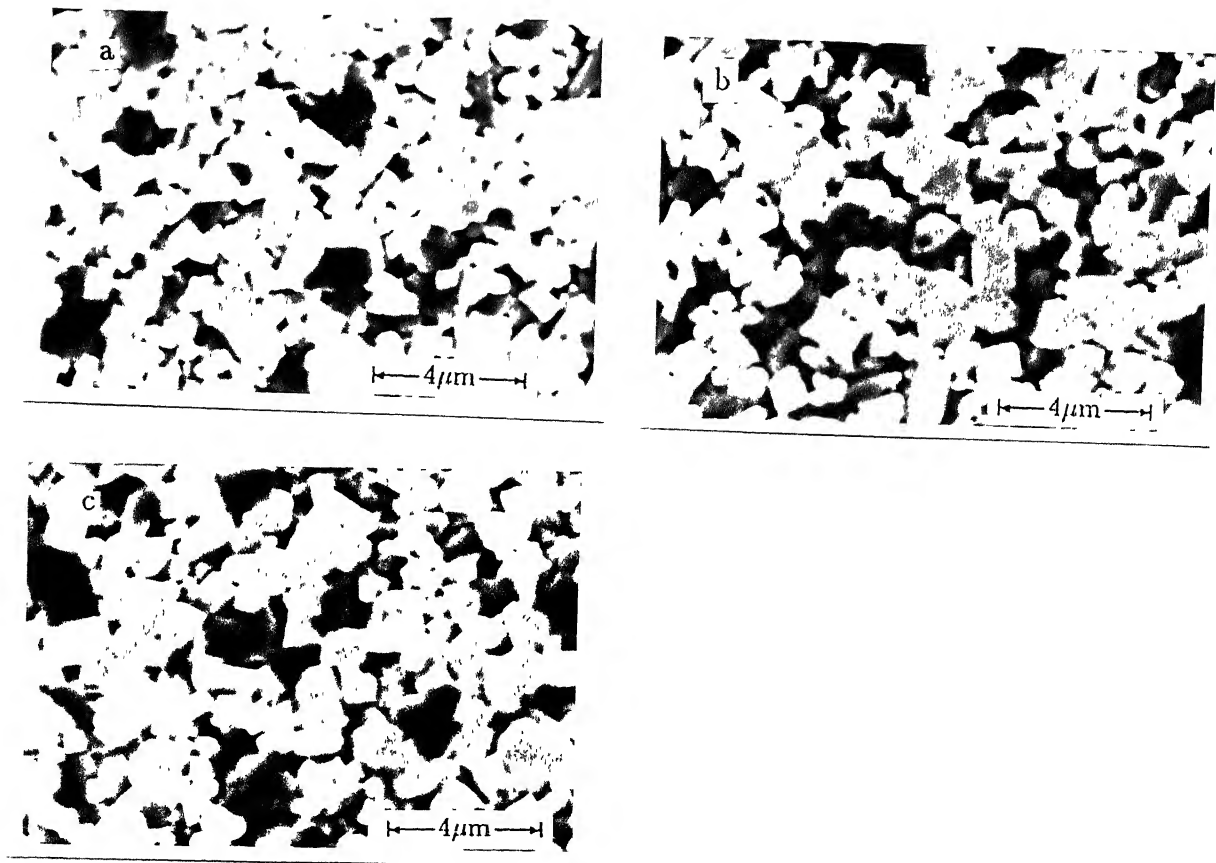


Figure 3.60 SEM microstructures of alloy H (a), alloy I (b), and alloy J (c) after HIP'ing at 1400°C.

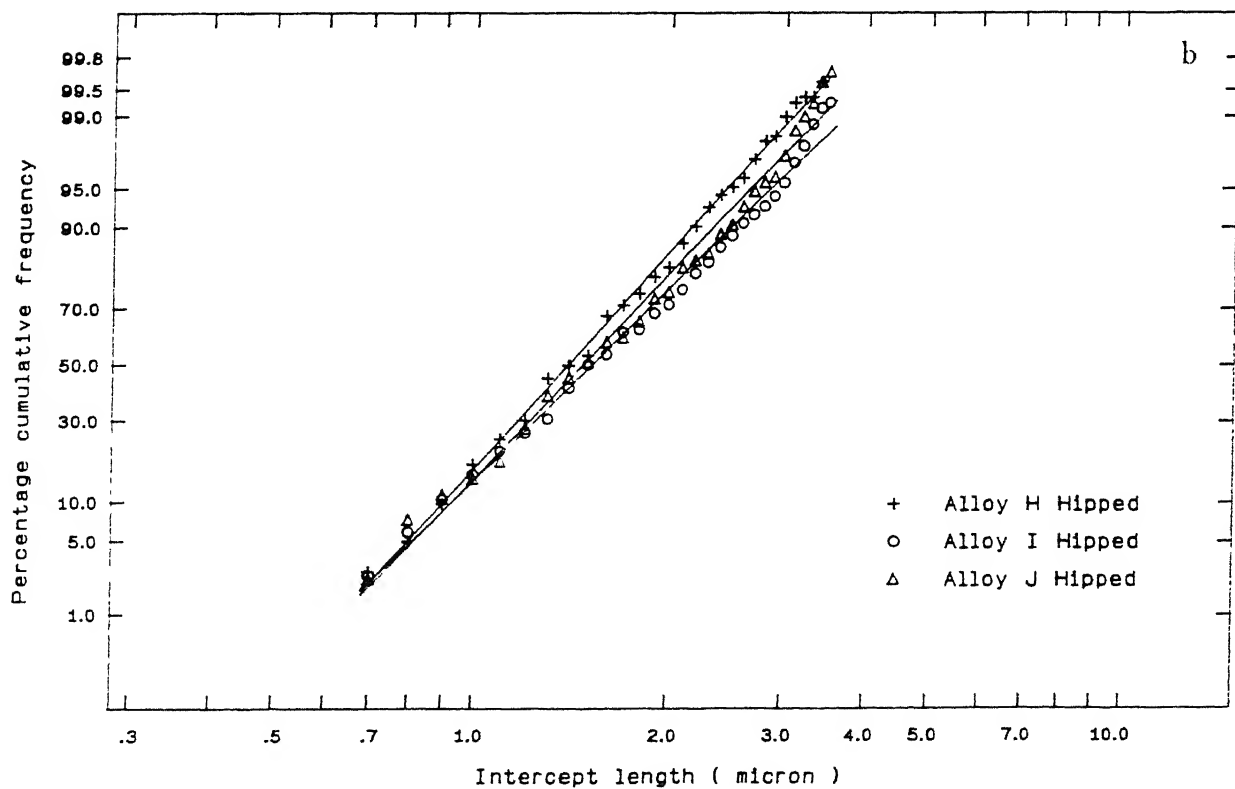
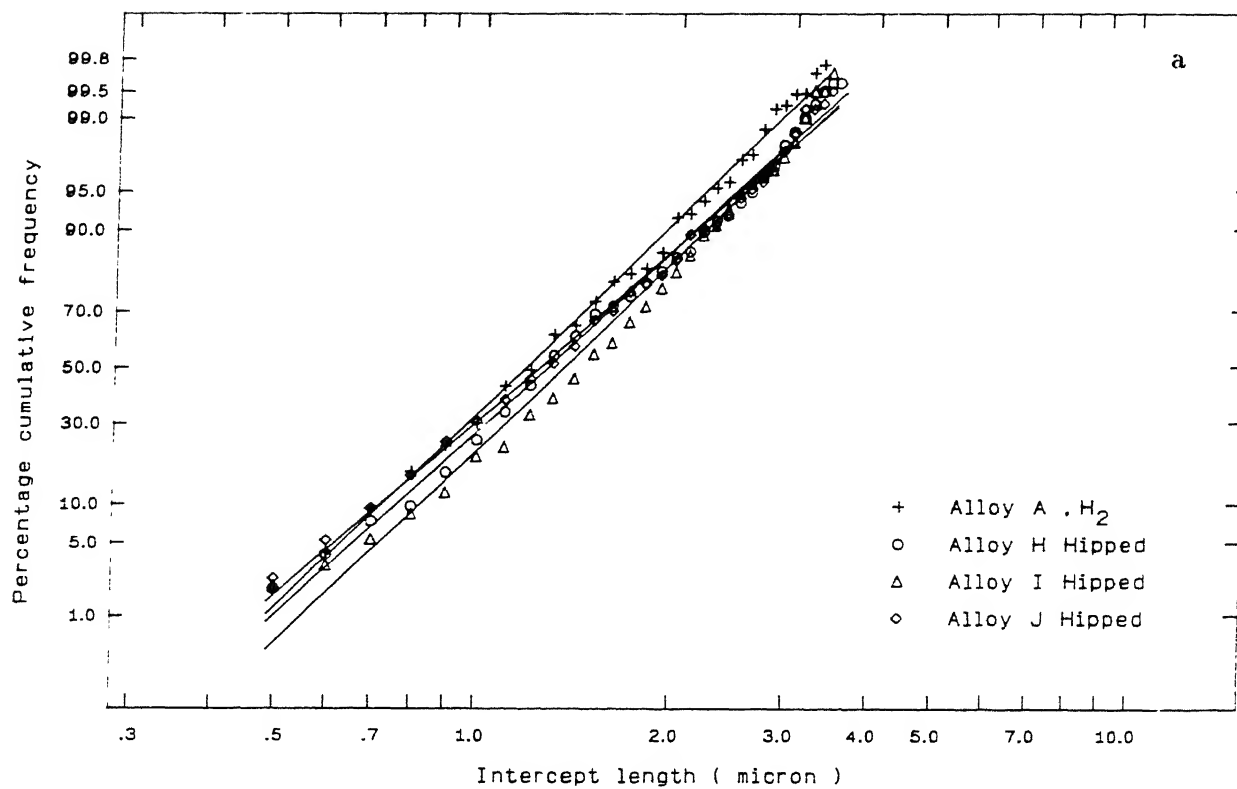


Figure 3.61 Cumulative frequency distribution of (a) WC, and (b) Ti(C,N) intercept lengths in alloys H, I and J after HIP'ing at 1400°C.

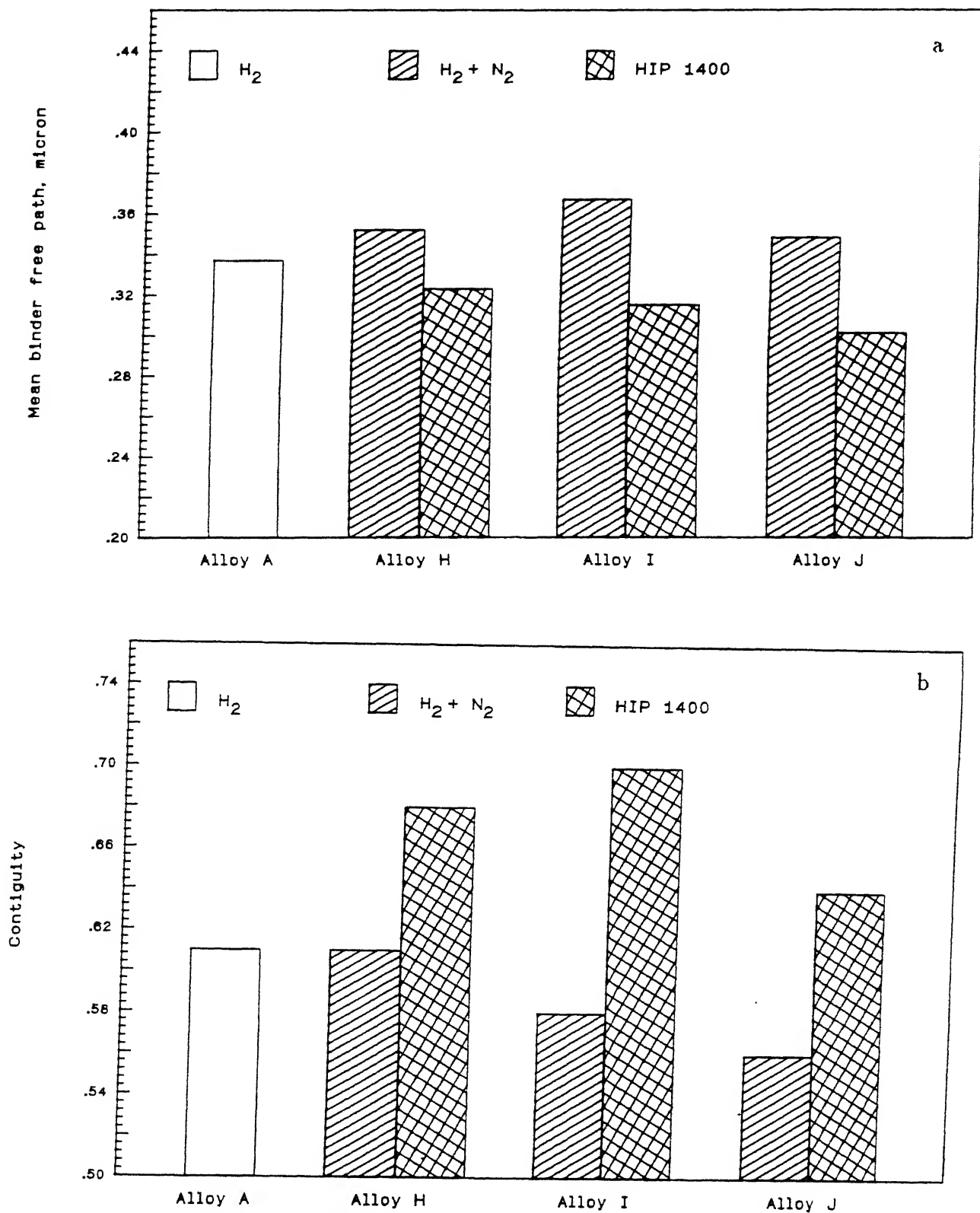


Figure 3.62 Mean binder free path (a) and contiguity (b) variations in alloys H, I and J.

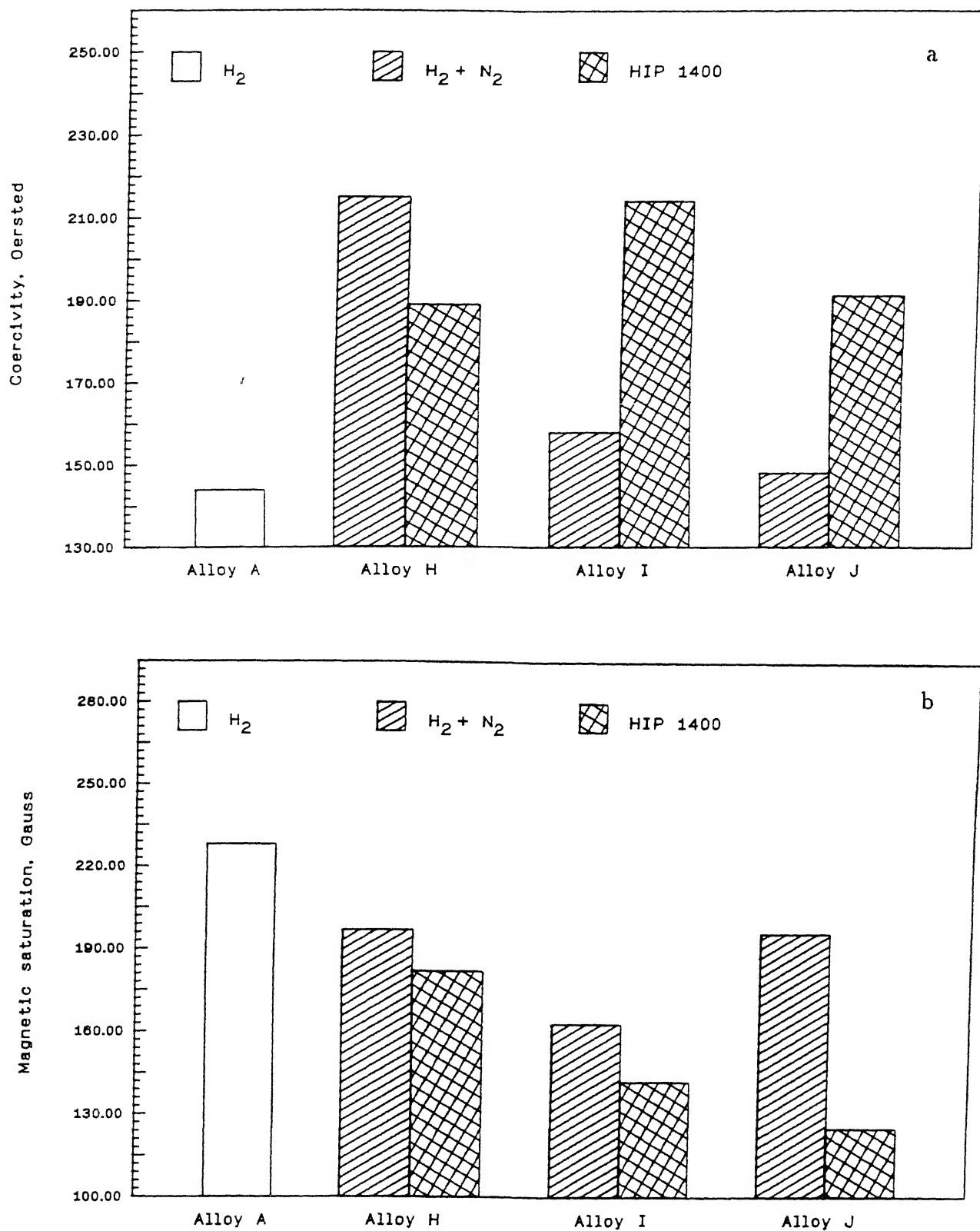


Figure 3.63 Coercivity (a), and magnetic saturation (b) variations in alloys H, I and J.

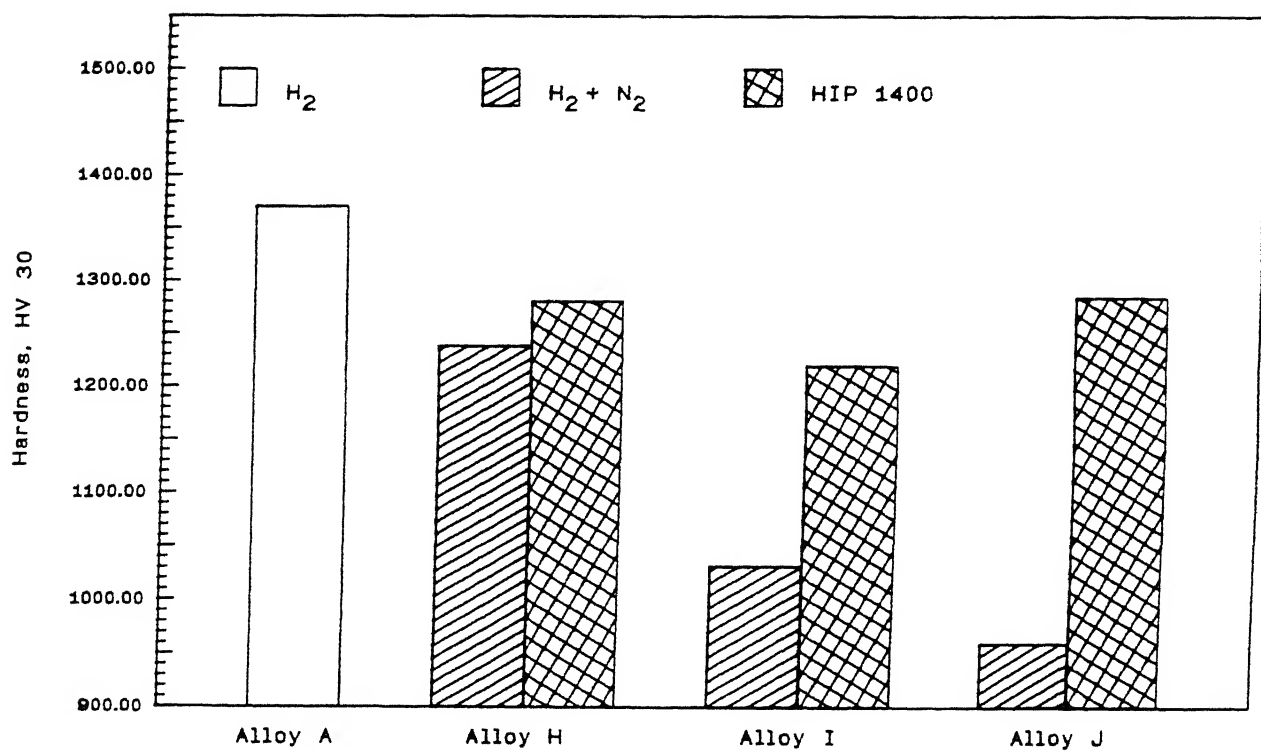


Figure 3.64 Hardness variations in alloys H, I and J.

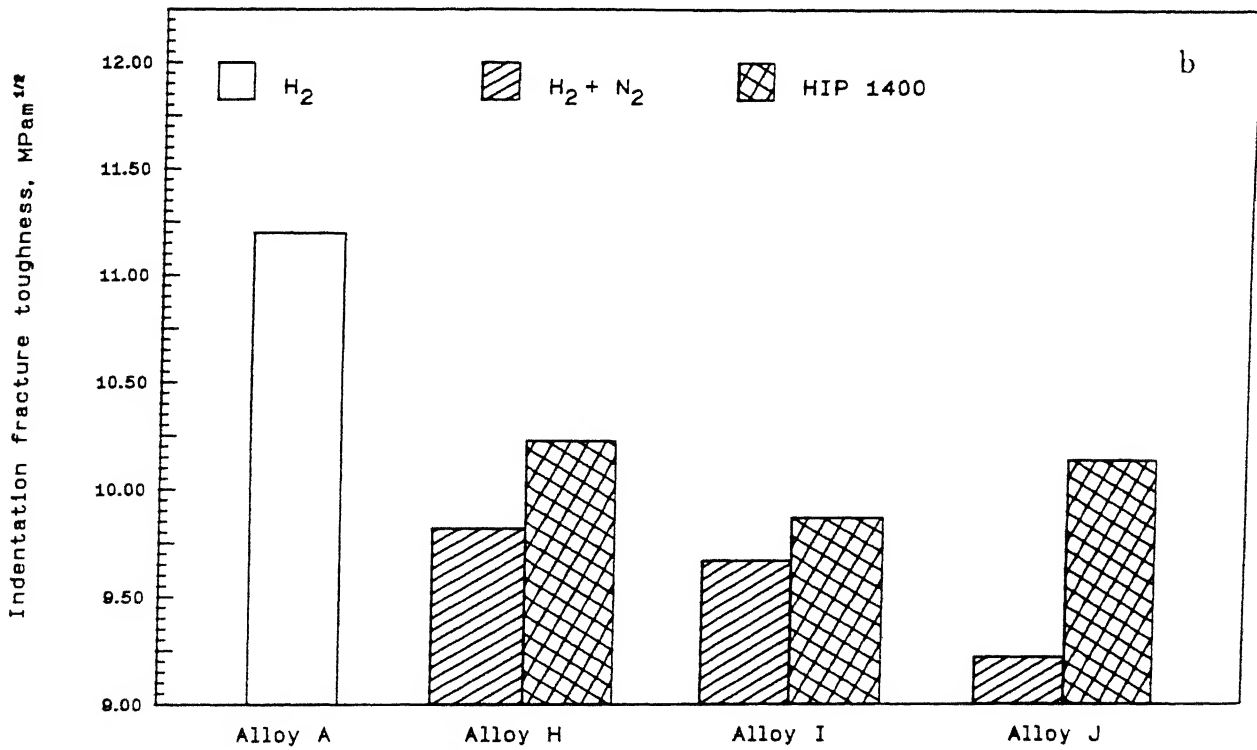
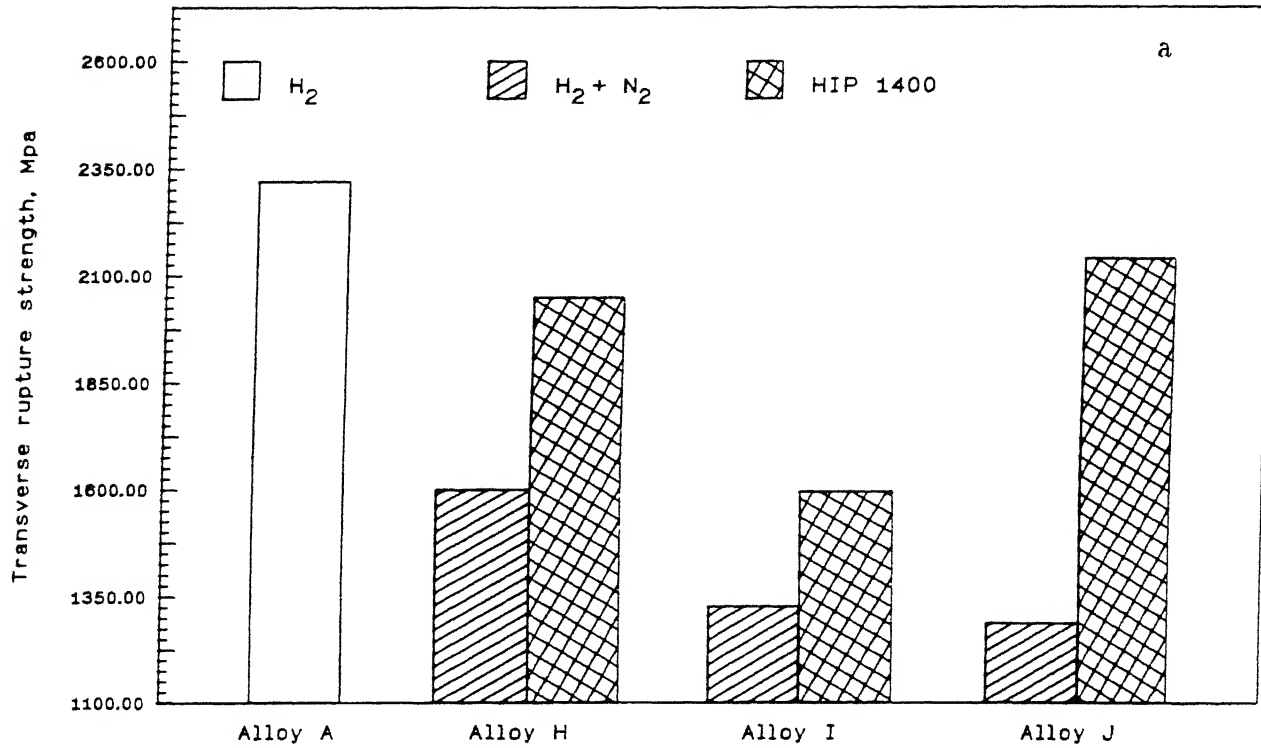


Figure 3.65 TRS (a), and indentation fracture toughness (b) variations in alloys H, I and J.

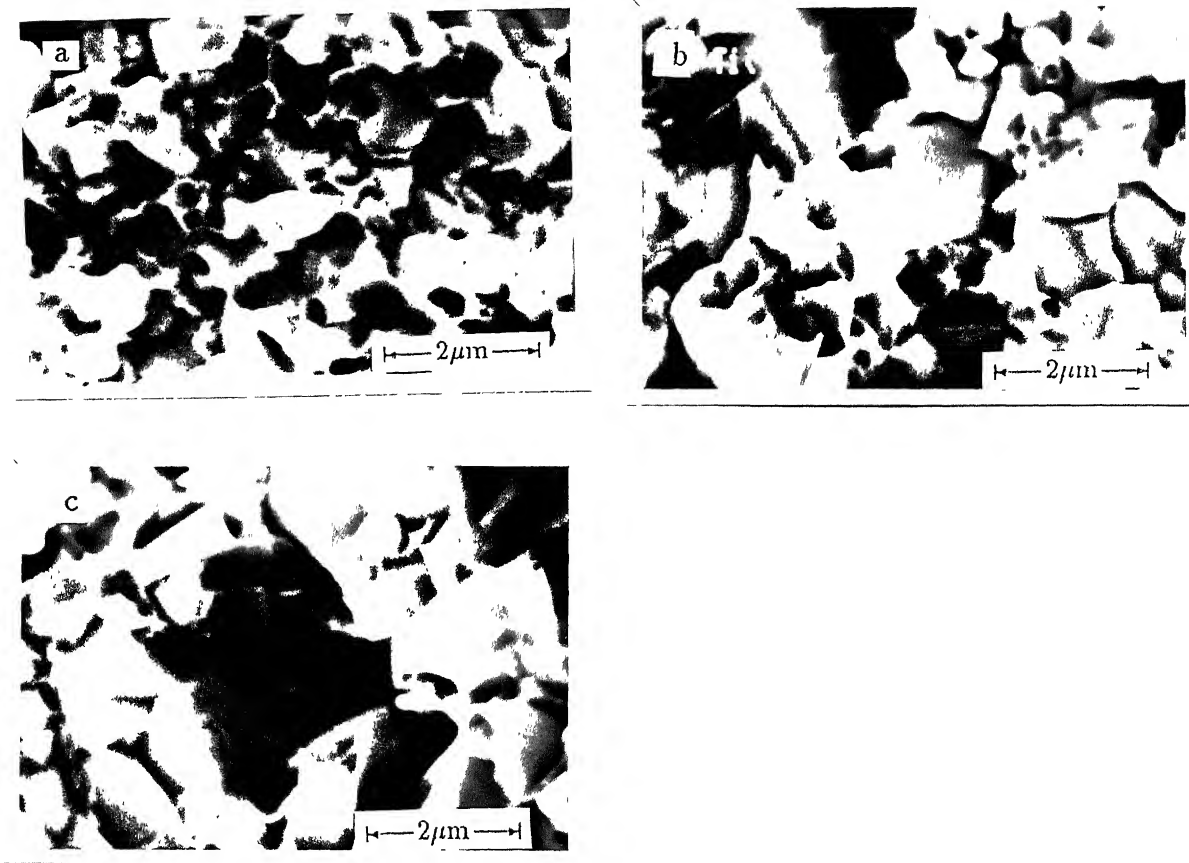


Figure 3.66 SEM fractographs of alloy H, showing : (a) ductile fracture in binder phase, (b) brittle fracture in hard phases, (c) transgranular fracture in large Ti(C,N) grain.

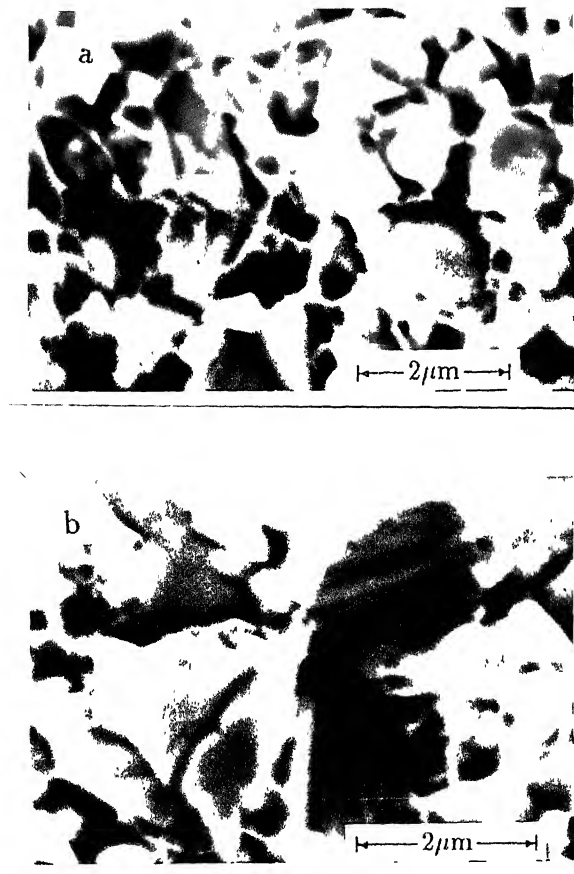


Figure 3.67 SEM fractographs of alloy I, showing: (a) fractured binder ligaments, and (b) crack initiation at the contiguous boundary.

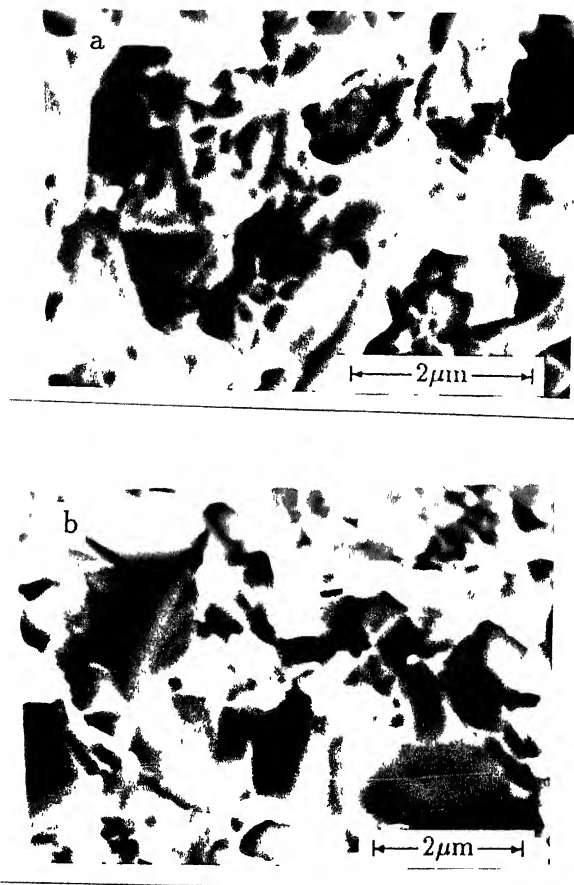


Figure 3.68 SEM fractographs of alloy J, showing : (a) dimpled structure in fractured binder phase, and (b) brittle fracture in hard phases.

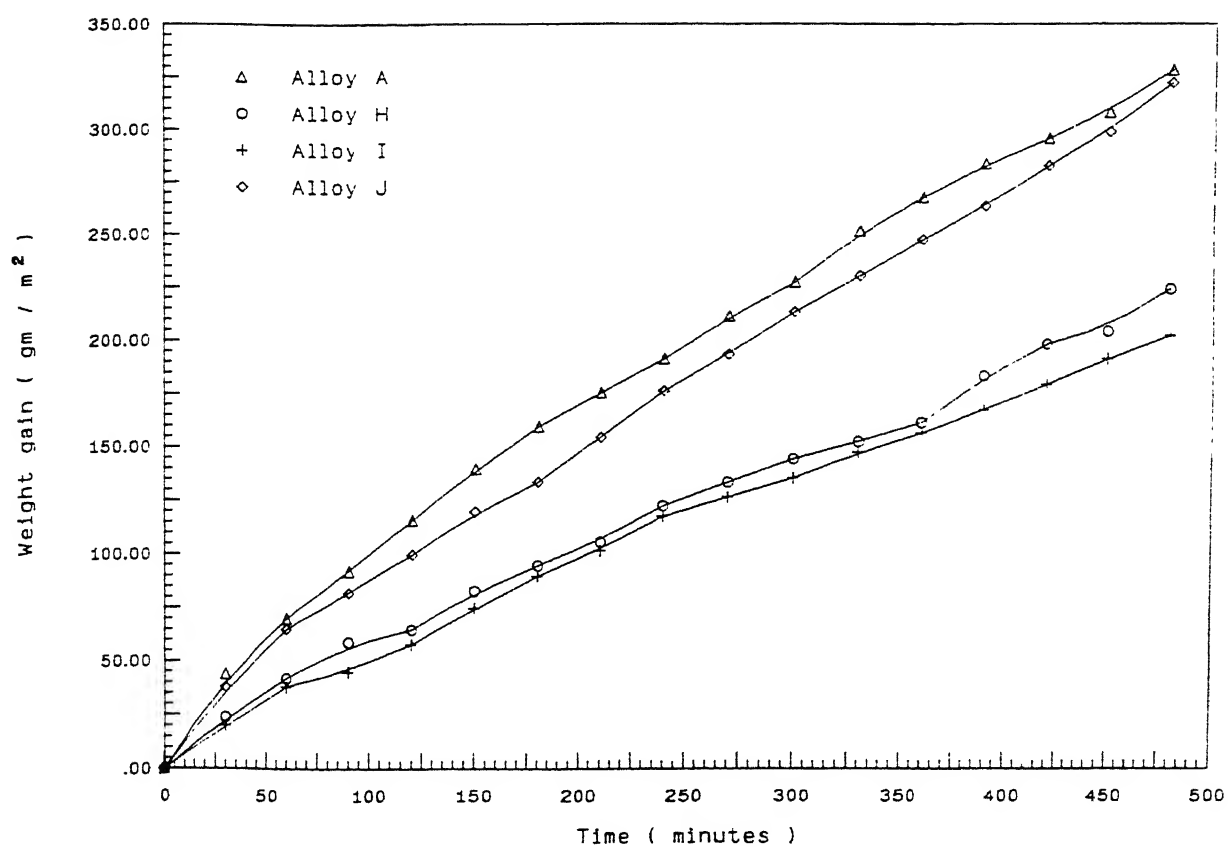


Figure 3.69 Weight gain Vs time plot of alloys H,I and J during oxidation in air at  $800^{\circ}\text{C}$  ( $1073\text{K}$ ).

# CHAPTER - IV

## DISCUSSION

In the present chapter the results on various grades of modified WC-10Co cemented carbides have been discussed. For each set of alloy densification behavior, microstructural characterisation, mechanical properties, oxidation and thermal shock resistance, and cutting performance have been discussed under separate sections.

### IV.1 WC-10Co CEMENTED CARBIDE (ALLOY A)

#### IV.1.1 Densification behavior

WC-Co system is an ideal system for liquid phase sintering where WC has a wetting angle of  $0^{\circ}$  (in vacuum) with liquid cobalt and has a maximum solubility of 22 mass% at  $1250^{\circ}\text{C}$  in it [13,169]. Based on the literature [163] the sintering temperature for WC-10Co cemented carbide was selected as  $1425^{\circ}\text{C}$  at which the full density of the alloy was achieved. The majority of densification in WC-Co system is achieved during the first stage of liquid phase sintering i.e., grain rearrangement. The good densification characteristics of WC-Co are due to the initial solution of the carbide by the cobalt. This results in an extensive densification even before the first liquid is formed. Cobalt diffuses in the solid state into interfaces between carbide grains and as the temperature increases dissolves carbide from the adjacent grain surfaces [9,10]. Once the liquid is formed its further formation and spreading over the grains are fast due to surface energy reasons. As soon as the liquid penetrates the grain boundaries, a capillary force is developed which leads to grain rearrangement for closer packing in the presence of liquid

becomes restricted due to the positive pressure of the insoluble gas in the pores. Such a case does not arise in vacuum sintering, because most of the insoluble gas is removed when the pores are interconnected and hence results in lower residual sintered porosity.

#### IV.1.2 Microstructural characterisation

WC-10Co cemented carbide has a two phase structure consisting of WC grains embedded in cobalt matrix (Fig.3.6b). WC grains exhibit simple geometric forms with straight edges (Fig. 3.7a). With isotropic substances a general redistribution of material takes place during sintering. This comes about as a result of diffusion gradients whereby interfaces grow at the expense of those with small radii. But in case of WC which has a highly anisotropic structure, the low energy surface and interfacial planes set up activity/diffusion gradients, whereby material tends to diffuse and deposit only on more favorable low energy orientations. This results in development of anisotropic crystal shapes during growth which can be described as flat triangular prism with truncated edges [11,13]. However, in technical cemented carbides, this shape is not fully developed, as was also observed in the present study, probably due to coalescence and impingement with other crystals. The typical grain shapes with rectangular or triangular faces suggest  $\{10\bar{1}0\}$  or  $\{0001\}$  orientations [15]. The dislocation density observed in WC crystals is low (Fig. 3.7b) and many of them are free from any form of defect structure. The observed dislocation may arise due to the deformation of the carbide crystals during milling and partly due to the residual stresses during sintering processes which are accommodated by plastic deformation [15-17]. Thermal

stresses develop during cooling from sintering temperature because of the large differences in thermal expansion coefficients and elastic moduli between the carbide and binder phases. In general, these stresses are compressive in the carbide phase and tensile in the binder phase [16].

In ideal case, the binder phase cobalt in the microstructure should be present as a continuous film separating each WC grain from others. This does not happen in practice and invariably each WC grain in the microstructure seems to be in contact with many neighboring grains (Fig. 3.7a). Whether the hard phase forms a continuous skeleton or not is debatable, but most of the reserchers do agree with the modified skeleton theory. However, contiguity which is a measure of the hard phase/hard phase boundary in the microstructure is frequently reported, which has a quantitative relationship with the mechanical properties of cemented carbides. The contiguity value varies with the hard phase grain size, volume fraction of binder phase and also depends on the processing parameters. The contiguity value obtained in the present alloy is 0.61 which is of the same order as reported in the literature [29] for similar compositions and grain size. Vacuum sintering resulted in a slightly lower contiguity value (Table 3.2), the reason being, wetting of WC grains by liquid cobalt in vacuum is better than that in hydrogen.

Binder phase cobalt was mostly present as a thin film between the carbide grains, but in some places in the microstructure it was also present as a pool. It was associated with high dislocation and stacking fault density (Fig. 3.7c). Cobalt has hcp structure at room temperature and fcc structure above  $417^{\circ}\text{C}$ . High temperature structure (fcc) is

stabilised below  $417^{\circ}\text{C}$  because of the residual stresses and because of the presence of dissolved tungsten and carbon [16]. Therefore, complete transformation of fcc to hcp structure never takes place and in cemented carbides this phase exists as a mixture of fcc and hcp structure. Moreover, the transformed hcp structure in fcc cobalt appears like stacking faults in microstructures.

There are basically two kinds of interfaces in cemented carbides viz. carbide/carbide (Fig. 3.7d) and carbide/binder (Fig. 3.7c). As previously mentioned, the  $\{10\bar{1}0\}$  prismatic plane and  $\{0001\}$  basal plane are the two main facets of WC crystals. These two crystallographic planes play an important role in the formation of tungsten carbide interfaces. Due to the particular crystal structure of WC and the shape of the crystal, the prismatic plane is highly promoted as a boundary plane during sintering process. Most grain boundaries between two WC crystals rotated around  $\langle 10\bar{1}0 \rangle$  parallel to prismatic plane which are classified as twist grain boundaries. On the other hand, the grain boundaries formed by rotation around  $\langle 11\bar{2}0 \rangle$  axis are described as asymmetric tilt boundaries [15]. However, the relationship between the orientations of the carbide grains and the cobalt at WC/Co interfaces is of interest. A lattice imaging technique for such studies was adopted [172] but no clear relationship between the two phases was found. Cobalt is used traditionally as the binder phase in WC based cemented carbides, as it results in a hard phase/ binder interface, which is strong enough to withstand interface separation.

#### IV.1.3 Mechanical properties and fracture behavior

Various mechanical properties viz. hardness, TRS, indentation fracture toughness obtained for the present alloy (Table 3.3) are comparable to those available in the literature [74,103,163]. Vacuum sintering resulted in a better TRS and indentation fracture toughness than that of hydrogen sintering (Table 3.3). The improvement in strength properties may be attributed to the fact that vacuum sintering results in a better binder phase distribution and less residual porosity than that of hydrogen sintered one.

The typical fracture surface of alloy A is composed of transgranular fracture of WC grains and ductile fracture of cobalt. The predominant fracture mode depends on the microstructural parameters such as carbide grain size, mean binder free path and the distribution of the binder phase. WC of grain size greater than 5  $\mu\text{m}$  are generally favored in fracturing transgranularly (Fig.3.8b) and smaller grains ( $<2\mu\text{m}$ ) in fracturing intergranularly. In general, the tendency of WC grains to cleave increases with increased grain size and cobalt content [107]. The most important micromechanism of fracture in WC-Co cemented carbide is the ductile fracture in binder phase, because this mode of fracture has the greatest influence on the strength [103,107]. WC/Co interface bond strength plays an important role in deciding the failure mode in the ductile phase. If the bond strength is sufficient enough to withstand the interface separation, the propagating crack is favored to pass through the binder phase and thus the maximum benefit of the matrix is obtained. In such a case, the binder phase fails by void nucleation and growth, and leaves a pattern of dimples on the fracture surface. On the other hand, when the WC/Co interface separation becomes easier because of inferior bond

strength, the binder phase fails by necking which is present on the fracture surface as fractured ligaments [110].

#### IV.1.4 Oxidation and thermal shock resistance

WC-Co cemented carbide follows parabolic type of oxidation behavior at  $800^{\circ}\text{C}$  ( $n = 1.36$ ). The oxide layers forming on this alloy are brittle. The oxide is in compression which is to be expected since the Pilling-Bedworth ratios for the oxides identified in this system are greater than one [119]. This results in some cracks at the substrate/oxide interface (Fig. 3.10a). These cracks are not just surface phenomena but they extend through the oxide layers from the substrate/oxide interface to oxide/gas interface (Fig. 3.10b) which would most probably lead to the fast oxidation kinetics observed in this alloy.

The stresses develop in cemented carbides during thermal shock resistance test (quenching test) are similar to those develop when cooling from sintering temperature. The only difference is that the cooling rate is faster in the former than that of the latter. The contraction mismatch between the binder phase and the carbide phase increases with the increase in the temperature from which the quenching is done. The resulting thermal stresses get relieved by the plastic deformation of the binder phase as well as carbide phase. As mentioned earlier, the stresses developed are compressive in carbide phase and tensile in binder phase. The binder phase cobalt is ductile and can accommodate the plastic deformation required to relieve the residual tensile stress of the order normally developed in this kind of test. But the limitation comes from the carbide phase. Since the carbide phase has almost negligible deformability below about  $800^{\circ}\text{C}$  [162], after

a certain stress level this phase fractures in a brittle manner which produces cracks on the surfaces of the sample. Moreover, since the cooling rate is highest at the surface, the cracks first appear there and then extend towards the core of the sample. Thermal shock resistance is very much microstructure sensitive as in the case of TRS or fracture toughness.

#### IV.1.5 Cutting performance

Inspite of having a very good combination of hardness, toughness and thermal shock resistance, alloy A has shown a poor performance in cutting steel. The diffusion wear was the major wear mechanism in limiting the tool life (Fig. 3.11b). The term diffusion wear signifies wear in which the tool shape is changed by diffusion of atoms of the tool material into the work material, equivalent to a dissolution of the tool surface by the chip material flowing over it [173]. Technologically this is known as 'cratering', which depends upon the solubility of tool material in the work material and the interface temperature obtained during cutting. The cratering phenomenon results from diffusion of carbon from the cemented tungsten carbide to the steel chip sliding over the rake face of the tools [127,132]. The interface temperature is proportional to the cutting speed, and diffusion wear is a major factor in limiting the cutting speeds for such types of cutting tools. This type of wear is extremely severe with WC-Co cemented carbides during steel cutting, so much so that such alloys have no practical application for cutting steel in continuous chip producing operations at economic cutting speed [127]. The present results obtained in case of alloy A are in complete agreement with the facts stated above.

## IV.2 WC-8TiC-12Co CEMENTED CARBIDE (ALLOY B)

## Densification behavior

Even though the volume percent binder phase cobalt was same in alloy A and B, the full density in alloy B was achieved at  $1475^{\circ}\text{C}$  which was  $50^{\circ}\text{C}$  higher than that of alloy A (Table 3.6). The increase in sintering temperature with respect to alloy A is believed to be due to poor wettability and solubility of TiC in liquid cobalt. Cobalt dissolves only 1 mass% TiC at  $1250^{\circ}\text{C}$  and has a wettability of  $25^{\circ}$  (in vacuum) at  $1420^{\circ}\text{C}$  [13,169]. Because of high dihedral angle, the liquid cobalt penetration into WC/TiC or TiC/TiC grain boundaries becomes restricted and thereby makes the first stage of sintering i.e., rearrangement of grains less efficient than that in WC-Co system. Secondly, since the solubility of TiC in cobalt is less, the TiC grain surface smoothening takes place very slowly, restricting further the rearrangement stage which contributes maximum to densification in liquid phase sintering. In this kind of situation a higher amount of liquid phase is required so as to obtain full density within practical sintering time. Increase in sintering temperature not only increases the amount of liquid phase but also lowers the solid/liquid interfacial energy which helps in a better liquid penetration into the solid grain interfaces and facilitates the solution reprecipitation.

The effects of sintering atmosphere on densification behavior in alloy B are similar as those explained in case of alloy A.

## Microstructural characterisation

Unlike WC, TiC possesses isotropic structure [162]. Therefore, while sintering in the presence of liquid phase, TiC grains have the tendency of developing rounded shape to decrease the specific liquid/TiC surface area and thus reduces the free energy of the system. On the other hand, addition of other transition metal carbides e.g., TiC, TaC etc. to WC-Co cemented carbides inhibits the grain growth of WC. When such grain growth inhibitors are added, they get partially dissolved in the binder phase and decrease the anisotropy of the WC/binder interfacial energy [155]. This also restricts the local material transfer from high energy planes to low energy planes in a single WC grain. As a consequence, the WC grain facets are not developed properly as in the case of WC-Co cemented carbides. However, such features were not observed in the present study in alloy B (Fig. 3.18a) where WC grains exhibited the same geometry as that of alloy A. The increase in sintering temperature by 50<sup>o</sup>C with respect to alloy A, thus appears to supersede the grain growth inhibition effects of TiC, because of a faster material transfer through the liquid phase which was more in volume and less viscous than that in alloy A. The cumulative effect was the grain growth in both WC and TiC, the magnitude in the former being less than in the latter (Fig. 3.16 and Table 3.7). Since the wettability of TiC by liquid cobalt is poor, more TiC/TiC interfaces were present in the compact during sintering which might have led to coalescence as the predominant grain growth mechanism. This would lead to a high contiguity of carbide phases in sintered compacts. The probability of spatial coincidence of carbides decreases with the increase of binder content and carbide grain size and thus results in a decreased contiguity value [19]. In

the present study the volume percent binder phase was kept constant for all the alloys and since the average carbide grain size in alloy B was higher than that in alloy A, a lower contiguity value in alloy B is expected. But the present results showed that there was only marginal drop in contiguity value to 0.56 (alloy B) from 0.61 (alloy A), which is actually higher than what it should be for WC-Co cemented carbides with equivalent grain size and binder phase amount. This leads to the conclusion that addition of TiC to WC-10Co cemented carbide results in high contiguity which may be attributed to the poor wettability of such carbide with the binder cobalt melt. Since the wettability of TiC is better in vacuum [169], vacuum sintering resulted in slightly less contiguity than that in  $H_2$  sintering.

The distribution of the binder phase in the microstructure is indicated by mean binder free path and coercivity [24]. The former is the physical measurement of the mean distance between two carbide grains whereas the latter is indirect measurement which relates with the specific surface area of cobalt. The smaller the binder mean free path and the higher the value of coercivity, better is the binder phase distribution. For a fixed volume of binder phase, mean binder free path increases and coercivity decreases with the increase in carbide grain size. Similar results were presently obtained in case of alloy B (Figs. 3.17a and 3.19a), but the abnormal increase in coercivity value after vacuum sintering is not clearly understandable.

The defect structure in WC and binder phase cobalt, and the nature of WC/Co interface in the present alloy are similar to those described for alloy A. However, the noticeable feature in the microstructure is TiC/Co interface

structure (Fig. 3.18b), which is indicative of the fact that there is negligible interaction as compared to WC/Co interface. This is due to the poor wettability and solubility of TiC in cobalt melt [13], which results in a highly incoherent TiC/Co interface boundary.

### **Mechanical properties and fracture behavior**

The poor TRS and indentation fracture toughness observed in alloy B is mainly because of rather nonuniform microstructure and high contiguity. TRS and fracture toughness of WC-Co cemented carbides increase with the decrease in mean carbide grain size and increase in mean binder free path, while increased carbide contiguity causes a decrease in both TRS and toughness [89]. In alloy B the large TiC grains in the microstructure act as stress concentration points causing early failure. Secondly, the initiated crack finds an easy way of propagation by separating the carbide/carbide interfaces since the contiguity value is high. However, the higher hardness of alloy B as compared to alloy A could be related to the presence of TiC in the former.

As mentioned earlier, the fracture modes in the binder phase and the carbide phase depend on the carbide/binder interface bond strength, carbide grain size and the contiguity of the carbides. Large carbide grains act as flaws in the microstructure and result in stress concentration points. Fracture surface analyses of alloy B have shown (Fig. 3.22) that the predominant local fracture modes were separation of TiC/Co or carbide/carbide interfaces followed by transgranular fracture of large carbide grains, specifically TiC. Since the energies required for either carbide/carbide interface separation or transgranular fracture of carbide phase are much

less than that required for ductile fracturing of binder cobalt [107], the present alloy exhibited rather poor TRS and toughness.

#### Oxidation and thermal shock resistance

With the addition of TiC to WC-10Co cemented carbide the oxidation resistance is enhanced. Viewing from the thermodynamic stand point, the formation of  $\text{TiO}_2$  from TiC is easier than the formation of  $\text{WO}_2$  or  $\text{WO}_3$  from WC at  $800^\circ\text{C}$  [174], which should have a deleterious effect on oxidation resistance.  $\text{TiO}_2$  forms a compact adherent layer on the substrate [173], which probably slows down the diffusion rate of oxygen through the oxide layer to fresh substrate surface and hence an improved oxidation resistance is achieved.

The drastic drop in thermal shock resistance in alloy B can be accounted by the same reasons as mentioned earlier for TRS and indentation fracture toughness. By now, it has been already established that in alloy B, TiC/Co interface bond strength is inferior to that of WC/Co interface. Therefore, the TiC/Co interface separation becomes energetically favorable and takes place at a lower stress level in the binder phase. Once the crack is produced, its further propagation is fast, since the contraction mismatch stress already exists between the carbide and binder phase. Moreover, alloy B is having rather nonuniform microstructure with large TiC grains, and high carbide contiguity, which also assist in easy propagation of the cracks produced at the carbide/binder interface.

## Cutting performance

The practical solution of diffusion wear mentioned in alloy A is to add TiC to WC-Co cemented carbide. High hardness of TiC and its chemical stability impart excellent resistance to crater wear [134,162]. Such a resistance is increased by reducing carbon diffusion from carbide tool to the steel chip. With addition of TiC in WC-Co base composition, TiC-WC solid solution is obtained which has better chemical stability at higher temperature. An improved cutting performance is, therefore, expected out of alloy B composition. But the poor TRS and toughness resulted in a catastrophic failure of the tools within a few minutes of cutting. The failed tool (Fig. 3.25a) is indicative of the fact that the failure took place by crack initiation at the cutting edge followed by its quick propagation. Moreover, a typical set of cracks were observed on the failed tool surface which are normally observed in tools used in interrupted cutting and mainly results due to thermal shock (Fig. 3.25b). The characteristic features of these are the initiation of cracks on the rake surface perpendicular to the cutting edge, above a specific cutting speed and load. Progressively a system of cracks, both parallel and perpendicular to the cutting edge on the rake and flank faces are formed [175]. Though it was unusual to form such thermal cracks in the present cutting conditions, the reason could be attributed to the combined effect of poor TRS and thermal shock resistance of alloy B.

### IV.3 WC-8TiC-6Co-6Ni CEMENTED CARBIDE (ALLOY C)

From the results so far obtained on alloy B, it seemed that the poor interaction of the TiC grains by the binder melt was one of the major reasons for the poor strength

and nonuniform microstructure. It was, therefore, decided to modify the binder phase by incorporating nickel into it so as to improve the wettability and solubility of TiC grains in the binder melt. Nickel dissolves 12 and 5 mass% of WC and TiC respectively into it at a temperature of  $1250^{\circ}\text{C}$  and they have contact angle of 0 and  $23^{\circ}\text{C}$  respectively in vacuum at a temperature of  $1380^{\circ}\text{C}$  [13,169]. As far as straight WC is concerned, nickel is inferior to cobalt binder from the solubility point of view, but the reverse is true for TiC in respect to both wettability and solubility. This suggests that cobalt-nickel binder instead of only cobalt could be a reasonably good compromise for the cemented carbides containing both WC and TiC.

#### Densification behavior

The liquid phase sintering process in cemented carbides is strongly dependent on the temperature of formation and volume fraction of liquid phase. Quasibinary phase diagrams of Ti-C-Co and Ti-C-Ni systems are available [176], which suggest that the minimum liquid phase formation temperature decreases as the binder metal is replaced from cobalt to nickel. But the reverse is true for W-C-Co and W-C-Ni systems [137]. Such a feature would relatively raise the sintering temperature of the present composition in order to achieve full density in comparison to WC-10Co cemented carbide (Alloy A). As mentioned earlier, the wettability and solubility of TiC in nickel is better than that in cobalt. The replacement of binder cobalt by nickel, therefore, promoted the solution reprecipitation of TiC without causing much problem with WC. This appears to be the main reason for a better densification of alloy C as compared to alloy B.

## Microstructural characterisation

The present investigation confirms that the modification of binder phase cobalt by incorporating nickel into it resulted in a somewhat better microstructure than that of alloy B. The microstructural changes of practical importance viz. grain size and size distribution, binder phase distribution, and the carbon adjustment in the binder phase mainly take place at the third stage of sintering in which solution-precipitation plays an important role [8,11,29]. Therefore, a better microstructure obtained in alloy C may be thought as a consequence of the modification in the binder phase chemistry. Moreover, a decreased carbide grain size and mean binder free path suggest that the overall wettability of carbide phases, in the cemented carbide systems containing WC and TiC, is better with Co-Ni than with only cobalt. For a fixed volume fraction binder phase the contiguity value increases with the decrease in carbide grain size [19], which was observed in the present alloy as well.

The change in binder phase chemistry did not lead to any noticeable change in WC/Co interface structure, but the TiC/Co interface observed in alloy C (Fig. 3.26c) was very different from those observed in alloy B (Fig. 3.18b), where an interfacial interaction between TiC and binder phase could be noticed. In presence of binder melt, WC grains dissolve out and diffuse into TiC grains to form (W,Ti)C solid solution [177]. In the present alloy composition the formation of (W,Ti)C solid solution is promoted, since TiC interacts better with Co-Ni than with only cobalt.

Apart from WC, TiC and cobalt some other phases could be present in the microstructure due to deviation of carbon content from the stoichiometric carbon content of the

alloy. Excess carbon precipitates as free carbon, whereas carbon deficiency results in the formation of a complex carbide (eta phase) which can exist in two forms, either  $M_6C$  carbide ranging from  $Co_{3.2}W_{2.8}C$  to  $Co_2W_4C$  or  $M_{12}C$  of fixed composition  $Co_6W_6C$  [47,48]. The 'eta' phase is nonmagnetic and very brittle which makes the cemented carbides brittle as well. Since the formation of 'eta phase' involves consumption of ferromagnetic cobalt, the magnetic saturation value drops with the presence of this phase in the alloy. Though no 'eta phase' was detected in the microstructure, a sharp drop in magnetic saturation value was observed in alloy C (Fig. 3.19b). The reason may be attributed to the fact that substitution of binder metal cobalt in WC based cemented carbides by nickel leads to the presence of some free carbon in the system [138] and even a slightly decarburised cemented carbide shows a drastic lowering of magnetic saturation [178].

### Mechanical properties and fracture behavior

The present investigation confirms that the modification of binder phase chemistry improved the TRS by about 325 MPa. Vacuum sintering resulted in further improvement in TRS, and the reasons are same as those mentioned earlier in alloy A. The drop in hardness value due to change in sintering atmosphere is not clearly understood.

In WC-10Co cemented carbide (Alloy A), the rupturing of cobalt leaves a pattern of dimples or tear ridges on the fracture surface. But in the present composition the binder phase is mostly present as ruptured ligaments between the carbide grains (Fig. 3.27a). As already mentioned such kind of failure in the binder phase takes place when the hard phase/binder interface is rather weak to withstand the

separation. Partial substitution of cobalt by nickel helps in producing a somewhat uniform microstructure than that of alloy B. On the other hand, since, the bond strength between WC and binder in the present case is much inferior to that in straight WC-10Co cemented carbide, this results in many small smooth WC grains on the fracture surface due to de-bonding of WC/binder interface. The inferior bond strength of WC/binder interface results in a lower indentation fracture toughness, since once the crack is produced by either fracturing the large carbide grains or interface separation, its further propagation requires less energy. As TiC is much more brittle in nature as compared to WC, the transgranularly fractured TiC very often leaves a river pattern on the fracture surface (Figs. 3.27b-c). From such patterns it can be easily inferred that the local fracture initiation is either from carbide/binder or carbide/carbide interface.

#### Oxidation and thermal shock resistance

Cobalt forms three oxides, cobaltus oxide ( $\text{CoO}$ ), cobaltic oxide ( $\text{Co}_2\text{O}_3$ ) and cobalto cobaltic oxide ( $\text{Co}_3\text{O}_4$ ). On the other hand Ni forms  $\text{NiO}$ ,  $\text{Ni}_2\text{O}$  and  $\text{Ni}_2\text{O}_3$ . From the thermodynamic data it is noted that change in free energy of formation of oxide at  $1100^\circ\text{K}$  for  $\text{CoO}$  and  $\text{Co}_3\text{O}_4$  are - 38,100 cal/gm mole, and - 124,650 cal/gm mole respectively whereas the corresponding value for  $\text{NiO}$  is 33,600 cal/gm mole [174]. These data confirm that the cemented carbides containing cobalt-nickel binder (alloy C) is comparatively more oxidation resistant than that of the nickel free one (alloy B).

The effects of microstructure and hard phase/binder interface bond strength on thermal shock resistance has already

been described for alloy B. The improved thermal shock resistance in alloy C (Table 3.5) is, therefore, attributed to the uniform microstructure and TiC/binder bond strength than that of alloy B.

#### Cutting performance

As the cutting performance is closely related to the TRS and toughness, the improvement in these properties resulted in a better tool life in the present alloy than that in alloy B. However, failed tool's microstructural analysis reveals that the tool made out of alloy C failed in a similar fashion to that of alloy B i.e., by cutting edge breaking even before any wear mechanism became operative. This suggests that the inadequate TRS and toughness of alloy C is the main reason of early failure of the tool.

#### IV.4 WC-6TiC-2Mo<sub>2</sub>C-6Co-6Ni CEMENTED CARBIDE (ALLOY D)

It is well known fact that the presence of molybdenum in cobalt-nickel binder lowers the solid/liquid interfacial energy and thus ensures a better wetting of the hard phase grains viz. WC and TiC [179]. With this in view, alloy C was further modified by including molybdenum into the system in the form of Mo<sub>2</sub>C.

#### Densification behavior

Molybdenum is free to diffuse into tungsten and titanium carbides and forms a continuous series of solid solution with them. During alloying a diffusion gradient across the solid/liquid interface results, which lowers the solid/liquid interfacial energy. This would lead to a better

wettability of the hard phase with the liquid binder and thus results in an improved densification behavior for alloy D.

### Microstructural characterisation

A rather uniform microstructure in alloy D (Fig. 3.15d) than that of alloy C (Fig. 3.15c) is, attributed to the improvements in wettability achieved through the modification in the alloy chemistry. This is further supplemented by the decreased mean binder free path and contiguity of the carbide phase observed in alloy D (Fig. 3.17).

The TiC/binder interface structure in alloy D reveals that TiC grain has a diffused interface (Fig. 3.29c), which is thought to be due to a better interaction of carbides with the binder. The better wettability of such alloys with molybdenum containing binder, finds a convincing conclusion from the TEM studies, which show a concentration gradient across the interface, particularly TiC/binder interface.

### Mechanical properties and fracture behavior

Relatively large size hard phase grains e.g., WC or TiC in cemented carbides result in stress concentration, which cannot be relieved by local plastic deformation so that the failure stress is reached at these points while the average applied stress is well below the failure stress. This results in a poor TRS and toughness as was seen in the case of alloys B and C, and in both the cases the TiC grain size is the major strength-determining microstructural parameter. However, such factors are less dominating in alloy D. More importantly this alloy has a narrower grain size distribution than that of either alloy B or alloy C (Fig. 3.16), which results in an improved TRS and fracture toughness. A slight improvement in

sintered hardness value observed in alloy D is expected because of the lowering of average grain size and mean binder free path with respect to alloy C. However, like alloy C, in the present alloy also a drastic drop in hardness value is observed after vacuum sintering (Fig.3.20).

Since the cobalt-nickel-molybdenum alloy has a better wettability with carbide, it makes the interface strong enough to favor the crack to pass through the binder phase. The partitioning of molybdenum between the binder phase and the carbides appears to have maintained a high toughness, possibly by forming a tough rim around WC or TiC grains. Due to such microstructural changes in alloy D, the binder phase has to undergo more plastic deformation before rupturing by void nucleation and growth, which produces dimples on the fracture surface (Fig. 3.30a). This is the major important change that could be observed in the fracture surfaces of alloy D from that of alloy C in which the binder phase was mostly present as ruptured ligaments between the carbide grains. As far as the TRS and fracture toughness are concerned, the failure of the binder phase is important, since it consumes most of the fracture energy by plastic deformation. A better mechanical property of the binder phase in alloy D is achieved by the combined effect of solid solution hardening by molybdenum and precipitation hardening with  $\gamma'$  ( $\text{Ni}_3\text{Ti}$ ) [147]. These factors are contributory to a better TRS and fracture toughness values in alloy D which are much superior than those in alloy B or alloy C.

#### Oxidation and thermal shock resistance

As mentioned in earlier section the nature of oxides forms on the substrate has great effect on the oxidation

behavior. A compact adherent oxide layer is always desirable for a better oxidation resistance. In the present cemented carbide, in addition to the other oxides  $\text{MoO}_3$  is formed (Table 3.4), which is responsible for the higher oxidation rate. Such a feature observed in alloy D than that in either alloy B or alloy C could most probably arise due to the unstable nature of  $\text{MoO}_3$  which melts and sublimates at relatively lower temperature of  $795^\circ\text{C}$  and  $1155^\circ\text{C}$  respectively [180,181].

As compared to alloy C, alloy D has a uniform microstructure and better carbide/binder bond strength which should result in a better thermal shock resistance. Such improvement is not observed in the present study and in fact alloy D has an equivalent thermal shock resistance to that of alloy C (Table 3.5). Once the cracks of critical size appear, their further propagation depends on the carbide grain size, carbide/binder bond strength and the ductility of the binder phase. It appears from the present results that molybdenum addition makes the binder phase less tougher because of solid solution/ precipitation hardening effects. As a result, the plastic zone ahead of the crack becomes narrower and allows the crack to pass through at a lower stress level.

### Cutting performance

A substantial increase in tool life in the present alloys is attributed to the better TRS and toughness brought about by the microstructural changes due to the compositional modification (Fig. 3.24). It again confirms the fact that the premature failure in alloys B and C was mainly because of the poor strength resulting from nonuniform microstructure. The power consumed in metal cutting is largely converted into heat near the cutting edge, which is of the order of  $600\text{--}1000^\circ\text{C}$

depending on the cutting speed, while the temperature is lower near the cutting edge itself [132,182]. Due to the rise in temperature during cutting, the oxidation of the tool surface is unavoidable. The positive role of TiC addition towards oxidation resistance as found in case of alloy B appears to get diluted after  $\text{Mo}_2\text{C}$  addition. As already mentioned,  $\text{Mo}_2\text{C}$  forms  $\text{MoO}_3$  which melts and sublimates at relatively lower temperature. Due to such unstable nature, the oxide layer formed on the tool of the present alloy does not have adequate strength and is carried away continuously along with the chip leaving a fresh tool surface. The nature of the oxides formed on the rake surface greatly, thus influences the sliding wear mode.

#### IV.5 WC-8.7TiN-12Co CEMENTED CARBIDE (ALLOY E)

##### IV.5.1 Liquid phase sintered alloy

##### Densification behavior

From the results it is obvious that the full density of the present cemented carbide was not achieved even at a sintering temperature of  $1500^\circ\text{C}$  which may be related to the poor wettability of TiN by cobalt [169]. Densification behavior in nitrogen containing cemented carbide is especially influenced by the sintering atmosphere. Such cemented carbides cannot be sintered in dynamic vacuum or in hydrogen, because TiN/Ti(C,N) have the tendency to emit nitrogen and thus causes the formation of micro- and macro- porosity [183-185]. It appears from the present results that such a feature occurred in alloy E as well. This diminishes the carbon content from WC, thus facilitating 'eta' phase formation, which is confirmed by magnetic saturation values (Fig. 3.43b). 'Eta' phase formation involves consumption of cobalt which otherwise

produces liquid at the sintering temperature. Secondly, depletion of carbon in the alloy reduces the fluidity of the liquid melt during sintering. These effects ultimately lead to higher sintered porosity in the hydrogen sintered cemented carbides of such grades.

#### Microstructure and mechanical properties

As far as the microstructural changes in alloy E are concerned not much differences were observed from those of WC-10Co cemented carbide (Alloy A). During liquid phase sintering, dissolved tungsten in the liquid binder diffuses into TiN which results in a more or less core/rim structures [185], as was observed in case of alloy D, where a rim was formed due to molybdenum diffusion. However, such cored microstructure was not observed in the present alloy which suggests that there was no observable alloying between WC and TiN. Due to the presence of porosity it was not possible to clearly isolate the effect of TiN addition on mechanical properties.

#### IV.5.2 Hot isostatically pressed alloy

It is virtually impossible by normal liquid phase sintering to achieve a fully dense product out of TiN/Ti(C,N) based cemented carbides, irrespective of any variation in the sintering atmosphere. This may arise from the fact that pores containing nitrogen arising out of denitrification are difficult to move out during sintering and invariably give rise to large pores in the sintered compacts [183,184]. These pores are the fracture origin and are responsible for low strengths in such cemented carbides. Hip'ing of such liquid phase

sintered compacts becomes obvious so as to eliminate such defects and to achieve increased strength.

### Densification behavior

HIP treatment after sintering was effective for eliminating large pores, though some small pores were still left out. HIP'ing at  $1400^{\circ}\text{C}$  did not eliminate all large pores in the sintered compact, which may be due to the fact that liquid phase sintering resulted in continuous hard phase skeleton formation and during HIP'ing at  $1400^{\circ}\text{C}$ , the contributions of power law creep/plastic deformation and amount of liquid phase were not sufficient enough to eliminate the large pores completely. However, such large pores were completely eliminated when HIP'ing temperature was raised to  $1450^{\circ}\text{C}$ .

### Microstructural characteristion

The microstructure of alloy E consists of straight faceted WC grains and equiaxed TiN grains. The hard phases exhibit substantial plastic deformation in the form of a high dislocation density (Fig. 3.42a) as a result of being under substantial stress during HIP'ing. Another characteristic feature of the microstructure is the formation of shear bands (Fig. 3.42b), which are normally observed to form in metals of low stacking fault energy where deformation by glide of partials are usually associated with slip in intense shear bands [186]. In the present alloy the observed bands can be attributed to a thermal softening mechanism brought about by heating to a high temperature during HIP'ing. However, the shear bands are mostly observed in TiN phase which suggests that while HIP'ing this phase has undergone more plastic

deformation than WC. It may be attributed to the fact that TiN softens rapidly with increasing temperature whereas WC retains the hardness [162]. Alloy E has a higher WC mean grain size than that of alloy A, which is expected, since during consolidation the alloy was heated to high temperature twice, i.e. for liquid phase sintering and HIP'ing and in both the cases the temperature was higher than the sintering temperature for alloy A. Because of the substantial pressure during HIP'ing, the liquid binder melt is squeezed out from the intergranular region of the hard phases to fill the voids and thus establishes a direct hard phase/ hard phase contact. This results in a higher contiguity value as compared to alloy A.

The binder cobalt is associated with high dislocation density and does not contain any stacking fault (Fig. 3.42a,c), which may be attributed to the fact that the high residual stresses resulting from HIP treatment might have completely suppressed the fcc to hcp cobalt transformation.

As far as the interfaces are concerned, they have more or less similar structure as those observed in alloy A, except hard phase/hard phase interfaces viz. WC/WC, WC/TiN and TiN/TiN which seem to be very different than those for alloy A. HIP'ing results in a substantial deformation at these interfaces. This can be clearly noticed in case of WC/TiN interfaces where WC grain invariably seems to be intruded into TiN (Fig. 3.42c) which has relatively much lower hardness at elevated temperature.

### Mechanical properties and fracture behavior

Cemented carbides, in general follow classic Griffith-type brittle fracture with failure initiating from preexisting flaws in the material [72]. Therefore, pores in the

microstructure above the critical flaw size act as defects and cause a drastic lowering in TRS. Thus, the increase in TRS after HIP treatment of the liquid phase sintered alloy is essentially entirely due to elimination of the largest flaws and hence a narrowing of critical flaw size range. Once the pores size is below the critical flaw size, pores no longer act as critical flaws; failure instead initiates from coarse grain agglomerates, cobalt rich areas or inclusions [52]. Poor interaction of TiN with binder cobalt and high contiguity are expected to result in an inferior TRS and toughness in alloy E as compared to that of alloy A as was noticed in case of alloy B. But such deterioration in properties was not observed in alloy E. This may be attributed to the fact that though TiN has poor wettability with cobalt, the diffusion of tungsten from the liquid binder into TiN might have maintained a concentration gradient across the liquid/TiN interface which results in reasonably good interface bond strength. Moreover, the micro-structure in the present alloy is more uniform than that of alloy B which also confirms that the solute atoms present in the liquid binder during sintering must have contributed in modifying the TiN/liquid interface so that a better wettability is achieved than that with pure cobalt melt. Moreover, as mentioned earlier, the binder phase is present as high temperature fcc phase which results in transformation toughening under stress. As a consequence, the TRS value obtained in alloy E is equivalent to that of alloy A. However, the indentation fracture toughness is slightly inferior to alloy A which is thought to be due to high contiguity. It is worth mentioning that TRS and hardness obtained in the present alloy are comparable to those reported by Tsuchiya et al. [164] for WC-10TiN-10Co cemented carbide.

The fracture behavior of the alloy E is not very different from those mentioned in the previous alloys. However, the predominant local fracture mode in alloy E is hard phase/hard phase viz. WC/WC, WC/TiN, and TiN/TiN interface separation (Fig. 3.46d) which is expected since it has high contiguity. Weak hard phase/binder interface results in a fracture surface like in alloy C (Fig. 3.27a) where binder phase is mostly present as ruptured ligaments. But a direct comparison of the fracture surface of the present alloy (Fig. 3.46a) with that of alloy C again confirms the fact that TiN/binder bond strength in WC-TiN-Co system is much better than what it should be in TiN-Co system. This leads to the conclusion that the presence of tungsten in the binder plays an important role in modifying the TiN/binder interfacial energy. The other distinctive feature on the fracture surface is the transgranularly fractured TiN grains which show a smooth cleaved surface with steps (Fig. 3.46c). This indicates that the cleavage in TiN grains takes place only along the planes which are favorably oriented with respect to the propagating crack.

#### Oxidation and thermal shock resistance

The present investigation confirms that the addition of TiN enhances the oxidation resistance of WC-10Co cemented carbide. Like TiC, TiN also forms  $\text{TiO}_2$  and therefore, the enhancement in oxidation resistance for alloy E can be accounted by the same facts as stated for alloy B. It is interesting to note that for a similar addition, the improvement in oxidation resistance is better with TiN (Alloy E) than with TiC (Alloy B). This could be due to the ease of formation of  $\text{TiO}_2$  from TiC compared to the formation of  $\text{TiO}_2$  from TiN, since

the free energies of formation of  $\text{TiO}_2$  at  $800^\circ\text{C}$  from  $\text{TiC}$  is  $-132 \text{ K.cal/mol.O}_2$  as compared to  $-117 \text{ K.cal/mol.O}_2$  for  $\text{TiN}$  [174,180].

Like  $\text{TiC}$ ,  $\text{TiN}$  addition does not lead to drastic deterioration of thermal shock resistance as observed presently in alloy E (Table 3.5). This is mainly because of uniform microstructure, relatively good  $\text{TiN/binder}$  bond strength and more importantly better thermal conductivity of  $\text{TiN}$  as compared to  $\text{TiC}$ .

### Cutting performance

The enhancement of tool life after addition of  $\text{TiN}$  to  $\text{WC-10Co}$  cemented carbide (Fig. 3.48), is mainly related to the improved combination of strength, toughness, thermal shock resistance and crater resistance of such alloys. The behavior of worn tool during cutting test at  $180 \text{ m/min}$  (Fig. 3.49) suggests that wear around the nose radius is of significance in this particular case. Several of the wear mechanisms viz. adhesion, abrasion, oxidation and subsequent adhesion wear, diffusion and plastic deformation of cutting edge can operate simultaneously, and may lead to wear below the nose radius of the turning tool [198]. The dominant wear mechanisms, however, vary according to the tool-work combination.

### IV.6 WC-8.7 $\text{TiN-6Co-6Ni}$ CEMENTED CARBIDE (ALLOY F)

It has been already mentioned that nickel is a better binder for titanium based refractory compounds viz.  $\text{TiC}$ ,  $\text{TiN}$  and  $\text{Ti(C,N)}$  whereas it is the other way for  $\text{WC}$ . Moreover, according to earlier results in case of alloy C, cobalt-nickel is a better binder alloy than only cobalt. Based on these

facts, the binder phase of the previous alloy i.e. alloy E has been modified by incorporating nickel into it in order to achieve a better densification. But it appears from the present results related to densification (Fig. 3.32a) that the overall wettability in alloy F deteriorated after such modifications. This can be related to rather poor interaction of TiN even with nickel. TiN has a contact angle of  $70^{\circ}$  with nickel at  $1550^{\circ}\text{C}$  in vacuum, whereas as it is  $38^{\circ}$  for TiC at  $1500^{\circ}\text{C}$  [169]. Since the basic idea of improving the binder-hard phase interaction was not successful, further studies on alloy F was not carried out.

#### IV.7 WC - 7.5 TiN - 1.8 Mo<sub>2</sub>C - 6 Co - 6 Ni CEMENTED CARBIDE (ALLOY G)

##### IV.7.1 Liquid phase sintered alloy

##### Densification behavior

Small additions to the well known binders can have positive effects on wetting and adhesion and may be useful in many technical alloys as was seen in case of alloy D, where molybdenum was added in cobalt-nickel binder. A similar result has been observed in the present alloy as well. Therefore, the better densification in alloy G than that in either alloy E or F is attributed to the improvement in wettability brought about by the change in binder chemistry. It is worth mentioning here that molybdenum which is added in the form of Mo<sub>2</sub>C in the alloy, gets dissolved in the liquid binder during sintering and modifies the binder phase.

## Microstructure and mechanical properties

It is evident that  $\text{Mo}_2\text{C}$  addition to previous alloy i.e., F promoted finer grain size and narrower grain size distribution which are because of the same facts stated earlier in case of alloy D. The improvement in mechanical properties can be related to the amount and size of the sintered porosity, since these flaws govern strength and toughness.

### IV.7.2 Hot isostatically pressed alloy

#### Densification behavior

The HIP'ed alloy G was found to have smaller pores and their better distribution than that of alloy E. This is mainly because of the improved wettability caused by the presence of molybdenum in the cobalt-nickel binder.

#### Microstructural characterisation

The earlier results on alloy D have shown that the presence of molybdenum in cobalt-nickel binder greatly improved the TRS and toughness values, which was mainly due to the appreciable modification of the  $\text{TiC}/\text{Co}$  interface interaction by the addition of better wetting additives such as nickel and molybdenum in the binder cobalt. A similar approach has been adopted in the present alloy G, but no noticeable change in the microstructure was observed. In fact, this alloy has more or less similar kind of microstructure to that of alloy E (Figs. 3.36, 3.42 and 3.50).

#### Mechanical properties and fracture behavior

Nickel in the cobalt binder stabilises the high temperature fcc cobalt and prevents it from transforming to

less ductile hcp phase during deformation. On the other hand, molybdenum addition to nickel-cobalt alloy, makes it harder by solid solution hardening/precipitation hardening and thereby reduces the toughness of the binder phase. This may be the reason of slightly inferior strength and toughness, and superior hardness values observed in alloy G to those of alloy E (Figs. 3.44 and 3.45). However, the present result contradicts the results obtained for alloy D, where an improvement in strength and toughness was observed due to such modifications. In TiC containing cemented carbides i.e. alloys B to D, the TiC grain size was very important in determining the strength. When an uniform microstructure with decreased grain size was obtained by binder phase modification, TRS and toughness naturally got improved. But in the case of TiN addition, no microstructural nonuniformity was observed. Secondly, as mentioned earlier, binder phase modification did not lead to any noticeable change in TiN/binder interface interaction. It is, therefore, probable that the decrease in binder phase ductility caused some deterioration in TRS and toughness of alloy G.

The only major change that could be observed in the fracture behavior of alloys E and G, is that in the latter many small WC grains were pulled out leaving clear impression on the fracture surface (Fig. 3.51d). This may be due to the fact that since WC has a better interaction with cobalt than with any other iron group transition metal, the change in binder chemistry leads to an inferior WC/binder bond strength.

#### Oxidation and thermal shock resistance

The inferior oxidation resistance and thermal

shock resistance of the present alloy can be based on the same reasons described earlier in case of alloy D.

#### Cutting performance

Most of the fracture energy in cemented carbides is consumed by the plastic deformation of the binder phase. Since the binder phase in alloy G is harder and less tougher than alloy E, the energy required to pass the propagating crack is less once the threshold value is reached. Therefore, it can be inferred that the inferior toughness of alloy G to that of alloy E could be the probable reason for the early failure of the tool.

### IV.8 CEMENTED CARBIDES CONTAINING Ti(C,N)

- (a) WC - 8.3 Ti(C,N) - 12 Co (Alloy H)
- (b) WC - 8.3 Ti(C,N) - 6 Co - 6 Ni (Alloy I)
- (c) WC - 7 Ti(C,N) -  $2\text{Mo}_2\text{C}$  - 6 Co - 6 Ni (Alloy J)

#### IV.8.1 Liquid phase sintered alloys

It appears from the present results that Ti(C,N) addition to WC-10Co cemented carbide imposes similar kind of processing difficulties as was observed in cemented carbides with TiN addition. Full density of the present alloys was not achieved even at a sintering temperature of  $1500^{\circ}\text{C}$  by normal liquid phase sintering, the reasons being the same explained earlier in case of alloys E, F and G. As far as the effects of binder phase compositions on sintering behavior are concerned, they are more or less similar to those with TiN addition except alloy J. A higher sintering temperature was required for alloy J to achieve even the same density level to that of alloy

I, which is unexpected. The reason for the deterioration in densification after  $\text{Mo}_2\text{C}$  addition to alloy I is not clear.

Microstructures of alloys H, I and J are very similar to those of cemented carbides containing TiN (Figs. 3.39 and 3.57). Like TiN, Ti(C,N) addition did not lead to any noticeable nonuniformity in the microstructure, which was a real problem after TiC addition. It's worth mentioning here that the present results agree with Suzuki [187] who suggests that addition of nitrogen to WC-TiC base cemented carbide promotes the formation of fine microstructure. The binder phase compositions do not seem to have any noticeable effects on the micro-structural development during sintering, such that the grain size and their distribution in all the alloys i.e., H, I and J follow almost similar trend (Fig. 3.58 and Table 3.7).

In general, the sintered compacts of alloys H, I and J contained considerable amount of porosity after liquid phase sintering (Table 3.8) which was the main source of catastrophic failure. It is, therefore, not possible at this stage to isolate the effects of microstructural variations that evolved through compositional changes, on mechanical properties.

#### IV.8.2 Hot isostatically pressed alloys

##### (a) Densification behavior :

HIP'ing at  $1400^{\circ}\text{C}$  eliminated all the large pores in the sintered compacts, and only some small pores were left out which were more or less uniformly distributed (Fig. 3.59). Alloy I exhibited relatively higher amount of residual porosity than that of either alloy H or alloy J. The reason

being the same as explained earlier in case of alloy F, where it has been mentioned that the hard phases viz. WC and TiN as a whole have inferior interaction with cobalt-nickel as compared to that with only cobalt. On the other hand, though alloy J required relatively higher sintering temperature to achieve the same density level to that of alloy I, the amount of residual porosity after HIP'ing was much less in the former. This suggests that the improvement in wettability did take place in the presence of  $\text{Mo}_2\text{C}$  in the alloy, which facilitated material transport during HIP'ing resulting in an efficient pore removal.

(b) Microstructural characterisation :

As mentioned earlier in liquid phase sintered alloys, the microstructures of alloys H, I and J are similar and resemble very much with those in cemented carbides containing TiN viz. alloys E, F and G. The change in binder phase composition did not lead to any observable change in the microstructure (Fig. 3.61 and Table 3.7). The characteristic features observed in alloys E, F and G are also present in the present series of alloys viz. H, I and J.

(c) Mechanical properties and fracture behavior :

Strength and toughness of liquid phase sintered alloys are greatly enhanced after HIP treatment, which is expected since all the preexisting fracture originating flaws i.e., relatively large pores are eliminated by such treatment. However, in general, Ti(C,N) addition to WC-10Co cemented carbide deteriorated both TRS and fracture toughness irrespective of the binder composition. The deterioration being more in the latter than in the former. Since in the

present series of alloys the microstructures were more or less uniform, the mechanical properties obtained were related mainly to the intrinsic properties of the hard phase additive i.e. Ti(C,N) and to the hard phase/binder interface bond strength. The inferior TRS and toughness of alloys H, I and J as compared to those for WC-10Co cemented carbide may be, therefore, attributed to the inferior WC/Ti(C,N)/binder bond strength and more brittle nature of Ti(C,N) than that of WC. In addition relatively high contiguity values in the present alloys (Fig. 3.62b) are also responsible for low TRS and toughness.

Coming to the individual cemented carbide compositions, alloy J exhibited best TRS and toughness among the alloys H, I and J (Fig. 3.65). Fracture surface analyses revealed that though the basic fracture modes were same in all the alloys, their behavior in binder phase changed noticeably with the alloy modification. The sequential properties changes from alloy H to alloy J are same as those observed in TiC containing cemented carbides viz. alloy B to alloy D. Incorporation of nickel into cobalt binder (alloy I), resulted in inferior hard phase/binder bond strength which favored the binder phase fracturing by necking (Fig. 3.67a). On the other hand,  $\text{Mo}_2\text{C}$  addition in alloy I, improved the hard phase/binder bond strength favoring void nucleation, growth and coalescence in the binder phase which resulted in dimpled structure on the fracture surface (Fig. 3.68a).

#### (d) Oxidation and thermal shock resistance

Oxidation resistance of the HIP'ped alloys H, I and J are better than those containing TiC but inferior to those containing TiN. The effects of binder phase composition

on oxidation resistance are similar to that mentioned for either TiC or TiN containing cemented carbides.

Thermal shock resistance of the present series of alloys are comparable to those with TiN addition and better than those with TiC addition (Table 3.5). This may be attributed to the fact that TiN and Ti(C,N) have better thermal conductivity than TiC. On the other hand, alloys H, I and J have inferior thermal shock resistance to that of WC-10Co cemented carbide. This is attributed to the fact that the latter has better hard phase/binder bond strength than the former and hence can withstand more thermal mismatch stress.

#### IV.9 COMPARATIVE ROLE OF DIFFERENT REFRACTORY COMPOUND ADDITIVES ON MICROSTRUCTURE AND PROPERTIES OF WC-10Co CEMENTED CARBIDES

The overall results of the investigations carried out presently are summarised in Figs. 4.1 - 4.2, where the refractory compound additives are TiC, TiN and Ti(C,N) respectively. From the view point of basic chemical bond in such compounds there are a number of similarities as they possess covalent/metallic type of bonding, apart from similar crystal structures of cubic NaCl type. The metallic component in these refractory compounds viz. titanium pertains to early transition metals containing unfilled d-shell. On the other hand, both nonmetal atoms viz. carbon and nitrogen correspond to sp-electronic configuration for their valency electrons. If one looks more deeply, there does exist a subtle distinction in the overall bonding of such compounds. Samsonov [188] discussed in detail the energetic stability of both types of metal/nonmetal elements and concluded that during formation of such compounds the transition metals act as donors of

electrons, so as to stabilise the  $sp^3$  configuration of nonmetal atoms to different extents. Carbon whose isolated atoms possess  $s^2 p^2$  electronic configuration tend to acquire stable  $sp^3$  configuration due to  $s \rightarrow p$  transition during TiC formation. However, in case of Nitrogen, whose isolated atoms have  $s^2 p^3$  configuration, owing to  $s \rightarrow p$  transitions by the scheme  $sp^4 \rightarrow sp^3 + p$ , they tend to acquire  $sp^3$  configurations with one weakly bonded electron of p configuration. It is this extra unbonded electron which is responsible for relatively lower hardness, higher plasticity and thermal conductivity in TiN as compared to strongly covalent bonded TiC. Such a treatment should bring forth a logical conclusion that the behavior of Ti(C,N) would be intermediate to that corresponding to either TiC or TiN, as both latter compounds form isomorphous solid solution among each other. When such refractory compounds are used as additives in a straight WC-Co cemented carbides, it is expected that the change in the end properties should bear a correlation. A look on the summary plots (Figs. 4.1-4.2) does confirm this feature. Considering the investigated properties there is much similarity in the role of TiN and Ti(C,N) in contrast to TiC containing cemented carbides. A detailed correlation with respect to various properties has been highlighted below.

In cemented carbides the major microstructural development takes place at the time of liquid phase sintering where the interaction of the carbides and binder melt is most important. The microstructure of WC-10Co cemented carbide is greatly altered when other cubic compounds, viz. carbides/nitrides/carbonitrides are added to it and which have important bearing on mechanical and physical properties. TiC addition to WC-10Co cemented carbide results in rather nonhomogeneous

microstructure, where grain coarsening in TiC phase is remarkable, combined with their tendency to form networks joined by carbide-carbide boundaries. To remove such defects from the microstructure, it is necessary to improve the wetting of TiC grains through binder phase modification. This is achieved through cobalt-nickel-molybdenum binder, where a well-wettable shell of molybdenum rich carbide is formed around the poorly wettable TiC grain. Improved wetting allows the production of a more or less uniform microstructure with much reduced carbide contiguity and thus bringing the end properties of WC-6TiC-2Mo<sub>2</sub>C-6Co-6Ni grade closer to those of WC-10Co cemented carbide.

Though the transition metal nitrides are very closely related to the corresponding carbides, they behave very differently during sintering and give rise to a variety of microstructures. TiN/Ti(C,N) addition to WC-10Co cemented carbide does not lead to any observable grain coarsening effect, but it gives rise to processing difficulties so that the full density is not achieved during normal liquid phase sintering. In addition, TiN in the cemented carbides does not remain thermodynamically stable at the sintering temperature; when in contact with carbon and Ti(C,N) gets formed [189-191]. This results in a core-rim structure where the thickness of the Ti(C,N) layer on TiN particle is determined by the total interstitial element concentration in the melt [53]. Moreover, the elements like W/Mo also diffuse into this shell forming a homogeneous solid solution (Ti, Mo/W)(C,N) during sintering. This results in spinodal transformation during cooling, which imparts grain refinement in such nitrogen containing cemented carbides [192-194].

solid in front of a migratory liquid film is not in equilibrium with the solute concentration of the boundary, then solute will either be depleted from or diffuse into this solid. When the boundary migrates at a constant velocity a steady state concentration profile will develop. The concentration gradient in the solid close to the liquid/solid interface will be very steep. The coherency strain at the interface will raise the free enthalpy of the stressed solid which is in contact with the boundary, resulting in differences of the local concentration equilibria at either side of the liquid films. These differences cause a constant traverse of host atoms through the liquid film, which results in the migration of the boundary.

A noted distinctive advantage of TiN addition over TiC addition is that it offers better oxidation, crater and thermal shock resistance with superior TRS and toughness (Fig. 4.2 and Tables 3.4 - 3.5. The combination of these properties results in a better cutting performance (Figs. 3.24 and 3.48). The tool life, in general, is a function of cutting tool composition. However, at the same time it may be emphasised that differing wear mechanisms may operate in different tools, which makes the absolute comparison of the tool lives rather difficult.

The above general discussion put forward, no doubt, is a qualitative one as in a complex binder systems the partitioning of solute atoms differ, which in its own turn does affect the microstructural characteristics. This naturally has a bearing on the mechanical as well as technological properties.

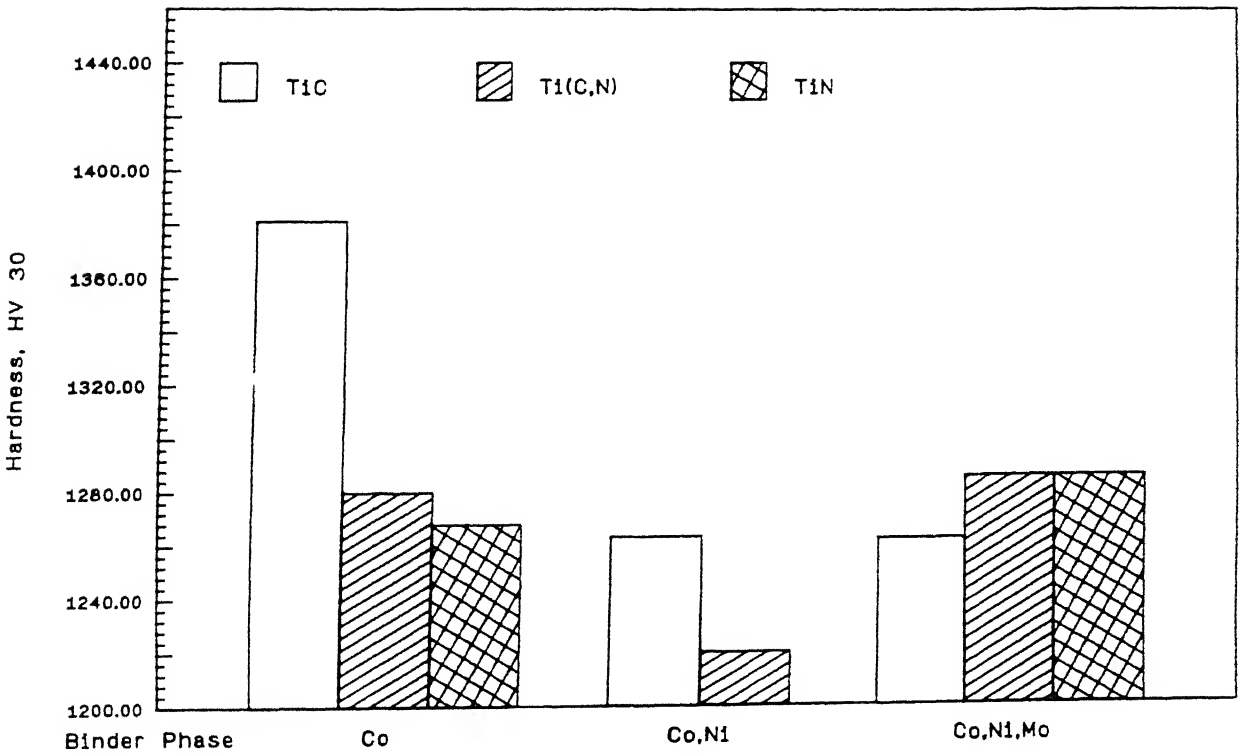


Figure 4.1 Hardness variations in various cemented carbides as a function of hard phase additives and binder phase compositions.

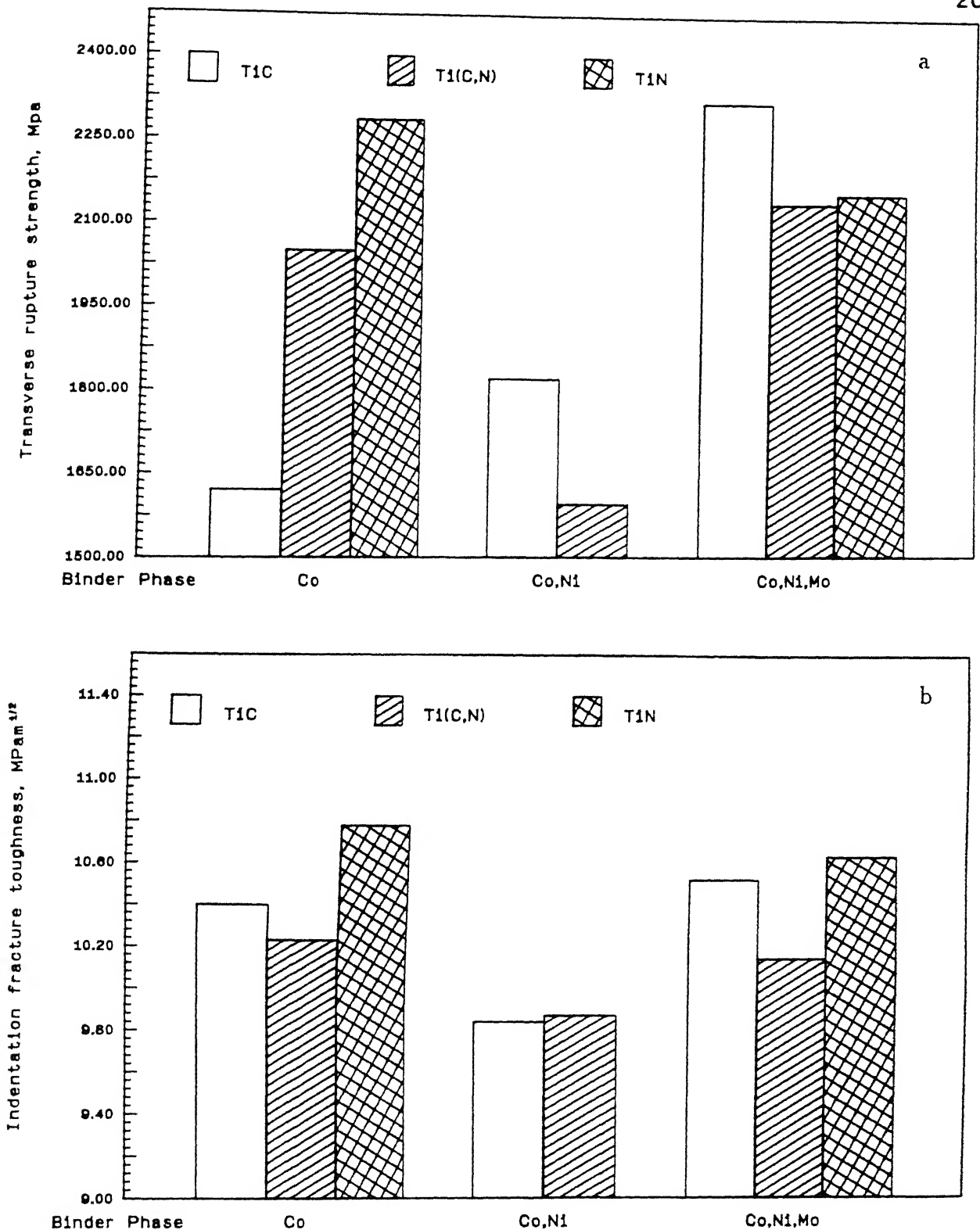


Figure 4.2 TRS and indentation fracture toughness variations in various cemented carbides as a function of hard phase additives and binder phase compositions.

## CHAPTER - V

### CONCLUSIONS

1. It is possible to substitute reasonable amount of WC by TiC/TiN/Ti(C,N) in WC-10Co cemented carbide without much sacrifice in strength and toughness with due modifications in the binder phase. However, a greater control over sintering atmosphere and post sintering treatment such as HIP'ing are required for cemented carbides with TiN/Ti(C,N) substitution.
2. Sintering experiments have shown that TiC addition to WC-10Co cemented carbide results in a nonuniform micro-structure with relatively large TiC grains. No such grain coarsening effect is observed when the additive hard phase is either TiN or Ti(C,N).
3. Grain coarsening suppression in TiC is achieved through the formation of well wettable Mo-rich shell around the poorly wettable TiC after the incorporation of nickel and molybdenum in the cobalt binder.
4. Addition of TiC to WC-10Co cemented carbide necessitates the incorporation of nickel and molybdenum in the binder cobalt so as to achieve equivalent TRS and indentation fracture toughness. In case of TiN/Ti(C,N) addition, with cobalt binder the properties are better than those corresponding to TiC containing alloys. Any change in the binder chemistry imparts some deterioration in properties in TiN/Ti(C,N) containing alloys.

5. Hardness value of WC-10Co cemented carbides improves with TiC addition but deteriorates with either TiN or Ti(C,N) addition. Binder compositions in all the systems do have a minor effect such that cobalt-nickel-molybdenum binder gives slightly better hardness than that with either cobalt or cobalt-nickel.
6. Addition of TiC/TiN/Ti(C,N) to WC-10Co improves the oxidation resistance, such that it is better with TiN as compared to either TiC or Ti(C,N). A further enhancement in oxidation resistance can be achieved through cobalt-nickel binder rather than only cobalt. However, incorporation of molybdenum in any of the alloy systems has significant deleterious effect on oxidation resistance.
7. All the hard phase additives viz. TiC, TiN and Ti(C,N) deteriorate the thermal shock resistance of WC-10Co cemented carbide, being more with TiC addition than that with either TiN or Ti(C,N) addition.
8. Among TiN and Ti(C,N) containing cemented carbides, the former offers a better combination of mechanical properties with a better resistance to oxidation and thermal shock.
9. In general, the properties of Ti(C,N) containing cemented carbides are intermediate to those containing TiC and TiN, irrespective of the change in the binder chemistry. The properties of the former are, however, much closer in magnitude with those containing TiN.

## REFERENCES

1. R.M. German, Liquid phase sintering, Plenum press, N.Y., 1985.
2. R.M. German, S. Farooq and C.M. Kipphut, Mat. Sci. Eng., Vol. A105/106, 1988, 215.
3. K. Schröter, U.S. Patent, 1,549,615.(application Oct. 1923; patented 1925)
4. P. Schwarzkopf, Deutsche Edelstahlwerke AG, German patent 720, 502 (patented 1929; issued 1942)
5. H.S. Cannon and F.V. Lenel, in 'Proc. 1st Plansee sem.', (F. Benesovsky, ed.), Metallwerk Plansee, Reutte, Austria, 1953, 106.
6. W.D. Kingery, J. Appl. Phys., Vol.30, 1959, 301.
7. C.J. Li and R.M. German, Metall. Trans. A, Vol. 14, 1983, 2031.
8. R.J. Nelson and D.R. Milner, Powd. Met., Vol. 15, No.30, 1972, 346.
9. R.F. Snowball and D.R. Milner, Powd. Met., Vol.11, No.21, 1968, 23.
10. B. Bengtsson, T. Johannesson and L. Lindan, Planseeber. Pulvermet., Vol.21, No.2, 1973, 110.
11. B. Meredith and D.R. Milner, Powd. Met., Vol.19, No.1, 1976, 38.
12. R. Edwards and T. Raine, in 'Proc. 1st Plansee Sem.', (F. Benesovsky, ed.), Metallwerk Plansee, Reutte, Austria, 1953, 232.
13. H.E. Exner, Int. Met. Rev., Vol.24, 1979, 149.
14. A. Hara, T. Nishikawa and T. Nishimota, J. Jap. Soc. Powd. and Powd. Met., Vol.16, 1970, 310.

15. J. Vicens, S. Lay, E. Laurent-Pinson and G. Nouet, in 'Surfaces and interfaces of ceramic materials', (L.C. Dufour, C. Monty and G. Petot-Ervas, eds.), Kluwer academic publishers, Dordrecht, 1989, 115.
16. M. Rettenmayer, H.E. Exner and W. Mader, Mat. Sci. Tech., Vol.4, 1988, 984.
17. B. Roebuck and E.A. Almond, Int. Matr. Rev., Vol.33, No.2, 1988,90.
18. E. Lardner, Powd. Met., Vol.13, No.26, 1970, 394.
19. R. Warren and M.B. Waldron, Powd. Met., Vol.15, No.30, 1972, 166.
20. H.E.Exner,in 'Science of hard materials',(R.K.Viswanadham, D.J. Rowcliffe and J. Gurland, eds.), Plenum press, N.Y., 1983, 233.
21. K.M. Friedrich, H.E. Exner and H. Tulhoff, in 'Proc. 10th Plansee sem.', ( H.M. Ortner, ed.), Metallwerk Plansee, Reutte, Austria, Vol.2, 1981, 795.
22. J. Gurland, Trans. AIME, Vol.200, 1954, 288.
23. J.W. Lee, D. Jaffery and J.D. Browne, Powd. Met., Vol.23, No.2, 1980, 57.
24. H.E. Exner and H.F. Fischmeister, Arch. Eisen., Vol.37, 1966, 417.
25. H. Tulhoff, in 'Mod. Dev. in P/M', (H.H.Hausner, A.W.Antes and G.D. Smith, eds.), APMI/MPIF, Princeton,N.J., Vol.14, 1981, 247.
26. M. Schreiner, E. Alizadeh, T. Schmitt, E. Lassner and B. Lux, in 'Proc. 10th Plansee Sem.', (H.M.Ortner, ed.), Metallwerk Plansee, Reutte, Austria, Vol.2, 1981, 811.
27. G.J. Rees and B. Young, Powd. Met., Vol.14, 1971, 1.
28. H.E. Exner, A. Walter, P. Walter and G. Petzow, Metall., Vol.32, 1978, 443.
29. B.Roebuck and E.G. Bennett, Metallography, Vol.19,1986,27.

30. Cobalt monograph, Centre D'information Du Cobalt, Bruxelles, 1960.
31. L.Akesson, in 'Science of hard materials', (R.K.Viswanadham, D.J. Rowcliffe and J. Gurland, eds.), Plenum press, N.Y., 1983, 71.
32. B.Roebuck, E.A.Almond and A.M. Cottenden, Mat. Sci. Eng., Vol.66, 1984, 179.
33. G. Wirmark and G.L. Dunlop, in 'Science of hard materials', (R.K.Viswanadham, D.J. Rowcliffe and J. Gurland, eds.), Plenum press, N.Y., 1983, 311.
34. V.K. Sarin, T. Johannesson, Mat. Sci., Vol.9, 1975, 472.
35. S. Mohajan, M.L. Green and D. Brasen, Metall. Trans., Vol.8A, 1977, 283.
36. H.E.Exner, J.Freytag, G.Petzow and P. Walter, Planseeber. Pulvermet., Vol.26, 1978, 90.
37. E. Lardner and D.J. Bettle, Metals and Materials, Vol.7, 1973, 540.
38. S. Amberg and H. Doxner, Powd. Met., Vol.20, 1977, 1.
39. H.F. Fischmeister, in 'Science of hard materials', (R.K. Viswanadham, D.J. Rowcliffe and J. Gurland, eds.), Plenum press, N.Y., 1983, 1.
40. J. Gurland and P.Bradzil, Trans. AIME, Vol.203, 1955, 311.
41. H.C.Lee and J.Gurland, Mat. Sci. Eng., Vol.33, 1978, 125.
42. H.E. Exner, Powd. Met., Vol.13, 1970, 429.
43. D.T.Quinto, G.J.Wolfe and M.N. Haller, in 'Science of hard materials', (R.K.Viswanadham, D.J. Rowcliffe and J. Gurland, eds.), Plenum press, N.Y., 1983, 947.
44. C. Lea and B. Roebuck, Met. Sci., Vol.15, 1981, 262.
45. V.Jayaram, R.Sinclair, J. Am. Cerm. Soc., Vol.66, 1983, 137.

46. J. Vicens, E. Laurent-Pinson, J.L. Chermant, G. Nouet, J. of Phys. Vol.49, No.C5, 1988, 271.
47. T. Johannesson, B. Uhrenius, Met. Sci., Vol.12, 1978, 83.
48. J.D. Bolton, R.J. Keely, Int. J. Refac. Met. and Hard Matr., Vol.1, 1982, 103.
49. J. Freytag and H.E. Exner, in 'Mod. Dev. in P/M', (H.H. Hausner and P.V. Taubenblatt, eds.), MPIF, Princeton, N.J., Vol.10, 1977, 511.
50. H. Jonsson, Planseeber. Pulvermet., Vol.21, 1973, 187.
51. Hardmetals - Metallographic Determination of Porosity and Uncombined Carbon, ISO 4505, 1978.
52. B. North, W.R. Pfouts, M.S. Greenfield, in 'Proc. 4th Int. Conf. on Isostatic Pressing', Stratford-upon-Avon, MPR Publishing Services Ltd., Shrewsbury, England, 1991, Paper-41.
53. G.S.Kreimer, V.J.Tumanov, D.S.Kamenskaya and Z.I.Pavolova, Fiz. i. Metalloved, Vol.17, No.4, 1964, 572.
54. J. Gurland, Mat. Sci. Eng., Vol.40, No.1, 1979, 59.
55. A. Miyoshi and A. Hara, J. Jap. Soc. Powd. and Powd. Met., Vol.12, 1965, 24.
56. M.Y. Lee, Metall. Trans. A, Vol.14A, 1983, 1625.
57. C. Chatfield, Powd. Met. Int., Vol.17, No.3, 1985, 113.
58. G.Altmayer and O.Jung, Z.Metallkd., Vol.52, No.9, 1961, 576.
59. J.L. Chermant and F. Osterstock, Powd. Met. Int., Vol.11, 1979, 106.
60. B. Roebuck and E.A. Almond, in 'Recent Advances in Hard Metal Production', Loughborough, Vol.1, 1979, 28-1.
61. V. Jayaram, R. Sinclair, D.J. Rowcliffe, Acta Metall., Vol.31, 1983, 373.

62. R.M. Greenwood, M.H. Loretto and R.E. Smallman, *Acta Metall.*, Vol.30, 1982, 1193.
63. J.L. Chermant, A. Deschanvres and F. Osterstock, *Powd. Met.*, Vol.20, 1977, 63.
64. H.E. Exner and J. Gurland, *Powd. Met.*, Vol. 13, No. 25, 1970, 13.
65. E.A. Almond and B. Roebuck, *Met. Sci.*, Vol.11, 1977, 458.
66. E.A. Almond, in 'Science of hard materials', (R.K. Viswanadham, D.J. Rowcliffe and J. Gurland, eds.), Plenum press, N.Y., 1983, 517.
67. R.K. Viswanadham and T.S. Sun, *Scripta Metall.*, Vol.13, 1979, 767.
68. R.K. Viswanadham, T.S. Sun, E.F. Drake and J.A. Peck, *J. Mat. Sci.*, Vol. 16, 1981, 1029.
69. H. Suzuki and K. Hayashi, *Planseeber. Pulvermet.*, Vol.23, 1975, 24.
70. S.B. Luyckx, *Acta Metall.*, Vol.23, 1975, 109.
71. E. Lardner and S. Ingstrom, in 'Proc. 10th Plansee sem.', (H.M. Ortner, ed.), *Metallwerk Plansee*, Reutte, Austria, Vol.1, 1981, 549.
72. U. Engel and H. Hubner, *J. Mat. Sci.*, Vol.13, 1978, 2003.
73. H. Kolaska, K. Dryer and G. Schaaf, *Powd. Met. Int.*, Vol.21, No.1, 1989, 22.
74. J. Gurland, *Trans. Met. Soc. AIME*, Vol. 227, 1963, 1146.
75. H. Suzuki and H. Kubota, *Planseeber. Pulvermet.*, Vol.14, 1966, 96.
76. G.S. Kreimer and M.R. Vakhovskaya, *Sov. Powd. Met. & Met. Cerm.*, 1965, 454.
77. H. Kubota, R. Ishida and A. Hara, *Trans. Indian Inst. Met.*, Vol.17, No.5, 1964, 132.

78. E. Lardner, *Powd. Met.*, Vol.21, No.2, 1978, 65.
79. British Standard BS 5447, 1977, 'Methods of test for plain strain fracture toughness ( $K_{IC}$ ) of metallic materials'.
80. ASTM Standard E 399-78, 'Test method for plain strain fracture toughness of metallic materials'.
81. J.R. Pickens and J. Gurland, *Mat. Sci. Eng.*, Vol.33, 1978, 135.
82. P. Kenny, *Powd. Met.*, Vol.14, 1971, 22.
83. E.A.Almond and B.Roebuck, *Met. Tech.*, Vol.5, No.4, 1978, 92.
84. G. Berry, *Met. Sci.*, Vol.10, No.10, 1976, 361.
85. H.E. Exner, A. Walter and R. Pabset, *Mat. Sci. Eng.*, Vol.16, 1974, 231.
86. H. Hubner and U. Engle, *Z. Werkstofftech*, Vol.9, 1978, 128.
87. R.C. Lueth, in 'Fracture Mechanics of Ceramics', (R.C. Bradt, D.P.H. Hasselman and F.F. Lange, eds.), Plenum press, N.Y., Vol.2, 1974, 791.
88. M.J. Murry and C.M. Perrott, in 'Proc. Advances in Hard Material Tool Tech.', Carnegie press, Pittsburgh, 1978, 314.
89. J. D. Bolton and R.J. Keely, *Fibre Science and Tech.*, Vol.19, 1983, 37.
90. L.M. Barker, *Eng. Fracture Mechanics.*, Vol.9, 1977, 361.
91. J.S. August and H.S. Kalish, in 'Proc. 10th Plansee sem. ', (H.M. Ortner, ed.), Metallwerk Plansee, Reutte, Austria, Vol.2, 1981, 743.
92. T.Mclaren and J.B.Lambert, in 'Science of hard materials', (R.K.Viswanadham, D.J. Rowcliffe and J. Gurland, eds.), Plenum press, N.Y., 1983, 689.
93. S. Palmqvist, *Jernkont. Ann.*, Vol.141, 1957, 300.
94. B.O. Jaensson, *Mat. Sci. Eng.*, Vol.8, 1971, 41.
95. H.E. Exner, *Trans. AIME*, Vol.245, 1969, 677.

96. A.Hara, M.Megata, S.Yazu, *Powd. Met. Int.*, Vol.2, 1970, 43.
97. M.T. Laugier, *Ceramics Int.*, Vol.15, 1989, 121.
98. C.B. Ponton and R.D. Rawlings, *Mat. Sci. Tech.*, Vol.5, 1989, 865 and 961.
99. C.B. Ponton and R.D. Rawlings, *Br. Ceram., Trans. J.*, Vol.88, 1989, 83.
100. S.H. Zhang and Y.X. Liu, in 'Mod. Dev. in P/M', (P.U. Gummeson and D.A.Gustafson, eds.), MPIF, Princeton, Vol.19, 1988, 33.
101. B.R.Lawn and E.R.Fuller, *J. Mat. Sci.*, Vol.11, 1976, 2016.
102. B.R. Lawn and M.V. Swain, *J. Mat. Sci.*, Vol.10, 1975, 113.
103. J. Dusza, L. Parilak and M. Slesar, *Ceramics Int.*, Vol.13, No.3, 1987, 133.
104. N.M. Parikh, *J. Am. Ceram. Soc.*, Vol.40, 1957, 335.
105. J.L. Chermant and F. Osterstock, *J. Mat. Sci.*, Vol.11, 1976, 1939.
106. M. Nakamura and J. Gurland, *Metall. Trans. A.*, Vol.11A, 1980, 141.
107. J. Hong and J. Gurland, in 'Science of hard materials', (R.K.Viswanadham, D.J. Rowcliffe and J. Gurland, eds.), Plenum press, N.Y., 1983, 649.
108. L.S. Sigl, H.E. Exner and H.F. Fischmeister, Paper presented at 2nd Int. Conf. on Science of Hard Materials, Rhodas, 1986.
109. C.Mian, *Int. J. Refrac Met. and Hard Matr.*, Vol.8, 1989, 49.
110. R. Spiegler, S. Schmander and H.F. Fischmeister, in 'Finite Elements in Engg. Applications', INTES GmbH, Stuttgart, 1990, 21.
111. R.Porat, J.Malek, *Mat. Sci. Eng.*, Vol.A 105/106, 1988, 289.
112. P.Walter, H. Grewe, *Powd. Met. Int.*, Vol.3, No.2, 1971, 88.

113. K.G. Stjernberg, *Powd. Met.*, Vol.13, No.25, 1970, 1.
114. H. Suzuki, T. Yamamoto and K. Hiyashi, *J. Jap. Soc. Powd. and Powd. Met.*, Vol.13, 1966, 304.
115. D.L.Tillwick and I.Joffe, *Scripta Metall.*, Vol.7, 1973, 479.
116. A. Nighiyama, R. Ishida, *Trans. Jap. Inst. Met.*, Vol.3, 1962, 185.
117. S.G. Kang and E. Fromm, in 'Proc. 10th Plansee sem.', (H.M. Ortner, ed.), Metallwerk Plansee, Reutte, Austria, Vol.1, 1981, 679.
118. O. Kubaschewski and B.E. Hopkins, 'Oxidation of metals and alloys', Butterworths, London, 1962.
119. J.M. West, 'Basic corrosion and oxidation', E. Horwood Publishers, Chichester, 1986.
120. J. Larsen-Basse, *Powd. Met.*, Vol.16, 1973, 1.
121. C.W. Merten, in 'Science of hard materials', R.K. Viswanadham, D.J. Rowcliffe and J. Gurland, eds.), Plenum press, N.Y., 1983, 757.
122. G.A. Schneider, in 'Cermaics today - Tommorow's ceramics', (P. Vincenzini, ed.), Elsevier Science Publishers B.V., Amsterdam, 1991, 2851.
123. G.A. Schneider, *Ceramics Int.*, Vol.17, 1991, 325.
124. S. Tomono, K. Tukumoto, A. Tanaka, *Nippon Tungsten Review*, Vol.22, 1989, 13.
125. K. Tukumoto, K. Terazaki, A. Tanaka, *Nippon Tungsten Review*, Vol.23, 1990, 59.
126. J. Larsen-Basse, *J. of Met.*, Vol.35, No11, 1983, 35.
127. E. Lardner, *Met. Tech.*, Vol.3, 1976, 237.
128. J. Larsen-Basse and E.T. Koyanagi, *Trans. ASME*, Vol. 101, 1979, 208.

129. J. Larsen-Basse, in 'Science of hard materials', (R.K. Viswanadham, D.J. Rowcliffe and J. Gurland, eds.), Plenum press, N.Y., 1983, 797.
130. T.A. Hack and C.T. Peters, in 'Proc. 11th Plansee sem.', (H. Blidstein and H.M. Ortner, eds.), Metallwerk Plansee, Reutte, Austria, Vol.1, 1985, 799.
131. C.T. Peters and S.M. Brabyn, in 'Proc. 11th Plansee sem.', (H. Blidstein and H.M. Ortner, eds.), Metallwerk Plansee, Reutte, Austria, Vol.1, 1985, 877.
132. E.M. Trent, 'Metal cutting', Butterworth, London, 1977.
133. H.S. Kalish, 'Some plain talk about carbides', Adamas Carbide Corporation, Reprint from American Machinist, May, 1978.
134. H.S. Kalish and J.S. August, Metal Progress, Vol.115, No.6, 1979, 64.
135. T. Yamaguchi and J.V. Biggers, Powd. Met. Int., Vol.7, No.2, 1975, 75.
136. W. Dawihl, Handbook of Hard Metals, H.M. stat. office, London, 1955, 68.
137. A. Gabriel, H. Pastor, D.M. Deo, S. Basu and C.H. Allibert, in 'Sintering '85', (G.C. Kuczynski, D.P. Uskokovic, H. Palmour III and M.M. Ristic, eds.), Plenum press, N.Y., 1987, 379.
138. V.A. Tracy and N.R.V. Hall, in 'Proc. Conf. on Recent Advances in Hard Metal Production', September 17-19, 1979, Metal Powder Report, Schrewsbury, 1979.
139. H. Suzuki, T. Tanase, F. Nakayama, K. Hayashi, J. Jap. Soc. Powd. and Powd. Met., Vol.25, 1978, 32.
140. H. Suzuki, T. Yamamoto and N. Chujo, J. Jap. Soc. Powd. and Powd. Met., Vol.14, 1967, 26.
141. G.S. Upadhyaya, S.K. Bhaumik, Mat. Sci. Eng., Vol. A 105/106, 1988, 249.
142. G. Barlow, in 'Proc. 4th Euro. P/M symp.', Grenoble, May, 1975, Priprints, Vol.2, Paper-5.

143. S. Ekemer, L. Lindholm and T. Hartzell, in 'Proc. 10th Plansee sem.', (H.M. Ortner, ed.), Metallwerk Plansee, Reutte, Austria, Vol.1, 1981, 477.
144. W. Precht, R.K. Viswanadham, J.D. Venables, in 'Science of hard materials', (R.K. Viswanadham, D.J. Rowcliffe and J. Gurland, eds.), Plenum press, N.Y., 1983, 815.
145. S. Ekemer, L. Lindholm and T. Hartzell, Int. J. Refrac. Met. and Hard Matr., Vol.1, No.1, 1982, 37.
146. E. Kny, L. Schmid, Int. J. Refrac. Met. and Hard Matr., Vol.6, No.3, 1987, 145.
147. E.A. Almond and B. Roebuck, Mat. Sci. Eng., Vol. A105/106, 1988, 237.
148. K. Nishigaki, H. Doi, N. Yukawa, M. Morinaga and T. Koie, in 'Proc. 11th Plansee sem.', (H. Blidstein and H.M. Ortner, eds.), Metallwerk Plansee, Reutte, Austria, Vol.2, 1985, 487.
149. D. Moskowitz, M.J. Ford and M. Humenik, Jr., Int. J. Powd. Met. Vol.6, No.4, 1970, 55.
150. L. Prakash, H. Holleck, F. Thummler and P. Walter, in 'Mod. Dev. in P/M', (H.H. Hausner, A.W. Antes and G.D. Smith, eds.), APMI/MPIF, Princeton, N.J., Vol.14, 1981, 255.
151. R.K. Viswanadham, P.G. Lindquist, Metall. Trans. A., Vol.18A, 1987, 2163 and 2175.
152. H. Suzuki, Y. Fuke, and K. Hayashi, J. Jap. Soc. Powd. and Powd. Met., Vol.19, 1972, 106.
153. E. Kny and H. Ortner, in 'Proc. 2nd Int. Conf. on Science of Hard Materials', Rhodas, Greece, 1984.
154. R. Warren, M.B. Waldron, Powd. Met., Vol.20, 1977, 180.
155. D.Y. Kim and A. Accary, in 'Sintering Process', (G.C. Kuczynski, ed.), Plenum press, N.Y., 1979, 235.
156. Y. Chaochen, in 'Horizon in Powd. Metall.', (W.A. Kaysser and W.J. Huppmann, eds.), Verlag-Schmid, Freiburg, Part I,

157. V.K. Sarin, in 'Advances in Powd. Tech.', (G.Y. Chin ed.), ASM, Ohio, 1982, 253.
158. H.S. Kalish and J.S. August, P/M '78 SEMP, Vol.2, Stockholm, 4-8 June, 1978, Jernkontaret, Sweden, 76.
159. H. Suzuki, K. Hayashi and K. Tukumoto, J. Jap. Soc. Powd. and Powd. Met., Vol.30, No.7, 1983, 263.
160. W. Dawihl and M.K. Mal, Cobalt, Vol.26, 1965, 25.
161. L. Zhonglin, in 'Horizon in Powd. Metall.', (W.A. Kaysser and W.J. Huppmann, eds.), Verlag-Schmid, Freiburg, Part I, 1986, 551.
162. L.E. Toth, 'Transition Metal Carbides and Nitrides', Academic press, N.Y., 1971.
163. P. Schwarzkopf and R. Kieffer, Cemented Carbides, McMillon, N.Y., 1960.
164. N. Tsuchiya, O. Terada, A. Sasaki and H. Suzuki, J. Jap. Soc. Powd. and Powd. Met., Vol.37, No.4, 1990, 80.
165. G. Arthur, J. Inst. Metals, Vol.83, 1954, P. 1329.
166. G.V. Samsonov, High temperature materials, No.2 Properties index, Plenum press, N.Y., 1964.
167. J. Gurland, in 'Practical application of quantitative metallography, STP 839', (J.L. McCall and J.H. Steele, Jr., eds.), ASTM, Philadelphia, 1984, 65.
168. D.K. Shetty, I.G. Wright, P.N. Mincer and A.H. Clauer, J. Mat. Sci., Vol.20, 1985, 1873.
169. P.S. Kisly, 'Kermeti', Naukova Dumka, Kiev, 1985 (in Russian).
170. K.J.A. Brooks, 'Cemented Carbides for Engineers and Tool Users', Int. Carbide Data, U.K., 1983.
171. G.E. Spriggs, Powd. Met., Vol.13, No.26, 1970, 369.
172. J.Y. Laval, J. Vicens and G. Nouet, J. of Phys., Vol.45, No. C2, 1984, 695.

173. E.M. Trent, in 'Treatise on Mat. Sci. and Tech.' (D.Scott, ed.), Academic press, N.Y., Vol.13, 1979, 443.
174. G.V. Samsonov (ed.), 'The Oxide Handbook', IFI/Plenum, N.Y., 1973.
175. H. Chandrasekaran, in 'Science of hard materials', (R.K. Viswanadham, D.J. Rowcliffe and J. Gurland, eds.), Plenum press, N.Y., 1983, 735.
176. L. Backerud, B. Carlsson, R. Oskarsson and M. Mikus, Scand. J. Met., Vol.3, 1974, 725.
177. A. Hara and M. Miyake, J. Jap. Soc. Powd. and Powd. Met., Vol. 17, 1971, 206, (HB translation no. 8467).
178. S.M. Brabyn, R. Cooper and C.T. Peters, in 'Proc. 10th Plansee sem.', (H.M. Ortner, ed.), Metallwerk Plansee, Reutte, Austria, Vol.2, 1981, 675.
179. J.M. Barranco and R.A. Warenchak, Int. J. Refrac. Met. and Hard Matr., Vol.8, 1989, 102.
180. O.Kubaschewski, E.L. Evans and C.B. Alcock, 'Metallurgical thermochemistry', Pergamon press, London, 1967.
181. J.A. Jehn and K.K. Schulze, in 'Physical metallurgy and technology of molybdenum and its alloys', (R.K.Miska, M. Semchyshen, E.P. Whelan and D.J. Kruzich, eds.), AMAX Speciality Metal Corporation, Greenwich, Conn., 1985, 107.
182. V.C. Venkatesh and H. Chandrasekaran, 'Experimental Methods in Metal Cutting', Prentice Hall of India Pvt. Ltd., New Delhi, 1982.
183. R. Kieffer, P. Ettmayer and M. Freudhofmeier, in 'Mod. Dev. in P/M', (H.H. Hausner, ed.), Plenum press, N.Y., Vol.5, 1971, 201.
184. P.S. Kisly and M.A. Kuzenkova, Powd. Met. Int., Vol.4, 1972, 67.
185. P. Ettmayer, H. Kolaska, K. Dreyer, Powd. Met. Int., Vol.23, 1991, 224.

186. T.B. Merala, H.W. Chan, G.G. Howitt, P.V. Kelsey, G.E. Korth and R.L. Williamson, *Mat. Sci. Eng.*, Vol. A105/106, 1988, 293.
187. H. Suzuki, *J. Jap. Soc. Powd. and Powd. Met.*, Vol.29, 1982, 25.
188. G.V. Samsonov, I.F. Pryadko and L.F. Pryadko, 'A configurational model of matter', Consultant Bureau, N.Y., 1973.
189. Y. Joonbaik, K.Y. Eun, *J. Am. Cerm. Soc.*, Vol.74, No.6, 1991, 1397.
190. B. Roebuck and M.G. Gee, in 'Proc. 12th Int. Plansee Sem.', (H. Bildstein and H.M. Ortner, eds.), *Metallwerk Plansee, Reutte, Austria*, Vol.2, 1989, 1.
191. H. Yoshimura, T. Sugizawa and H. Doi, in 'Proc. 11th Int. Plansee Sem.', (H. Bildstein and H.M. Ortner, eds.), *Metallwerk Plansee, Reutte, Austria*, Vol.2, 1985, 795.
192. E. Rudy, *J. Less. Comm. Met.*, Vol.33, 1973, 43.
193. E. Rudy, S. Worcester and W. Elkington, in 'Proc. 8th Plansee sem.', *Metallwerk Plansee, Reutte, Austria*, 1974, Paper-30.
194. M. Fukuhara and H. Mitani, *Powd. Met.*, Vol.25, No.2, 1982, 62.
195. J. Gurland, in 'Materials for metal cutting', ISI Publication No. 126, Institute of Metals, London, 1970, 152.
196. R. Kieffer, N. Reiter, and D. Fister in 'Materials for metal cutting', ISI Publication, No. 126, Institute of Metals, London, 1970, 157.
197. ISO 3685-1977, Specification for tool life testing with single point turning tools.
198. P.K. Wright, A. Bagchi and J.G. Horne, in 'Cutting tool materials', ASM, Ohio, 1981, 7

